THE JOURNAL
OF
CHEMICAL PHYSICS

VOLUME 17, NUMBER 1 JANUARY, 1949

Chemical Properties of Astatine. I.

G. L. JOHNSON, R. F. LEININGER, AND E. SEGRÈ
Radiation Laboratory, Department of Physics, University of California, Berkeley, California

(Received June 1, 1948)

This work is a report on studies of the chemistry of astatine on a tracer scale, using the various methods of tracer chemistry. A general discussion of preparation of materials and analytical methods is included. The properties of astatine and its solutions as they appear in work on a tracer scale are discussed. Migration experiments show that astatine when ionized in aqueous solution is negatively charged. Electro chemical, solvent extraction, and carrying studies are presented.

In general, (a) elemental astatine is extractable by organic solvents; (b) the -1 state may be prepared by powerful reducing agents; and (c) at least two positive oxidation states exist.

I. INTRODUCTION

EARLIER work on the radioactive element 85, astatine, has been reported in 1940.[1] At that time the nature of the various radiations produced by astatine 211 were well worked out, and, in addition, the chemical properties of this new element were briefly sketched. Soon after, all work on the subject was dropped because of the pressure of war activities. This paper is the first report of a more detailed investigation of the chemistry of astatine; we hope to continue this research.

As a first step in extending our knowledge of astatine, we have tried to find some isotope of longer life than At^{211}, with the hope of accumulating visible amounts of the substance. This quest has been unsuccessful, although two new isotopes, astatine 212 and 210, with half-lives of 0.2 second and 8.3 hours, respectively, have been recognized.[2] Astatine 212 is an alpha-emitter, and astatine 210 decays by K-capture. Other reported isotopes of astatine[3,4] have even shorter half-lives, and from this it appears that at the present time all of the chemical research on astatine must be done on a tracer scale. For reasons of convenience we have used almost exclusively astatine 211 of 7.5-hour half-life. 650 atoms of this isotope produce one alpha-particle per minute. The most concentrated solution so far prepared is approximately 10^{-8} molar, and the usual experiments are performed with 10^{-11} to 10^{-15} molar astatine; a molar solution of At^{211} would emit $1.54\times10^{16}\alpha$ cm^{-3} sec.$^{-1}$. Since tracer scale experiments are difficult to interpret, wherever there is any doubt we shall include sufficient experimental data to enable

[1] D. R. Corson, K. R. Mackenzie, and E. Segrè, Phys. Rev. **57**, 672 (1940). For the name "astatine," see D. R. Corson, K. R. Mackenzie, E. Segrè, Nature (London) **159**, 24 (1947).

[2] At^{210}: E. Kelly and E. Segrè, to be published elsewhere; At^{212}: T. Putnam and M. Weissbluth, to be published elsewhere.

[3] At^{217}; $T_{\frac{1}{2}}$ 0.02 sec.: Hageman, Katzin, Studier, Ghiorso, and Seaborg, Phys. Rev. **72**, 252 (1947); English, Cranshaw, Demers, Harvey, Hincks, Jelley, and May, *ibid.* **72**, 253 (1947).

[4] At^{215}, At^{216}, At^{218}: B. Karlik and T. Bernert, Zeits. f. Physik **123**, 51 (1944).

the reader to draw his own conclusions. Also, in work at these dilutions the concentration effects on the thermodynamic properties are very large. The correction to macro quantities of astatine will be very large in all cases except when the same numbers of astatine atoms or molecules appear on both sides of the reaction equations. As this is a report of current work, some of our conclusions are rather hypothetical and may be corrected in future articles. The experimental parts of this paper will be described in general sections according to the property of astatine used in the experiment (volatility, solvent extraction, etc.). Since the details of the experiments will not be of interest to all readers, the final section includes a summary of the results with the conclusions which we have drawn from them.

II. PREPARATION OF MATERIALS

Bismuth, when bombarded by alpha-particles in the energy range 21–29 Mev, produces astatine 211 free of other activities. Above 28 Mev astatine 210 is also produced by the reaction $(\alpha, 3n)$.[5] This substance decays by orbital electron capture to polonium 210, the presence of which is very undesirable in all of our experiments.

The bismuth samples that were bombarded were produced by evaporating bismuth from a molybdenum boat in a high vacuum upon aluminum disks of one-mil thickness. Bismuth samples prepared in this way were of uniform thickness and could be made up to 40 milligrams per square centimeter thick. These samples were subsequently clamped in a water-cooled target holder and bombarded by the sixty-inch cyclotron of the Crocker Radiation Laboratory. The beam energy was reduced to less than 28 Mev by aluminum absorbers in front of the target in order to avoid producing polonium 210. In some bombardments an additional bismuth-aluminum foil was exposed to the full energy of the beam to produce polonium 210 for comparison experiments. A detailed study of the bismuth-alpha-excitation function by E. Kelly will be published elsewhere. Here it suffices to say that if we limit the energy to 29 Mev to prevent production of polonium 210, the thick target yield for a short bombardment is approximately 1.2×10^{9} disintegrations per minute per microampere hour.

For most of our experiments we wished to extract the activity from the bombarded target. As the high volatility of astatine from bismuth was known,[1] we used a high vacuum distillation method to concentrate the activity.

The procedure used was to distill the astatine from bismuth at its melting point in an all-glass system, and collect the carrier-free element in a four-millimeter diameter U tube cooled by liquid nitrogen. The U tube while still cold was washed with one drop of concentrated nitric acid, allowed to stand 1 hour, and then washed with distilled water into a stock bottle. By this method three-milliliter solutions were prepared containing 0.5-molar nitric acid and 10^{7} disintegrations/sec. of astatine. Such a solution is 2.1×10^{-10} molar with respect to astatine. Yields up to 0.95 were obtained with less than 0.001 of any polonium present in the original target coming over.

Experiments to be described later in the volatility section indicate that astatine evaporated on glass is very poorly held by this surface at room temperature. Based on this information, a double separation of astatine from bismuth and polonium was accomplished. A bismuth plate was bombarded in such a way as to accumulate in it approximately equal numbers of polonium and astatine atoms, after which a first distillation was carried out in the usual way. The tube containing the bismuth was sealed off and the astatine then distilled at room temperature to a second U tube cooled by liquid nitrogen. The yield of this experiment was 0.83 of the astatine present on the original target, with less than 10^{-6} of the polonium coming over.

III. ANALYTICAL METHODS

Astatine 211 can be measured by its alpha or x-ray radiations, and either radiation can be used to follow a chemical process. For most purposes the alpha-particles are counted because of the higher counting efficiency of the equipment used to detect this type of radiation. However, for certain experiments where self-absorption prohibits the use of alpha-counting techniques, x-ray counters were used. At^{210} is even more favorable than At^{211} for thick sample counting because it emits γ-rays in addition to the x-rays. However,

[5] E. L. Kelly and E. Segrè, Phys. Rev. **72**, 746 (1947).

because in our alpha-bombardments At^{210} is always produced together with polonium and with relatively small yield, we did not use it extensively.

For alpha-counting, the samples were mounted on flat platinum disks 2 mils thick and one inch in diameter. A slurry of the precipitate to be studied was pipetted on a freshly flamed platinum disk and allowed to dry. In general, the thickness of the sample was limited to one milligram per square centimeter except in cases where poor spreading of the precipitate made the sample thicker in spots.

Samples for x-ray measurement were placed in three-milliliter centrifuge cones. These samples were counted with a Geiger-Müller counter; the efficiency of the counter was not accurately known, but was kept constant during the various experiments.

Frequently during the course of this investigation weightless samples of astatine and its compounds were deposited on supports of a variety of materials for analytical purposes. It was easily recognized that such samples occasionally lost more activity by evaporation than by decay, and for this reason studies were made on their volatilities under various conditions.

The volatility of astatine from glass is most striking. When elemental astatine was evaporated upon glass the loss of astatine from that surface at room temperature was so rapid that, if the evaporation follows an exponential law, the "half-life for evaporation" is approximately 1 hour. From metallic surfaces the losses were much less; for instance, about sixteen hours were required for half of the astatine to evaporate from a gold or platinum surface. When the astatine was initially dissolved in cold concentrated nitric acid, and the samples dried at 80°C on the surface investigated, the losses were much smaller. From glass the "half-life for evaporation" of the residue was approximately four hours. There was no observable loss from gold and platinum in a period of 24 hours after the samples were evaporated at 80°C on these supports.

These experiments indicated that elemental astatine would not provide samples suitable for counting but that nitric acid solutions of astatine dried on gold or platinum would give satisfactory samples if we knew the loss undergone in the drying process. Furthermore, since gold consistently showed a higher initial loss than platinum when identical amounts of the same tracer solution were evaporated upon them at 80°C, platinum was used in all cases. The absolute loss of astatine, when a nitric acid solution was dried, was measured by counting the x-rays from a small sample as the solution went to dryness. In three experiments on different solutions, the losses were 26, 26, and 28 percent, respectively. Subsequent experiments with solvent extraction have shown that astatine dissolved in cold concentrated nitric acid is present principally as the zero state.

The losses in the experiment just described are attributed to partial loss of some astatine zero. The principal losses always took place just as the samples were going to dryness.

IV. VOLATILITY EXPERIMENTS

Since our analytical experiments indicated that astatine had variable affinities for various surfaces, an experiment was devised to measure the relative adsorption power of various metals. A 0.3×2.5-cm strip of each of the metals listed in Table I was suspended in an evacuated Pyrex tube of one-inch diameter. In the first experiments the metals were exposed to astatine vapor for approximately 16 hours at room temperature. In the second experiment the metal foils were heated in an evacuated system to 325°C for one-half hour together with a previously bombarded bismuth foil. The data are given in Table I. Since Al, Ni, and Cu showed low adsorption, in some of the later experiments we omitted them and used duplicate strips of the other metals. The surfaces of the metals in each

TABLE I. Adsorption of astatine on metallic surfaces in high vacuum expressed as percent of the total astatine on the surfaces.

Metal	Room temperature		325°C		
	(1)	(2)	(1)	(2)	(3)
Al	0.3		0.2	0.3	
Ni	0.2		0.6	0.7	
Cu	0.5		0.6	4.3	
Pt	36.3	20	33.5	6.5	16
Au	38.4	65	0.1	0.7	4
Ag	24.3	15	65.0	87.5	80
	100.0%	100%	100.0%	100.0%	100%

TABLE II. Distillation of astatine solutions.

Initial solution	Initial volume 10 ml Percent of At in each successive ml of distillate (1)	(2)	(3)	(4)	(5)	(6)	(7)	(8)	(9)	Percent left in still	(a)
$16M$ HNO_3	0.1	0.1	0.1	0.3	0.1	0.2				86	0.87
$5M$ HNO_3+3 mg I^-	2.0*									98	—
$12M$ HCl	0	0	0	0.4	0.1	0.8	3.7	9.5		70	0.84
1:1 H_2SO_4	0.6	0	0.2	0.3	0.4	0.2	0.1	0		91	0.92
60% $HClO_4$	0	0.1	0	0	0	0.1	0	0.2	0.4	101	1.02
$0.5M$ H_2SO_4+$0.05M$ Fe^{++}	48	21	5.0	4.0	3.6	2.6	3.0	4.0		7.4	—
CCl_4	1.1	0.8	0.7	0.6	0.6	0.8	1.0	2.0	7.8	64	0.78
Benzene	3.5	3.5	3.4	3.2	3.5	3.6	4.6	4.8	7.7	62	—

[a] Amount of astatine in distillate and still pot divided by initial amount of astatine.
* First 10 percent of distillate contained all of the I_2 but only 2 percent of the At.

case were previously cleaned in the apparatus by heating to ~400°C in a hydrogen atmosphere.

The selective nature of the adsorption indicates a special affinity of astatine for some metallic surfaces. Aluminum (certainly oxidized on the surface) and glass showed very poor adsorption; bismuth too is not a good adsorber.

We have also run some experiments on the distillation of various solutions containing astatine. Table II lists the various combinations tested, the yields of astatine in the distillate, and the material balances when obtained. In all experiments the astatine was detected by thick sample counting of the x-rays.

Special attention is called to the differing behavior of astatine and iodine. The dissimilarity of astatine and iodine under these conditions was noted in the paper of 1940.[1] The failure of astatine to distill under conditions in which iodine distills, therefore, was not surprising. This anomaly will be explained further in the section on solvent extraction.

These results indicate that astatine in aqueous solution may be manipulated without loss in the presence of oxidizing agents. Organic solvent solutions and aqueous solutions containing reducing agents (Fe^{++} or better) must be handled with care.

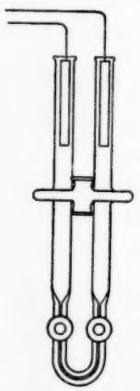

FIG. 1. Migration apparatus.

V. MIGRATION EXPERIMENTS

We performed some experiments to determine the direction of migration of astatine in a solution subject to an electric field. The simple apparatus[6] used consisted of a U tube, the bottom section of which was made of one-millimeter capillary tubing (see Fig. 1). The capillary tubing, which was about two inches long, could be isolated from the rest of the U tube by one-millimeter bore stopcocks.

Solutions containing astatine were placed in the capillary tube with care so that no bubbles were left. The stopcocks were then closed and the excess material in the side arms of the U tube carefully washed out. A solution of the same composition but without astatine was placed in the U tube arms, two platinum electrodes inserted, and the entire apparatus clamped in a thermostat. The solutions in the side arms were leveled by opening the connecting stopcock, which was above the capillary section of the U tube containing astatine. The leveling stopcock was then closed and the two capillary stopcocks opened. A voltage difference of 100 volts was applied across the cell for approximately one hour, after which the stopcocks were closed and the side arms analyzed for astatine. The normal migration current was less than 10 milliamperes; however, in concentrated acid solutions, currents

[6] See, e.g., M. Haïssinsky, *Electrochimie des Substances Radioactives* (Hermann and Company, Paris, 1946), p. 19.

as high as 90 milliamperes occurred. In all solutions tested the astatine migrated as a negative ion. The conditions checked are listed in Table III.

VI. ELECTROCHEMISTRY

The electrochemistry of astatine has been studied using the method of Hevesy and Paneth[7] with the refinements of Joliot.[8] The electrolysis was carried out in a glass cell (*a*) made in the form of a tee (see Fig. 2). Gold windows (*b*), eight to ten milligrams per square centimeter in thickness, were fastened over the ends of the tee by a rigid clamping arrangement similar to that used by Joliot. The windows were one centimeter in diameter, and the cell had a volume of ten milliliters. The alpha-particles of astatine were deposited on the gold windows, penetrated the thin gold, and caused ionization in the air beyond. These ions were collected by an electric field and the resultant current measured by an FP-54 electrometer. By this arrangement the ionization of 50 alpha-particles per minute was easily detected.

Joliot used a system of parallel plates perpendicular to the thin gold window to collect the ions formed. We used this arrangement at first, but later abandoned it in favor of another which gave better results. The changes were as follows: A thin aluminum leaf (*c*) was mounted by Aquadag on a brass ring spaced one centimeter from and parallel to the gold windows. A potential difference of 700 volts was maintained on this ring with respect to ground by a battery. Behind the ring and spaced two centimeters from it was a brass disk (*d*) of the same size. The disk was insulated by polystyrene and was connected to the grid of the FP-54 tube. In addition, a movable shutter was arranged over the gold windows to absorb the alpha-particles coming through so that the FP-54 circuit could be adjusted to zero while an electrolytic process was in progress. Since both windows were equipped with electrometers, the activity deposited on either window could be measured at any time.

Considerable difficulty was experienced in finding thin gold free from pin holes. The gold foils were finally manufactured by evaporating gold from a tungsten boat in a high vacuum upon freshly split mica. When the gold-coated mica was placed in water, the gold films were detached cleanly from the mica by the wetting power of the water.

Initially, the electrolysis was carried on between the two gold windows. The potentials of the gold windows with respect to a saturated calomel reference electrode were measured with a Beckman Laboratory type *p*H meter. Later, however, the two electrodes were connected together and the electrolysis conducted between the combined electrodes and a working calomel electrode. Figure 2 is a schematic diagram of the apparatus and electrical circuit used.

The results of the cathode electrolytic experiments are shown in Table IV. The critical deposition potentials listed are obtained by extrapolation of deposition rate *vs.* potential curves back to zero rate. An example of typical data and their extrapolation are given in Figs. 3 and 4.

Special experiments performed were as follows: (a) When the astatine was previously oxidized

TABLE III. Composition of solutions in which astatine migration experiments were run; astatine was initially dissolved in concentrated nitric acid and then treated as described below.

(1)	Made 1*M* in HNO_3
(2)	Made 0.1*M* in HNO_3
(3)	*p*H = 3 in phosphate buffer
(4)	*p*H = 5 in phosphate buffer
(5)	*p*H = 7 in phosphate buffer
(6)	*p*H = 9 in phosphate buffer
(7)	*p*H = 11 in phosphate buffer
(8)	*p*H = 13 0.1*M* NaOH
(9)	Reduced by SO_2 in 0.1*M* HNO_3
(10)	Reduced by $NaSO_3$ in 0.1*M* NaOH
(11)	Oxidized by hot $K_2S_2O_8$ in 0.1*M* HNO_3
(12)	Oxidized by HClO in 0.1*M* NaOH
(13)	Oxidized by Br_2 in 0.5*M* HNO_3

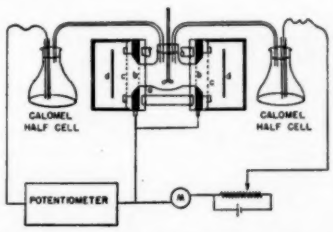

FIG. 2. Schematic diagram of the electrolytic apparatus and the electrical circuit.

[7] G. v. Hevesy and F. Paneth, Wien Ber. **123**, 1619 (1914), and **122**, 1049 (1913).
[8] F. Joliot, J. de Chemie Phys. **27**, 119 (1930).

TABLE IV. Critical deposition potential of astatine at the cathode from various solutions.

Solution	Concentration of At mole/liter	Critical deposition potential/normal H_2 electrodes
0.066*M* HNO_3	2.8×10^{-13}	-1.225 ± 0.025v
1.0*M* HNO_3	5×10^{-14}	-1.24 ± 0.025v
0.075*M* H_2SO_4 0.1*M* $Na_2Cr_2O_7$	6×10^{-13}	-1.20 ± 0.025v
0.066*M* HNO_3+3 mg Au	1×10^{-13}	-1.22 ± 0.025v
0.066*M* HNO_3 (repeat)	4×10^{-14}	-1.22 ± 0.025v

TABLE V. Critical deposition potential of astatine at the anode from various solutions.

Solution	Concentration of At in mole/liter	Critical deposition potential/normal H_2 electrode
0.066*M* HNO_3	2.4×10^{-13}	-1.46 ± 0.02v
0.066*M* HNO_3	5.3×10^{-13}	-1.45 ± 0.02v
0.1*M* HNO_3 0.1*M* $K_2S_2O_8$	5.4×10^{-13}	-1.445 ± 0.02v

by hot (60°C) persulfate for 15 minutes there was no consistent deposition at the cathode. The initial spontaneous deposition was smaller than in any previous experiment. The possible ions present in the oxidized solution will be discussed in the sections on solvent extraction and carrying.

(b) When astatine zero was dissolved in sulfuric acid no deposition took place at the cathode until dichromate ion was added to the cell.

We endeavored to determine the reversibility of the cathodic deposition. In every experiment tried the deposition appeared to be quite reversible. After depositing astatine on the cathode at potentials greater than the critical deposition potential, the material was rapidly removed by lowering the cathode potential below -1.25v by a few hundredths of a volt. A further decrease of the gold potential to about -1.45v caused the astatine to deposit on the gold anodically.

A study of this anodic deposit was also attempted (Table V). Since the potentials involved are close to those required to decompose water and dissolve gold, the problems are more difficult than those involved in the cathodic work. The experiments were run in 0.1*M*, or less, nitric acid to avoid excessive electrolytic currents.

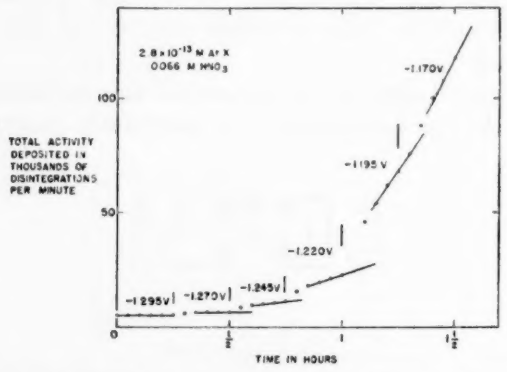

FIG. 3. Typical data showing the total activity deposited on the gold window as a function of the deposition potential and the time.

The anodic deposition was not reversible. Vigorous treatment, such as concentrated nitric acid or strong electrolytic currents with repeated reversals of direction, was necessary to remove the deposited material.

The nature of the astatine compounds deposited in the electrolytic experiments is as yet unknown. A large variety of products are possible at both the anode and the cathode.

VII. SOLVENT EXTRACTION

Solvent extraction studies proved to be our most powerful single tool in the study of astatine chemistry. Since solvent extraction methods work well in very dilute solutions, the method is particularly adaptable to our problems and although no quantitative results were attempted for the time being, solvent extraction methods should prove to be very useful in determining the thermodynamics of astatine even in these extremely dilute solutions. As an example, the reaction

$$At^- = At^0 + e^-$$

would be unaffected by astatine concentration, whereas

$$2At^- = At_2^0 + 2e^-$$

would be greatly affected. Concentration studies of solvent extraction in solutions stabilized with respect to oxidation-reduction are contemplated.

The solvents used were Baker's analyzed carbon tetrachloride and benzene. Initially, it was believed that in the case of carbon tetrachloride astatine might conceivably react with or replace the chlorine of the solvent, affecting the results of the experiments. No such effect was observed in the work, and the behavior of CCl_4 is qualitatively identical with that of benzene.

Solutions were prepared by dissolving astatine in the various solvents, and using them as

stock solutions for the experiments involved. All extraction experiments were run in the range of 3×10^{-11} to 10^{-12} molar astatine. When such a stock solution was repeatedly extracted with $0.01M$ HNO_3, a series of partition coefficients was obtained which increased to a maximum value. This maximum value is not necessarily the true partition coefficient, but approaches it as a limit, the limit being set by the mechanics of the experiment and the presence of traces of oxidizing or reducing agents. All work was done on a one-milliliter scale. Since the extraction experiments involved usually a series of consecutive extractions on a single sample of astatine, the results of the experiments are recorded in tabular form in Table VI with comment at the end.

It is noteworthy that the experiment on tracer I_2 falls far short of the accepted value of 85.

In basic solution the behavior of astatine is very different. The experiments were as follows. A stock solution of astatine in organic solvent was extracted three times by $0.01M$ HNO_3 until a large partition coefficient was obtained. The solvent phase was then extracted with $0.1M$ NaOH and the partition coefficient measured. Finally, the water layer was acidulated and the partition coefficient remeasured. The results are given in Table VII.

The simplest interpretation of this experiment is that in alkaline solution astatine disproportionates to At^- and an oxidized state, and passes from the solvent to the water layer. In this hypothesis a fractional part of the astatine in the water layer should precipitate with AgI as a carrier, and another fraction should not precipitate because it is in a higher oxidation state. However, when we precipitated silver iodide from the 0.1-M NaOH solution in the presence of excess ammonia, the silver iodide carried all the astatine. This objection to the hypothesis of the disproportionation of astatine in alkaline solution does not seem of great importance, however, because we are not certain that the higher oxidation states of astatine would not coprecipitate in alkaline solution with silver iodide. In acid solution they do not coprecipitate with silver iodide.

TABLE VI. Partition coefficient of At and tracer I in successive extractions.

	At $CCl_4-0.01M$ HNO_3		At $C_6H_6-0.01M$ HNO_3		I $CCl_4-0.01M$ HNO_3	
Extraction	Exp. 1	Exp. 2	Exp. 1	Exp. 2	Exp. 1	Exp. 2
1	58	9.8	46	40	18	14
2	86	53	86	83	15	17
3	91	64	140	112	21	25
4		90	155	106	31	28
5			242	89		
6			227			

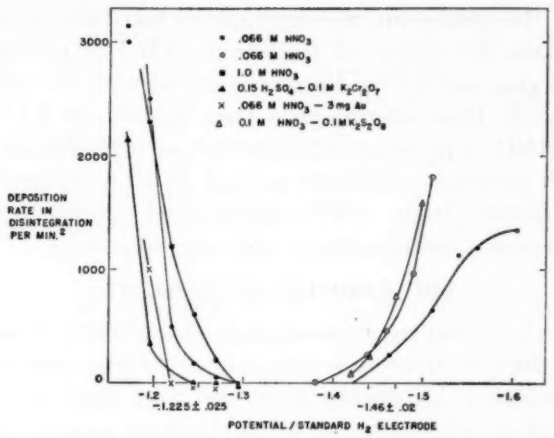

FIG. 4. The rate of electrochemical deposition of astatine on gold at the cathode and the anode from various acid solutions. All points below zero indicate zero rate of deposition.

So far we have discussed simple extractions in acid and basic solutions of astatine. Solvent extraction has been used also to study oxidation and reduction of astatine zero by adding an oxidizing or reducing agent to the water phase and observing the effect on the partition coefficient. In the experiments to be described, astatine dissolved in the organic solvent was repeatedly extracted by $0.01M$ HNO_3 to give the partition coefficient listed in column 3 of Table VIII. The solvent layer was then extracted by the final aqueous phase, listed in column 2, to give a new value of partition coefficient, listed in column 4.

TABLE VII. Comparison of partition coefficients of At in acid and basic solution.

Solvent	CCl_4	C_6H_6
First acid extraction	58	29
Second acid extraction	86	42
Third acid extraction	91	52
Extracted by $0.1M$ NaOH	0.85	1.5
Aqueous layer made $0.1M$ in HNO_3, the layers recombined and reextracted	25.0	21

In addition to the experiments listed above we have also dissolved astatine in 16M HNO_3 from a glass surface by 2-hour treatment with the cold acid. This solution was then diluted to 0.1M HNO_3 and extracted with carbon tetrachloride. A partition coefficient as high as 10 was found, showing that cold concentrated nitric acid oxidizes astatine slowly and incompletely.

VIII. CARRYING EXPERIMENTS

Carrying experiments have been made in an effort to determine the nature of the ions in solution. Experimental results have been found which emphasize the resemblance of astatine to iodine. Reference should also be made to the paper of 1940[1] which described many more of the carrying experiments.

Since astatine has a slight tendency to stick to glass surfaces, as do many other substances on tracer scale, precautions must be taken to avoid this cause of error. In general, confusion from this source has been avoided by measuring separately the activities of the supernatant, precipitate, and precipitation vessel. X-ray counting methods have been used extensively for these measurements.

TABLE VIII. Oxidation reduction studies using solvent extraction.

Solvent	Final aqueous layer	Partition coeff. in 0.01M HNO_3	Partition coeff. with final aq. layer	Comments
(1) C_6H_6	0.25M $FeSO_4$ 0.01M HNO_3	91	89	At^0 is neither reduced nor oxidized
(2a) CCl_4	saturated H_3AsO_3	90	49	after 10 minutes
(2b)	solvent reextracted with same aqueous layer	—	31	after 20 m[illegible]
(3) CCl_4	1.1M KI in 0.01 HNO_3	50	0.4	approx. 10 minute extraction. Decrease of coefficient due to formation of inter halogen compounds
(4) C_6H_6	saturated I_2 0.01M HNO_3	200	64	slight effect
(5a) C_6H_6	saturated SO_2 0.01M HNO_3	200	3	reduction of At^0 to At^-. AgI precipitated from this solution carries all the activity.
(5b) CCl_4	same	85	0.8	same
(6) CCl_4	0.25M $Fe(NO_3)_3$ 0.01M HNO_3	85	2	partial oxidation of astatine
(7)	0.5M $Hg(NO_3)_2$ 0.01M HNO_3	200	0.01	possible complexing by Hg^{++} causing At^0 to disproportionate
(8) CCl_4	Br_2 <0.1M 0.01M HNO_3	85	0.05	rapid oxidation of astatine by bromine; see carrying experiments.
(9a) C_6H_6	cold 0.01M $K_2S_2O_8$	200	5	slow oxidation of astatine
(9b) C_6H_6	50°C 0.1 $K_2S_2O_8$	200	0.1	rapid oxidation by hot $K_2S_2O_8$
(10) C_6H_6	3M HCl	50	0.66	possible compound formation with Cl^-
(11) C_6H_6	0.1M KIO_3 0.01M HNO_3	200	16	slight oxidation by IO_3^- in 10 minutes

(a) When the stock solutions were centrifuged, erratic losses were observed in different solutions of the same composition. However, no additional loss was produced by repeated centrifuging of an astatine tracer solution which had lost activity to the glass walls in the initial centrifugation. Since fresh centrifuge tubes were used each time, the loss was not dependent on the glass surface but on impurities (i.e., dust, etc.) in the initial solution. In general, centrifugation of the stock solutions improved the consistency of the subsequent experiments. Two-hour centrifugations at 2000 times gravity have produced negligible losses from 10-M HNO_3, 0.5-M HNO_3, and 0.1-M NaOH solutions.

(b) Various hydroxides carry astatine differently. The results are summarized in Table IX.

It is noteworthy that lanthanum hydroxide carries astatine differently, according to the oxidation of the solution. The reason for this behavior may be related to the insolubility of compounds of the type $La(AtO_3)_3$ in alkaline solution.

(c) Precipitation of mercuric sulfide in HCl solution carries astatine. The percent carried as a function of acidity is given below.

M HCl	0.5	1	5	10
Percent of At carried by HgS	69	81	93	92
Same in repeat exp.	88			96

(d) Astatine when reduced by sulfur dioxide in acid solution, is partially carried by TlI. Silver iodide carries At completely, but this effect is due to the formation of metallic silver on which astatine deposits (see under (e) below).

(e) If astatine is reduced by zinc in 1M sulfuric acid, and potassium iodide and silver nitrate are added *after the zinc is completely dissolved*, the astatine is carried completely by silver iodide. The carrying is also complete when TlI is used. If, however, we start from AgI containing astatine and reduce it by zinc, all of the astatine is found on the precipitated metallic silver which is formed, whereas all the iodine is in the solution.

(f) When silver iodide or chloride is precipitated from nitric acid solution of astatine, less than 2 percent of the activity is found in the precipitate.

(g) When silver iodate is precipitated from a nitric acid solution of astatine, the carrying depends upon the order of addition of the reagents. When silver is added first, poor carrying (5–20 percent) is observed; when iodate is added first, fair carrying (40–80 percent) occurs. This may be due to the fact that iodate can oxidize astatine, as discussed in the section on solvent extraction.

(h) When silver iodate is precipitated from a bromine oxidized solution, the iodate carries astatine poorly (5–15 percent).

(i) When silver iodate is precipitated from an oxidized solution of astatine (hot $K_2S_2O_8$ or HClO), carrying (90–100 percent) is independent of the order of addition of the reagents.

IX. CONCLUSIONS

In a work of this nature, the interpretation of the experimental data is often difficult because of the extreme dilution at which the experiments are run. This circumstance affects the results not only through dilution effects, but also through the presence of impurities in the reagents, which although negligible under ordinary circumstances, may materially influence some reactions. For the time being we have not tried to purify reagents beyond the ordinary quantitative analysis standards. For these reasons, although the facts and the results which have been described seem to us reasonably established, we may later change some of our current interpretations as additional research uncovers further facts in the complicated study of astatine chemistry.

The problem of data interpretation would be greatly simplified if the chemistry of iodine on a tracer scale were known. At the present time little is known of the behavior of iodine at concentrations of the order of $10^{-10}-10^{-16}$ molar. Studies on this subject would also be highly desirable from the general point of view of radio-chemistry. However, such a study would be very difficult since any reagent, even of highest quality, would be likely to increase the iodine concentration unwittingly manyfold.

TABLE IX. Carrying of astatine by various hydroxides.

	Starting material			
	HNO_3 stock solution		HNO_3 stock solution oxidized by hot $K_2S_2O_8$	
Precipitant	NaOH	NH_4OH	NaOH	NH_4O
Aluminum hydroxide		7–15%		7–15%
Bismuth hydroxide	40–60%		50–60%	
Ferric hydroxide	40–50%	30–40%	97–99%	85–90%
Lanthanum hydroxide	5–8%		97–99%	

Unfortunately, astatine is one of the few elements which can be studied in truly carrier free solutions.

In conclusion, we shall discuss individually the various oxidation species thus far ascertained.

The Zero State

The solvent extraction experiments give ample evidence for the existence of the zero state. Since the extraction coefficients which have been measured for the halogens show a trend increasing from chlorine to iodine, we expected the corresponding coefficients for astatine to exceed numerically those of iodine. The maximum values so far determined are

	At	I_2 literature	I_2 on tracer scale experiments
Benzene	240	400	—
Carbon tetrachloride	91	85	31

The attempt at solvent extraction of I_2 on a tracer scale, using carrier free iodine from Oak Ridge, yielded the coefficient included in the data.

The zero state is very easy to prepare and is stable in water solution. It is reduced by SO_2 and oxidized by ferric salts. (See solvent extraction.) It is the form obtained when astatine is distilled from bismuth at elevated temperatures, as proved by the fact that initial extraction coefficients as high as 40 have been obtained from such distilled materials.

The zero state is slowly oxidized by cold concentrated nitric acid. Oxidized solutions, however, are readily reduced to the zero state by ferrous compounds. These same ferrous compounds are incapable of reducing the zero state to the -1 state. (There is no effect on the distribution coefficient in CCl_4 with $0.25M$ $FeSO_4$.)

Astatine zero appears to disproportionate in basic solutions with $p\mathrm{H}=13$.

The −1 State

There is little doubt as to the assignment of the −1 state. As was pointed out, the zero state is not reduced by the −1 by 0.25*M* $FeSO_4$. There is slight evidence for a slow reduction by arsenious acid (see solvent extraction data). However, sulfur dioxide and zinc reduce astatine zero. Silver iodide, precipitated after SO_2 reduction, carries astatine completely in both acid and basic solutions (see (d) under carrying experiments). Zinc reduction in sulfuric acid solution followed by silver or thallous iodide precipitation carries astatine completely. On the other hand, if the reduction is performed in the presence of silver, the astatine is found entirely in the precipitated metallic silver. Experiments described in the section on volatility of astatine showed a strong affinity of At^0 in the gaseous state for silver. This may be due to either compound formation (astatides) or adsorption upon the metallic lattice. The carrying of the astatine by the reduced silver is perhaps to be regarded as a related phenomenon, rather than as an electrochemical deposition. The difficulties described in the earlier paper[1] regarding the method of purification used by Buch-Anderson in his search for element 85 in nature are easily resolved by these results.

The Plus States

Ferric compounds are sufficiently strong oxidizing agents to oxidize the zero state to a plus state. Br_2 rapidly and completely oxidizes astatine. (See solvent extraction studies.)

Carrying experiments with $AgIO_3$ have shown a difference between the plus states formed by Br_2 oxidation and those formed by HClO oxidation. One-half hour oxidation by cold Br_2 oxidizes the astatine completely (CCl_4 extraction coefficient of 0.1 and less), and the astatine so oxidized carries poorly on $AgIO_3$ (less than 15 percent). However, oxidation by HClO produces an astatine state which carries completely on $AgIO_3$, when the iodate is precipitated under the same condition as just described for the Br_2 experiment.

These experiments make is plausible that there are two positive oxidation states, one of which is formed by Br_2 oxidation, and the other by more powerful oxidation (HClO or $K_2S_2O_8$).

ACKNOWLEDGMENTS

We wish to acknowledge the stimulating help of many discussions with Doctors R. E. Connick, J. G. Hamilton, G. Hevesy, J. H. Hildebrand, and E. F. Orlemann.

Mr. T. Putnam and the 60-inch cyclotron crew have materially contributed to this investigation by the cooperation given in the bombardments.

This paper is based on work performed under Contract W7405-eng-48 with the A.E.C. in connection with the Radiation Laboratory, University of California, Berkeley, California.

THE JOURNAL OF CHEMICAL PHYSICS VOLUME 17, NUMBER 1 JANUARY, 1949

Short-Lived Halogen Fission Products†

NATHAN SUGARMAN
Argonne National Laboratory and Institute for Nuclear Studies, University of Chicago, Chicago, Illinois
(Received April 23, 1948)

Half-life values have been determined for some short-lived Br and I fission products. The chemical isolation of Br from irradiated uranyl nitrate led to a half-life for Br^{85} of 3.00±0.05 min. The energy of the β-radiation of Br^{85} was found to be 2.5 Mev by Feather analysis of the Al absorption curve. The half-lives found for Br^{87} and Br^{88} by extraction of the Kr daughter activities from AgBr precipitates were 56.1±0.7 sec. and 15.5±0.3 sec., respectively, on the basis of a 3-min. half-life for Br^{85}. Attempts to measure the half-lives of Br^{89} and Br^{91} by extraction of the descendant Sr activity were unsuccessful because of the absence of activity. The identity in half-lives of Br^{87} and the 55.6-sec. Br delayed neutron emitter makes it probable that the mass assignment of the delayed neutron emitter is 87.

The half-life of I^{137} was found to be 19.3±0.5 sec. by extraction of Xe^{137} from AgI precipitates, on the assumption of constant chemical yield of the Xe extraction. Isolation of Cs^{138} both from the gas separated from AgI precipitates and from the precipitates directly led to a half-life determination for I^{138} of 5.9±0.4 sec. Extractions of Ba^{149} yielded a value of 2.7±0.1 sec. for the half-life of I^{139}. The absence of Ba^{140} activity in AgI precipitates made it impossible to determine the half-life of I^{140}. Because of the agreement in half-lives of I^{137} and the 22.0-sec. I delayed neutron emitter it is probable that the two are identical.

The low retention of the decay products of the short-lived halogens by the silver halide precipitates led to an estimate of 20 sec. for the "setting" time of the precipitate.

1. INTRODUCTION

EXPERIMENTS have been performed on the search for new short-lived fission products of Br and I and the determination of the mass numbers of the three longer-lived delayed neutron emitters identified as isotopes of Br and I. The fission chains showing the region of investigation in the light and heavy groups of fission products as given in the table of "Nuclei Formed in Fission" [1] are listed in Table I.

In these experiments a solution of uranyl nitrate containing Br^- or I^- carrier is irradiated for a fixed time after which AgBr(I) is precipitated from the active solution. The AgBr(I) precipitate collected by filtration is examined for known fission products which could arise from the decay of active Br or I isotopes; e.g., Kr and Xe, Rb and Cs, Sr and Ba. The activity levels of these decay products will be determined by the neutron flux, time of irradiation, and quantity of uranium irradiated, and by the time of precipitation after the end of irradiation and the half-life of the halogen activity. In experiments performed under standard conditions where only the time of precipitation is varied, the variation in activity of a decay product will be a measure of the half-life of its halogen ancestor. For example, in chain of mass 85, the half-life of the Br isotope is 3 min. The initial activity of the 4.5-hr. Kr^{85} found in the precipitate should decrease one-half for each 3 min. elapsed between the end of irradiation and precipitation of AgBr, provided the loss of Kr from the precipitate is constant from experiment to experiment and the chemical operations are performed quantitatively. In practice it is rather difficult to perform some of the operations quantitatively so that the chemical yield must be determined in another way. This is discussed more fully under the specific isotopes studied.

The co-precipitation of radioactive ancestors or descendants of the halogens on the silver-halide precipitates would affect the measured half-lives. Fission yields and half-life considerations make it unlikely that Se or Te parents of the halogen activities would seriously interfere with these measurements. Contamination of the precipitates by descendant activities, Kr or Xe, Rb or Cs, Sr or Ba, would be expected to be small and would affect only those measurements where the descendant activity in the precipitate is small relative to the total descendant activity present. A discussion of this effect is given later in the pertinent cases (cf. Sections 8 and 9).

† This document is based on work performed at the Argonne National Laboratory, Chicago, Illinois, operated by the University of Chicago for the Atomic Energy Commission.

[1] "Nuclei Formed in Fission," issued by the Plutonium Project, J. Am. Chem. Soc. 68, 2411 (1946); Rev. Mod. Phys. 18, 513 (1946).

TABLE I.* Fission chains investigated for Br and I ancestry.**

Mass 85:	3.0-min. Br→ 4.5-hr. Kr→*Stable* Rb ↘ ↗ ~10-yr. Kr
Mass 86:	*Stable* Kr 19.5-da. Rb→*Stable* Sr ↑ (neutron)
Mass (87):	55.6-sec. Br→ v. short Kr └→? Kr
Mass 87:	50-sec. Br→ 75-min. Kr→6.3×10^{10}-yr. Rb→*Stable* Sr
Mass 88:	3-hr. Kr→17.8-min. Rb→*Stable* Sr
Mass 89:	2.6-Min. Kr→15.4-min. Rb→53-da. Sr→*Stable* Y
Mass 90:	~33-sec. Kr→short Rb→25-yr. Sr→65-hr. Y→*Stable* Zr
Mass 91:	9.8-sec. Kr→short Rb→9.7-hr. Sr→51-min. Y ↘ ↓ 57-da. Y→*Stable* Zr
Mass 135:	<2-min. Te→6.7-hr. I→ 13-min. Xe ↘ ↓ 9.2-hr. Xe→>2.5×10^{4}-yr. Cs→*Stable* Ba
Mass (136):	1.8-min. I→ *Stable* Xe←13-da. Cs→*Stable* Ba ↑ (neutron)
Mass (137):	22.0-sec. I→ v. short Xe └→? Xe
Mass 137:	30-sec. I→3.4-min. Xe→33-yr. Cs→*Stable* Ba
Mass 138:	17-min. Xe→32-min. Cs→*Stable* Ba
Mass 139:	41-sec. Xe→7-min. Cs→85-min. Ba→*Stable* La
Mass 140:	16-sec. Xe→short Cs→12.8-da. Ba→40.0-hr. La→*Stable* Ce

* Uncertain mass assignments are given in parentheses.
** See reference 1.

Another effect which could alter the half-life observed for the halogen species is a time-dependent exchange between the halogen carrier added (Br^- or I^-) and the halogen activity in higher valence states. A serious perturbation in the observed half-life would occur only when the exchange constant is of the same order as the radioactive decay constant of the halogen. The concentrations used in these experiments are: $(H^+)\cong0.01\ M$, $(Br^-)\cong0.01\ M$, and $(I^-)\cong0.01\ M$. Using these concentrations and assuming the well established rapid exchange of Br^- with Br_2, one calculates an effective exchange constant for carrier Br^- with radio-Br as BrO_3^- from kinetic data on the interaction of Br^- with BrO_3^- to give Br_2.[2] This constant proves to be much smaller than the radioactive decay constants of the Br isotopes studied. The exchange constant of carrier I^- and radio-I as IO_3^- from reactions analogous to those of Br is much larger than the radioactive decay constants of the I isotopes studied. Although kinetic information on the reaction of I^- or Br^- with other oxidation species of halogens is not known, it would be fortuitous if the effective exchange constants were of the same order as the decay constants.

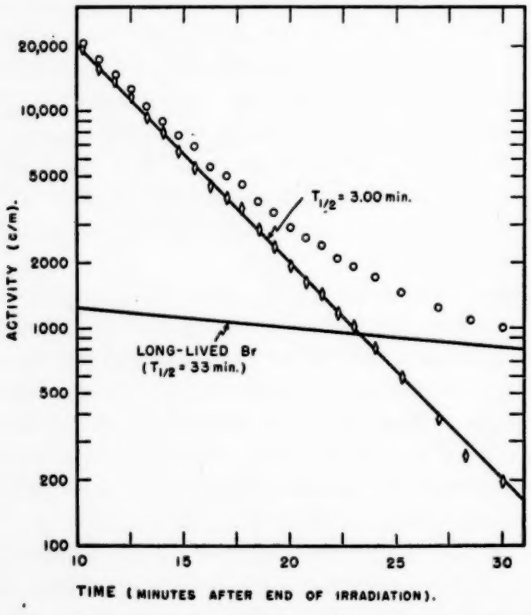

FIG. 1. Decay curve of Br isolated from irradiated uranyl nitrate solution. Counted through 211 mg Al/cm². ○ original points; ◇ subtracted curve, activities of 30-min. Br^{84} and 2.4-hr. Br^{83} determined from later part of curve (average $T_{\frac{1}{2}}=33$ min.).

Observations made on the 4.5-hr. Kr^{85}, 75-min. Kr^{87}, 2.8-hr. Kr^{88} and its 17.8-min. Rb^{88} daughter led to determination of the half-lives of Br^{87} and Br^{88}. Attempts to find the half-lives of Br^{89} and Br^{91} by extraction of the Sr were unsuccessful. Extractions of the Xe and Cs from AgI pre-

[2] *International Critical Tables*, 7, 149 (1930).

cipitates determined the half-lives of I^{137} and I^{138}. The half-life of I^{139} was determined by analyzing for Ba^{139}, and no activity of Ba^{140} was observed from AgI precipitates.

2. CHARACTERISTICS OF Br^{85}; HALF-LIFE AND RADIATIONS

Strassmann and Hahn[3] found two short-lived Br activities of 50±10 sec. and 3.0±0.5 min. half-life in fission by chemically separating Br soon after irradiation. Seelmann-Eggebert and Born[4] have shown that the 75-min. Kr and 4.5-hr Kr could be extracted from the short-lived Br fraction and that the variation of their intensities with time related the 75-min. Kr to the 50-sec. Br and the 4.5-hr. Kr to the 3-min. Br provided no other short-lived Br activities were present. Later, cross-bombardments led to mass assignments of 85 to the 3-min. Br and 87 to the 50-sec. Br.[5]

The use of Br^{85} as a normalizing activity in experiments on the half-life of Br^{87} and Br^{88} (Sections 3 and 4), made it necessary to determine its half-life more precisely. Because of the greater neutron fluxes available it was possible to separate quickly sufficient activity for measurement after short irradiations of small amounts of uranium. These conditions enhance the activity of the Br^{85} relative to the longer-lived isotopes, 30-min. Br^{84} and 2.4-hr. Br^{83} because of the hold-up in growth from their Se ancestors, ~2-min. Se^{84}, 67-sec. Se^{83} and 25-min. Se^{83}.[1]

The active Br was isolated from a uranyl nitrate solution irradiated for 10 sec. in the pneumatic tube of the Argonne heavy water pile. The chemical procedure was modified from that of Glendenin, Edwards, and Gest.[6] Carriers of Br^- and I^- are added to the irradiated solution which is then transferred to a separatory funnel containing CCl_4 and $KMnO_4$ acidified with HNO_3. The liberated Br is transferred to the CCl_4 layer. This Br extraction is performed within 30 sec. from the end of irradiation. The CCl_4 extract is added to a funnel containing H_2O and $NH_2OH \cdot HCl$. The Br is transferred to the H_2O layer. Two oxidation-reduction cycles with $KMnO_4$ as oxidant and $NaHSO_3$ as reductant are then performed. The last aqueous $NaHSO_3$ layer is acidified with HNO_3, the solution is boiled to expel SO_2, and AgBr is precipitated. The precipitate is filtered on a filter paper disk and mounted for counting. In general, radioactivity measurements began within 7 min. after the end of irradiation. Aqueous samples used for half-life determination were washed with extra CCl_4 to remove suspended material and insure purity. These samples were counted within 10 min. from the end of irradiation.

Decay curves were obtained through various Al absorbers. The ratio of the activity of Br^{85} to the 55.6-sec. Br^{87}, 30-min. Br^{84}, and 2.4-hr. Br^{83} decreased with increasing absorber weight beyond 325 mg Al/cm². The optimum absorber weight for determination of the half-life of Br^{85} was found to be in the range 100 to 325 mg Al/cm². Ten decay curves taken through 101, 211, and 311 mg Al/cm² yielded a half-life for Br^{85} of 3.00±0.05 min. A typical decay curve through 211 mg Al/cm² is given in Fig. 1.

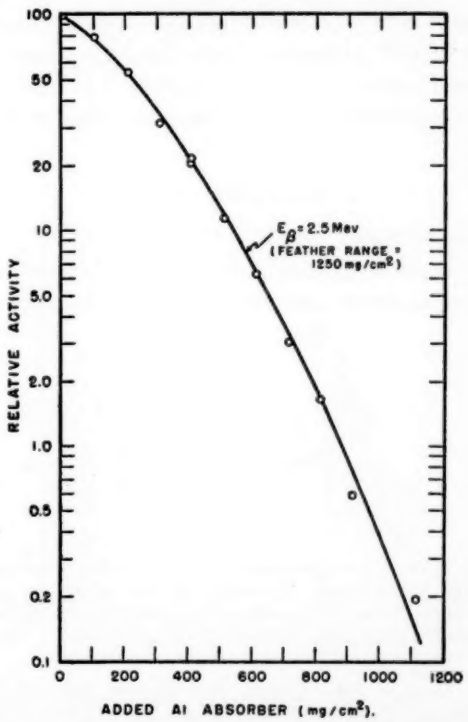

FIG. 2. Aluminum absorption curve of 3.00-min. Br^{85}. Absorber thickness at zero added Al estimated at 35 mg/cm².

[3] F. Strassmann and O. Hahn, Naturwiss. **28**, 817 (1940).
[4] W. Seelmann-Eggebert and H. J. Born, Naturwiss. **31**, 59 (1943).
[5] H. J. Born and W. Seelmann-Eggebert, Naturwiss. **31**, 86 (1943).
[6] L. E. Glendenin, R. R. Edwards, and H. Gest, Plutonium Project Record, Vol. 9B, 8.4.2 (1946).

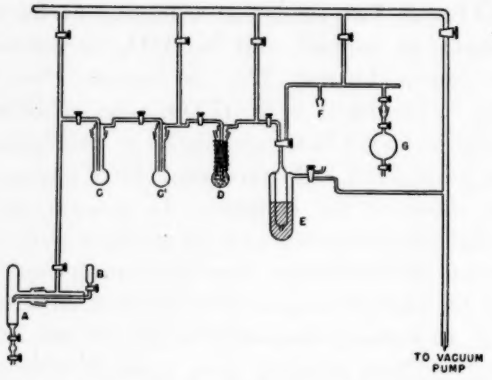

FIG. 3. Vacuum line for removing active gases from dissolved AgBr(I) precipitates. *A*. Dissolver; *B*. Port for introducing NaCN; *C*, *C'*. Traps (surrounded by liquid nitrogen or filled with Drierite); *D*. Charcoal trap; *E*. Toepler pump; *F*. Lead to gas cell; *G*. Bulb for removing aliquot of gas for Rb or Cs analysis.

The absorption characteristics of Br^{85} were determined by following the decay of active samples through sets of two Al absorbers differing by about 200 mg Al/cm², the activity through one absorber being used for normalization of the activity through the other. The Al absorption curve of the 3.00-min. Br^{85} is given in Fig. 2. The β-energy was found to be 2.5 Mev by a Feather comparison method[7] of the absorption curve of Br^{85} with that of the 1.5 Mev β-particles of the 17-min. Se^{81}.[1] It is apparent from Fig. 2 that γ-radiation is not present in a high counting rate.

3. HALF-LIFE OF Br^{87}

The 55.6-sec. delayed neutron emitter* identified as an isotope of Br by Snell and co-workers[8] was tentatively assigned by them to Br^{87} and was thought to be the 50-sec. Br referred to earlier.[3] Glendenin, Coryell and Edwards[9] in their discussion of the variation in yield as a function of charge found it difficult to correlate the variation in yield of the 55.6-sec. delayed neutron emitter in the thermal neutron fission of U^{233}, U^{235}, and Pu^{239} with their postulate of "equal chain length" and a mass of 87. They suggested that the mass of the delayed neutron emitter might be 89 or 90 and that therefore there might be two Br activities with half-lives of ~50 sec. The experiments reported here establish the half-life of Br^{87} as 56.1 sec., identical within experimental error with the 55.6-sec. Br delayed neutron emitter, and suggest the improbability of another Br activity of the same half-life at mass 89 or 90.

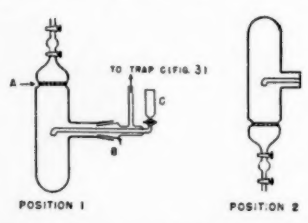

FIG. 4. Details of dissolver. Position 1—for dissolving of AgBr(I) precipitates; Position 2—for sweeping active gases from solutions of dissolved AgBr(I) precipitates. *A*. Sintered glass plate (fine); *B*. Ground joint; *C*. Solution port.

The half-life of Br^{87} was determined by measuring the variation in intensity of the 75-min. Kr^{87} in the active AgBr samples precipitated from irradiated uranyl nitrate solutions at various times after short irradiations. The solution of uranyl nitrate containing Br^- carrier was irradiated for 10 sec. At the desired time after irradiation the active material was poured into a heated solution of $AgNO_3$ acidified with HNO_3. The solution was allowed to stand for about 20 min. and was then filtered through a filter paper disk and the precipitate washed with water and dried with alcohol and ether. The precipitate on the filter disk was transferred to a dissolver on a vacuum line (Fig. 3) and after evacuation was dissolved in NaCN. The dissolver was made from a 30-ml fine sintered glass funnel sealed off at the top, with a ground joint side arm attached to the vacuum line for evacuation, gas flow, and introduction of solutions under vacuum (see Fig. 4). During the solution process the dissolver was in the position in which the precipitate and NaCN solution were off the sintered glass plate (position 1, Fig. 4). The dissolver was then rotated so that the solution rested on the sintered plate and introduction of air from the bottom resulted in efficient sweeping of the solution (position 2, Fig. 4). This apparatus was used earlier by Hoagland and Sugarman[10] in their study of Xe^{135}

[7] N. Feather, Proc. Camb. Phil. Soc. **34**, 599 (1938).

* The half-lives of the delayed neutron emitters adopted in this paper are those of D. J. Hughes, J. Dabbs, A. Cahn, and D. Hall, Phys. Rev. **73**, 111 (1948). (Also reference 1.)

[8] A. H. Snell, J. S. Levinger, E. P. Meiners, Jr., M. B. Sampson, and R. G. Wilkinson, Phys. Rev. **72**, 545 (1947).

[9] L. E. Glendenin, C. D. Coryell, and R. R. Edwards, Clinton Laboratory Memo CL-LEG No. 1, July 25, 1946.

[10] E. J. Hoagland and N. Sugarman, Metallurgical Laboratory Report, CC-3007, April 5, 1945; Plutonium Project Record, Vol. 9B, 7.37.3 (1946).

and was adapted from the techniques developed by Turkevich and co-workers[11] in investigating the short-lived Kr and Xe activities in fission.

The active gases were swept from the solution containing the dissolved precipitate and passed successively through two traps cooled with liquid nitrogen and a charcoal trap at room temperature. Desorption of the gases from the charcoal at room temperature by a Toepler pump yielded an active gas fraction containing Kr nearly free of Xe. The gas was transferred to a glass counting cell with a mica window and counted with a standard Eck-Krebs counter of 30 mg/cm² wall thickness. The decay of the gas activity showed the presence of two major components, the 4.5-hr. Kr^{85} and the 75-min. Kr^{87}. The 75-min. Kr activity was determined more easily by counting through 405 mg Al/cm² which absorbed the β-activity of the 4.5-hr. Kr. After the decay of the 75-min. Kr, the 4.5-hr. Kr activity was determined by counting without absorber. In the experiments in which precipitations were performed within two minutes after the end of irradiation the gas activity contained some contribution from the 2.8-hr. Kr^{88} arising from its Br^{88} parent. Since the fission yields of the neighboring Br isotopes vary by only a factor of 4, and since Br^{88} has a much shorter half-life than Br^{87} or Br^{85}, the 2.8-hr. Kr^{88} activity grown from it was negligibly small relative to the activities of the 75-min. Kr and 4.5-hr. Kr for later precipitations (cf. Section 4).

Intercomparison of the activities of the 75-min. Kr^{87} and the 4.5-hr. Kr^{85} in samples obtained from AgBr precipitated at various times after irradiation permit determination of the half-lives of the Br ancestors provided operations are quantitative or at least chemical yields are constant. Since it proved difficult to maintain a constant yield for the gas sweeping and desorption process the 4.5-hr. Kr activity was used as a monitor for the over-all chemical yield. A 3-min. Br parent was used. The activity of the 75-min. Kr was then normalized for changes in irradiation conditions and loss in activity by correcting the 4.5-hr. Kr activity to a 3-min. decay curve and normalizing the 75-min. Kr activity by this factor. The variation of the normalized 75-min. Kr activity as a function of time of precipitation yielded the half-life of the Br^{87} parent (Fig. 5). The data for the gas activities from the various experiments are given in Table II.

TABLE II. Activities of 4.5-hr. Kr^{85} and 75-min. Kr^{87} extracted from AgBr precipitates.

Time of precipitation of AgBr	4.5-hr. Kr^{85} Activity at AgBr precipitation (no Al absorber) (c/m)	4.5-hr. Kr^{85} Activity from arbitrary 3-min. decay curve (c/m)	Normalization factor	75-min. Kr^{87} Activity at AgBr precipitation (405 mg Al/cm²) (c/m)	75-min. Kr^{87} Normalized activity (c/m)
8 sec.	12400	6100	0.492	25400	12500
15 sec.	27000	5900	0.219	48250	10550
25 sec.	23300	5700	0.245	45500	11150
41 sec.	25300	5400	0.213	42000	8950
55 sec.	11650	5100	0.438	17600	7700
70 sec.	15400	4800	0.312	18500	5800
85 sec.	11500	4550	0.396	12700	5030
90 sec.	21800	4450	0.204	24000	4900
100 sec.	16000	4300	0.269	15800	4250
115 sec.	17600	4050	0.230	15800	3630
2.5 min.	13800	3530	0.256	8000	2050
3.07 min.	3020	3100	1.026	1390	1430
3.5 min.	33200	2800	0.0843	13100	1100
4.0 min.	21900	2500	0.114	6825	780
4.5 min.	6600	2220	0.336	1585	530
5.0 min.	10900	1990	0.183	2000	365
5.5 min.	8800	1780	0.202	1260	255
6.0 min.	5500	1580	0.287	520	149

The half-life of Br^{87} is found to be 56.1±0.6

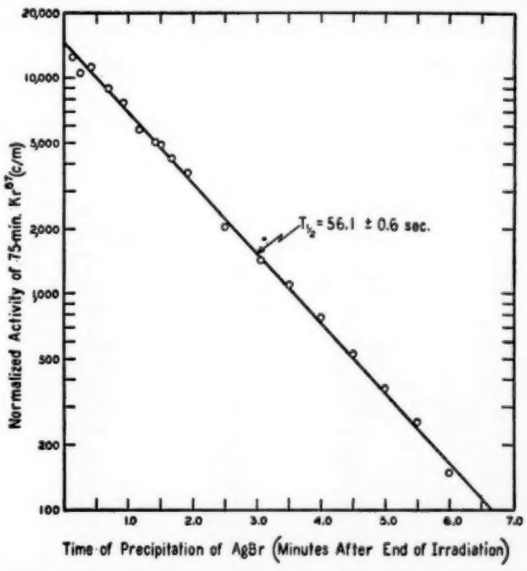

FIG. 5. Decay curve of Br^{87} from 75-min. Kr^{87} activities extracted from AgBr precipitates. Activities of 75-min. Kr^{87} multiplied by normalization factors of 4.5-hr. Kr^{85} obtained by correcting to arbitrary 3-min. Br^{85} decay curve (data of Table II).

[11] C. Dillard, R. M. Adams, H. Finston, and A. Turkevich, Metallurgical Laboratory Reports, CC-1805, July 14, 1944, CC-2310, Jan. 1, 1945; Plutonium Project Record, Vol. 9B, 7.5.3, 7.5.5, (1946).

sec. by least squares analysis of the normalized activity data of Table II. Including the error in the half-life of Br^{85}, one finds the error in the half-life of Br^{87} to be 0.7 sec. The good fit of the data by an exponential decay curve suggests that, if Kr is lost from the AgBr precipitate between the time of precipitation of AgBr and the introduction of the precipitate into the dissolver about 30 minutes later, the loss occurs either very soon after precipitation or very slowly relative to 3 minutes. This condition must hold to preserve the activity ratio of 75-min. Kr and 4.5-hr. Kr generated by parents whose half-lives are quite different, 56.1 sec. and 3 min., respectively. A more complete discussion of this question is given later (cf. Section 12).

4. HALF-LIFE OF Br^{88}

The half-life of Br^{88} was determined in a manner similar to that of Br^{87} except that the activity of Kr^{88} could not be measured directly in the gas because of the interference of Kr^{85} and Kr^{87}. Instead, the activity of the Kr^{88} was measured by analyzing for the 17.8-min. Rb^{88} activity in the gas. An aliquot of each gas sample counted was transferred to a bulb, and a wash solution of Rb carrier acidified with HAc was added. The Rb activity was allowed to grow for 1 hour during which time the bulb was shaken periodically to effect interchange between the Rb activity and carrier. The wash solution was then removed, the solution boiled to expel the active gases, the Rb precipitated as the cobaltinitrite by adding 15 ml of sodium cobaltinitrite reagent solution according to the procedure of Treadwell and Hall,[12] and the solution allowed to stand for 3 min. after filtration. Rubidium analysis as a measure of Kr activity was tested by determining the apparent half-life of Kr^{88} through successive Rb extractions of a single gas sample. A value of 2.8 hr. was found, in good agreement with published values.[13] The Rb samples were counted without absorber, and the decay curves were followed to check the radio-chemical purity. After corrections were made for the chemical yield of Rb, for decay of the 2.8-hr. Kr before growth of 17.8-min. Rb started, and for growth of 17.8-min. Rb during the standing period (1 hour), the Kr activities so derived were extrapolated to the time of AgBr precipitation and normalized by the 4.5-hr. Kr normalization factors of Table II. Least squares analysis of the normalized activities *versus* the time of precipitation (Table III) yielded a half-life of 15.5 ± 0.3 sec. for Br^{88}. The error in the half-life of Br^{85} does not appreciably affect this result. A graphical representation of the data of Table III is given in Fig. 6.

5. SEARCH FOR Br^{89} AND Br^{91}

A search was made for Br^{89} through its active descendants 2.6-min. Kr^{89}, 15.4-min. Rb^{89}, and 53-da. Sr^{89}. In the first experiments the active Kr

TABLE III. Activity of 2.8-hr. Kr^{88} from analysis for 17.8-min. Rb^{88} in gas samples extracted from AgBr precipitates.

Time of precipitation of AgBr	Activity of 17.8-min. Rb^{88} at time of separation from Kr^{88} (c/m)	Milligrams Rb precipitate	Activity of 17.8-min. Rb^{88} corrected to 50 mg Rb precipitate (c/m)	Decay factor for Kr^{88} from time of AgBr precipitation to Rb growth	Rb growth factor (1 hr. growth)	Activity of 2.8-hr. Kr^{88} at time of AgBr precipitation (Rb counting geometry) (c/m)	Normalization factor, 4.5-hr. Kr^{85} (Table II)	Normalized activity (c/m)
8 sec.	19000	52.5	18100	1.368	1.30	32100	0.492	15800
15 sec.	28000	49.8	28100	1.302	1.30	47600	0.219	10400
25 sec.	18200	50.0	18200	1.255	1.30	29700	0.245	7250
41 sec.	8900	40.3	11040	1.255	1.30	18000	0.213	3830
55 sec.	2080	35.8	2905	1.247	1.30	4710	0.438	2060
70 sec.	880	28.5	1544	1.371	1.30	2750	0.312	860
85 sec.	790	46.4	851	1.270	1.30	1405	0.396	555
90 sec.	960	33.5	1433	1.224	1.30	2280	0.204	465
100 sec.	600	48.8	615	1.286	1.30	1030	0.269	275
115 sec.	225	38.8	290	1.281	1.30	483	0.230	110

[12] F. P. Treadwell and W. T. Hall, *Analytical Chemistry* (John Wiley & Sons, Inc., New York, 1942), Vol. II, p. 275.

[13] J. C. Jacobsen and O. Kofoed-Hansen ($T_{\frac{1}{2}}=2.7$ hr.), D. Kgl. Danske Vidensk. Selskab Mat.-fys. Medd., **23**, No. 12 (1945); G. N. Glasoe and J. Steigman ($T_{\frac{1}{2}}=2.8$ hr.), Phys. Rev. **58**, 1 (1940); A. Langsdorf ($T_{\frac{1}{2}}=3$ hr.). Phys. Rev. **56**, 205 (1939).

fraction from AgBr precipitated at 8 sec. after a 10-sec. irradiation was examined for a short-lived component by performing the operations quickly enough to start the counting 10 min. after the end of irradiation. No short-lived activity was observed. An effort was then made to isolate the 15.4-min. Rb^{89}. Active AgBr samples precipitated from a $AgNO_3$ solution containing Rb carrier 6 to 9 sec. after the end of 10-sec. irradiations were examined. The variation in this activity might be used to measure the half-life of Br^{89}. This procedure was unsuccessful, however. The 17.8-min. Rb^{88} interfered with the measurement of the 15.4-min. Rb^{89} present even when Rb was removed from the dissolved AgBr precipitate within 10 min. after the end of irradiation. At this time the 2.6-min. Kr^{89} has almost completely decayed to 15.4-min. Rb^{89} whereas the 17.8-min. Rb^{88} is only at ~30 percent of its equilibrium value. From the ratio in half-lives of 15.4-min. Rb^{89} and 2.8-hr. Kr^{88} and the relative growth factors for Rb^{89} and Rb^{88} which should emphasize Rb^{89} relative to Rb^{88}, one concludes that Br^{89}, if it exists, is present in low yield and/or its half-life is much shorter than 16 sec., the half-life of Br^{88}. Still another attempt was made to identify Br^{89} by isolation of Sr from the AgBr precipitated at 7 sec. after a 10-sec. irradiation from a $AgNO_3$ solution containing Rb, Cs, Ba and Sr carriers. No activity of 53-da. Sr^{89} in the precipitate was observed. If the activity of Sr^{89} in the Sr fraction isolated from the AgBr precipitate is <4 c/m, the ratio of Sr^{89} activity in the precipitate to Sr^{89} in the uranyl nitrate supernate is <0.001. This suggests that Br^{89} has either a very low yield in fission and/or its half-life is short. The short half-life of the halogen would lead to low activity of decay products both because of radioactive decay before precipitation and because of the marked loss of Kr from the precipitate during coagulation (cf. Section 12).

Experiments on the half-life of Br^{91} yielded similar results. The Sr samples isolated for the study of Br^{89} were isolated early enough to detect any 9.7-hr. Sr^{91} if present. A negligibly small activity was observed in the precipitate samples (~10 c/m) giving a ratio of Sr^{91} activity in the AgBr precipitate to the supernate of $<2\times10^{-5}$, leading to the same conclusion on half-life and yield of Br^{91} as for Br^{89}.

6. MASS ASSIGNMENTS OF THE 55.6-SEC. Br AND 4.51-SEC. Br DELAYED NEUTRON EMITTERS

The determination of the half-life of Br^{87} for β^--emission to be 56.1 ± 0.7 sec., identical within experimental error with the 56.6-sec. half-life for the Br delayed neutron emitter and the unsuccessful attempts to detect Br^{89} and Br^{91}, make it probable that the mass number of the delayed neutron emitter is 87. If the assignment of the mass to 89 or 90 suggested by Glendenin *et al.*[9] were correct, on the basis of the fission yields expected for Br^{89} or Br^{90} from their postulate, one should have found activity in later members of these chains. No effort was made to study Br^{90} because of the inconveniently short half-life of Kr^{90} (~33 sec.) and long half-life of Sr^{90} (25 yr.). However, Sr^{89} would have been detected if the 55.6-sec. Br were of mass 90, because of the change in mass following the delayed neutron emission.

The assignment of the mass number of the 4.51-sec. Br delayed neutron emitter to masses

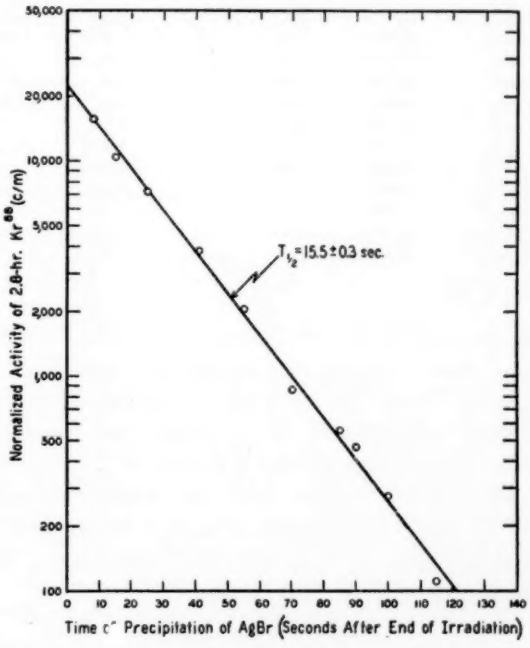

FIG. 6. Decay curve of Br^{88} from 2.8-hr. Kr^{88} activities extracted from AgBr precipitates. Activities of 2.8-hr. Kr^{88} multiplied by normalization factors of 4.5-hr. Kr^{85} obtained by correcting to arbitrary 3-min. Br^{85} decay curve (data of Table III).

87 to 88[14] was based on mass 87 for the 55.6-sec. Br. Now that the half-lives of Br^{87} and Br^{88} are established, the 4.51-sec. Br must be of mass higher than 88 unless it is an isomer of Br^{87} or Br^{88} and was not observed in these studies because of the adverse conditions of the experiment, namely, the long irradiation time of 10 sec., the time elapsed before precipitation of 7 to 8 seconds, and the loss of Kr from the precipitate during coagulation (cf. Section 12). Each of these factors would reduce the production of daughter activity from the 4.51-sec. Br relative to that grown from a longer-lived isomeric state. Although loss of 4.51-sec. Br from the first two factors would be decreased by shorter irradiations and quicker precipitations, the loss of activity from the precipitate would seriously hamper observation of a short-lived isomeric state. Assignment of the 4.51-sec. Br to mass 89 or 90 does not conflict with the failure to detect Sr^{89} in AgBr precipitates (Section 5) since it is expected that most of the Kr^{89} would leave the precipitate during coagulation.

TABLE IV. Activity of 3.8-min. Xe^{137} extracted from AgI precipitates.

Time of precipitation of AgI	Activity of 3.8-min. Xe^{137} observed at 15 min. after precipitation of AgI (c/m)	Pile power (kw)	Milliliters $UO_2(NO_3)_2$ solution irradiated	Normalization factor to 300 kw and 10 ml U solution	Activity of 3.8-min. Xe^{137} normalized (c/m)
8 sec.	23300	200	5	3.0	69900
9 sec.	32000	300	5	2.0	64000
12 sec.	38200	300	5	2.0	76400
15 sec.	23800	250	5	2.4	57120
17 sec.	22900	300	5	2.0	45800
20 sec.	28000	300	5	2.0	56000
20 sec.	14800	200	5	3.0	44400
25 sec.	35000	300	10	1.0	35000
27 sec.	32000	300	10	1.0	32000
30 sec.	32000	300	10	1.0	32000
32 sec.	30000	300	10	1.0	30000
35 sec.	25700	300	10	1.0	25700
40 sec.	22000	250	10	1.2	26400
45 sec.	19000	300	15	0.667	12670
50 sec.	20700	300	15	0.667	13800
1.5 min.	3800	250	15	0.80	3040
2.0 min.	1350	250	15	0.80	1080
2.5 min.	680	250	15	0.80	545

7. HALF-LIFE OF I^{137}

Strassmann and Hahn[3] chemically separated two short-lived I activities of 30±6-sec. and 1.8±0.4-min. half-life in fission. Seelmann-Eggebert and Born[4] isolated the short-lived I fraction from irradiated uranium solutions, and extracting the gas activity found that a 3.8-min. Xe activity could be related to the 30-sec. I, and that no active gas grew from the 1.8-min. I. Irradiation of Xe with neutrons[15] led to the formation of 3.4-min. Xe^{137} and a mass assignment of 137 to the 30-sec. I. The agreement in half-lives of the 30-sec. I^{137} and the 22.0-sec. I delayed neutron emitter led Snell *et al.*[8] to assign mass 137 to the 22.0-sec. I activity. Glendenin and co-workers[9] suggested the possibility of 138 or 139 as the mass assignment of the 22.0-sec. delayed neutron emitter on the basis of a comparison of the variation of the yields of this activity among the fissionable isotopes with those predicted by their postulate of "equal chain length." The experiments reported here show that the 22.0-sec. I delayed neutron emitter is probably of mass 137, and cannot be of mass 138, 139, or 140.

The half-life of I^{137} was studied via the activity of its Xe daughter. The experiments were performed in a manner similar to that used for Br^{87} and Br^{88}. The irradiated uranyl nitrate solution contained both Br^- and I^- carriers since it proved difficult to filter the solution containing AgI alone. The presence of AgBr enhanced the coagulation of the precipitate and did not interfere with subsequent operations. The AgI precipitate was transferred to the vacuum line (Figs. 3 and 4) and dissolved in NaCN. The active gases were passed successively through two drying traps filled with Drierite and a charcoal trap at room temperature. The Xe activity was enriched in the gas fraction relative to Kr by discarding the gas removed from the charcoal at room temperature, and the first gas fraction from the charcoal after heating it to ~100°C. Later gas samples from the heated charcoal showed a Xe enrichment of about 15-fold. The time elapsed between the AgI precipitation and filling of the gas cell was about 15 minutes.

The variation of Xe^{137} activity with time of precipitation can be used to find the half-life of I^{137} in two ways. First, the chemical yield of Xe extracted from the AgI precipitates can be

[14] N. Sugarman, J. Chem. Phys. 15, 544 (1947).

[15] W. Riezler, Naturwiss. 31, 326 (1943).

assumed to be constant in the various experiments and the activity then plotted *versus* time of precipitation. Secondly, another I activity can be used as the monitor of the chemical yield by measuring the activity of its Xe daughter and correcting this Xe activity to the half-life of the I parent. The difficulty in this procedure is that the only I activity which can be used, I^{138}, has a half-life of about 6 sec. (see Section 8), so that a relatively small error (10 percent) in the half-life of the normalizing activity causes a considerably larger error in the half-life of I^{137}.

The half-life found for I^{137} via its Xe daughter (3.8-min. half-life observed) assuming constant chemical yield in the Xe extraction is 19.3±0.5 sec. by least squares analysis of the normalized activities of Table IV. The marked deviation of the points from an exponential curve (Fig. 7) is not surprising in view of the large differences in chemical yield which can occur.

Lower neutron fluxes in the larger samples used for later precipitations arising from the neutron absorption of the uranyl nitrate solution may explain the shorter half-life found for I^{137} than that expected of 22 sec.

The discrepancy in the half-life values of Xe^{137} of 3.4 min. found by Riezler[15] by (n, γ) activation of Xe and 3.8 min. observed by Seelmann-Eggebert and Born[4] and in this work when extracted from I, has been resolved. Activation of spectroscopically pure Xe with neutrons led to a half-life determination of 3.9±0.1 min. in good agreement with the value found for Xe^{137} from fission.

8. HALF-LIFE OF I^{138}

The half-life of I^{138} was determined in a manner similar to that used for Br^{88} (cf. Section 4). The activity used for normalization of the irradiations was Xe^{137} on the basis of a 22.0-sec. half-life for its parent activity, I^{137}. A fraction of the gas separated in the manner described in Section 7 is counted to determine the 3.8-min. Xe^{137} activity, and an aliquot transferred to a bulb for determination of the 17-min. Xe^{138} activity via its 32-min. Cs daughter after a 30 min. growth period of Cs from Xe. The gas and bulb are washed with a solution containing Cs and Rb carriers and the wash solution is analyzed for Cs. In this analysis the only separation necessary is that of the 32-min. Cs from the 17.8-min. Rb (grown from the 2.8-hr. Kr^{88} in the gas). The separation is effected through the use of BiI_3 in HI as a specific precipitating reagent for Cs.

The procedure used is a modification of one devised by Evans.[16] The Cs is precipitated from the wash solution containing 40 mg Cs and 10 mg Rb carriers, 10 ml H_2O, and 1 ml. 6*M* HAc by adding 3 ml BiI_3—HI reagent (10 g BiI_3 in 50 ml 55 percent HI). The solution is cooled in an ice bath and centrifuged. The precipitate is washed twice with 5 ml H_2O containing 3 drops

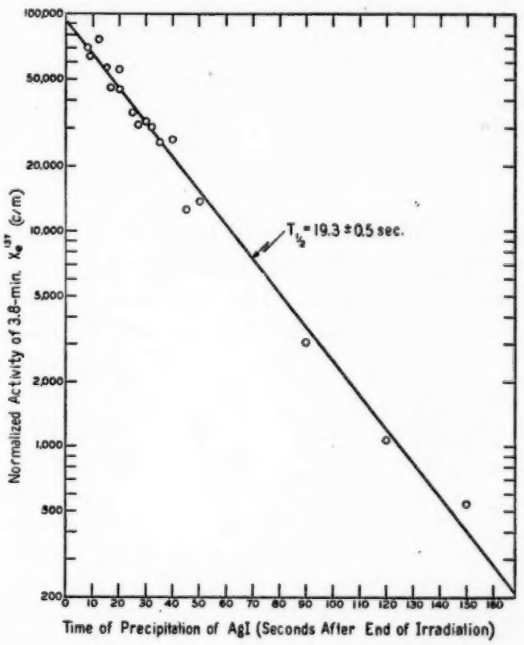

FIG. 7. Decay curve of I^{137} from 3.8-min. Xe^{137} activities extracted from AgI precipitates. Activities of 3.8-min. Xe^{137} multiplied by normalization factors for pile power and milliliters of solution irradiated on the assumption of constant chemical yield (data of Table IV).

6*N* HCl and 0.5 ml BiI_3-HI reagent, and cooled before centrifugation. The precipitate is then dissolved by adding 10 ml H_2O, 10 mg Rb carrier, and 7 drops conc. HCl, and heating. After cooling, the Cs is reprecipitated and washed twice. The precipitate is dissolved by boiling out the I_2 after adding 3 ml 6*M* HNO_3 and 2 ml Fe^{+++} carrier solution (~10 mg Fe^{+++}/ml). The solution is diluted to 10 ml and the Fe and Bi are precipitated as hydroxides with NaOH. After

[16] H. B. Evans, Plutonium Project Record, Vol. 9B, 8.22.2 (1946).

TABLE V. Activities of 3.8-min. Xe^{137} and 32-min. Cs^{138} in gas samples extracted from AgI precipitates.

Time of precipitation of AgI	3.8-min. Xe^{137} Activity at 15 min. after AgI precipitation (c/m)	3.8-min. Xe^{137} Activity from arbitrary 22-sec. decay curve (c/m)	Normalization factor	32-min Cs^{138} Activity at time of separation from Xe after 30 min. growth of Cs from Xe (c/m)	Correction factor for decay of Xe to bulb filling time of 15 min.	Milligrams Cs precipitate	Activity corrected for Xe decay to bulb filling time of 15 min. and to 50 mg Cs precipitate (c/m)	Normalized activity (c/m)
8 sec.	23300	47000	2.015	9050	0.98	38.7	11450	23100
9 sec.	32000	45500	1.420	5500	1.02	19.8	14150	20100
12 sec.	38200	41500	1.085	6100	1.01	19.8	15550	16900
15 sec.	23800	37800	1.590	1820	1.02	17.4	5330	8450
17 sec.	22900	35200	1.535	2140	1.02	19.4	5630	8650
20 sec.	28000	32000	1.145	2290	0.98	23.3	4820	5520
20 sec.	14800	32000	2.160	2000	0.98	38.2	2570	5550
25 sec.	35000	27300	0.780	1400	1.01	17.2	4110	3210
27 sec.	32000	25800	0.805	1390	1.02	22.4	3160	2540
32 sec.	30000	22000	0.735	618	1.04	17.6	1825	1340
35 sec.	25700	20000	0.780	500	1.02	22.6	1130	880
40 sec.	22000	17000	0.775	110	1.02	9.4	597	465
45 sec.	19000	14700	0.775	108	1.02	19.2	287	220
50 sec.	20700	12400	0.600	71	1.06	18.1	208	125

acidification with HAc, the Cs is precipitated as the cobaltinitrite by adding 15 ml of the sodium cobaltinitrite reagent. The chemical yield of Cs is ~50 percent and the time of analysis about 1 hr. The Cs is freed from the Rb contamination very effectively by this procedure as is evidenced by the decay curves of Cs obtained from samples where the Rb activity was many times that of the Cs.

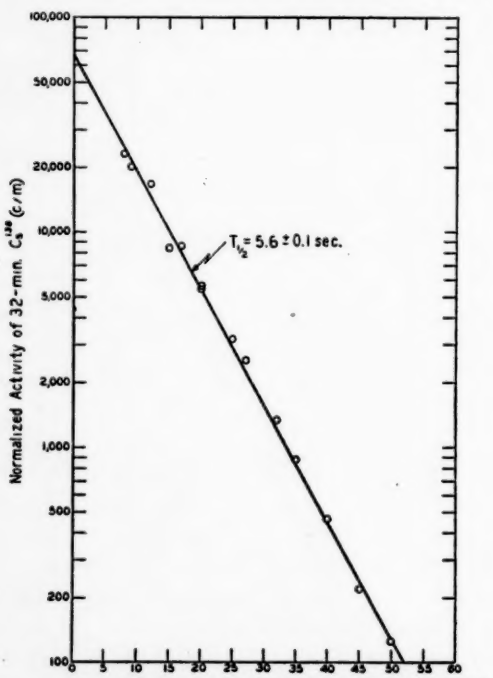

FIG. 8. Decay curve of I^{138} from 32-min. Cs^{138} activities separated from the gas fractions extracted from AgI precipitates. Activities of 32-min. Cs^{138} multiplied by normalization factors of 3.8-min. Xe^{137} obtained by correcting to arbitrary 22.0-sec. I^{137} decay curve (data of Table V).

After correcting the Cs activities for chemical yield, decay of Xe, etc., one can normalize these activities by the factor found for Xe^{137} on the basis of a 22.0-sec. half-life for I^{137}. The normalized activities of the 32-min. Cs^{138} (Table V) as a function of the time of AgI precipitation give a half-life for I^{138} of 5.6±0.1 sec. (Fig. 8) as determined by least squares analysis.

Another measurement of the half-life of I^{138} was made by analyzing the AgI precipitates for 32-min. Cs^{138} and comparing this activity as a function of time of precipitation of AgI with the 32-min. Cs activity in the supernates. Since it was shown that most of the activity of the 32-min. Cs (>99.5 percent) is in the supernate, its activity should not be affected by time of precipitation and can be used as a monitor of the irradiations. In these experiments the AgI was precipitated from a solution containing Rb and Cs carriers to minimize the adsorption of Cs activity on the AgI precipitate. The solution was allowed to stand for 1 hr. before filtration to permit growth of the 32-min. Cs from its 17-min. Xe parent. The precipitate on the filter disk was washed thoroughly with H_2O, alcohol, and ether,

transferred to a centrifuge tube containing Rb and Cs carriers, and dissolved in NaCN. The NaCN solution was analyzed for 32-min. Cs along with an aliquot of the supernate.

In the first experiments the analytical procedure used was modified from that of Glendenin and Nelson[17] in which Rb and Cs are separated by precipitation of Cs as silicotungstate. The procedure consists of a cobaltinitrite precipitation, solution of the precipitate in HCl, a silicotungstate precipitation, two HCl washings of the silicotungstate, solution in NaOH, fuming with $HClO_4$ to precipitate SiO_2 and WO_3, a $CsClO_4$ precipitation, two $Fe(OH)_3$ scavengings and a final cobaltinitrite precipitation. The Cs samples from the supernate solutions decayed with a 32- to 33-min. half-life, but those of the precipitate samples of precipitations later than 25 sec. decayed with somewhat shorter half-lives (27 to 30 min.). In the latter samples the 17.8-min. Rb^{88} activity grown from the 15.5-sec. Br^{88} is considerably greater than that of the 32-min. Cs and must be removed efficiently to determine the 32-min. Cs activity. The activities so determined led to a 7-sec. half-life for I^{138}. However, since the weakly active samples of later precipitations are contaminated with some 17.8-min. Rb activity, the true half-life is expected to be somewhat shorter than that measured.

The half-life of I^{138} was redetermined after a desirable chemical procedure was devised for the separation of Cs in the precipitate from Rb and the other fission products. The Cs is precipitated from the NaCN and supernate solutions as the cobaltinitrite. The precipitate is washed once with 10 ml 10-percent HAc. The precipitate is then dissolved in 1 ml 6*N* HCl by heating, 8 ml 70-percent $HClO_4$ is added, and the solution heated until dense fuming occurs. The solution is cooled and $CsClO_4$ is precipitated by addition of 15 ml absolute ethyl alcohol. The precipitate is washed once with 10 ml absolute ethyl alcohol. The precipitate is dissolved in 10 ml H_2O, and 3 ml BiI_3—HI reagent added to precipitate the Cs. Following the procedure given earlier in this section, the precipitate is washed twice, the I_2 expelled, two hydroxide precipitations are performed and the Cs is precipitated as the covaltinitrite. The chemical yield is ~60 percent and the time for analysis of two samples about 1½ hrs. The Cs is freed from contamination by Rb and the other fission products very effectively by this procedure as is evidenced by the decay curves of Cs obtained from samples of later precipitations where the Cs activity was much lower than that of Rb or the other fission products.

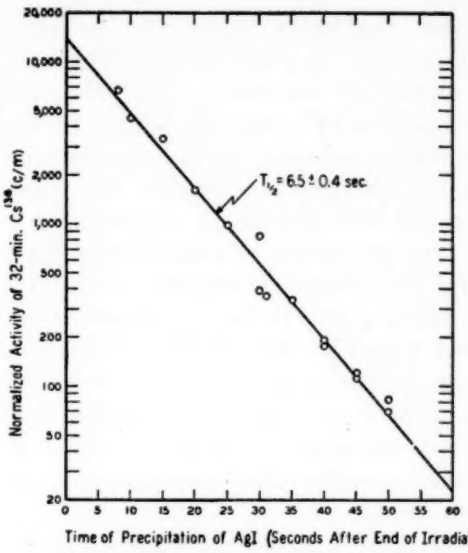

FIG. 9. Decay curve of I^{138} from 32-min. Cs^{138} activities extracted from AgI precipitates. Activities of 32-min. Cs^{138} in precipitates multiplied by normalization factors obtained by correcting Cs activities in supernates to 10^6 c/m (data of Table VI).

The measured activities of the Cs samples of the precipitate and supernate from a given experiment are corrected for chemical yield and aliquot of solution taken. Since the Cs activity is predominately in the supernate, this activity is used for monitoring the irradiations by normalizing the activity to a constant level, 10^6 c/m. The half-life found for I^{138} by least squares analysis is 6.5±0.4 sec. (Fig. 9) using the normalized activity data of Table VI.

The half-lives found for I^{138} by the two methods, 5.6±0.1 sec. and 6.5±0.4 sec., differ by more than the estimated errors of the determination. Such a discrepancy would result if Cs activity coseparated with Ag(Br, I) to the extent of one part in 5×10^4. This possibility was tested under conditions identical with those of the experiments already reported. Approximately one part in 5×10^5 of the Cs activity was found

[17] L. E. Glendenin and C. M. Nelson, Plutonium Project Record, Vol. 9B, 8.22.1 (1946).

with the precipitate when the former was present at time of precipitation. When Cs activity was added one minute after precipitation, only one part in 10^6 coseparated. Thus the source of the discrepancy lies elsewhere. Coseparation of the Xe activity will lengthen the apparent half-lives in both procedures although the error in the first case should be smaller since the Xe^{137} used for normalization will also coseparate. If other fission products are not removed to the required degree by the isolation procedure used for radio-Cs, the apparent half-life of I^{138} will be longer in the second method. In the first method Xe^{138} was separated from the precipitate and non-volatile radioactive contaminants before analysis for Cs.

The average half-life by weighting the first determination twofold relative to the second is 5.9 ± 0.4 sec.

9. HALF-LIFE OF I^{139}

The half-life of I^{139} was determined by analyzing the AgI precipitate and supernatant solution containing Rb, Cs, Sr, and Ba carriers for 85-min. Ba^{139}. After thorough washing of the precipitate on the filter disk, it was dissolved in NaCN solution containing Ba carrier and analysis for Ba was performed on this solution and an aliquot of the supernatant solution. The Ba was precipitated as $BaCO_3$ about 1 hr. after the end of irradiation. At this time the 7-min. Cs^{139} has completely decayed to the 85-min. Ba^{139}. After dissolving this precipitate in acid the Ba was separated by the procedure of Glendenin[18] which includes two precipitations of Ba as $Ba(NO_3)_2$ from fuming HNO_3 solution, a $Fe(OH)_3$ scavenging, and two precipitations of $BaCl_2$ using conc. HCl—ether reagent. The Ba was then converted to $BaCrO_4$ and counted. The 85-min. Ba^{139}

TABLE VI. Activity of 32-min. Cs^{138} extracted from AgI precipitates and supernatant solutions.

Time of precipitation of AgI	Sample	Activity of 32-min. Cs at 3 hrs. after AgI precipitation (c/m)	Milligrams Cs precipitate	Aliquot	Activity of 32-min. Cs corrected to 25 mg precipitate* and for aliquot	Normalization factor for supernate activities (corrected to 10^6 c/m)	Activity of Cs in precipitate (normalized) (c/m)
	precipitate	4150	24.4	1.0	4250	—	6720
8 sec.	supernate	13300	25.8	0.02	0.630×10^6	1.58	—
	precipitate	1720	14.9	1.0	2885	—	4500
10 sec.	supernate	13100	26.1	0.02	0.640×10^6	1.56	—
	precipitate	2910	24.9	1.0	2920	—	3360
15 sec.	supernate	17200	25.2	0.02	0.870×10^6	1.15	—
	precipitate	1310	24.7	1.0	1325	—	1615
20 sec.	supernate	13900	21.6	0.02	0.820×10^6	1.22	—
	precipitate	371	22.5	1.0	412	—	985
25 sec.	supernate	9100	27.7	0.02	0.420×10^6	2.39	—
	precipitate	388	26.0	1.0	373	—	388
30 sec.	supernate	19200	25.4	0.02	0.965×10^6	1.04	—
	precipitate	435	21.4	1.0	508	—	845
30 sec.	supernate	12200	25.8	0.02	0.605×10^6	1.66	—
	precipitate	280	25.1	1.0	279	—	360
31 sec.	supernate	14500	23.8	0.02	0.775×10^6	1.29	—
	precipitate	148	25.3	1.0	146	—	340
35 sec.	supernate	8550	25.5	0.02	0.430×10^6	2.33	—
	precipitate	88	17.7	1.0	124	—	192
40 sec.	supernate	12250	24.2	0.02	0.645×10^6	1.55	—
	precipitate	152	24.8	1.0	153	—	177
40 sec.	supernate	16200	24.0	0.02	0.860×10^6	1.16	—
	precipitate	88	23.0	1.0	92	—	111
45 sec.	supernate	17200	26.6	0.02	0.825×10^6	1.21	—
	precipitate	68	25.7	1.0	66	—	120
45 sec.	supernate	10800	25.0	0.02	0.550×10^6	1.82	—
	precipitate	31	13.0	1.0	60	—	70
50 sec.	supernate	17600	26.3	0.02	0.855×10^6	1.17	—
	precipitate	61	26.4	1.0	58	—	83
50 sec.	supernate	13800	25.1	0.02	0.700×10^6	1.43	—

* Supernate activities multiplied by another factor of 1.02 to correct for Cs carrier originally present in solution at AgI precipitation.

[18] L. E. Glendenin, Plutonium Project Record, Vol. 9B, 8.23.1 (1946).

activity is predominately in the supernate (>99.98 percent) so that the supernate activity can be used for monitoring the irradiations. The half-life found for I^{139} by least squares analysis was 2.7±0.1 sec. (Fig. 10) using the normalized activity data of Table VII.

The half-life found for I^{139} is quite sensitive to the coseparation of Ba^{139} activity or its antecedents since so small a fraction of the total Ba activity is in the precipitate. For the coseparated activity to be less than 10 percent of the total activity of the samples from later precipitations (17 sec.), the coseparation factor must be less than 10^{-6}. Coseparation tests with Cs and Ba yielded factors of this magnitude, $\sim 1\times10^{-6}$ for Cs and $<2\times10^{-6}$ for Ba. Since the factor for Xe and the fate of the Cs and Ba decay products of coseparated Xe are unknown, the half-life found for I^{139} may be somewhat higher than the true value.

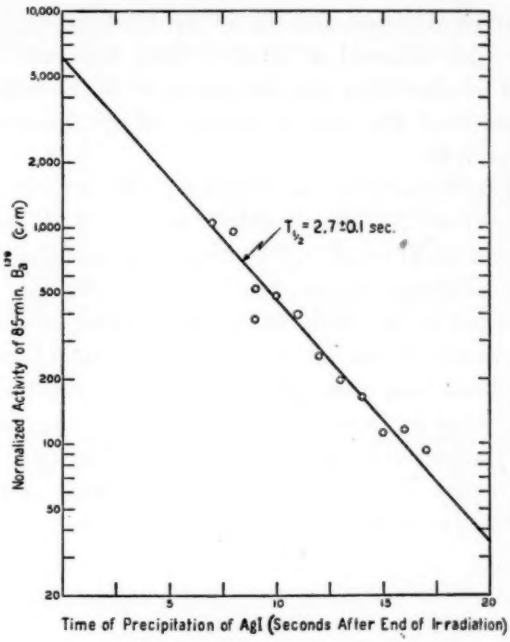

Fig. 10. Decay curve of I^{139} from 85-min. Ba^{139} activities extracted from AgI precipitates. Activities of 85-min. Ba^{139} in precipitates multiplied by normalization factors obtained by correcting Ba activities in supernates to 10^7 c/m (data for Table VII).

10. SEARCH FOR I^{140}

Two of the Ba samples isolated for the study of I^{139} (Section 9) were followed long enough to detect any activity of 12.8-days Ba^{140}, if present. None was observed in the AgI samples precipitated at 7 and 10 sec., and on the assumption that an activity of 4 c/m would have been detected, a ratio of $<5\times10^{-5}$ for the 12.8-days Ba^{140} activity in the precipitate to that in the supernate was obtained. The conclusion from this is that the half-life of I^{140} is short and/or the isotope is formed in low yield.

11. MASS ASSIGNMENT OF THE 22.0-SEC. I DELAYED NEUTRON EMITTER

The half-life of I^{137} has been determined on the assumption of constant chemical yield of Xe extraction to be 19.3±0.5 sec. (Section 7). It seems probable that I^{137} and the 22.0-sec. I delayed neutron emitter are identical. This result and the half-lives found for I^{138} and I^{139} eliminate the possibility of the assignment of the mass of the 22.0-sec. I to 138 or 139.[9]

Another uncertainty introduced into the assignment of the 22.0-sec. I delayed neutron emitter to mass 137 by the relatively lower yield of the stable isotope Xe^{136} compared to Xe^{134} found in fission by Thode and Graham,[19] has been removed. An assignment of the delayed neutron emitter to I^{136} was proposed[14] to explain the lower yield of Xe^{136} and the fission yield of 9.2-hr. Xe^{135} formed independently of the 6.7-hr. I^{135}. On the basis of a mass of 136, the 9.2-hr. Xe activity in a AgI precipitate should arise from two sources, the 22.0-sec. I decaying to the 9.2-hr. Xe^{135} by a process of β^--decay followed by

TABLE VII. Activity of 85-min. Ba^{139} extracted from AgI precipitates and supernatant solutions.

Time of precipitation of AgI	Activity of 85-min. Ba in precipitate at time of AgI precipitation (c/m)	Activity of 85-min. Ba in supernate at time of AgI precipitation (c/m)	Normalization factor for supernate activities (corrected to 10^7 c/m)	Activity of Ba in precipitate (normalized) (c/m)
7 sec.	1025	0.975×10^7	1.025	1050
8 sec.	389	0.405×10^7	2.470	960
9 sec.	340	0.905×10^7	1.105	376
9 sec.	630	1.200×10^7	0.835	525
10 sec.	1015	2.085×10^7	0.480	485
11 sec.	650	1.655×10^7	0.605	393
12 sec.	410	1.605×10^7	0.625	256
13 sec.	342	1.725×10^7	0.580	198
14 sec.	110	0.675×10^7	1.480	163
15 sec.	117	1.045×10^7	0.955	112
16 sec.	173	1.475×10^7	0.680	118
17 sec.	138	1.485×10^7	0.675	93

[19] H. G. Thode and R. L. Graham, Can. J. Research **25**, 1 (1947).

neutron emission, and the 6.7-hr. I^{135} decay during the time interval of about 6 min. between the AgI precipitation and the sweeping of the active gases from the NaCN solution of the dissolved precipitate.

This hypothesis can be tested. The activity of the 9.2-hr. Xe should show variation with time of precipitation of AgI leading to a resolution of the composite decay curve into two periods, 22 sec. and 6.7 hr. Some of the Xe samples used for the study of the half-life of I^{137} (Section 7) were followed long enough to measure the 9.2-hr Xe activities in them. It was found that the ratio of the activity of 9.2-hr. Xe to 3.8-min. Xe increased 70-fold for AgI precipitations in the time interval 15 sec. to 2.5 min., showing a much

TABLE VIII. Activity of 9.2-hr. Xe^{135} extracted from AgI precipitates.

	3.8-min. Xe^{137}			9.2-hr. Xe^{135}	
Time of precipitation of AgI	Activity of 3.8-min. Xe^{137} at 15 min. after AgI precipitation (c/m)	Activity from arbitrary 22-sec. decay curve (c/m)	Normalization factor	Activity of 9.2-hr. Xe^{135} at 24 hr. after AgI precipitation (c/m)	Normalized activity (c/m)
15 sec.	23800	62500	2.62	39	102
30 sec.	32000	39000	1.22	108	132
35 sec.	25700	33500	1.30	92	119
40 sec.	22000	28500	1.29	98	127
50 sec.	20700	21000	1.01	143	144
1.5 min.	3800	6000	1.58	72	114
2.0 min.	1350	2300	1.71	72	123
2.5 min.	680	900	1.32	74	98

slower decrease of the 9.2-hr. Xe activity relative to the 3.8-min. Xe activity as a function of time of AgI precipitation. Normalizing the 3.8-min. Xe^{137} activities to a 22-sec. half-life for I^{137} and multiplying the 9.2-hr. Xe^{135} activities by these normalization factors, one finds that the 9.2-hr. Xe activity is roughly constant for AgI precipitations from 15 sec. to 2.5 min. (last column of Table VIII). These results show that the delayed neutron emitter cannot be I^{136} since the contribution of 9.2-hr. Xe from this species would have resulted in a considerably higher activity in the 15 sec. AgI precipitate relative to the 2.5-min. sample. The lower yield of Xe^{136} relative to Xe^{134} observed by Thode and Graham[19] must, therefore, arise from some other source.

12. LOSS OF ACTIVITY FROM SILVER HALIDE PRECIPITATES

In the course of this work some semi-quantitative information was obtained on the loss of the active decay products from AgBr(I) precipitates. A comparison of the activity in the precipitate with that in the supernate yields the composite value of the fraction of the halogen activity precipitated and the fraction of the activity of the decay products retained by the precipitate. The fraction of the halogen activity precipitated with AgBr may be expected to be less than unity since activity present chemically in oxidized states of the halogens will not precipitate unless the carrier species (Br^- or I^-) reacts fast enough to reduce them to states exchangeable with I^- or Br^- before precipitation. The retention factor expresses the loss of activity from the precipitate by the diffusion of Kr or Xe which may be expected to occur rapidly during coagulation while considerable surface is exposed, and more slowly afterward. This factor will be approximately the exponential decay of the halogen activity during the time of rapid diffusion.

The ratio of the Ba^{139} activity in the AgI precipitate to the activity in the supernate at the end of a 10-sec. irradiation is 6.2×10^{-4} (see Fig. 10). After correcting for the saturation of the 2.7-sec. I^{139} during irradiation, and assuming the fission yield of I^{139} to be about 0.3 that of Ba^{139},[9] one finds the product of the fraction of the I activity precipitated as AgI and the fraction of the decay products retained by the precipitate is 0.006. Similarly, this value for the 5.9-sec. I^{138} is 0.05. A rough value of $\sim$0.25 is found for the 15.5-sec. Br^{88} by comparing the 17.8-min. Rb^{88} activity with that of the 32-min. Cs^{138} activity in a mixed Ag(Br+I) precipitate where no separation of Rb from Cs is made in the analysis for Cs. From these results there is found a marked variation in the fraction of the decay products found in the precipitate as a function of the half-life of the halogen ancestor. Assuming the fraction of Br or I activity exchanged with Br^- or I^- carriers is about 0.5, one can correlate the derived retention factors with a time required for retention of about 20 sec.

The precision of the half-life determination of the halogen by the method employed here will

be affected by the difference in time required for "setting" of the precipitate from experiment to experiment. In those cases where the half-life of the halogen is long relative to ~20 sec., e.g., Br^{85} and Br^{87}, the loss of activity during "setting" will not be significant and the scattering of the data from time variations in "setting" will be small. This result is borne out by the good precision of the determination of the half-life of Br^{87} based on normalization values of Br^{85} (cf. Section 3 and Fig. 5). On the other hand, where the half-life of the halogen is short relative to ~20 sec., e.g., I^{138}, I^{139}, there is considerable loss of activity during the "setting" process and greater scatter of the points due to differences in "setting" time (see Fig. 10). It should be noted, however, that the variation in "setting" time is probably small relative to 2.7 sec. or considerably more scattering would have resulted.

The considerations above offer an explanation for the absence of 53-day Sr^{89} in AgBr precipitates if the mass assignment of the 4.51-sec. delayed neutron emitter is 89 or 90 (cf. Section 6). Little activity would be retained by the precipitate because of the short-half-life of the halogen, leading to difficulty in observing either an increase in Kr^{88} activity above that formed from decay of 15.5-sec. Br^{88} or the Sr^{89} activity if the mass is 89, or Sr^{89} activity formed via neutron emission and subsequent β^- decay if the mass is 90.

13. SUMMARY

The results of these experiments on the half-lives of the halogen fission products clarify some of the ambiguities in mass assignment formerly existing in the table of "Nuclei Formed in Fission." [1] Some new short-lived Br and I activities have also been found. The chain relations as modified in this work are given below:**

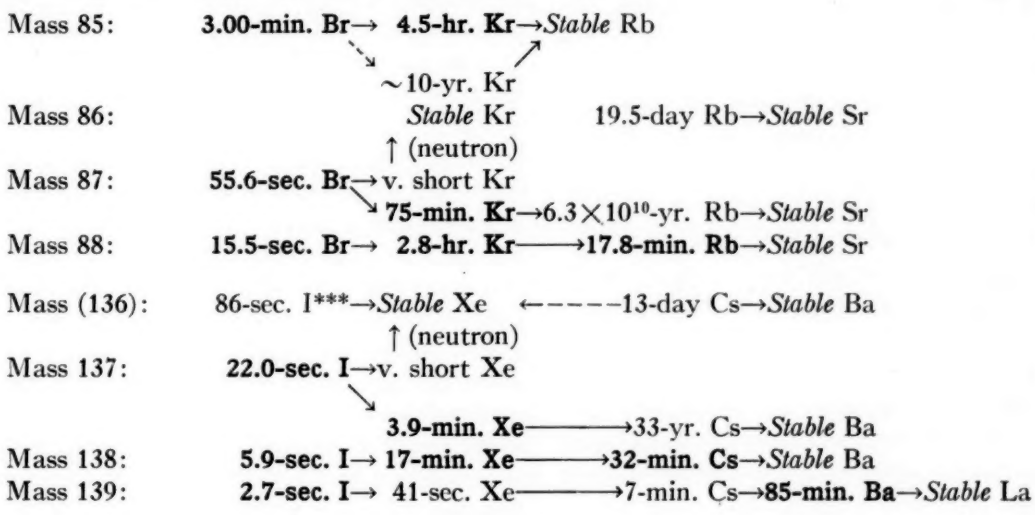
Mass 85: 3.00-min. Br→ 4.5-hr. Kr→Stable Rb
~10-yr. Kr
Mass 86: Stable Kr 19.5-day Rb→Stable Sr
↑ (neutron)
Mass 87: 55.6-sec. Br→v. short Kr
75-min. Kr→6.3×10¹⁰-yr. Rb→Stable Sr
Mass 88: 15.5-sec. Br→ 2.8-hr. Kr→17.8-min. Rb→Stable Sr
Mass (136): 86-sec. I***→Stable Xe ←13-day Cs→Stable Ba
↑ (neutron)
Mass 137: 22.0-sec. I→v. short Xe
3.9-min. Xe→33-yr. Cs→Stable Ba
Mass 138: 5.9-sec. I→ 17-min. Xe→32-min. Cs→Stable Ba
Mass 139: 2.7-sec. I→ 41-sec. Xe→7-min. Cs→85-min. Ba→Stable La

ACKNOWLEDGMENT

It is a pleasure to acknowledge the assistance given the author in these experiments by Mr. Harold Richter of the Argonne National Laboratory.

** Boldface indicates activities studied in this paper.

*** This value is taken from recent work of S. Katcoff and C. W. Stanley, Los Alamos Report, La-628, March 25, 1947.

THE JOURNAL OF CHEMICAL PHYSICS VOLUME 17, NUMBER 1 JANUARY, 1949

Motions of Molecules in Condensed Systems. IV. The Infra-Red Spectra for Ammonium Nitrate and Thallous Nitrate

WILLIAM E. KELLER AND RALPH S. HALFORD*
Mallinckrodt Chemical Laboratory, Harvard University, Cambridge, Massachusetts

(Received July 6, 1948)

The infra-red absorption spectra from 680 to 3600 cm^{-1} have been recorded for five crystalline modifications of NH_4NO_3 at 150°, 105°, 55°, 25°, and −40°; also the spectra from 680 to 1450 cm^{-1} of three modifications of $TlNO_3$ at 170°, 100°, and 25°. Fundamental frequencies of the nitrate ion were found for NH_4NO_3 at 715, 830, 1050, and 1350 cm^{-1} (those for $TlNO_3$ were found at approximately the same positions) and of the ammonium ion at 1430, 1760, 3100, 3200 cm^{-1}. The spectrum of each compound remains essentially the same with change of temperature, except that in NH_4NO_3 at 150° and 105° the band at 715 cm^{-1} is absent. It is notable that bands at 1050, 1760, and 3100 cm^{-1}, supposedly caused by symmetric vibrations, remain active in all crystal forms investigated.

INTRODUCTION

FOR some years it has been known that the character of the infra-red absorption spectrum of a compound depends largely upon the environment in which the molecules find themselves. Recently one of us[1] has advanced the thesis, subsequently verified[2] experimentally for the case of benzene, that (1) while the selection rules for the vapor are determined solely by the symmetry of the individual molecule; (2) for the liquid, in general, there are no strict selection rules; (3) the selection rules for the solid may be approximated by considering a single molecule and the symmetry of the potential field created by its neighbors. In passing from the liquid to the solid, it is expected that prohibitions may become operative, since in the latter the symmetry of the surroundings of a given molecule are more nearly space and time-fixed, than in the former.

It was thought of interest to extend experiments to include infra-red spectra of a single compound exhibiting several different crystal modifications. Presumably, with change in crystal structure, the change of potential field about any given molecule might alter the spectrum. Ammonium nitrate, capable of existing in five modifications over a short temperature range at normal pressures, was chosen for this study.

In order to treat the problem in accordance with the stated principles, it is necessary to know beforehand the "site" symmetry of the molecules or ions in the crystal; that is, we must at least have knowledge of the space group and the number of molecules per unit cell for each of the five modifications of ammonium nitrate. Unfortunately, only two of the polymorphs have been sufficiently defined. These are NH_4NO_3 IV (orthorhombic) stable from about −18° to +32°C, having space group V_h^{13} ($P2_1/m2_1/m2/n$) and two molecules per unit cell,[3,4] and NH_4NO_3 III (orthorhombic) stable from 32° to 84°C with space group V_h^{16} ($P2_1/n2_1/m2_1/a$) and four molecules per unit cell.[3] The remaining modifications have been described as NH_4NO_3 I (cubic) stable from 125° to 169°C (melting point) with one molecule per unit cell; NH_4NO_3 II (tetragonal) assigned to space group D_{2d}^3 or C_{4v}^2 with two molecules per unit cell;[5] and NH_4NO_3 V (hexagonal ?) with six molecules per unit cell.

During the course of our investigations the spectra of forms I and II were found to be irregular with respect to the nitrate ion. Lack of crystallographic knowledge prompted us to treat thallous nitrate as we had ammonium nitrate, since the former possesses a high temperature cubic modification ($TlNO_3$ α, space group un-

* Present address: Department of Chemistry, Columbia University, New York, New York.

[1] R. S. Halford, J. Chem. Phys. **14**, 8 (1946). The same symmetry argument for crystals was first used, in another connection, by H. Bethe, Ann. d. Physik **3**, 133 (1929).

[2] R. S. Halford and O. A. Schaeffer, J. Chem. Phys. **15**, 141 (1946).

[3] S. B. Hendricks, E. Posnjak, and F. C. Kracek, J. Am. Chem. Soc. **54**, 2780 (1932).

[4] C. D. West, J. Am. Chem. Soc. **54**, 2256 (1932).

[5] R. Tiemeyer, Zeits. f. Krist. **97**, 386 (1937).

known) having cell dimensions[6] almost those of NH_4NO_3 I. From these considerations we infer that the nitrate ions in the two compounds may exist in similar environments in the high temperature forms and could therefore give rise to correspondingly similar spectra. $TlNO_3$ exists in two other forms, thereby providing further possibilities of changes in spectra and of comparison with NH_4NO_3.

In this article we shall describe the experimental methods and results of a study of the spectra of the five forms of ammonium nitrate and of the three forms of thallous nitrate.

EXPERIMENTAL AND RESULTS—NH_4NO_3

The requirements for the preparation of a solid sample for investigation in the infra-red include that the sample be transparent to infra-red radiations in the regions of non-absorption and that the sample not extensively scatter the radiation incident upon it. In the case of ammonium nitrate we found these requirements best met by preparing the sample in the following manner.

Analytical reagent NH_4NO_3 supplied by the Mallinckrodt Chemical Company was finely ground and spread in a thin layer upon a disk, 50 mm in diameter and 1 mm thick, of rolled silver chloride obtained from Harshaw Chemical Company. Then a similar disk of AgCl was placed on top of the NH_4NO_3 layer. This sandwich was placed upon a small aluminum plate and the whole heated by a cone heater to the melting point of NH_4NO_3. Once the entire layer was fused, another aluminum plate was laid upon the sandwich and on top of this a weight of about a kilogram, thereby squeezing out excess sample. The heater was removed and the specimen allowed to cool undisturbed. This last sequence of operations was carried out quickly since vaporized NH_4NO_3 slowly decomposes to water and nitrous oxide at the melting point of the salt. By varying the amount of salt and the weight placed upon the sandwich, the thickness of the sample could be roughly adjusted. An apparent drawback of this procedure was the indeterminacy of the exact thickness of the specimen. However, for the investigation under discussion the main aim was a sample that would display the fundamental absorption bands. To this end, the above treatment was entirely satisfactory.

Since ammonium nitrate is highly volatile at the relatively high temperatures at which spectra were to be taken, it was desirable that the sample cell be closed from the atmosphere. The sandwich was held between cork insulators with an ordinary *c*-clamp, while a hot glass rod was applied to the rim of the AgCl disks, thus welding them together.

It was found that upon passing from one modification to another the sample became more opaque to infra-red radiations—it was by this evidence that we were assured a transition had occurred. Moreover, the sample would begin to scatter the shorter waves quite severely after several transitions. This was remedied by "rejuvenating" the salt layer: the sandwich was merely heated above the nitrate's melting point and allowed to cool to the modification desired. This had to be done twice during the investigation.

Because polymorphic transitions in NH_4NO_3 are often delayed,[7] in all cases, with the exception of modification V, the various crystal forms were obtained by maintaining the suitable temperature for at least twelve hours before recording the spectra. The low temperature form was precooled for two hours.

The electric heating cell and the liquid nitrogen cooling apparatus employed for temperature control were those described by Carpenter,[8] and Carpenter and Halford.[9]

An automatic recording prism spectrophotometer[10] was used for measurements of the spectra. At all times a cell, made of two disks of AgCl treated exactly as those used in the sample, was used as a photometric standard. The spectra were recorded in the following order: (1) NH_4NO_3 IV at room temperature; (2) III at 55°C; (3) II at 105°C; (4) I at 150°C; (5) IV again at room

[6] C. Finbak and O. Hassel, Zeits. f. physik. Chemie **B35**, 25 (1937).

[7] O. Lehmann, Zeits. f. Kryst. **1**, 108 (1877).

[8] G. B. Carpenter, thesis for the doctorate, Harvard University (1947).

[9] G. B. Carpenter and R. S. Halford, J. Chem. Phys. **15**, 99 (1947).

[10] H. Gershinowitz and E. B. Wilson, Jr., J. Chem. Phys. **6**, 197 (1938).

temperature; (6) V at −40°C; and (7) V at −65°C. Each spectrum was measured at least twice. In the region up to 1250 cm^{-1} a NaCl prism was used, while from 1250 to 3600 cm^{-1} a CaF_2 prism was employed.

Figure 1 shows the absorption spectra in the range 680 to 3600 cm^{-1} of NH_4NO_3 in its five modifications. The regions of transparency have been corrected to read 100 percent by using a sliding correction factor in order to compensate for the small though increasing losses of radiation toward the short wave end of the spectra. The absorption bands have been corrected accordingly. The spectra at −40° and −65°C are virtually identical despite the fact that these temperatures straddle a reported lambda-point[11, 12] of NH_4NO_3 at about −60°C. Furthermore, the specimen gave the same spectrum at room temperature before and after it had been heated up to 150°C in the stages mentioned above.

It is altogether plausible that all the distinct fundamental frequencies of nitrate (four) and of ammonium (four) ions appear in the spectra. The fundamental absorption bands of the two ions are confined to separate frequency regions

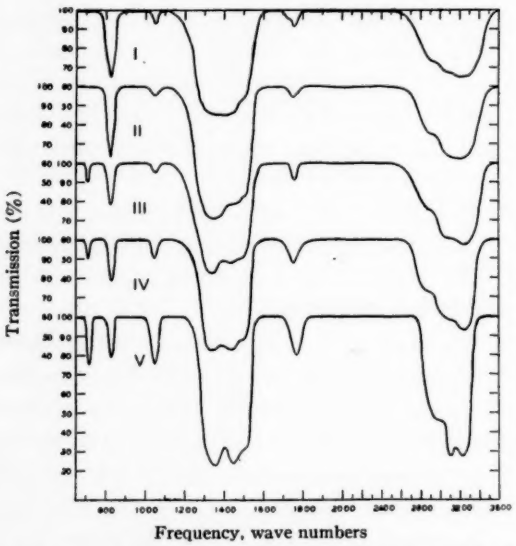

FIG. 1. Infra-red absorption spectra from 680 to 3600 cm^{-1} of five crystalline forms of NH_4NO_3: I at 150°C; II at 105°C; III at 55°C; IV at room temperature; V at −40°C. Measurements from 680 to 1250 cm^{-1} were made with a rock salt prism, from 1250 to 3600 cm^{-1} with a fluorite prism.

[11] J. L. Crenshaw, I. Ritter, Zeits. f. physik. Chemie **B16**, 148 (1932).
[12] R. Pohlman, Zeits. f. Physik **79**, 419 (1932).

and have been assigned[13] elsewhere as shown in Table I, regarding nitrate ion as planar and ammonium ion as tetrahedral. Also listed is an overtone frequency.

Although the method of obtaining data does not lend itself to giving a quantitative picture of intensity changes in the five spectra, some qualitative information is readily presented. Most obvious is the disappearance in forms I and II of the band at 715 cm^{-1}. Another unusual feature displayed by the group of spectra is the comparative increase in intensity of the 830 cm^{-1} band, which contrasts with the losses of intensity at 715, 1050 and 1760 cm^{-1}.

EXPERIMENTAL AND RESULTS—$TlNO_3$

Specimens of thallous nitrate of high purity were prepared by a method similar to that used for ammonium nitrate, but with the following variations. Melted $TlNO_3$ in contact with AgCl and oxygen of the air readily oxidizes to Tl_2O_3; to avoid this it was found sufficient to cool the melt soon after its formation as well as to keep the initial layer of powdered $TlNO_3$ compact so as to exclude as much air as possible from the sandwich filling. The cell was not sealed as before; but instead the sandwich was placed in a holder consisting of threaded male and female parts, both parts having equal apertures for traversal by the light beam. The rim of the sandwich was in this way held secure.

TABLE I. Assignment (13) of frequencies for ammonium and nitrate ions as found in NH_4NO_3.

Ion	Frequency (cm^{-1})	Assignment
NO_3^-	715	Doubly degenerate bend in plane
NO_3^-	830	*N* in-and-out of plane
NO_3^-	1050	Symmetric stretch in plane
NO_3^-	1350	Doubly degenerate unsymmetric stretch in plane
NH_4^+	1430	Triply degenerate bend
NH_4^+	1760	Doubly degenerate totally symmetric bend
NH_4^+	3100	Totally symmetric stretch
NH_4^+	3200	Triply degenerate stretch
NH_4^+	2880	Overtone of 1430

$TlNO_3$ freezes at 206°C to form a clear mass of cubic crystals (form α); at 145°C the salt undergoes a transition to a trigonal form (β);

[13] G. Herzberg, *Infra-red and Raman Spectra*, Vol. II (D. Van Nostrand Company, Inc., New York, 1945), p. 167, 178.

and at 75°C it passes into an orthorhombic form (γ) stable down to very low temperatures. Of these modifications only the latter has been well defined crystallographically: possible space groups are given as D_2^2 ($P222_1$) and D_2^3 ($P2_12_12$) the latter being most probable, with four molecules per unit cell.[14] Upon passing from one form to another, $TlNO_3$ crystals do not fracture[15] into microcrystals as do those of NH_4NO_3,[3] so that the occurrence of a transition was not immediately obvious. Also, the sample never required rejuvenation. Absorption measurements were made in the following order: (1) γ-form at room temperature; (2) β-form at 100°C; (3) α-form at 170°C; and (4) γ-form at room temperature again. Each of the absorption regions was measured at least in duplicate. The same electrical heating cell as mentioned above was employed for temperature control.

Figure 2 depicts the spectra of the three forms of $TlNO_3$ in the fundamental region from 680 to 1450 cm^{-1}. For this work the NaCl prism only was used. (680 cm^{-1} seemed to be the lower useful limit for work with the NaCl prism on $TlNO_3$; in this region the KBr prism has poor resolving power. Hence the band at 715 cm^{-1} is covered as well as can be done on our instrument.) The data as presented appears uncorrected for any effect of light-scattering that might be operative.

The presence of all the nitrate fundamentals in all the modifications is evident, but the envelopes of the bands near 700 and 1050 cm^{-1} are quite different from the corresponding absorptions in the ammonium compound. Aside from the effect of temperature in broadening out the absorption envelopes, very little can be said concerning the changes in intensity of the various components of the spectra.

DISCUSSION

In view of the wide variety of environments in which the respective ions exist in NH_4NO_3 and $TlNO_3$, it is indeed singular that the spectra of the different modifications are so similar. Group theoretical considerations show that only the totally symmetric vibration of NO_3^- (1050 cm^{-1}) and symmetric stretch and bend of NH_4^+ (3100 and 1760 cm^{-1} respectively) would be expected to become infra-red inactive if the ions were either in no potential field or in a very symmetrical one. Yet it is evident that these frequencies remain active in all the polymorphs investigated. It may be mentioned that in the two cases for which space-group information is complete (NH_4NO_3 IV and III) the proposed criteria for selection rules are in agreement with the results.

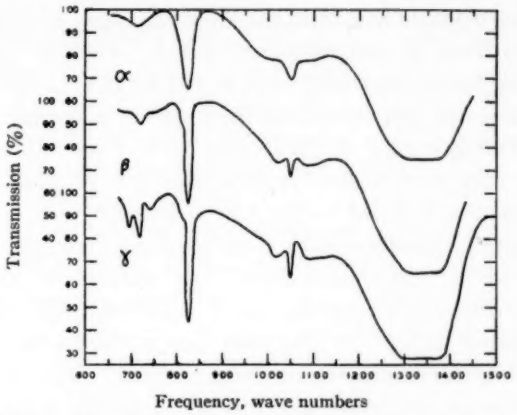

FIG. 2. Infra-red absorption spectra from 680 to 1450 cm^{-1} of three crystalline forms of $TlNO_3$: α at 170°C; β at 100°C; and γ at room temperature. All measurements were made with a rock salt prism.

Finbak and Hassel[6] have shown by x-ray diffraction powder-diagrams that NH_4NO_3 I has a cubic structure, $a_0=4.39$A at 150°C and that $TlNO_3$ also is cubic, $a_0=4.31$A at 170°C. Pauling[16] lists the crystal radii of NH_4^+ and Tl^+ as 1.48A and 1.44A, respectively. In the light of this information, structural considerations do not readily explain the apparent failure of these two crystals to give similar spectra (i.e., in NH_4NO_3 the absorption at 715 cm^{-1} is missing).

The band near 715 cm^{-1} is comparatively quite sensitive to the environment in which the nitrate ion finds itself. In two of the five modifications of NH_4NO_3 this band seems to be absent altogether, while it becomes noticeably less intense as one progresses toward higher temperatures through either the remaining three modifications of this substance or the three modifications of $TlNO_3$. Moreover, loss of intensity is accompanied by small but definite shifts of the band

[14] L. Rivoir and M. Abbad, Anales fis. quim. **39**, 306 (1943).

[15] G. Tammann and W. Boehme, Zeits. f. allgem. anorg. Chemie **223**, 365 (1935).

[16] L. Pauling, *The Nature of the Chemical Bond* (Cornell University Press, Ithaca, New York, 1939), p. 350.

toward lower frequencies. These changes are not paralleled in our observations by any of the other bands, although ones at 1050 and 1760 cm^{-1} do become less intense at higher temperatures.

The behavior of this band at 715 cm^{-1} is of the sort that might be expected[1] if it originates with a molecular mode whose capacity for absorption results solely from perturbations produced by the environment, one that could not contribute to the infra-red spectrum of the isolated molecule. The only fundamental mode that is forbidden to contribute to the infra-red spectrum of the isolated nitrate ion is the totally symmetric one. On the basis of strong evidence from the Raman effect[17] in inorganic nitrates, this mode is assigned the frequency 1050 cm^{-1}: the Raman line at this frequency is intense, sharp, and strongly polarized, all features characteristic of a completely symmetric vibration. The Raman line for nitrate ion at 715 cm^{-1}, on the other hand, is not polarized and has for some compounds been resolved into a doublet,[18] indicating that the mode may be doubly degenerate. It is interesting to note that light scattering experiments with single crystals of KNO_3 (isomorphous with NH_4NO_3 IV) at different temperatures[19] show that the 715 cm^{-1} line shifts to lower frequency with increasing temperature, in accord with the infra-red behavior of this vibration. Considering this data and that of earlier workers on the infra-red spectra of nitrates,[20] we cannot seek the explanation for the strange disappearance of the NH_4NO_3 band at 715 cm^{-1} in a mere shuffling of the assignment of nitrate ion frequencies. We are of the opinion, however, that a proper understanding of this anomaly will require some knowledge of the lattice modes and their combinations with the molecular modes. This question is being investigated currently with a more powerful spectrometer, using single crystals in polarized light, and, accordingly, additional comment will not be offered at this time.

[17] See, for example: P. Grassmann, Zeits. f. Physik **77**, 616 (1932); P. A. Moses, Proc. Ind. Acad. Sci. **10A**, 71 (1939); T. M. K. Nedungadi, Proc. Ind. Acad. Sci. **14A**, 242 (1941).

[18] P. Grassmann, see reference 17.

[19] T. M. K. Nedungadi, see reference 17.

[20] See, for example: C. Shaefer and C. Bormuth, Zeits. f. Physik **67**, 508 (1930); D. Williams and L. Decherd, J. Am. Chem. Soc. **61**, 1382 (1939).

THE JOURNAL OF CHEMICAL PHYSICS VOLUME 17, NUMBER 1 JANUARY, 1949

The Vibration-Rotation Mechanics of the Allene Molecule. Part I. Classical Vibration Problem

ROBERT C. HERMAN,
Applied Physics Laboratory, The John Hopkins University, Silver Spring, Maryland
AND
WAVE H. SHAFFER
Mendenhall Laboratory of Physics, The Ohio State University, Columbus 10, Ohio

(Received May 27, 1948)

Symmetry coordinates are set up from the standpoint of group theory for describing the normal modes of oscillation of the allene molecular model in such a manner that maximum factorization of the secular determinant is accomplished. The cubic and quartic portions of the anharmonic potential function are derived, and the components of vibrational angular momentum are set down. The complete valence-type potential function is discussed. Explicit relations are derived between the force constants occurring in the secular determinant and the physical valence force constants.

I. INTRODUCTION

THE infra-red and Raman spectra of the allene molecule, C_3H_4, have been studied experimentally by several observers.[1] The non-degenerate normal modes of vibration have been investigated by Thompson and Linnett[2] and by

[1] M. Bourguel and L. Piaux, Bull. Soc. Chim. **51**, 1041 (1932); H. Kopper and A. Pongratz, Wien. Ber. **141**, 840 (1932); L. G. Bonner and R. Hofstadter, Phys. Rev. **52**, 249 (1937); E. H. Eyster, J. Chem. Phys. **6**, 580 (1938); J. W. Linnett and W. H. Avery, J. Chem. Phys. **6**, 686 (1938).

[2] H. W. Thompson and J. W. Linnett, J. Chem. Soc. London, p. 1384 (1937).

TABLE I. Masses and equilibrium coordinates.

atom	r	m_r	x_{or}	y_{or}	z_{or}
H	1	m	a_o	0	c_o
H	2	m	$-a_o$	0	c_o
H	3	m	0	$-a_o$	$-c_o$
H	4	m	0	a_o	$-c_o$
C	5	M	0	0	b_o
C	6	M	0	0	$-b_o$
C	7	M	0	0	0

Ta-You Wu.[3] The symmetry properties of the vibrations and assignments of the experimental data have been discussed by Herzberg.[4]

II. MOLECULAR CONFIGURATION AND SYMMETRY

The available experimental evidence indicates for the allene molecule an equilibrium (vibrationless) configuration belonging to symmetry point group D_{2d}. In this configuration the three C atoms lie on a straight line, the symmetry axis, and the two CH_2 groups lie in planes passing through the symmetry axis at right angles to each other. The equilibrium model adopted for the allene model is shown in Fig. 1 along with a right-handed rectangular coordinate system, xyz, whose origin coincides with the center of mass and whose axes are principal axes of inertia. The respective atoms are indicated by an arbitrary index $r(r=1, 2\cdots7)$ for reference. The three C atoms lie on the z axis, H atoms 1 and 2 lie in the xz plane, and H atoms 3 and 4 lie in the yz plane. The masses (m_r) and equilibrium coordinates (x_{or}, y_{or}, z_{or}) of the respective atoms are listed in Table I.

The eight covering operations of symmetry point group D_{2d} or V_d form five classes as follows:

TABLE II. Characters of point group D_{2d}.

	E	C_2	$2S_4$	$2C_2'$	$2\sigma_d$
A_1	1	1	0	1	1
A_2	1	1	1	−1	−1
B_1	1	1	−1	1	−1
B_2	1	1	−1	−1	1
E	2	−2	0	0	0

[3] Ta-You Wu, *Vibrational Spectra and Structure of Polyatomic Molecules* (National University of Peking, Kun-Ming, China, 1939) (Edwards Brothers, Inc., Ann Arbor, Michigan, 1946), p. 287 ff.

[4] G. Herzberg, *Infrared and Raman Spectra of Polyatomic Molecules* (D. Van Nostrand Company, Inc., New York, 1945).

E, the identity operation; C_2, rotation by π around the z axis; $2S_4$, rotations by $\pm\pi/2$ around the z axis plus reflection in the xy plane; $2C_2'$, rotation by π around either of 2 axes in the xy plane which bisect angles between the x and y axes; and $2\sigma_d$, reflection in the xz and yz planes. Table II contains the characters of the various classes of covering operations performed on the five possible species (A_1, A_2, B_1, B_2, E) of physical quantities. The species A and B are nondegenerate and E is twofold degenerate. Quantities associated with the vibrations and rotations of the allene model have the following species assignments: (a) of the components of linear displacement, x and y form an E pair and z is B_2;

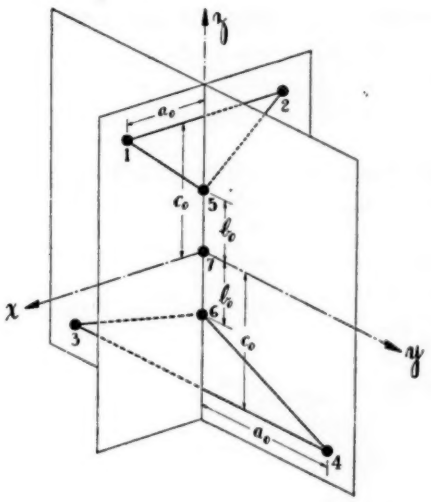

FIG. 1. Equilibrium configuration of the allene molecular model.

(b) of the components of angular momentum, P_x and P_y form an E pair and P_z is A_2; (c) of the components of the electric dipole moment, M_x and M_y form an E pair and M_z is B_2; (d) the polarizability tensor has components of species A_1, B_1, B_2, and E.

III. COORDINATES FOR INFINITESIMAL VIBRATIONS

The body-fixed rectangular coordinate system, which was introduced in Section II for description of the equilibrium configuration, is suitable for analytical discussion of the rotations and modes of vibration of the molecular model if it moves with the molecular framework subject to

the following two conditions:[5,6] (a) the coordinate origin remains at the center of mass, and (b) none of the modes of vibration results in angular momentum of rotation of the molecular framework as a whole inside the coordinate system.[7]

The instantaneous coordinates of the rth atom during infinitesimal vibrations will be given by $x_r=x_{or}+x_r'$, etc., where x_{or}, y_{or}, and z_{or} denote equilibrium values of the coordinates and x_r', y_r', z_r' denote components of displacement from the equilibrium position. Conditions (a) and (b) are satisfied by the following relations which are given in terms of the displacement coordinates:

$$\sum_r m_r x_r' = \sum_r m_r y_r' = \sum_r m_r z_r' = 0, \quad (1)$$

$$p_{ox} = \sum_r m_r (y_{or}\dot{z}_r' - z_{or}\dot{y}_r') = 0, \quad (2a)$$

$$p_{oy} = \sum_r m_r (z_{or}\dot{x}_r' - x_{or}\dot{z}_r') = 0, \quad (2b)$$

$$p_{oz} = \sum_r m_r (x_{or}\dot{y}_r' - y_{or}\dot{x}_r') = 0. \quad (2c)$$

For the allene model, these conditions are satisfied by the following equations:

$$m(x_1'+x_2'+x_3'+x_4') + M(x_5'+x_6'+x_7') = 0, \text{ etc.}, \quad (1')$$

and

$$ma_o(z_4'-z_3') - mc_o(y_1'+y_2'-y_3'-y_4') - Mb_o(y_5'-y_6') = 0, \quad (2'a)$$

$$ma_0(z_2'-z_1') + mc_0(x_1'+x_2'-x_3'-x_4') - Mb_o(x_6'-x_5') = 0, \quad (2'b)$$

$$ma_o(x_3'-x_4'+y_1'-y_2') = 0. \quad (2'c)$$

The methods of group theory show that the fifteen normal modes of vibration of the allene molecule of symmetry D_{2d} have the following species classifications: three of A_1, none of A_2, one of B_1, three of B_2, and four pairs of E. The complete vibrational secular determinant can accordingly be broken up at once, if one uses generalized coordinates with proper symmetry properties, into steps as follows: one onefold, two threefold, and two identical fourfold steps. It can be shown with the aid of group theory methods that the following fifteen linear combinations of the displacement coordinates form a set of linearly independent and mutually orthogonal generalized coordinates of appropriate symmetries for setting up the normal vibration problem:

$$\begin{aligned}
&u_1 = (x_1'-x_2'-y_3'+y_4')/4,\\
A_1:\quad &u_2 = (z_1'+z_2'-z_3'-z_4')/4,\\
&u_3 = (z_5'-z_6')/2.\\
A_2:\quad &(x_3'-x_4'+y_1'-y_2') = 0, \text{ from } p_{oz}=0.\\
B_1:\quad &v_4 = (x_3'-x_4'-y_1'+y_2')/4\\
&\quad = (x_3'-x_4')/2 = (y_2'-y_1')/2.\\
&w_5 = (x_1'-x_2'+y_3'-y_4')/4,\\
B_2:\quad &w_6 = z_7',\\
&w_7 = (z_5'+z_6')/2.\\
&s_8 = x_7'; \qquad t_8 = y_7',\\
&s_9 = \gamma^{-1}(z_1'-z_2')/2; \quad t_9 = \gamma^{-1}(z_3'-z_4')/2,\\
E:\quad &s_{10} = (x_5'+x_6')/2; \quad t_{10} = (y_5'+y_6')/2,\\
&s_{11} = \alpha^{-1}(x_5'-x_6')/2; \quad t_{11} = \alpha^{-1}(y_6'-y_5')/2,
\end{aligned} \quad (3)$$

where

$$\alpha = mc_o/Mb_o, \text{ and } \gamma = c_o/a_o. \quad (3a)$$

Combination of Eqs. (1') and (2') with the above definitions of symmetry coordinates leads to the following expressions for the $3N$, or twenty-one displacement coordinates:

$$\begin{aligned}
x_1' &= u_1+w_5-(1/2)[2\beta s_8-s_9+4\beta s_{10}+s_{11}],\\
x_2' &= -u_1-w_5-(1/2)[2\beta s_8-s_9+4\beta s_{10}+s_{11}],\\
x_3' &= v_4-(1/2)[2\beta s_8+s_9+4\beta s_{10}-s_{11}],\\
x_4' &= -v_4-(1/2)[2\beta s_8+s_9+4\beta s_{10}-s_{11}],\\
x_5' &= s_{10}+\alpha s_{11},\\
x_6' &= s_{10}-\alpha s_{11},\\
x_7' &= s_8.\\
y_1' &= -v_4-(1/2)[2\beta t_8+t_9+4\beta t_{10}-t_{11}],\\
y_2' &= v_4-(1/2)[2\beta t_8+t_9+4\beta t_{10}-t_{11}],\\
y_3' &= -u_1+w_5-(1/2)[2\beta t_8-t_9+4\beta t_{10}+t_{11}],
\end{aligned}$$

[5] C. Eckart, Phys. Rev. **47**, 552 (1932).
[6] E. B. Wilson, Jr. and J. B. Howard, J. Chem. Phys. **4**, 260 (1936).
[7] It cannot also be true, in general, that the coordinate axes remain instantaneously principal axes of inertia, but such a condition could be imposed in place of condition (b).

$$
\begin{aligned}
y_4' &= u_1 - w_5 - (1/2)[2\beta t_8 - t_9 + 4\beta t_{10} + t_{11}],\\
y_5' &= t_{10} - \alpha t_{11},\\
y_6' &= t_{10} + \alpha t_{11},\\
y_7' &= t_8.\\
z_1' &= u_2 - \beta[w_6 + 2w_7] + \gamma s_9,\\
z_2' &= u_2 - \beta[w_6 + 2w_7] - \gamma s_9,\\
z_3' &= -u_2 - \beta[w_6 + 2w_7] + \gamma t_9,\\
z_4' &= -u_2 - \beta[w_6 + 2w_7] - \gamma t_9,\\
z_5' &= u_3 + w_7,\\
z_6' &= -u_3 + w_7,\\
z_7' &= w_6,
\end{aligned}
\tag{4}
$$

where

$$\beta = \frac{M}{4m}, \tag{4a}$$

while α and γ are as defined in Eqs. (3a).

The vibrational kinetic energy T_v must be of symmetry species A_1 and is given by the expression:[8]

$$2T_v = \sum_{r=1}^{7} m_r(\dot{x}_r^2 + \dot{y}_r^2 + \dot{z}_r^2).$$

In terms of the intermediate symmetry coordinates this becomes:

$$
\begin{aligned}
2T_v = &\sum_{i=1}^{3}[\mu_i \dot{u}_i^2 + 2\sum_{i'>i}\mu_{i,i'}\dot{u}_i\dot{u}_{i'}] + \mu_j \dot{v}_j^2\\
&+ \sum_{k=5}^{7}[\mu_k \dot{w}_k^2 + 2\sum_{k'>k}\mu_{kk'}\dot{w}_k\dot{w}_{k'}]\\
&+ \sum_{l=8}^{11}[\mu_l(\dot{s}_l^2 + \dot{t}_l^2) + 2\sum_{l'>l}\mu_{ll'}(\dot{s}_l\dot{s}_{l'} + \dot{t}_l\dot{t}_{l'})],
\end{aligned}
\tag{5}
$$

in which the non-vanishing mass coefficients are

$$
\begin{aligned}
&\mu_1 = \mu_2 = \mu_4 = \mu_5 = 4m; \quad \mu_3 = 2M;\\
&\mu_6 = \mu_8 = M(1+\beta); \quad \mu_7 = \mu_{10} = 2M(1+2\beta);\\
&\mu_9 = m(1+2\gamma^2); \quad \mu_{11} = m(1+8\alpha^2\beta);\\
&\mu_{6,7} = \mu_{8,10} = 2M\beta; \quad \mu_{9,11} = -m,
\end{aligned}
\tag{5a}
$$

if α, β, and γ are as defined in Eqs. (3a) and (4a).

The harmonic or zero-order potential energy function U_o must be of symmetry species A_1 and is given by the following general expression,

$$
\begin{aligned}
2U_0 = &\sum_{i=1}^{3}[k_i u_i^2 + 2\sum_{i'>i}k_{i,i'}u_i u_{i'}] + k_j v_j^2\\
&+ \sum_{k=5}^{7}[k_k w_k^2 + 2\sum_{k'>k}k_{k,k'}w_k w_{k'}]\\
&+ \sum_{l=8}^{11}[k_l(s_l^2 + t_l^2) + \sum_{l'>l}k_{l,l'}(s_l s_{l'} + t_l t_{l'})],
\end{aligned}
\tag{6}
$$

in which the generalized force constants, k_i, etc., must be determined from data and can be given in terms of physical force constants of the valence type. Since there are twenty-three generalized force constants and only fifteen fundamental frequencies, some approximations must be made in the evaluation of the force constants or some of them must be evaluated from data on isotopic molecules.

IV. THE NORMAL MODES OF VIBRATION

The frequencies, ω_n, of the normal or characteristic modes of vibration of the molecular model are obtained from the solution of Lagrange's determinantal equation, $|\lambda T_v - U_o| = 0$, where $\lambda_n = 4\pi^2 c^2 \omega_n^2$, if c is velocity of light in cm/sec., and ω_n is the frequency in cm^{-1}. The steps of the secular determinant associated with the various symmetry species have the following forms:

A_1:
$$\begin{vmatrix} \lambda\mu_1 - k_1 & -k_{1,2} & -k_{1,3} \\ -k_{1,2} & \lambda\mu_2 - k_2 & -k_{2,3} \\ -k_{1,3} & -k_{2,3} & \lambda\mu_3 - k_3 \end{vmatrix} = 0. \tag{7a}$$

A_2: None.

B_1:
$$\begin{vmatrix} \lambda\mu_4 - k_4 \end{vmatrix} = 0. \tag{7b}$$

B_2:
$$\begin{vmatrix} \lambda\mu_5 - k_5 & -k_{5,6} & -k_{5,7} \\ -k_{5,6} & \lambda\mu_6 - k_6 & \lambda\mu_{6,7} - k_{6,7} \\ -k_{5,7} & \lambda\mu_{6,7} - k_{6,7} & \lambda\mu_7 - k_7 \end{vmatrix} = 0. \tag{7c}$$

[8] In the remainder of this paper, coordinates of species A_1 will be denoted by subscripts $i=1$, 2, or 3; B_1 by $j=4$; B_2 by $k=5$, 6, or 7; and E by $l=8$, 9, 10, or 11.

$$E: \begin{vmatrix} \lambda\mu_8-k_8 & -k_{8,9} & \lambda\mu_{8,10}-k_{8,10} & -k_{8,11} \\ -k_{8,9} & \lambda\mu_9-k_9 & -k_{9,10} & \lambda\mu_{9,11}-k_{9,11} \\ \lambda\mu_{8,10}-k_{8,10} & -k_{9,10} & \lambda\mu_{10}-k_{10} & -k_{10,11} \\ -k_{8,11} & \lambda\mu_{9,11}-k_{9,11} & -k_{10,11} & \lambda\mu_{11}-k_{11} \end{vmatrix} = 0. \tag{7d}$$

The following relations among the frequencies of various symmetry species can be obtained from expansion of the steps of the secular determinant:

$$\lambda_1+\lambda_2+\lambda_3=(k_1/\mu_1)+(k_2/\mu_2)+(k_3/\mu_3),$$

$$A_1: \quad \lambda_1\lambda_2+\lambda_1\lambda_3+\lambda_2\lambda_3 = [(k_1k_2-k_{1,2}^2)/(\mu_1\mu_2)] + [(k_1k_3-k_{1,3}^2)/(\mu_1\mu_3)] + [(k_2k_3-k_{2,3}^2)/(\mu_2\mu_3)], \tag{8a}$$

$$\lambda_1\lambda_2\lambda_3=[k_1k_2k_3+2k_{1,2}k_{1,3}k_{2,3}-k_1k_{2,3}^2-k_2k_{1,3}^2-k_3k_{1,2}^2]/(\mu_1\mu_2\mu_3).$$

$$B_1: \quad \lambda_4=(k_4/\mu_4). \tag{8b}$$

$$\lambda_5+\lambda_6+\lambda_7=[(\mu_6k_7+\mu_7k_6-2\mu_{6,7}k_{6,7})/(\mu_6\mu_7-\mu_{6,7}^2)]+(k_5/\mu_5),$$

$$B_2: \quad \lambda_5\lambda_6+\lambda_5\lambda_7+\lambda_6\lambda_7=[\mu_5(k_6k_7-k_{6,7}^2) + \mu_6(k_5k_7-k_{5,7}^2)+\mu_7(k_5k_6-k_{5,6}^2) + 2\mu_{6,7}(k_{5,6}k_{5,7}-k_5k_{6,7})]/[\mu_5(\mu_6\mu_7-\mu_{6,7}^2)], \tag{8c}$$

$$\lambda_5\lambda_6\lambda_7=[k_5k_6k_7+2k_{5,6}k_{5,7}k_{6,7}-k_5k_{6,7}^2-k_6k_{5,7}^2-k_7k_{5,6}^2]/[\mu_5(\mu_6\mu_7-\mu_{6,7}^2)].$$

Similar relations, too long to record here, can be obtained for the frequencies of species E.

The following equations give the trasnformations from the intermediate coordinates of Eq. (3) to the normal coordinates, Q_n: for species A_1,

$$u_r=\sum_{i=1}^{3} n_{ri}Q_i, \quad r=1, 2, 3, \tag{9}$$

where n_{ri} is the normalized cofactor of the ir element of the secular determinant in Eq. (7a) with $\lambda=\lambda_i$; for species B_1,

$$v_4=n_{44}Q_4, \tag{10}$$

where

$$n_{44}=\mu_4^{-\frac{1}{2}};$$

for species B_2,

$$w_r=\sum_{k=5}^{7} n_{rk}Q_k, \tag{11}$$

where n_{rk} is the normalized cofactor of the kr element of the secular determinant in Eq. (7c) with $\lambda=\lambda_k$; for species E,

$$s_{rx}=\sum_{l=8}^{11} n_{rl}Q_{lx}, \tag{12a}$$

$$t_{ry}=\sum_{l=8}^{11} n_{rl}Q_{ly}, \tag{12b}$$

where n_{rl} is the normalized cofactor of the lr element of the secular determinant in Eq. (7d) with $\lambda=\lambda_l$. In terms of the normal coordinates, the kinetic and harmonic potential energies of vibration become

$$T=(1/2)\left\{\sum_{i=1}^{3}\dot{Q}_i^2+\dot{Q}_4^2+\sum_{k=5}^{7}\dot{Q}_k^2 + \sum_{l=8}^{11}(\dot{Q}_{lx}^2+\dot{Q}_{ly}^2)\right\}, \tag{13}$$

and

$$U_o=(1/2)\left\{\sum_{i=1}^{3}\lambda_iQ_i^2+\lambda_4Q_4^2+\sum_{k=5}^{7}\lambda_kQ_k^2 + \sum_{l=8}^{11}\lambda_l(Q_{lx}^2+Q_{ly}^2)\right\}. \tag{14}$$

It is convenient to introduce dimensionless coordinates q_n, which are given by the transformation, $Q_n=(\hbar/2\pi c\omega_n)^{\frac{1}{2}}q_n$, and in terms of which the zero-order vibrational energy is given in the

Hamiltonian form as

$$H_{ov}=(hc/2)\Big\{\sum_{i=1}^{3}\omega_i[(p_i^2/\hbar^2)+q_i^2]$$
$$+\omega_4[(p_4^2/\hbar^2)+q_4^2]$$
$$+\sum_{k=5}^{7}\omega_k[(p_k^2/\hbar^2)+q_k^2]$$
$$+\sum_{l=8}^{11}\omega_l[(p_{lx}^2+p_{ly}^2)/\hbar^2$$
$$+(q_{lx}^2+q_{ly}^2)]\Big\}. \quad (15)$$

The normal modes of oscillation of the allene model are illustrated in Fig. 2. The actual modes of species A_1 are not necessarily those shown in the diagram, but they will be linear combinations of the three shown. Similar remarks hold for species B_2 and E.

V. ANHARMONIC POTENTIAL FUNCTION

Since each term in the expression for the total energy must belong to symmetry type A_1, it can be shown by direct multiplication of the characters in Table II that the cubic combinations of normal coordinates occurring in the anharmonic potential function of a molecule belonging to symmetry group D_{2d} are: A_1^3, $[A_2^2A_1]$, $B_1^2A_1$,

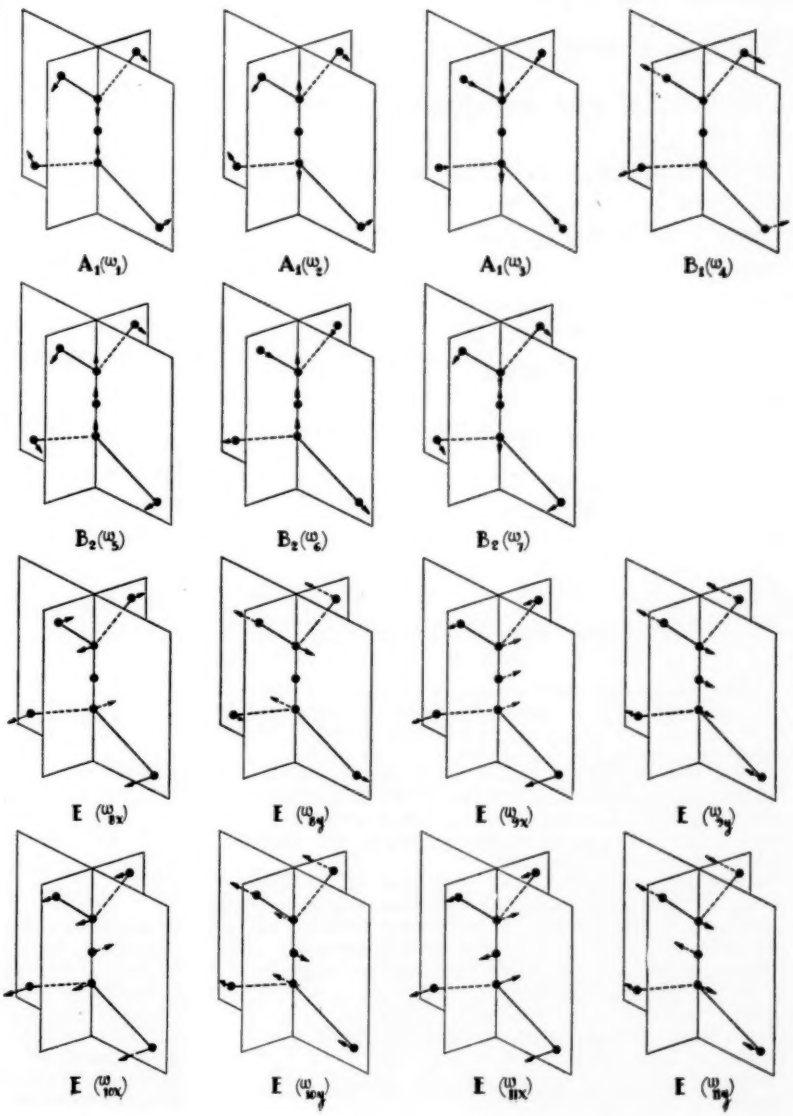

FIG. 2. Normal modes of vibration of the allene molecular model.

$B_2^2A_1$, $[A_2B_1B_2]$, $A_1A_1^{(2)}$, $[A_2A_2^{(2)}]$, $B_1B_2^{(2)}$, and $B_2B_2^{(2)}$. Likewise the quartic combinations occurring are: A_1^4, $A_1^2A_1^{(2)}$, $(A_1^{(2)})^2$, $[A_2^4]$, $(A_2^{(2)})^2$, B_1^4, $(B_1^{(2)})^2$, B_2^4, $(B_2^{(2)})^2$, $[A_1^2A_2^2]$, $A_1^{(2)}A_2^2$, $A_1^2B_1^2$, $A_1^{(2)}B_1^2$, $A_1^2B_2^2$, $A_1^{(2)}B_2^2$, $[A_2^2B_1^2]$, $[A_2^2B_2^2]$, $B_1^2B_2^2$, $A_1A_2B_1B_2$ and $A_2^{(2)}B_1B_2$. The terms in square brackets, such as $[A_2^2A_1]$, do not occur in the case of allene because there is no normal coordinate of first degree of type A_2. The designations $X^{(2)}$ are used to refer to the quadratic combinations of degenerate normal coordinates of the various symmetry types.[9]

The most general cubic portion U_1 of the anharmonic potential function of the allene molecular model is given by:[10]

$$\begin{aligned}U_1/hc=&\sum_i\{\beta_{iii}q_i^3+\sum_{i'}\beta_{iii'}q_i^2q_{i'}\\&+\sum_{i'}\sum_{i''}\beta_{ii'i''}q_iq_{i'}q_{i''}+\beta_{ijj}q_jq_j^2\\&+\sum_k\beta_{ikk}q_iq_k^2+\sum_k\sum_{k'}\beta_{ikk'}q_iq_kq_{k'}\\&+\sum_l\beta_{ill}q_i(q_{lx}^2+q_{ly}^2)\\&+\sum_l\sum_{l'>l}\beta_{ill'}q_i(q_{lx}q_{l'x}+q_{ly}q_{l'y})\}\\&+\sum_l\{\beta_{jll}q_jq_{lx}q_{ly}\\&+\sum_{l'>l}\beta_{jll'}q_j(q_{lx}q_{l'y}+q_{l'x}q_{ly})\}\\&+\sum_k\sum_l\{\beta_{kll}q_k(q_{lx}^2-q_{ly}^2)\\&+\sum_{l'>l}\beta_{kll'}q_k(q_{lx}q_{l'x}-q_{ly}q_{l'y})\}.\end{aligned}\tag{16}$$

To second-order approximation[11] the quartic portion U_2 of the anharmonic potential function is given by:[10]

$$\begin{aligned}U_2/hc=&\sum_i\{\gamma_{iiii}q_i^4+\sum_{i'}\gamma_{iii'i'}q_i^3q_{i'}^2\}+\gamma_{jjjj}q_j^4\\&+\sum_k\{\gamma_{kkkk}q_k^4+\sum_{k'}\gamma_{kkk'k'}q_k^2q_{k'}^2\}\\&+\sum_l\{\gamma_{lll}(q_{lx}^2+q_{ly}^2)+\sum_{l'>l}\gamma_{ll'l'}(q_{lx}q_{l'x}+q_{ly}q_{l'y})^2\\&+\sum_{l'>l}\gamma_{ll'l'}(q_{lx}^2+q_{ly}^2)(q_{l'x}^2+q_{l'y}^2)\\&+\sum_{l'>l}\gamma_{ll'l'}(q_{lx}q_{l'y}-q_{l'x}q_{ly})^2+\gamma_{lll}q_{lx}^2q_{ly}^2\\&+\sum_{l'>l}\gamma_{ll'l'}(q_{lx}q_{l'y}+q_{l'x}q_{ly})^2+\gamma_{lll}(q_{lx}^2-q_{ly}^2)^2\\&+\sum_{l'>l}\gamma_{ll'l'}(q_{lx}^2-q_{ly}^2)(q_{l'x}^2-q_{l'y}^2)\\&+\sum_{l'>l}\gamma_{ll'l'}(q_{lx}q_{l'x}-q_{ly}q_{l'y})^2\}\\&+\sum_i\{\gamma_{iijj}q_i^2q_j^2+\sum_k\gamma_{iikk}q_i^2q_k^2\\&+\sum_l\gamma_{iill}q_i^2(q_{lx}^2+q_{ly}^2)\}+\sum_k\gamma_{jjkk}q_j^2q_k^2\\&\sum_l\gamma_{jjll}q_j^2(q_{lx}^2+q_{ly}^2)\\&+\sum_k\sum_l\gamma_{kkll}q_k^2(q_{lx}^2+q_{ly}^2).\end{aligned}\tag{17}$$

VI. VIBRATIONAL ANGULAR MOMENTUM

The components of internal angular momentum of vibration p_x, p_y, and p_z have importance in connection with the Coriolis interaction between the total and internal angular momenta and are of the same symmetry types as the components of total angular momentum. An E pair is formed between p_x and p_y, and while p_z is of type A_2. These components are defined as

$$\begin{aligned}p_x&=\textstyle\sum_r m_r(y_r'\dot z_r'-z_r'\dot y_r'),\\p_y&=\textstyle\sum_r m_r(z_r'\dot x_r'-x_r'\dot z_r'),\\p_z&=\textstyle\sum_r m_r(x_r'\dot y_r'-y_r'\dot x_r'),\end{aligned}$$

and are expressed in terms of the dimensionless normal coordinates q_k and conjugate momenta

---

[9] These quadratic combinations are as follows: $(q_{lx}^2+q_{ly}^2)$ and $(q_{lx}q_{l'x}+q_{ly}q_{l'y})$ of type $A_1^{(2)}$; $(q_{lx}q_{l'y}-q_{l'x}q_{ly})$ of type $A_2^{(2)}$; $(q_{lx}q_{ly})$ and $(q_{lx}q_{l'y}+q_{l'x}q_{ly})$ of type $B_1^{(2)}$; $(q_{lx}^2-q_{ly}^2)$ and $(q_{lx}q_{l'x}-q_{ly}q_{l'y})$ of type $B_2^{(2)}$.

[10] For the subscript notation employed see footnote 8. Primed and unprimed subscripts in a given summation refer to different coordinates of the same symmetry type. Each combination of subscripts may occur only once i.e., permutations are not allowed.

[11] The most general quartic portion of the anharmonic potential function contains the following additional terms which are of odd degree in at least one coordinate and do not ordinarily contribute to the allowed energies: $q_i^3q_{i'}$, $q_i^2q_{i'}q_{i''}$, $q_kq_{k'}q_{k''}$, $q_k^3q_{k'}$, $(q_{lx}^2+q_{ly}^2)(q_{lx}q_{l'x}+q_{ly}q_{l'y})$, $(q_{lx}^2+q_{ly}^2)(q_{l'x}q_{l''x}+q_{l'y}q_{l''y})$, $(q_{lx}q_{l'x}+q_{ly}q_{l'y})(q_{lx}q_{l''x}+q_{ly}q_{l''y})$, $(q_{lx}q_{l'x}+q_{ly}q_{l'y})(q_{l'x}q_{l''x}+q_{l'y}q_{l''y})$, $q_{lx}q_{ly}q_{l'x}q_{l'y}$, $(q_{lx}q_{l'y}-q_{l'x}q_{ly})(q_{lx}q_{l''y}-q_{l''x}q_{ly})$, $(q_{lx}q_{l'y}-q_{l'x}q_{ly})(q_{l'x}q_{l''y}-q_{l''x}q_{l'y})$, $(q_{lx}q_{l'y}+q_{l'x}q_{ly})(q_{lx}q_{l''y}+q_{l''x}q_{ly})$, $(q_{lx}q_{l'y}+q_{l'x}q_{ly})(q_{l'x}q_{l''y}+q_{l''x}q_{l'y})$, $q_{lx}q_{ly}(q_{lx}q_{l'y}+q_{l'x}q_{ly})$, $q_{lx}q_{ly}(q_{lx}q_{l'x}+q_{ly}q_{l'y})$, $(q_{lx}q_{l'x}-q_{ly}q_{l'y})(q_{lx}q_{l'x}+q_{ly}q_{l'y})$, $(q_{lx}q_{l'y}+q_{l'x}q_{ly})(q_{l'x}q_{l''y}+q_{l''x}q_{l'y})$, $(q_{lx}q_{l'x}-q_{ly}q_{l'y})(q_{lx}q_{l''x}-q_{ly}q_{l''y})$, $(q_{lx}q_{l'x}-q_{ly}q_{l'y})(q_{l'x}q_{l''x}-q_{l'y}q_{l''y})$, $(q_{lx}^2-q_{ly}^2)(q_{lx}q_{l'x}-q_{ly}q_{l'y})$, $(q_{lx}^2-q_{ly}^2)(q_{l'x}q_{l''x}-q_{l'y}q_{l''y})$, $q_i^2(q_{lx}q_{l'x}+q_{ly}q_{l'y})$, $q_iq_{i'}(q_{lx}^2+q_{ly}^2)$, $q_iq_{i'}(q_{lx}q_{l'x}-q_{ly}q_{l'y})$, $q_iq_{i'}q_j^2$, $q_j^2(q_{lx}q_{l'x}-q_{ly}q_{l'y})$, $q_i^2q_kq_{k'}$, $q_iq_{i'}q_k^2$, $q_iq_{i'}q_kq_{k'}$, $q_k^3(q_{lx}q_{l'x}+q_{ly}q_{l'y})$, $q_kq_{k'}(q_{lx}^2+q_{ly}^2)$, $q_kq_{k'}(q_{lx}q_{l'x}+q_{ly}q_{l'y})$, $q_j^2q_kq_{k'}$, $q_jq_k(q_{lx}q_{l'y}-q_{l'x}q_{ly})$.

p_h as follows:

$$
\begin{aligned}
p_x=&\sum_{i,\,l}\xi_{il}[(\omega_l/\omega_i)^{\frac{1}{2}}q_ip_{ly}-(\omega_i/\omega_l)^{\frac{1}{2}}q_{ly}p_i]\\
&+\sum_{l}\xi_{4l}[(\omega_l/\omega_4)^{\frac{1}{2}}q_4p_{lx}-(\omega_4/\omega_l)^{\frac{1}{2}}q_{lx}p_4]\\
&+\sum_{k,\,l}\xi_{kl}[(\omega_l/\omega_k)^{\frac{1}{2}}q_kp_{ly}-(\omega_k/\omega_l)^{\frac{1}{2}}q_{ly}p_k],\\
p_y=&\sum_{i,\,l}\xi_{il}[(\omega_l/\omega_i)^{\frac{1}{2}}q_ip_{lx}-(\omega_i/\omega_l)^{\frac{1}{2}}q_{lx}p_i]\\
&+\sum_{l}\xi_{4l}[(\omega_l/\omega_4)^{\frac{1}{2}}q_4p_{ly}-(\omega_4/\omega_l)^{\frac{1}{2}}q_{ly}p_4]\\
&-\sum_{k,\,l}\xi_{kl}[(\omega_l/\omega_k)^{\frac{1}{2}}q_kp_{lx}-(\omega_k/\omega_l)^{\frac{1}{2}}q_{lx}p_k] \qquad (18)\\
p_z=&\sum_{l}\zeta_l(q_{lx}p_{ly}-q_{ly}p_{lx})\\
&+\sum_{l,\,l'}\zeta_{ll'}[(\omega_{l'}/\omega_l)^{\frac{1}{2}}(q_{lx}p_{l'y}-q_{ly}p_{l'x})\\
&+(\omega_l/\omega_{l'})^{\frac{1}{2}}(q_{l'x}p_{ly}-q_{l'y}p_{lx})]\\
&+\sum_{k}\zeta_{4k}[(\omega_k/\omega_4)^{\frac{1}{2}}q_4p_k\\
&\qquad -(\omega_4/\omega_k)^{\frac{1}{2}}q_kp_4],
\end{aligned}
$$

in which the Coriolis parameters are given by the following expressions:

$$
\begin{aligned}
\xi_{il}=&2m\{[n_{2i}-(c_o/a_o)n_{1i}]n_{9l}\\
&\qquad -[n_{2i}-(c_o/b_o)n_{3i}]n_{11l}\},\\
\xi_{4l}=&-m^{\frac{1}{2}}(c_o/a_o)n_{9l},\\
\xi_{kl}=&2m(c_o/a_o)n_{5k}n_{9l}-(\mu_6n_{6k}+\mu_{6,7}n_{7k})n_{8l}\\
&\qquad -(\mu_{6,7}n_{6k}+\mu_7n_{7k})n_{10l}, \qquad (19)\\
\zeta_l=&1-2m(1+\gamma^2)n_{9l}^2-2\mu_{11}n_{11l}^2+4mn_{9l}n_{11l},\\
\zeta_{ll'}=&-2m(1+\gamma^2)n_{9l}n_{9l'}-2\mu_{11}n_{11l}n_{11l'}\\
&\qquad +2m(n_{9l}n_{11l'}+n_{11l}n_{9l'}),\\
\zeta_{4k}=&2m^{\frac{1}{2}}n_{5k}.
\end{aligned}
$$

VII. VALENCE SYMMETRY COORDINATES

The generalized symmetry coordinates defined in Eqs. (3) were used in setting up the general quadratic potential function given in Eq. (6). The generalized force constants occurring in Eq. (6) do not have obvious physical significance and are not appropriate for use in the analysis of experimental data. It has been found in many cases that a suitable potential function for analysis of data is that based on so-called valence coordinates which are changes in the lengths of valence bonds and changes in the included valence angles. For infinitesimal displacements there are linear relationships between the valence coordinates and the generalized symmetry coordinates defined in Eqs. (3). One can readily obtain linear relations between the generalized force constants in Eq. (6) and those in a valence type quadratic potential function.

The valence coordinates can best be described in terms of changes in distances between pairs of atoms. The infinitesimal change in distance δp_{mn} between the mth and nth atoms is given in terms of the original rectangular coordinates and displacements as follows:

$$
\begin{aligned}
\delta p_{mn}=&[(x_{om}-x_{on})(x_m'-x_n')\\
&+(y_{om}-y_{on})(y_m'-y_n')\\
&+(z_{om}-z_{on})(z_m'-z_n')]/p_{omn}. \qquad (20)
\end{aligned}
$$

The valence coordinates suitable for description of infinitesimal vibrations of a group of three atoms (m, n, and a central atom C) are illustrated in Fig. 3, where $r_m=r_{om}+\delta r_m$, $r_n=r_{on}+\delta r_n$, and $\beta_{mn}=\beta_{omn}+\delta\beta_{mn}$; r_m, r_n, and β_{mn} denote, respectively, the instantaneous values of the two valence bond lengths and the included bond angle, while r_{om}, r_{on}, and β_{omn} denote their equilibrium values and δr_m, δr_n, and $\delta\beta_{mn}$ denote changes occurring during vibration. The quantity $\delta\beta_{mn}$ is given for infinitesimal vibrations by

$$
\begin{aligned}
\delta\beta_{mn}=&p_{omn}\delta p_{mn}-(r_{om}-r_{on}\cos\beta_{omn})\delta r_m\\
&-(r_{on}-r_{om}\cos\beta_{omn})\delta r_n/\\
&\qquad (r_{om}r_{on}\sin\beta_{omn}), \qquad (21)
\end{aligned}
$$

where p_{mn} is the distance between atoms m and n. Additional angular coordinates required for the allene problem are defined as follows:

$$\delta\beta_t=(x_3'-x_4'+y_2'-y_1')/2a_o,$$

where $\delta\beta_t$ is the change in angle between the two CH_2 planes resulting from torsional vibration.

$$\delta\beta_{567x}=(x_5'-x_7'+x_6'-x_7')/b_o,$$

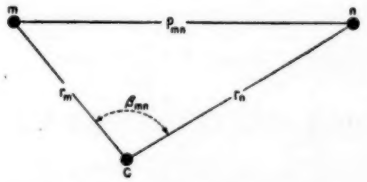

FIG. 3. Valence coordinates.

and

$$\delta\beta_{567y}=(y_5'-y_7'+y_6'-y_7')/b_o,$$

where $\delta\beta_{567x}$ and $\delta\beta_{567y}$ are, respectively, the changes in angle of the C−C−C configuration in the xz and yz planes.

$$\delta\beta_{347x}=[(x_3'+x_4'-2x_6')/2(c_o-b_o)]+(x_7'-x_6')/b_o,$$

and

$$\delta\beta_{127y}=[(y_1'+y_2'-2y_5')/2(c_o-b_o)]+(y_7'-y_5')/b_o,$$

where $\delta\beta_{347x}$ and $\delta\beta_{127y}$ are the changes in the angles between the CH_2 planes and the C−C−C line.

Following the procedure outlined by Shaffer and Herman,[12] one can obtain the combination of valence coordinates listed below for the allene type molecular model which belong to the various symmetry species.

Species A_1:

$$\begin{aligned}
\Delta_1&=(\delta r_1+\delta r_2+\delta r_3+\delta r_4)/4=\sum_{i=1}^{3}a_{1i}u_i,\\
\Delta_2&=(\delta r_5+\delta r_6)/2=\sum_{i=1}^{3}a_{2i}u_i,\\
\Delta_3&=r_o(\delta\beta_{12}+\delta\beta_{34})/4=\sum_{i=1}^{3}a_{3i}u_i,\\
\Delta_o&=r_o(\delta\beta_{17}+\delta\beta_{27}+\delta\beta_{37}+\delta\beta_{47})/4=-\Delta_3.
\end{aligned}\tag{22}$$

Species A_2: none.

Species B_1:

$$\Delta_4=a_o\delta\beta_t=2v_4.\tag{23}$$

Species B_2:

$$\begin{aligned}
\Delta_5&=(\delta r_1+\delta r_2-\delta r_3-\delta r_4)/4=\sum_{k=5}^{7}a_{5k}w_k,\\
\Delta_6&=(\delta r_6-\delta r_5)/2=\sum_{k=5}^{7}a_{6k}w_k,\\
\Delta_7&=r_o(\delta\beta_{12}-\delta\beta_{34})/4=\sum_{k=5}^{7}a_{7k}w_k,\\
\Delta'_o&=r_o(\delta\beta_{17}+\delta\beta_{27}-\delta\beta_{37}-\delta\beta_{47})/4=-\Delta_7.
\end{aligned}\tag{24}$$

[12] W. H. Shaffer and R. C. Herman, J. Chem. Phys. **12**, 494 (1944).

Species E:

$$\begin{aligned}
\Delta_{8x}&=(\delta r_1-\delta r_2)/2=\sum_{l=8}^{11}a_{8l}s_l,\\
\Delta_{8y}&=(\delta r_4-\delta r_3)/2=\sum_{l=8}^{11}a_{8l}t_l,\\
\Delta_{9x}&=b_o\delta\beta_{567x}=\sum_{l=8}^{11}a_{9l}s_l,\\
\Delta_{9y}&=b_o\delta\beta_{567y}=\sum_{l=8}^{11}a_{9l}t_l,\\
\Delta_{10x}&=(c_o-b_o)\delta\beta_{347}=\sum_{l=8}^{11}a_{10l}s_l,\\
\Delta_{10y}&=(c_o-b_o)\delta\beta_{127}=\sum_{l=8}^{11}a_{10l}t_l,\\
\Delta_{11x}&=b_o(\delta\beta_{17}-\delta\beta_{27})/2=\sum_{l=8}^{11}a_{11l}s_l,\\
\Delta_{11y}&=b_o(\delta\beta_{47}-\delta\beta_{37})/2=\sum_{l=8}^{11}a_{11l}t_l,
\end{aligned}\tag{25}$$

where

$$\begin{aligned}
&a_{1,1}=-a_{3,2}=a_{3,3}=a_o/r_o,\\
&a_{1,2}=-a_{1,3}=a_{3,1}=(c_o-b_o)/r_o,\\
&a_{2,1}=a_{2,2}=0,\quad a_{2,3}=1;
\end{aligned}\tag{22a}$$

$$\begin{aligned}
&a_{5,5}=a_0/r_0,\quad a_{6,5}=0,\quad a_{7,5}=(c_o-b_o)/r_0,\\
&a_{5,6}=-\beta a_{7,5},\quad a_{6,6}=1;\quad a_{7,6}=\beta a_{5,5},\\
&a_{5,7}=-(1+2\beta)a_{7,5},\quad a_{6,7}=-1,\\
&\qquad\qquad a_{7,7}=(1+2\beta)a_{5,5};
\end{aligned}\tag{24a}$$

$$\begin{aligned}
&a_{8,8}=-\beta(a_0/r_0),\\
&a_{8,9}=(a_o/r_o)\{(1/2)+[c_o(c_o-b_o)/a_o^2]\},\\
&a_{8,10}=-(1+2\beta)(a_0/r_0),\\
&a_{8,11}=-(1+2\alpha)(a_o/2r_o),\\
&a_{9,8}=-2,\quad a_{9,9}=0,\quad a_{9,10}=2,\quad a_{9,11}=0,\\
&a_{10,8}=(c_o/b_o)-1-\beta,\quad a_{10,9}=-\tfrac{1}{2},\\
&a_{10,10}=-(c_o/b_o)-2\beta,\\
&a_{10,11}=(1/2)+(\alpha c_o/b_o),\\
&a_{11,8}=-1+\beta\epsilon,\quad a_{11,9}=b_o(c_o+b_o)/(2r_o^2),\\
&a_{11,10}=1+(1+2\beta)\epsilon,\\
&a_{11,11}=\alpha+(1+2\alpha)(\epsilon/2),
\end{aligned}\tag{25a}$$

if, $\alpha=(mc_o/Mb_o)$, $\beta=(M/4m)$, $\gamma=c_o/a_o$, and $\epsilon=b_o(c_o-b_o)/r_o^2$.

One needs the inverse transformations giving the intermediate symmetry coordinates, u_i, v_4, w_k, s_l, and t_l defined in Eqs. (3) in terms of the valence symmetry coordinates defined above, in order to set up the kinetic and potential energy expressions in terms of the valence coordinates. These relations are given below.

$$u_i=\sum_{h=1}^{3} b_{ih}\Delta_h, \quad i=1, 2, 3; \tag{26}$$

$$v_4=b_{44}\Delta_4; \tag{27}$$

$$w_k=\sum_{h=5}^{7} b_{kh}\Delta_h, \quad k=5, 6, 7; \tag{28}$$

$$s_l=\sum_{h=8}^{11} b_{lh}\Delta_{hx}, \quad t_l=\sum_{h=8}^{11} b_{lh}\Delta_{hy} \qquad l=8, 9, 10, 11, \tag{29}$$

where

$$\begin{aligned} &b_{1,1}=-b_{2,3}=a_o/r_o,\\ &b_{1,2}=b_{3,1}=b_{3,3}=0,\\ &b_{1,3}=b_{2,1}=(c_o-b_o)/r_o,\\ &b_{2,2}=b_{3,2}=1; \end{aligned} \tag{26a}$$

$$b_{4,4}=\tfrac{1}{2}, \tag{27a}$$

$$\begin{aligned} &b_{5,5}=a_o/r_o, \quad b_{5,6}=0, \quad b_{5,7}=(c_o-b_o)/r_o,\\ &b_{6,5}=-b_{5,7}/(1+3\beta)=b_{7,5},\\ &b_{6,6}=(1+2\beta)/(1+3\beta), \quad b_{6,7}=b_{7,7}=b_{5,5}/(1+3\beta),\\ &b_{7,6}=-\beta/(1+3\beta), \end{aligned} \tag{28a}$$

and, if $\sigma_o=2m/(3M+4m)$, $\phi_o=(c_o-b_o)/b_o$, $I_{ex}=I_{cy}=2ma_o^2+4mc_o^2+2Mb_o^2$, and $I_{cz}+4ma_o^2$,

$$\begin{aligned} &b_{8,8}=-(a_o/r_o)\sigma_o,\\ &b_{8,9}=-(c_o\sigma_o/b_o)(1+2^{-1}\alpha^{-1}),\\ &b_{8,10}=-\sigma_0, \quad b_{8,11}=\sigma_o\phi_o,\\ &b_{9,8}=(a_ob_o/r_oc_o)[\phi_o+(I_{cz}/2I_{ex})],\\ &b_{9,9}=-(a_o^2/2b_o^2)[1-(I_{cz}/2I_{ex})],\\ &b_{9,10}=-(I_{cz}/2I_{ex}),\\ &b_{9,11}=(a_o^2/b_oc_o)[1-(a_o^2+b_oc_o\phi_o)(I_{cz}/2a_o^2I_{ex})], \end{aligned} \tag{29a}$$

$$\begin{aligned} &b_{10,8}=-a_o\sigma_o/r_o, \quad b_{10,9}=\sigma_0(\beta-\phi_0),\\ &b_{10,10}=-\sigma_0, \quad b_{10,11}=\sigma_0\phi_0,\\ &b_{11,8}=-(a_ob_o/r_oc_o)b_{11,10},\\ &b_{11,9}=-(a_o^2/2b_oc_o)b_{11,10}, \quad b_{11,10}=2Mb_o^2/I_{cz},\\ &b_{11,11}=[(a_o^2/b_oc_o)-\phi_o]b_{11,10}. \end{aligned}$$

The vibrational kinetic energy, T_v, can be written in terms of the valence symmetry coordinates with the aid of Eqs. (26)–(29) and Eq. (5) and is given by the following relation:

$$\begin{aligned} 2T=&\sum_{i=1}^{3}[M_i\dot{\Delta}_i^2+2\sum_{i'>i}M_{ii'}\dot{\Delta}_i\dot{\Delta}_{i'}]+M_4\dot{\Delta}_4^2\\ &+\sum_{k=5}^{7}[M_k\dot{\Delta}_k^2+2\sum_{k'>k}M_{kk'}\dot{\Delta}_k\dot{\Delta}_{k'}]\\ &+\sum_{h=8}^{11}[M_h(\dot{\Delta}_{hx}^2+\dot{\Delta}_{hy}^2)\\ &+2\sum_{h'>h}M_{hh'}(\dot{\Delta}_{hx}\dot{\Delta}_{h'x}+\dot{\Delta}_{hy}\dot{\Delta}_{h'y})], \end{aligned} \tag{30}$$

where, if $\sum_o=4m+3M$,

$$\begin{aligned} &M_1=M_3=4m, \quad M_2=4m+2M,\\ &M_{1,2}=4m[(c_o-b_o)/r_o], \quad M_{1,3}=0,\\ &M_{2,3}=-4m(a_o/r_o);\\ &M_4=m;\\ &M_5=(4m/\textstyle\sum_o)[3M+4m(a_o/r_o)^2],\\ &M_6=(2M/\textstyle\sum_o)(2m+M),\\ &M_7=(4m/\textstyle\sum_o)[3M+4m(c_o-b_o)^2/r_o^2],\\ &M_{5,6}=-(4mM/\textstyle\sum_o)[(c_o-b_o)/r_o],\\ &M_{6,7}=(4mM/\textstyle\sum_o)(a_o/r_o),\\ &M_{5,7}=(16m^2/\textstyle\sum_o)(a_o/r_o)[(c_o-b_o)/r_o], \end{aligned}$$

and

$$\begin{aligned} M_h=&\sum_{l=8}^{11}\mu_lb_{lh}^2+2\mu_{8,10}b_{8h}b_{10h}+2u_{9,11}b_{9h}b_{11h},\\ M_{hh'}=&\sum_{l=8}^{11}\mu_lb_{lh}b_{hh'}+\mu_{8,10}(b_{8h}b_{10h'}+b_{8h'}b_{10h})\\ &+\mu_{9,11}(b_{9h}b_{11h'}+b_{9h'}b_{11h}). \end{aligned}$$

VIII. VALENCE POTENTIAL FUNCTION

The most general quadratic potential function, U_o, satisfying the symmetry conditions is given

in terms of the valence symmetry coordinates by:

$$2U_0=\sum_{i=1}^{3}[K_i\Delta_i^2+2\sum_{i'>i}K_{ii'}\Delta_i\Delta_{i'}]+K_4\Delta_4^2$$
$$+\sum_{k=i}^{7}[K_k\Delta_k^2+2\sum_{k'>k}K_{kk'}\Delta_k\Delta_{k'}]$$
$$+\sum_{h=8}^{11}[K_h(\Delta_{hx}^2+\Delta_{hy}^2)$$
$$+\sum_{h'>h}K_{hh'}(\Delta_{hx}\Delta_{h'x}+\Delta_{hy}\Delta_{h'y})], \quad (31)$$

in which the cross products occur only among symmetry coordinates of the same species. The complete valence-type potential function U_o for the allene molecular model can be written in terms of the valence coordinates as

$$2U_o=c_1[(\delta r_1)^2+(\delta r_2)^2+(\delta r_3)^2+(\delta r_4)^2]$$
$$+c_1'[(\delta r_5)^2+(\delta r_6)^2]$$
$$+c_2r_o^2[(\delta\beta_{12})^2+(\delta\beta_{34})^2]+c_2'a_o^2(\delta\beta_t)^2$$
$$+c_2''b_o^2[(\delta\beta_{567x})^2+(\delta\beta_{567})^2]$$
$$+c_2'''(c_o-b_o)^2[(\delta\beta_{347})^2+(\delta\beta_{127})^2]$$
$$+c_2^{\mathrm{iv}}b_o^2[(\delta\beta_{17})^2+(\delta\beta_{27})^2+(\delta\beta_{37})^2+(\delta\beta_{47})^2]$$
$$+c_3(\delta r_1\delta r_2+\delta r_3\delta r_4)$$
$$+c_3'(\delta r_1+\delta r_2)(\delta r_3+\delta r_4)+c_3'''\delta r_5\delta r_6$$
$$+c_3'''[(\delta r_1+\delta r_2)\delta r_5+(\delta r_3+\delta r_4)\delta r_6]$$
$$+c_3^{\mathrm{iv}}[(\delta r_1+\delta r_2)\delta r_6+(\delta r_3+\delta r_4)\delta r_5]$$
$$+c_4r_o[(\delta r_1+\delta r_2)\delta\beta_{12}+(\delta r_3+\delta r_4)\delta\beta_{34}]$$
$$+c_4'r_o[(\delta r_1+\delta r_2)\delta\beta_{34}+(\delta r_3+\delta r_4)\delta\beta_{12}]$$
$$+c_4''r_o[\delta r_5\delta\beta_{14}+\delta r_6\delta\beta_{34}]$$
$$+c_4'''r_o[\delta r_5\delta\beta_{34}+\delta r_6\delta\beta_{12}]$$
$$+c_5b_o[(\delta r_1-\delta r_2)\delta\beta_{567x}+(\delta r_4-\delta r_3)\delta\beta_{567y}]$$
$$+c_5'(c_o-b_o)[(\delta r_1-\delta r_2)\delta\beta_{347}$$
$$+(\delta r_4-\delta r_3)\delta\beta_{127}]$$
$$+c_5''b_o[(\delta r_1-\delta r_2)(\delta\beta_{17}-\delta\beta_{27})$$
$$+(\delta r_4-\delta r_3)(\delta\beta_{47}-\delta\beta_{37}]+c_6r_o^2\delta\beta_{12}\delta\beta_{34}$$
$$+c_6'b_o^2(\delta\beta_{17}\delta\beta_{27}+\delta\beta_{37}\delta\beta_{47})$$
$$+c_6''b_o(c_o-b_o)[\delta\beta_{567x}\delta\beta_{347}+\delta\beta_{567y}\delta\beta_{127}]$$
$$+c_6'''b_o^2[\delta\beta_{567x}(\delta\beta_{17}-\delta\beta_{27})$$
$$+\delta\beta_{567y}(\delta\beta_{47}-\delta\beta_{37})]$$
$$+c_6^{\mathrm{iv}}b_o(c_o-b_o)[\delta\beta_{347}(\delta\beta_{17}-\delta\beta_{27})$$
$$+\delta\beta_{127}(\delta\beta_{47}-\delta\beta_{37})], \quad (32)$$

where

$$K_1=2(2c_1+c_3+2c_3'),$$
$$K_2=2c_1'+c_3',$$
$$K_3=4(2c_2+c_6),$$
$$K_{1,2}=2(c_3'''+c_3^{\mathrm{iv}}),$$
$$K_{1,3}=4(c_4+c_4'),$$
$$K_{2,3}=2(c_4''+c_4'''),$$
$$K_4=c_2',$$
$$K_5=2(2c_1+c_3-2c_3'),$$
$$K_6=2c_1'-c_3',$$
$$K_7=4(2c_2-c_6),$$
$$K_{5,6}=2(c_3^{\mathrm{iv}}-c_3'''),$$
$$K_{5,7}=4(c_4-c_4'), \quad (32a)$$
$$K_{6,7}=2(c_4'''-c_4''),$$
$$K_8=2c_1-c_3,$$
$$K_9=c_2'',$$
$$K_{10}=c_2''',$$
$$K_{11}=4c_2^{\mathrm{iv}}=2c_6',$$
$$K_{8,9}=c_5,$$
$$K_{8,10}=c_5',$$
$$K_{8,11}=c_5'',$$
$$K_{9,10}=c_6''/2,$$
$$K_{9,11}=c_6''',$$
$$K_{10,11}=c_6^{\mathrm{iv}}.$$

Substitution of Eqs. (22)–(25) into Eq. (31) and comparison of the resulting expression with Eq. (6) lead to the relations between the K's of Eq. (31) and the generalized force constants of Eq. (6); substitution of Eq. (32a) into the latter relations yields the expressions for the generalized force constants of Eq. (6) in terms of the valence force constants.

In the analysis of experimental data one must assume as a first approximation that some of the valence force constants of Eq. (32) are negligible because sufficient data are not ordinarily available to evaluate all of them accurately. One must exercise judgment in determining which of the constants to neglect.

In conclusion the authors wish to thank Mr. W. L. Drevo for his drawing of Fig. 2 and Miss Shirley Thomas for her aid in the preparation of the manuscript.

Diffusion of Radioactive Copper during Oxidation of Copper Foil

GILBERT W. CASTELLAN AND WALTER J. MOORE
Department of Chemistry, The Catholic University of America, Washington, D. C.

(Received July 8, 1948)

Strips of copper foil were plated with a thin deposit of radioactive copper and the specimens then oxidized in air at 800°, 900°, 1000°C. From the distribution of radioactive copper in the oxide diffusion coefficients, D, for cuprous ion in cuprous oxide were calculated. Over the temperature range D was found to be $0.0358 \exp(-37{,}000/RT)$ cm² sec.$^{-1}$. The activation energy for the oxidation of copper is 39 ± 2 kcal./mole, so that these measurements provide further evidence that diffusion of Cu^+ in Cu_2O is the rate-determining step in the oxidation.

BARDEEN, Brattain, and Shockley[1] have recently determined the distribution, after oxidation in air at 1000°C, of radioactive copper deposited in a thin layer on a copper blank. The results were interpreted in terms of Wagner's[2] theory of oxidation. We have made more extensive measurements of the same kind over a range of temperatures, and from our data have derived values for the diffusion coefficient of Cu^+ in Cu_2O under the conditions of the oxidation process.

EXPERIMENTAL PROCEDURE

Copper 64, a β-emitter of 12.8-hours half-life, was prepared by a d, p reaction with copper 63. We are indebted to Dr. D. B .Cowie and Dr. M. A. Tuve of the Carnegie Institution of Washington for their kind cooperation in supplying this material. After separation from the cyclotron target, the copper was precipitated as thiocyanate, ignited to CuO, and made up into a cyanide plating solution.[3] The copper was plated at 6 volts and a current density of 4 ma/cm² on both sides of a strip of copper foil $2 \times 7.5 \times 0.005$ cm. The calculated thickness of the deposit of copper was around 10^{-5} cm. The total count, measured with a Victoreen VG-10 Geiger counter and a Herbach and Rademann GL532B scaling circuit, was 3000 to 4000 counts per minute.

After weighing, the strips were suspended in air in a furnace for times varying from 0.50 to 2.00 minutes. The temperature was controlled manually within ±5°C. Oxidations were made at 800°, 900°, and 1000°C. The time required for the thin strip to reach the furnace temperature uniformly was calculated on the assumption that the slow step in the heating is conduction of heat from the surface to the interior. This time was of the order of 4×10^{-2} second.

After oxidation, the strip was reweighed, the calculated thickness of the oxide being 1 to 2×10^{-3} cm. One side of the active area was coated with Glyptal, and the strip was dried in an oven at 100°C. The exposed active area was etched in 1:3 hydrochloric acid to remove successive layers of the oxide. Four etchings were made. The copper in the solutions was precipitated as CuCNS, which was filtered off on filter paper, dried, and counted on the filter paper. The precipitate was then dissolved and analyzed colorimetrically for copper. The total copper found by analysis was generally a few percent

TABLE I. Typical data showing the distribution of radioactivity in the different layers of Cu_2O. Layers are numbered beginning at the oxide-gas interface. Count is corrected for background.

800° Layer No.	% total thickness	% total count	900° Layer No.	% total thickness	% total count	1000° Layer No.	% total thickness	% total count
1	32	50	1	17	27	1	25	43
2	28	34	2	19	26	2	24	35
3	32	13	3	27	20	3	24	15
4	8	3	4	37	27	4	27	7
Total thickness: 1.12×10^{-3} cm			Total thickness: 2.19×10^{-3} cm			Total thickness: 2.12×10^{-3} cm		
Total time: 120 sec.			Total time: 120 sec.			Total time: 30 sec.		
1	33	55	1	21	34	1	34	58
2	43	35	2	24	38	2	33	32
3	24	10	3	26	20	3	22	7
4	—	—	4	29	8	4	11	3
Total thickness: 0.91×10^{-3} cm			Total thickness: 2.36×10^{-3} cm			Total thickness: 2.15×10^{-3} cm		
Total time: 120 sec.			Total time: 120 sec.			Total time: 30 sec.		

[1] J. Bardeen, W. H. Brattain, and W. Shockley, J. Chem. Phys. **14**, 714 (1946).
[2] C. Wagner and K. Grunewald, Zeits. f. physik. Chemie **B40**, 455 (1938).
[3] H. J. Creighton and W. A. Koehler, *Principles and Applications of Electrochemistry* (John Wiley and Sons, Inc., New York, 1935), Vol. II, p. 117.

TABLE II. Values of the diffusion coefficient computed from the data of Table I by the use of Eq. (2).

800°C		900°C		1000°C	
Layer No.	$D\times10^{10}$	Layer No.	$D\times10^{10}$	Layer No.	$D\times10^{10}$
1	11.8	1	48.5	1	145
2	9.5	2	49.6	2	120
3	9.4	3	65.2	3	122
1	6.6	1	52.9	1	137
2	7.4	2	40.3	2	128
1	10.7	3	38.2	3	130
2	8.4			*1	(145)
1	11.4			*2	(123)
2	9.1			*3	(115)
Average: 9.4±1.3		Average: 49.1±6.8		Average: 130±7	

* Data of Bardeen *et al.*

higher than that calculated from the weight gain on oxidation, indicating, perhaps, a slight attack on the underlying copper during etching.

RESULTS AND DISCUSSION

Typical data from the experiments are tabulated in Table I. In order to evaluate diffusion coefficients from these data, the solution of the diffusion equation for diffusion into a semi-infinite solid from an instantaneous plane source was employed.[4] This has the form

$$C=\frac{Q}{(\pi Dt)^{\frac{1}{2}}}\exp(-x^2/4Dt), \qquad (1)$$

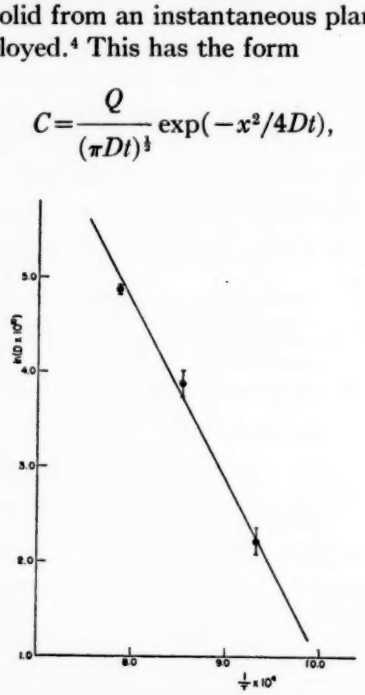

FIG. 1. Variation of D with temperature.

[4] R. M. Barrer, *Diffusion in and through Solids* (Cambridge University Press, Teddington, England, 1941), p. 43 ff.

where C is the concentration of radioactive copper at the point x, Q is the total quantity of radioactive copper, D is the diffusion coefficient, t is the time of the diffusion, and the origin is at the oxide-gas interface.

The use of Eq. (1) is equivalent to the physical assumption that the distribution of the radioactive copper throughout the oxide will be essentially the same as would be obtained if an equivalent amount of radioactive cuprous oxide were deposited on top of a cuprous oxide strip and this specimen maintained at temperature for a time equal to that in the oxidation experiments. This assumption seems reasonable in view of the fact that the thickness of radioactive copper originally deposited on the strip is very much less than the thickness of oxide finally obtained; as a result, the thickness corresponding to the original active deposit is oxidized in a time which is (roughly) less than one-thousandth of the total time of oxidation. Hence, it seems that the great part of the diffusion of the radioactive Cu^+ must be from an active layer of oxide into another layer of oxide. The approximation of the semi-infinite solid is supported by the observed approach of the activity in the layer adjacent to the metal interface to a low value. It is true, of course, that the cuprous oxide which is being studied is not ordinary equilibrium Cu_2O, so that the diffusion coefficient is not necessarily that for equilibrium Cu_2O, but rather that for the particular slab of Cu_2O formed on oxidation.

Equation (1) can be brought into convenient form for calculation by dividing through by Q and integrating from a to b to give the fraction of activity between a and b. The result is

$$\int_a^b \frac{C}{Q}dx=f_{ab}=H\left(\frac{b}{2(Dt)^{\frac{1}{2}}}\right)-H\left(\frac{a}{2(Dt)^{\frac{1}{2}}}\right), \qquad (2)$$

where f_{ab} is the fraction of activity between a and b, and $H(t)$ is the error function. Since f_{ab}, a, b, and t are known, D can be calculated.

Table II shows the values of D at the three temperatures and the average values. The value of D has also been computed from the data of Bardeen, Brattain, and Shockley. This value is within 2 percent of our value at 1000°C. Although the values of D vary from layer to layer, there is not a very marked dependence on layer number.

In Fig. 1, the logarithm of D is plotted against $1/T$, and a straight line has been drawn through the points. From the slope of the line an activation energy of 37 kcal. is obtained for the diffusion.

This energy of activation for the diffusion agrees within experimental error with the energy of activation of the oxidation reaction. The data of Pilling and Bedworth[5] yield an energy of activation of 40 kcal.[6] between 800 and 1000°C. The weight gain data from the present experiment correspond to an energy of activation of 38 ± 3 kcal. These activation energies provide additional evidence that diffusion of copper in cuprous oxide is the rate determining step in the oxidation reaction.

The Eyring equation[7] for the diffusion constant is

$$D=d^2\frac{kT}{h}\exp(\Delta S^{\neq}/R)\exp(-\Delta H^{\neq}/RT). \quad (3)$$

The value of the frequency factor calculated from Fig. 1 is 0.0358 cm^2 sec.$^{-1}$. If the observed energy of activation is set equal to $\Delta H^{\neq}$, and d is taken as the equilibrium separation of the Cu^+ ions in Cu_2O (3.01×10^{-8} cm), the entropy of activation, $\Delta S^{\neq}$, from Eq. (3), is 0.8 e.u.

The value of D at 1000°C can be calculated from the theoretical expressions

$$v=\sigma\tau/en, \quad (4)$$

$$eD=vkT. \quad (5)$$

Here v is the mobility of the Cu^+ ion, σ is the electrical conductivity of Cu_2O, τ is the transport number of the Cu^+ ions, n is the number of copper ions per cc in Cu_2O. The experimental values of these quantities are[8] $\sigma=4.8$ ohm^{-1} cm^{-1}, $\tau=4\times10^{-4}$, $n=5.05\times10^{22}$/cc. This calculation yields a value for D at 1000°C of 260×10^{-10} cm^2 sec.$^{-1}$, as compared with our average value of 130×10^{-10} cm^2 sec.$^{-1}$. This difference might be ascribed to the fact that Eq. (5) is derived for a condition of no net flow of current, while the apparent diffusion coefficient is measured during growth of the oxide film.

ACKNOWLEDGMENT

We wish to thank the Research Corporation for a Frederick Gardiner Cottrell grant-in-aid of research.

[5] N. E. Pilling and R. E. Bedworth, J. Inst. Metals **29**, 529 (1923).

[6] N. F. Mott and R. W. Gurney, *Electronic Processes in Ionic Crystals* (Oxford University Press, London, 1940), p. 254 ff. See also J. S. Dunn, Proc. Roy. Soc. (A) **111**, 203 (1926).

[7] S. Glasstone, K. J. Laidler, and H. Eyring, *The Theory of Rate Processes* (McGraw-Hill Book Company, Inc., New York, 1941), p. 539.

[8] C. Wagner, Zeits. f. physik Chemie **B21**, 25 (1933).

THE JOURNAL OF CHEMICAL PHYSICS VOLUME 17, NUMBER 1 JANUARY, 1949

Hydrocarbon Ion Appearance Potentials

J. J. MITCHELL AND F. F. COLEMAN*
Beacon Laboratories of The Texas Company, Beacon, New York
(Received June 7, 1948)

Discussion of the effect of impact parameter, distribution of electron energy and transition efficiency upon the appearance potential for ions from hydrocarbons in the mass spectrometer leads to the conclusion that initial ion current onset is a correct measure of the appearance potential. In order to calibrate the appearance potential voltage scale, the spectroscopic ionization potentials for seven gases were correlated with their apparent appearance potentials to give a calibration curve. Heretofore only one gas had been used to give a simple additive constant. Appearance potentials were determined for ions from six paraffins and four olefins. For methane, ethane and propane the agreement with previous determinations is excellent. For the other hydrocarbons the values reported here are higher than those reported by others. It is concluded that dissociation energies computed from these appearance potentials are greater than true bond energies because electron collision processes give rise to excited fragments. The excitation energy appears to be greater for larger molecules.

INTRODUCTION

IT has been recognized for many years that the electron energy necessary to produce ions from gas molecules under electron bombardment is intimately connected with the energy states both of the ion and of the molecule from which it was formed. If in some way that energy could be used to determine the strengths of bonds in the molecule under study, one would be in an advantageous position for the prediction of its behavior in chemical reactions. The desire to determine molecule energy states and bond strengths has led to a considerable amount of work on hydrocarbon ion appearance potentials in the mass spectrometer.[1–18] No one can argue that the results obtained are not important. However, their interpretation in terms of energy states and bond strengths is not yet on solid ground. The difficulties arise from two sources, the problem of deducing the appearance potential accurately from the experimental data and the problem of relating the appearance potentials to molecular energy states. This paper will first discuss the former problem, then give the results obtained by applying the conclusions derived, and finally will discuss the latter problem of applying the results.

DETERMINING APPEARANCE POTENTIALS

As a first step in developing a proper interpretation of the experimental data, some thought should be given to the way in which the data are obtained. In Fig. 1 is shown schematically the ionization chamber of the mass spectrometer used in this work.** Gas molecules present are ionized by the electron beam E to give rise to the ion beam I. The electrons come from filament A and are accelerated by potentials on electrodes B and C. The ions in ion beam I will thus have been produced by electrons with an energy in electron volts numerically equal to the potential drop between A and C. Since the ionization

* Present address: U. S. Navy Electronics Laboratory, San Diego, California.

[1] S. H. Bauer and T. R. Hogness, J. Chem. Phys. **3**, 687–692 (1935).
[2] W. Bleakney, E. U. Condon and L. G. Smith, J. Phys. Chem. **41**, 197–208 (1937).
[3] C. S. Cummings and W. Bleakney, Phys. Rev. **58**, 787–792 (1940).
[4] J. M. Delfosse and W. Bleakney, Phys. Rev. **56**, 256–260 (1939).
[5] V. H. Dibeler, J. Research Nat. Bur. Stand. **38**, 329–336 (1947).
[6] J. A. Hipple and W. Bleakney, Phys. Rev. **47**, 802(A) (1935).
[7] J. A. Hipple, Phys. Rev. **53**, 530–533 (1938).
[8] J. A. Hipple and D. P. Stevenson, Phys. Rev. **63**, 121–126 (1943).
[9] R. E. Honig, J. Chem. Phys. **16**, 105–112 (1948).
[10] A. Hustrulid, P. Kusch and J. T. Tate, Phys. Rev. **54**, 1037–1044 (1938).
[11] M. B. Koffel and R. A. Lad, J. Chem. Phys. **16**, 420–422 (1948).
[12] P. Kusch, A. Hustrulid and J. T. Tate, Phys. Rev. **52**, 843–844 (1937).
[13] L. G. Smith, Phys. Rev. **51**, 263–275 (1937).
[14] D. P. Stevenson, J. Am. Chem. Soc. **65**, 209–212 (1943).
[15] D. P. Stevenson and J. A. Hipple, J. Am. Chem. Soc. **64**, 1588–1594 (1942).
[16] D. P. Stevenson and J. A. Hipple, J. Am. Chem. Soc. **64**, 2766–2768 (1942).
[17] D. P. Stevenson and J. A. Hipple, J. Am. Chem. Soc. **64**, 2769–2772 (1942).
[18] J. T. Tate, P. T. Smith and A. L. Vaughan, Phys. Rev. **48**, 525–531 (1935).

** Consolidated Engineering Corporation Type 21-101.

chamber is part of a mass spectrometer, the ion beam can be resolved so that the current due only to ions of a given mass to charge ratio will be measured. If now the gas pressure and the current in the electron beam are kept constant, then changing the potential between A and C gives rise to a change in ion current such as is shown by the points in Fig. 2. The curve defined by these points is called the ionization efficiency curve, in this case, for $C_3H_7^+$ $(m/e=43)$ from n-butane.

All of this is elementary and straightforward. However, as is generally the case with experimental data if a sufficiently open scale is used, these points lie about rather than on a smooth curve. Thus, if the scale is open enough to permit accurate location of the points, very small ion currents and instrument background are so difficult to separate that it becomes quite impossible to pick out the exact electron voltage at which ions of given m/e first appear.

TRANSFER OF ENERGY FROM ELECTRON TO MOLECULE

Various procedures can be and have been used to resolve this impasse. The most logical scheme would be one based on a hypothesis explaining the shape of the ionization efficiency curve. There are several factors which contribute to the curve shape. In what follows each will be treated as if it were the sole determining factor. The first factor to be considered is the transfer of energy from an electron to the molecule with which it collides. Oldenberg[19] has pointed out that the transfer of kinetic energy of the electron into internal energy in the molecule will start with zero probability of transfer for electrons with just the energy necessary for the formation of an ion and increase with increasing electron energy. This statement is based on a consideration of the collision process. If the electron has exactly the critical energy, it must make an exactly central impact in order to excite the molecule. As the energy of the electrons becomes larger, the allowable impact parameter increases from the zero value for central impact to values corresponding to glancing collisions. If now P is the energy of the electrons and V_0 the critical

[19] O. Oldenberg, J. Chem. Phys. **13**, 196–198 (1945).

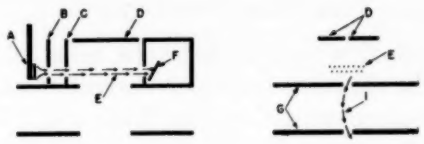

FIG. 1. Schematic cross sections (at right angles to each other) through a typical ionization chamber. A, filament supported on heavy legs; B, first electron accelerating plate; C, second electron accelerating plate; D, "pusher" plates to supply small ion ejecting field; E, electron beam; F, electron catcher; G, ion accelerating plates; and I, ion beam.

energy in electron volts and if one assumes that the molecules are hard spheres and that if it were not for this effect the ionization efficiency curve would be a straight line, one can write for the ion current I_p at electron energy P the following equations:

$$I_p=0 \qquad P\leqq V_0,$$
$$I_p=(1-V_0/P)(a+bP) \qquad P>V_0.$$

The curve drawn in Fig. 2 shows the result of fitting these equations by least squares to the experimental data shown by the points. It is clearly apparent that the critical energy $V_0=7.46$ electron volts determined by this curve is not a good representation of the data.

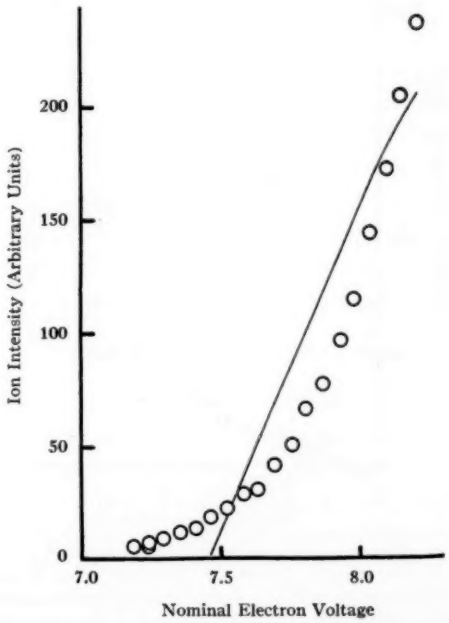

FIG. 2. Ionization efficiency curve showing experimental points for C_3H_7+ from n-butane. The smooth curve is that fitted to this data by least squares using an equation based on the electron impact parameter.

ELECTRON ENERGY SPREAD

Up to this point it has been assumed tacitly that the electrons are mono-energetic. Inasmuch as the electrons are emitted from a hot filament this is not true. They possess a distribution of energies based on P and corresponding to the absolute temperature T of the filament. If one assumes that this distribution is Maxwellian[20] and that the number of ions produced is directly proportional to the excess of the electron energy P above a critical value V_0, one can write for the ion current I_p produced by electrons accelerated through a potential P:[21]

$$I_p = A\left(\frac{3}{2}\frac{T}{11{,}606} + P - V_0\right) \quad \text{for } P \geqq V_0,$$

$$I_p = \frac{2A}{(\pi)^{\frac{1}{2}}}\frac{T}{11{,}606}\left\{\frac{3}{2}B^{\frac{1}{2}}\exp(-B) + \frac{(\pi)^{\frac{1}{2}}}{2}\left[\frac{3}{2} - B\right]\right.$$

$$\left.\times[1 - H(B^{\frac{1}{2}})]\right\} \quad \text{for } P < V_0,$$

where

$$B = (11{,}606/T)(V_0 - P),$$

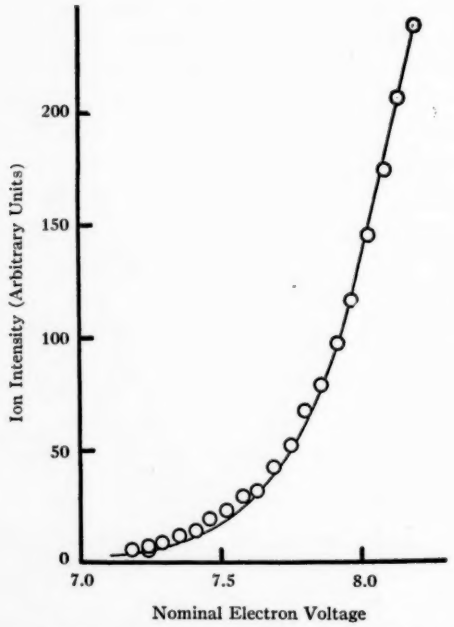

FIG. 3. The same data as in Fig. 2 fitted by a curve based on the energy spread of electrons from a hot filament. Apparent temperature 2349°K; apparent appearance potential, 8.06 volts.

and

$$H(B^{\frac{1}{2}}) = \frac{2}{(\pi)^{\frac{1}{2}}}\int_0^{B^{\frac{1}{2}}} \exp(-x^2)dx.$$

Figure 3 shows how well one can fit these equations to the data by a few steps of successive approximation. The curve, which is defined by the parameters $A = 534$, $V_0 = 8.06$ electron volts, and $T = 2349°\text{K}$, fits the data with a standard error of estimate of $s = \pm 3.6$ divisions of ion intensity. Although the parameter T corresponds to a fairly reasonable temperature for a tungsten filament and the fit is also reasonable, the fact that there must be an additional electron energy spread as a result of voltage drop along the filament throws considerable doubt on the validity of identifying $V_0 = 8.06$ volts with the appearance potential.

After the experimental work reported in this paper was completed, a paper by R. E. Honig[9] appeared in which is described a procedure for locating V_0 also based on the view that the curvature of the foot of the ionization efficiency curve is due to the electron energy spread. The procedure uses a critical slope to locate the point at which the electron energy P corresponds to a critical voltage V_0. Although the critical slope is derived on the assumption of a Maxwellian electron energy distribution and of the ion current being proportional to the square of the excess of the electron energy over the critical voltage, the fact that the effective absolute temperature of the electrons was measured independently from the ionization efficiency curve eliminates the difficulty just raised about potential drop along the filament. Using this effective temperature, Honig was able to fit his ionization efficiency curves very accurately. More important is the fact that the values for V_0 determined by the critical slope for the rare gases and nitrogen agree with the spectroscopic values within experimental error. On the other hand, it is also a fact that the simpler procedure of identifying initial current onset with V_0 also gives results agreeing with spectroscopic values for the rare gases.

TRANSITION EFFICIENCIES

Since it is the curved foot of the ionization efficiency curve which causes the difficulty in

[20] C. del Rosario, Phys. Rev. **28**, 769–780 (1926).
[21] D. P. Stevenson and J. A. Hipple, Phys. Rev. **62**, 237–240 (1942).

estimating an appearance potential from the data, any argument which would validate the use of an extrapolation of the straight line portion would remove the difficulty. Vought[22] has advanced a plausible argument which asserts that the voltage determined by the extrapolation of the straight line portion is just that necessary for the most probable or Franck-Condon transition to the ionized state. This argument ascribes a good portion of the curvature to the transition probabilities between the lowest electron energy state of the molecule and that which leads to ionization. Thus the analysis which was just developed of the curvature in terms of electron energy spread can be only partially correct.

Table I shows how well experimentally determined appearance potentials correlate with spectroscopic ionization potentials for seven gases. It will be noted that the correlation is every bit as good for appearance potentials determined from the extrapolated straight line portions of the ionization efficiency curves as those determined from the estimated first appearance of ions.

An equally plausible argument has been advanced[23] to show that, with the sensitivity of the modern mass spectrometer, the point of first onset of ion current is more closely related to the energy differences of molecular and ionic energy states than is the linear extrapolation. However, the real test of a hypothesis is not how plausible it may be but how well it stands up in a crucial experimental test. Stevenson and Hipple[21] showed that whereas the onset of ion current for A^+ and A^{++} gave appearance potentials spaced according to the corresponding spectroscopic ionization potentials the linear extrapolations gave values which differed from the spectroscopic values by considerably more than experimental precision. Other workers[24] using the initial current onset showed that relative to A^+ the mass spectrometer gave the correct ionization potentials for He^+, Ne^+, Ne^{++}, A^{++}, Kr^{++} and Xe^+. It can be argued, with some force, that these results refer only to monatomic molecules. However, as Hagstrum[25] points out, the use of

TABLE I. Calibration curves for two interpretations of ionization efficiency data.

Set of data	Calibration curve for extrapolated straight line	Fit of curve (standard error of estimate in volts)	Calibration curve for first appearance of ions	Fit of curve (standard error of estimate in volts)
1	$V_0=5.98+24.0P+411P^2$	0.25	$V_0=7.78-0.704P+618P^2$	0.25
2	$V_0=5.47+32.2P+411P^2$	0.29	$V_0=6.12+38.0P+407P^2$	0.25
3	$V_0=4.25+61.3P+251P^2$	0.24	$V_0=4.76+76.2P+171P^2$	0.24

the potential for initial current onset as the appearance potential for ions from H_2, N_2 and NO gives rise to dissociation energies for the corresponding molecules which agree very well with spectroscopic values.

Thus, although the data of Table I are inconclusive, it appears from independent evidence that the initial onset of ion current should be identified with the appearance potential. The decision to use initial current onset was clinched when it was found that appearance potentials based on straight line extrapolations for $C_2H_5^+$ from ethane, *n*-butane and *n*-pentane when used to compute bond strengths in the manner of D. P. Stevenson[26] gave 122 and 144 kcal/mole as the energy to remove the first hydrogen from ethane and propane respectively, whereas the initial current onset interpretation of the same data gave 114 and 134 kcal/mole. While the fact that the bond strengths calculated using the straight line extrapolation interpretation were further from chemical experience and thus led to the decision to use the initial current onset interpretation, present ignorance with regard to the excitation of the fragments produced by electron collision prevents one from claiming on the basis of this evidence that one interpretation is more nearly correct than the other.

EXPERIMENTAL PROCEDURE

The ionization chamber shown in Fig. 1 was operated in the standard manner recommended by the manufacturer except for the potentials on electrodes *C* and *D*. Electrode *B* was maintained at +40 volts with respect to the filament *A*. Electrode *F* was kept at the same potential as *C*, and the electron current to it was kept constant at 9.0 microamperes. The ionization chamber is wholly immersed in an homogeneous magnetic

[22] R. H. Vought, Phys. Rev. **71**, 93–101 (1947).
[23] T. Mariner and W. Bleakney, Phys. Rev. **72**, 807–814 (1947).
[24] V. H. Dibeler, F. L. Mohler and R. M. Reese, J. Research Nat. Bur. Stand. **38**, 617–620 (1947).
[25] H. D. Hagstrum, Phys. Rev. **72**, 947–963 (1947).
[26] D. P. Stevenson, J. Chem. Phys. **10**, 291 (1942).

field parallel to the electron beam, the energizing current for which was kept constant at 0.54 ampere.

The various gases to be studied were allowed to leak into the ionization chamber from a 2-liter sample flask in which the initial pressure was in the neighborhood of 40×10^{-3} mm of Hg. The leak rate of the gas out of the sample flask into the chamber was about -0.3 percent/min. for $m/e=58$ from n-C_4H_{10}. The ions to be studied were then brought into register on the current detector of the mass spectrometer by adjustment of the ion accelerating voltage. Under

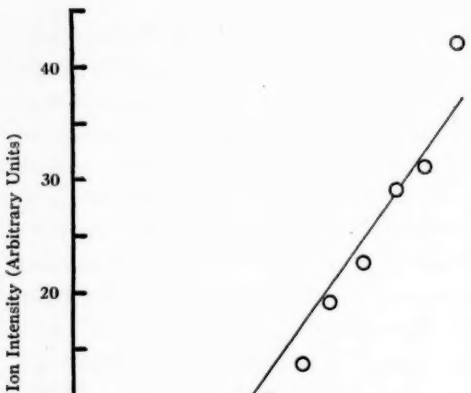

FIG. 4. Part of the data of Figs. 2 and 3 plotted on an enlarged scale. The straight line is that fitted by least squares. Its intersection with the zero axis is taken to be the $C_3H_7^+$ appearance potential.

these conditions $m/e=58$ from n-C_4H_{10} gave 16 chart divisions per 10^{-3} mm of Hg sample pressure at the beginning of the work and declined steadily to 3 divisions per 10^{-3} mm of Hg five months later.

Even though the decision has been made to use the "first break" or initial onset of ion current as a measure of appearance potential, one must carefully define the location of this point. Inasmuch as the ionization efficiency curves approach the axis in an exponential manner, one must have some objective method of locating a break-off point. Stevenson and Hipple have proceeded by plotting each set of data on a scale adjusted so as to make the curves similar. They then extrapolate by eye to the zero axis. This is an advance over simple extrapolation by eye. However, any extrapolation by eye becomes an exercise in personal judgment when the data are plotted on a scale large enough to permit accurate extrapolation.

Figure 4 shows an application of the scheme adopted in this work for locating the initial onset of ion current. After the ion accelerating voltage had been adjusted to bring the ion to be studied into focus (705 volts for $m/e=58$), the potential on electrode C (see Fig. 1), and hence the electron voltage, was raised in steps of 0.05 volt from a point well below the expected appearance potential. At each step the ion accelerating voltage was swept from a value slightly greater than the value for focus to one slightly below. The ion current was determined by the height of the peak produced on the chart. This was continued until the peak height reached about one chart division. The values found were then corrected to specific ion intensity by dividing by the pressure of the sample. On the basis of the observation that this short section of the ionization efficiency curve differed negligibly from a straight line, such a line was fitted to the specific ion intensity data. Its intersection with the zero axis was then taken to be a measure of the appearance potential.

ELECTRON ENERGY SCALE

Although this procedure identifies a point on the electron energy axis with the appearance potential, there is still the problem of defining the scale to be used on this axis in order to obtain true values. There are several factors which cause the actual electron energies to be different from those expected from the potentials impressed on the accelerating electrodes.

The thermal energy of the electrons and the contact potentials of the electrode surfaces have an effect on the total electron energy. Even more important the "pushers" (see Fig. 1) are kept at a constant potential of $+3.1$ volts, a portion of which contributes to the electron beam acceleration. In all of the previously published work[1–18] on appearance potentials, this difference between applied electron accelerating voltage and actual electron energy has been adjusted for by means

TABLE II. Convenient gases of known spectroscopic ionization potential

Gas	Spectroscopic ionization potential (volts)	Experimental precision (volts)
Argon[a]	15.75	0.02*
Nitrogen[b]	15.572	0.002
Carbon Monoxide[c]	14.1	0.1
Carbon Dioxide[d]	13.78	0.02
Water[e]	12.61	0.02
Ethylene[f]	10.50	0.04
Acetone[g]	10.26	0.04*

[a] G. Herzberg, *Molecular Spectra*, I (Prentice-Hall, Inc., New York, 1939).
[b] R. E. Worley and F. A. Jenkins, Phys. Rev. **54**, 305 (1938).
[c] A. D. Walsh, Trans. Faraday Soc. **42**, 56 (1945).
[d] W. C. Price and D. M. Simpson, Proc. Roy. Soc. **169A**, 501–512 (1938).
[e] W. C. Price, J. Chem. Phys. **4**, 147–153 (1936).
[f] W. C. Price and W. T. Tutte, Proc. Roy. Soc. **174A**, 207–220 (1940).
[g] A. B. F. Duncan, J. Chem. Phys. **3**, 131–132 (1935); **8**, 444–446 (1940).
* These precisions are not those given by the reference but are merely estimates.

of an additive constant. The apparent appearance potential V of a monatomic gas, such as mercury or argon, has been compared to its accurately known spectroscopic ionization potential V_0. The difference between the two is then added algebraically to the apparent appearance potentials for other ions to obtain true values. This procedure of using one calibrating point and the assumption of a calibration curve which is a straight line of unit slope should not be expected to yield accurate results for appearance potentials very different from that of the calibrating gas. For that reason in the present work seven gases whose spectroscopic ionization potentials were known were used to construct a calibration curve. Table II shows the ionization potentials which were used. Of these values only that for CO is at all doubtful. The reference[27] given by Walsh[28] for 14.1 electron volts relates only to transition to the $^3\pi$ state of CO. A more recent paper of Long and Walsh[29] cites a value of 14.55 electron volts calculated from a Rydberg series by B. M. Anand.[30] However, this value does not fit in at all smoothly with the mass spectrometer results found in this work. What is more, a value of 14.006 electron volts corresponds to the limit of a Rydberg series assigned by Takamine, Tanaka and Iwata[31] to the (0, 0) vibration series in CO. Inasmuch, as 14.1 electron volts agrees with this and with earlier electron collision results,[32] it has been used as a calibration point but with a reduced weight corresponding to the larger precision limit of ±0.1 electron volt.

TABLE III. Calibration curves.

Date	Curves	Standard error of estimate (electron volts)
5–31–46	$V_0=7.362+5.262V+555.3V^2$	0.14
	$V_0=2.742+108.7V$	0.21
6–25–46	$V_0=7.230+4.835V+569.6V^2$	0.14
	$V_0=2.516+110.7V$	0.21
7–12–46	$V_0=6.523+18.27V+479.9V^2$	0.16
	$V_0=2.314+110.0V$	0.22
7–26–46	$V_0=6.086+31.50V+415.7V^2$	0.12
	$V_0=2.56+109.7V$	0.15
8– 6–46[a]	$V_0=9.78-55.15V+939.8V^2$	0.26
	$V_0=3.94+98.6V$	0.45
8– 7–46	$V_0=4.79+62.69V+272.0V^2$	0.23
	$V_0=2.62+112.3V$	0.22
9– 5–46	$V_0=8.06-23.85V+679.0V^2$	0.17
	$V_0=1.48+112.3V$	0.28
9–12–46	$V_0=10.06-56.91V+821.6V^2$	0.27
	$V_0=2.46+104.5V$	0.36
9–13–46[a]	$V_0=7.57-7.10V+600.9V^2$	0.24
	$V_0=2.13+109.6V$	0.30
9–17–46	$V_0=10.53-72.68V+933.4V^2$	0.31
	$V_0=1.85+110.7V$	0.37
9–23–46	$V_0=7.61-11.56V+589.7V^2$	0.19
	$V_0=1.87+107.1V$	0.25
10– 3–46	$V_0=7.13-2.561V+55.0V^2$	0.16
	$V_0=1.60+110.2V$	0.22
2–13–47	$V_0=7.78-0.704V+618.5V^2$	0.25
	$V_0=3.18+108.5V$	0.30
2–20–47	$V_0=6.12+37.98V+406.9V^2$	0.25
	$V_0=3.04+110.4V$	0.24
3– 5–47	$V_0=4.76+76.25V+170.8V^2$	0.24
	$V_0=3.43+106.8V$	0.21
3–30–47	$V_0=7.11+16.72V+511.3V^2$	0.14
	$V_0=3.17+108.7V$	0.20
3–30–47[b]	$V_0=8.48+39.00V+653.3V^2$	0.22
	$V_0=6.78+110.1V$	0.28
3–30–47	$V_0=7.05+15.16V+536.8V^2$	0.23
	$V_0=3.02+110.4V$	0.26

[a] Calibration made at high electron catcher bias.
[b] Calibration made at high pusher bias.
V_0 is the true appearance potential; V is the potentiometer reading.

The apparent appearance potentials in the mass spectrometer of these seven gases were used to construct a calibration curve. In order to determine the applied electron voltage accurately a constant fraction from a voltage dividing network was measured with a semi-precision potentiometer (Leeds and Northrup Type 7655). The potentiometer readings were used directly with

[27] L. Gerö, G. Herzberg and R. Schmid, Phys. Rev. **52**, 467 (1937).
[28] See Table II, reference c.
[29] L. H. Long and A. D. Walsh, Trans. Faraday Soc. **43**, 342 (1947).
[30] B. M. Anand, Science and Culture **8**, 278–279 (1942).
[31] T. Takamine, Y. Tanaka and M. Iwata, Sci. Papers Inst. Phys. Chem. Research (Tokyo) **40**, 371–378 (1943).
[32] H. D. Hagstrum and J. T. Tate, Phys. Rev. **59**, 354 (1941).

the corresponding spectroscopic appearance potentials to give points to which a second degree curve was fitted by least squares. Table III shows both these curves and the corresponding least squares straight lines. It is interesting to note that the slopes of these latter are not the same and hence any assumption of a simple additive constant for a Consolidated mass spectrometer cannot be correct.*** The standard errors of estimate, $S_2=\pm(\sum d_i^2/(n-3))^{\frac{1}{2}}$, for the second degree curves are in general smaller than those, $S_1=\pm(\sum d_i^2/(n-2))^{\frac{1}{2}}$, for the straight lines so all of the true appearance potentials have been calculated from the second degree curve determined just prior to the experimental determinations.

Since this work was completed, Honig[9] has made some experimental observations which throw doubt on this scheme of calibrating. First, he demonstrated that, when using his interpretation of the ionization efficiency curve, it was necessary to use a mixture of the calibrating gas and the gas giving the ions to be measured.

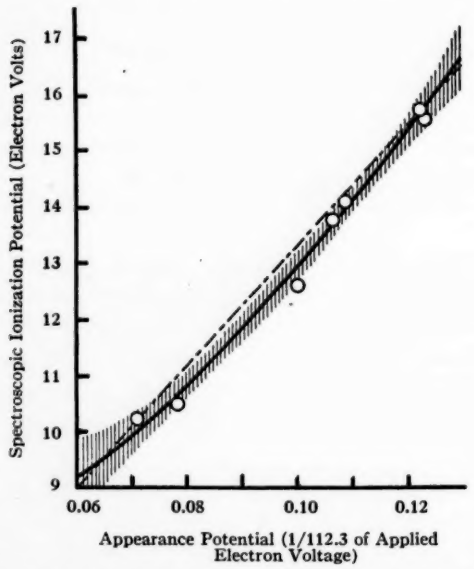

FIG. 5. The solid curve is the calibration curve produced by fitting a second degree curve by least squares to the seven points given by acetone, ethylene, water, carbon dioxide, carbon monoxide, argon, and nitrogen (reading from left to right). The shaded area is the 95 percent confidence band. The dashed straight line is the calibration curve one would get using only argon and a simple additive correction voltage.

*** A slope of 112.3 corresponds to unit slope if both variables are expressed in volts since 112.3 ± 0.1 is the voltage divider factor.

Otherwise the effective electron temperature would be different for different gases and the critical slope would be shifted. Since the shape of the lower part of the ionization efficiency curve must be due in part to electron energy spread, shifts in effective electron temperature could conceivably interfere with calibration. Second and more serious, the fact that there is agreement between mass spectrometer and spectroscopic results for rare gases and nitrogen but not for ethylene or benzene in Honig's work raises the issue of whether polyatomic molecules such as acetone and ethylene should be used as reference points. The view taken in the work reported here is that electron impact and photon absorption should give the same ionization potentials on the ground that a Rydberg series of electronic states is observed only when the electronic state potential curves are located directly above each other so that only the $0-0$ band appears for each state.[33] Thus the idea of a simple additive calibration constant which gives a discrepancy between appearance potential and spectroscopic ionization potential for some molecules has been abandoned in favor of a calibration based on the identity of the two values for all molecules where a Rydberg series is available. This issue will be discussed further in connection with a comparison of the results obtained by the two methods.

It should be pointed out that since the spectroscopic values, the ordinates of the calibration curve, are more accurately known than the experimental apparent appearance potentials, which are the corresponding abscissas, the usual least squares method theoretically should not have been used. The usual method assumes complete accuracy in the abscissas and ascribes all the error to the ordinates. However, application of the exact method[34] gave results which did not differ significantly from the usual method so that the latter was used because of its simplicity. Figure 5 shows some of the additional information that the exact method yielded with regard to one of the cases (9–13–46 calibration) for which it was applied. The dashed straight line is

[33] G. Herzberg, *Molecular Spectra and Molecular Structure. I. Diatomic Molecules* (Prentice-Hall, Inc., New York, 1939), page 231.

[34] W. E. Deming, *Statistical Adjustment of Data* (J. Wiley and Sons, Inc., New York, 1938).

TABLE IV. Stability of calibration scheme with regard to ionization chamber voltages.

Compound and ion	Electrode voltage Pusher bias*	Apparent appearance potential (potentiometer reading)	True appearance potential (electron volts)
n-Butane, $m/e=58$	+ 3.1	0.0740	11.15
	+10.9	0.0386	10.96
	+ 3.1	0.0739	11.10
	Electron catcher bias*		
Ethylene, $m/e=27$	0	0.1114	13.92
	+47.5	0.1089	13.93
	0	0.1109	13.95
n-Pentane, $m/e=57$	0	0.0861	11.25
	+47.5	0.0840	11.22
	0	0.0862	11.20

* These electrodes are biased with respect to the final electron accelerating electrode which is at the same potential as the plate containing the first ion beam defining slit.

the calibration curve one would obtain by using argon alone as a calibrating gas. It can be seen that it lies partly outside the shaded area representing the 95-percent confidence band. This band, which can be calculated from information derived from the exact least squares method, defines the range of ordinate within which the chance is 95 out of 100 that, for a particular value of V, the true appearance potential is located. Thus there is a region in which the straight line can be considered to be in error.

EXPERIMENTAL VERIFICATION OF THE CALIBRATION METHOD

In order to be certain that the above calibration scheme was one which would compensate for changes in ionization chamber conditions, the voltages impressed on the pushers and the electron catcher were deliberately varied by large amounts. Table IV shows that the calibration procedure is stable against changes which are far more severe than would ever be met in practice.

EXPERIMENTAL RESULTS

The hydrocarbon ion appearance potentials shown together with their standard deviations in Tables V, VI and VII were measured with Phillips Research Grade hydrocarbons. These hydrocarbons are 99-mole percent pure or better. The appearance potentials are given in terms of

TABLE V. Ionization potentials of hydrocarbons.

Hydrocarbon	No. of measurements	V_0 (kcal/mole)	Literature value (kcal/mole)	Reference
Methane	2	300.8±0.5	304.5±9.2	13
			299.9±4.6	11
			300.8±0.5	9
Ethane	6	271.7±0.5	269.0±2.3	15
			265.3±4.6	11
			271.3±0.5	9
Propane	4	260.7±1.2	260.2±2.3	17
			258.4±6.9	11
			258.6±0.2	9
n-Butane	8	256.3±0.9	240.1±2.3	15
			237.6±6.9	11
			249.1±0.2	9
Isobutane	1	255.1	240.1±2.3	15
			237.6±4.6	11
n-Pentane	2	250.8±0.2	242.2±6.9	11
			243.4±0.2	9
Propylene	1	231.8	226.8±2.3	17
			227.0	9
Butylene-1	1	230.7	222.6±2.3	13
			225.1	9
Isobutylene	5	222.6±1.6	206.0±2.3	17

kilocalories per mole so that they may be compared directly with thermochemical data.†

Figures 6 and 7 have been plotted to show the trends established for the appearance potentials of ions from succeeding members of the normal paraffin series.

DISCUSSION OF RESULTS

There are several remarks which should be made about the data in Tables V, VI and VII before discussing their interpretation. First, the experimental precision is as good as any previously published results. These precisions are standard errors, $S_0=\pm(\sum d_i^2/n(n-1))^{\frac{1}{2}}$, for the averages of independent determinations. They do not take into account explicitly the accuracy of calibration. This latter has been computed as standard error of estimate, $S=\pm(\sum d_i^2/(n-3))^{\frac{1}{2}}$, which expresses only the "vertical" fit of the calibration curve to the points from which it was constructed. Thus, it would not be easy to state the absolute accuracy of the appearance poten-

† The conversion factor used was 1 international electron volt per molecule equals 23.0682±0.0024 kilocalories per mole.

TABLE VI. Paraffin ion appearance potentials.

Ion (m/e)	No. of measurements	V_0 (kcal/mole)	Literature value (kcal/mole)	Reference
Methane				
15	2	336.3±1.2	334.5±9.2	13
			332.2±6.9	11
Ethane				
15	6	361.5±3.2	329.9±6.9	7
			334.5±6.9	11
28	4	263.9±1.2	280.5±2.3	15
			279.1±4.6	11
29	6	293.0±0.9	297.8±2.3	15
			295.3±4.6	11
Propane				
15	1	584.1	392.2±4.6	17
28	1	268.3	274.0±2.3	17
			272.2±6.9	11
29	2	277.2±2.1	283.3±2.3	17
			283.3±6.9	11
42	1	281.4	286.0±6.9	4
			281.4±6.9	11
43	2	271.3±2.3	270.8±2.3	17
			265.3±6.9	11
n-Butane				
15	1	473.1	>460	15
27	1	331.7	327.6±6.9	15
			362.2±6.9	11
28	3	279.1±0.7	266.7±2.3	15
			263.0±4.6	11
29	9	290.0±3.0	279.4±2.3	15
			290.6±6.9	11
41	2	315.6±7.2	303.6±2.3	15
			306.8±6.9	11
42	2	258.1±0.7	254.0±2.3	15
			246.8±6.9	11
43	4	259.7±1.4	258.6±2.3	15
			251.4±6.9	11
56	2	287.2±3.7		
57	4	293.6±1.8	279.1±6.9	15
			272.2±6.9	11
Isobutane				
27	4	327.8±2.8	339.1±6.9	15
			366.8±6.9	11
28	4	323.4±4.4	279.1±4.6	15
			313.7±6.9	11
29	6	353.2±8.5	295.3±4.6	15
			392.2±11.5	11
42	2	255.8±1.8	249.4±2.3	15
			246.8±4.6	11
43	2	259.7±0.9	254.0±2.3	15
			253.8±6.9	11
57	4	284.4±2.3	267.6±6.9	15
			267.6±6.9	11
n-Pentane				
27	1	335.0	426.8±4.6	11
28	2	299.6±2.8	449.5±11.5	11
29	8	310.0±1.2	343.7±6.9	11
41	1	299.4	332.2±4.6	11
42	5	246.8±8.3	258.4±4.6	11
43	5	256.0±0.7	272.2±4.6	11
56	1	267.1	260.7±6.9	11
57	5	260.4±0.9	267.6±6.9	11
70	1	295.0		
71	5	307.0±6.9	279.1±6.9	11

TABLE VII. Olefin ion appearance potentials.

Ion (m/e)	No. of measurements	V_0 (kcal/mole)	Literature value (kcal/mole)	Reference
Ethylene				
27	4	321.1±0.2	327.6±2.3	12
Propylene				
15	3	532.2±30.4		
27	3	314.4±1.6	336.8±6.9	4
28	2	296.4±1.8		
41	2	276.8±1.8	277.5±2.3	17
Butylene-1				
27	2	383.6±10.2		
28	1	284.9		
29	4	316.3±1.6	276.1±2.3	14
40	1	283.7	269.9±4.6	14
41	2	268.7±2.3	268.7±2.3	14
55	2	276.1±2.5	255.4±2.3	14
Isobutylene				
28	2	281.0±0.9	281.4±11.5	17
40	3	276.8±0.9	269.7±2.3	17
41	5	272.2±2.8	267.1±2.3	17
55	5	278.9±1.6	262.7±2.3	17

tials presented. However, since the various determinations of any appearance potential were carried out using different calibrations, the excellent precision shown must include implicitly the effect of calibration accuracy. Second, the agreement for the normal paraffins through propane between these data and those previously published is excellent. The agreement between the results of Koffel and Lad[11] and other workers is remarkable in view of the fact that the former used the straight line extrapolation interpretation and the latter used the ion current onset or critical slope interpretation. The literature results prior to 1941 in Tables V, VI and VII have been corrected for the change in the value of e and the consequent change in calibration point. Third, as evidenced in Table V, for the paraffins beyond propane and for olefins the ionization potentials obtained in this work are systematically higher than others reported. It is interesting to note, that, if one recalculates literature values for the olefin molecule ions so as to shift from one point calibration to seven points, the discrepancies are reduced as is shown in Table VIII. The shift in calibration was effected by substituting in the calibration curve,

$$V_0 = A + BV + CV^2,$$

the value for V from the relation

$$V' = a + 112.3V,$$

based on an additive constant giving $V' = 15.75$

volts for the argon apparent appearance potential V. $V=0.0662$ for propylene which, since it was referred to the calibration curve for 6–25–46 in Table III, corresponded to $V_0=10.05$ ev $V=0.1189$ for argon was used in calculating the 6–25–46 calibration so $a=2.40$ and

$$V_0=7.39-0.174\,V'+0.045\,V'^2.$$

Thus, the literature value for propylene, $V'=9.83$ ev, corresponds to $V_0=10.02$ ev. As illustrated in Fig. 5 for another pair of calibrations, the two schemes give the same electron voltage at two points. For the data just described these are 15.32 ev and 10.68 ev. Between these two values $V_0<V'$ and beyond them $V_0>V'$. Thus the difference between results is evidently a difference in calibration method.

If, on the other hand, one were to assume that the apparent value for ethylene corresponds to 10.60 ev as stated by Honig[9] and that for acetone 10.46 ev should be used instead of the spectroscopic value, recalculation of the 6–25–46 calibration curve gives

$$V_0=8.25-13.12\,V+648.3\,V^2$$

with a standard error of estimate of 0.15 ev. Thus a curve can be fitted to these data just as well as to the original ones. However, this calibration gives a propylene ionization potential of 10.22 ev or 235.8 kcal/mole.

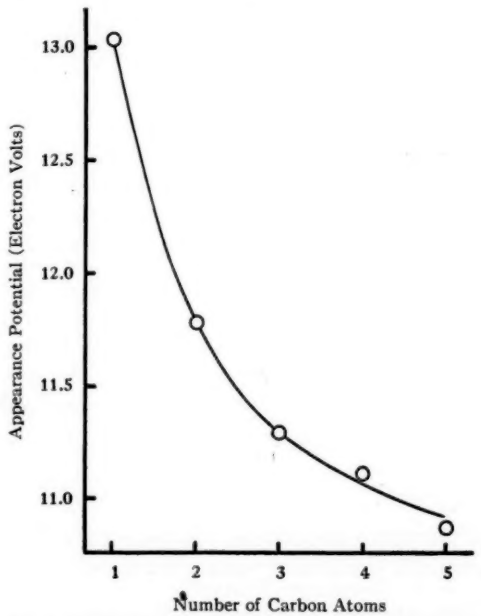

FIG. 6. The appearance potentials of the molecule ions from normal paraffins.

TABLE VIII. Result of changing basis of calibration.

Compound	Literature	Literature recalculated	Values from Table VII
Propylene	9.83[a]	10.02	10.05
Butylene-1	9.65[b]	9.88	10.00
Isobutylene	8.93	9.35	9.65

[a] See reference 17.
[b] See reference 14.

Since this procedure increases the discrepancy, it is evident that, at least in this case, the assumption that electron impact gives higher values than found in spectroscopic work for large molecules does not reconcile the two calibration schemes. If the difference in results is wholly due to different calibration procedure, then the two sets plotted against each other as in Fig. 8 can be used to convert from one voltage scale to the other. Until some independent means of calibration for the 10-volt region is available, there is no way to decide which is the correct scale.

Finally, as is apparent in Figs. 6 and 7, while the molecule ion appearance potentials for the normal paraffins form a decreasing sequence with the differences becoming smaller, the $m/e=29$ ion appearance potentials for the same molecules show a reverse trend.

DISSOCIATION ENERGIES

Further discussion of the results tabulated in Tables V, VI and VII can best be carried on in

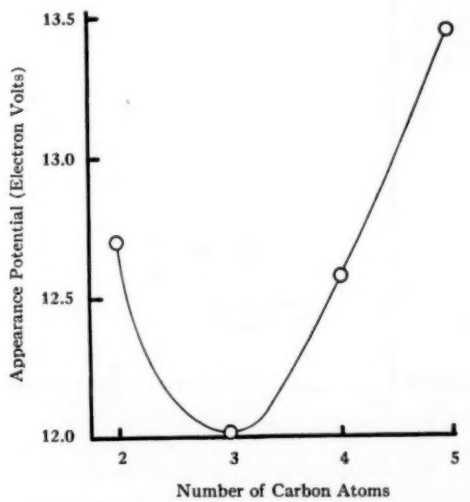

FIG. 7. Appearance potentials of the ion $C_3H_5^+$ from the normal paraffins.

relation to a statement of the energies which define the appearance potential. In equation form, the statement reads:

$$V_0(R_1^+) = D(R_1-R_2) + I(R_1) + E(R_1^+) + E(R_2) - E(R_1R_2) + \text{K.E.}(R_1^+) + \text{K.E.}(R_2) - \text{K.E.}(R_1R_2).$$

In this equation $V_0(R_1^+)$ represents the appearance potential, or the minimum energy necessary for the production of the ion R_1^+ from the molecule R_1R_2. $D(R_1-R_2)$ is the energy of the bond between R_1 and R_2 in the original molecule. It is defined as the energy necessary to produce the two fragments in their lowest energy states from the molecule in its lowest energy state. $I(R_1)$ is the energy necessary to remove an electron from the fragment R_1. The various E's represent internal energy which the corresponding fragments or molecule have in excess of that of their lowest energy state. The K.E.'s represent the kinetic energies of the molecules. Both $E(R_1R_2)$ and K.E.(R_1R_2) can be neglected since the original gas will be at 250–300°C. Most molecules at that temperature are still in their lowest vibration state, and the corresponding kinetic energy is 0.05 electron volt. While the latter is of the order of experimental error, it is not large enough to account for the discrepancies to be described later. The kinetic energy of the neutral fragment can be deduced by conservation of momentum from that of the ion. Washburn and Berry[35] have determined the kinetic energies of ions from *n*-butane bombarded by 50 electron volt electrons. These varied from 0.04 to 2.4 electron volts. For two ions of interest to this discussion, $m/e=29$ and $m/e=43$, they found respectively 0.08 ± 0.01 and 0.045 ± 0.005 electron volt. In view of the fact that bombarding electron energies of about 15 electron volts are used in appearance potential work, the kinetic energies can be expected to be smaller, and one can neglect them in the same manner as one has the other terms just discussed.

D. P. Stevenson[26] has gone a step farther and assumed that the excitation energies of the fragments are also negligible. On this basis, he was then able to set up closed energy cycles such as the following:

$$\begin{aligned} C_2H_6+CH_4 &= C_3H_8+2H && -117.1 \text{ kcal/mole}^{36} \\ C_3H_8 &= C_2H_5^+ + CH_3 && -277.3\pm2.1 \\ H+C_2H_5^+ &= C_2H_6 && +293.0\pm0.9 \\ \hline CH_4 &= CH_3+H && -101.4\pm2.3 \end{aligned}$$

or

$$\begin{aligned} C_2H_4+CH_4 &= C_3H_6+2H && -111.1 \text{ kcal/mole}^{33} \\ C_3H_6 &= C_2H_3^+ + CH_3 && -314.4\pm1.6 \\ H+C_2H_3^+ &= C_2H_4 && +321.1\pm0.2 \\ \hline CH_4 &= CH_3+H && -104.4\pm1.6 \end{aligned}$$

In other words, from heats of formation and ion appearance potentials, one can calculate an energy related to a given bond in a molecule. In Table IX is a compilation similar to Stevenson's[14] of energies calculated from data from Tables V, VI and VII for the bonds indicated.

While the two energy cycles for $D(CH_3-H)$ check each other and values obtained from ther-

TABLE IX. Values of $D(R'-R'')$ for the reaction $R'R'' = R'+R''-D(R'-R'')$ as calculated according to D. P. Stevenson.

	(kcal/mole)				
R'' / R'	H	CH_3	$CH=CH_2$	C_2H_5	C_3H_7
H	103.8[a]				
CH_3	103.5±1.5	87.8±2.5			
$CH=CH_2$	135.1±2 0	125.4±3.1	164.6±2.8		
C_2H_5	111.5±3.9	94.8±4.6	133.8±4.4	117.5±5.5	
C_3H_7	130.8±1.7	115.6±3.0	154.9±2.6	126.1±4.2	148.2±2.4

[a] See reference 11.

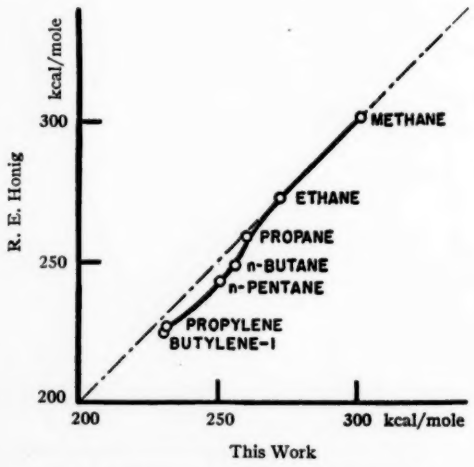

FIG. 8. Hydrocarbon ionization potentials.

[35] H. W. Washburn and C. E. Berry, Phys. Rev. **70**, 559 (1946).

[36] American Petroleum Institute Research Project 44 at the National Bureau of Standards, "Selected Values of Properties of Hydrocarbons," April 30, 1945.

mochemical data, such as $D(CH_3-H)=102\pm1$ kcal/mole,[37] Table IX shows that whatever confidence this engenders in the assumption of negligible excitation energies is destroyed by the upward trends in calculated energies with molecular weight. The differences between this table and the similar one presented by Stevenson[14] are the result of the differences in the corresponding appearance potentials.

In the light of thermochemical evidence with regard to chemical bonds, these upward trends must be taken to be the result of differences between dissociation energy as measured by electron impact and the corresponding bond energy. Long and Norrish[38] have pointed out that it would be surprising if inelastic collision produced unexcited fragments from large molecules. At least there will be an energy corresponding to the change in atomic arrangement between the fragment as it is in the molecule and the fragment after release from the molecule. For this reason they define a dissociation energy which may be represented as:

$$D'(R_1-R_2)=D(R_1-R_2)+E(R_1^+)+E(R_2).$$

Their position is that although the energy D' will be necessary to cause the breaking of the R_1-R_2 bond, thermochemical data, being obtained under equilibrium conditions, will give values for the bond energy D because any excitation energies E imparted to the fragments in the process under study are returned to the reacting system. Electron impact, on the other hand, is a non-equilibrium process so that the excitation energies must be taken into account, and one obtains values for D' and not for D. An excellent example of electron collision producing an excited ion is found in the production of CH^+ from HCN. Spectroscopic evidence[39] has shown that the mass spectrometer ionization potential for this ion[12] includes 85 kcal/mole "excess" energy. Thus, an accurate knowledge of the energy states of the fragments produced is necessary before ionization potentials can be used to calculate bond energies.

It is interesting to note that if one makes the crude assumption that the energy needed to produce the ion R_1^+ from the molecule R_1R_2 is in excess of $D(R_1-R_2)$ and $I(R_1^+)$ by an amount which is a linear function of the number of methylene groups in R_1R_2 less one, one can obtain an approximately consistent correction for the excess energy for the production of $C_2H_5^+$. Since thermochemical data[40] give $D(C_2H_5-H)=98\pm2$ kcal/mole, one can compute that 13.5 ±4.4 kcal/mole, according to the assumption, is the excess energy for the production of $C_2H_5^+$ from *n*-butane, and that therefore 27 ± 6 kcal/mole is that for $C_2H_5^+$ from *n*-pentane. The value $D(C_3H_7-H)=104\pm6$ kcal/mole, calculated from the corrected appearance potential of $C_2H_5^+$ from *n*-pentane, is larger than that for $D(C_2H_5-H)$, which is contrary to chemical experience,[38] but the experimental uncertainty is so large that one could say that the correction is roughly satisfactory.

CONCLUSIONS

Although the appearance potentials discussed in this paper are as precise experimentally as any previously published, the difference between them and those published previously raises doubt as to the absolute accuracy of both sets of data. The difference arises from the method used for calibrating the voltage scale.

It seems entirely reasonable that for larger molecules the energy necessary to produce a given ion will be partially due to simultaneous internal excitation of the fragments produced and that the amount of excitation energy will increase with molecule size. Thus mass spectrometer appearance potentials cannot be used in calculating bond energies unless some knowledge about the states of the fragments produced is available.

ACKNOWLEDGMENTS

We wish to thank the Misses C. I. Benson, C. McKinley, and R. H. Perkins for carrying out many of the measurements and calculations. We also wish to thank L. C. Roess for many helpful discussions.

[37] H. C. Anderson and G. B. Kistiakowsky, J. Chem. Phys. **11**, 6–10 (1943); G. B. Kistiakowsky and E. R. Van Artsdalen, J. Chem. Phys. **12**, 469–478 (1944).

[38] L. H. Long and R. G. W. Norrish, Proc. Roy. Soc. **187A**, 337–357 (1946).

[39] A. E. Douglas and G. Herzberg, Can. J. Res. **20A**, 71–82 (1942).

[40] H. C. Anderson and E. R. Van Artsdalen, J. Chem. Phys. **12**, 479–483 (1944).

THE JOURNAL OF CHEMICAL PHYSICS VOLUME 17, NUMBER 1 JANUARY, 1949

Chemical Reaction During Adiabatic Flow through a Rocket Nozzle*

DAVID ALTMAN AND S. S. PENNER
Jet Propulsion Laboratory, California Institute of Technology, Pasadena, California

(Received June 14, 1948)

An analysis has been carried out for isentropic expansion through a representative rocket nozzle. The rate of change of temperature of an element of gas with distance and time in the vicinity of the nozzle throat is discussed in some detail. By use of Daniels' rate constant for the formation of nitric oxide from nitrogen and oxygen, it is shown that the temperature changes so rapidly that the reaction $2NO \rightleftarrows O_2+N_2$ produces insignificantly small composition changes below about 2800°K when the temperature in the rocket chamber is 3000°K.

I. INTRODUCTION

PERFORMANCE calculations for a propellant system in a rocket motor require the determination of thermodynamic properties at rocket chamber and nozzle exit conditions. It is customary to perform rocket calculations on the assumption that equilibrium among the internal energy states is maintained.[1,2] This assumption is also made in the present discussion without, however, proving its validity. In fact, a more detailed analysis of the rate of attainment of equilibrium among the internal energy states may lead to a refinement of performance calculations in rockets. Relevant experimental and theoretical data can be found in the literature.[3,4,5,6]

It is the purpose of this paper to consider flow through a nozzle with reference to composition changes which may occur as the result of chemical reactions. The flow equations which are used correspond to the well-known one-dimensional approximation.**

The numerical analysis of the changes in chemical composition during isentropic expansion described in the present paper is related to the general problem of gas reactions in flow systems which has been discussed by a number of authors.[7,8,9,10] In order to calculate the extent of changes in chemical composition during flow, it is necessary to know the rates of the various reactions involved, as well as the rate of change of temperature and pressure with time. Theoretical estimates of the order of magnitude of the reaction rates[11] or extrapolations from low-temperature measurements may be sufficient in some cases, since only relatively fast reactions will permit extensive composition changes during isentropic expansion through the rocket nozzle. The present analysis is limited to a study of the changes in composition according to the reaction

$$2NO \rightleftarrows O_2+N_2.$$

Rate constants for the formation of nitric oxide from oxygen and nitrogen are available in the literature.[12,13,14] These rate data are combined with the time-temperature relations for an adiabatic flow process in a rocket nozzle in order to predict the extent of composition change pro-

* Presented as Paper 26 before the 112th meeting of the American Chemical Society in New York City, September, 1947.

[1] F. J. Malina, J. Franklin Inst. **230**, 433 (1940).

[2] H. S. Seifert, M. Mills, and M. Summerfield, Am. J. Phys. **15**, 1–21, 121–140, 255–275 (1947).

[3] H. O. Kneser, J. Acous. Soc. Am. **5**, 122 (1933).

[4] L. Landau and E. Teller, Physik. Zeits. Sowjetunion **1**, 34 (1936).

[5] A. Kantrowitz, J. Chem. Phys. **14**, 150 (1946).

[6] P. W. Huber and A. Kantrowitz, J. Chem. Phys. **15**, 275 (1947).

** A number of papers concerned with the problem of one-dimensional flow through a nozzle have been published since the preparation of this article. Among these may be mentioned the papers by A. H. Shapiro *et al.*, J. App. Mech. **14**, 317, 344 (1948), and by B. L. Hicks, D. J. Montgomery, and R. H. Wasserman, J. App. Phys. **18**, 891 (1947).

[7] Th. von Förster and K. H. Geib, Ann. d. Physik **20**, 250 (1934).

[8] H. M. Hulburt, Ind. Eng. Chem. **36**, 1012 (1944); **37**, 1063 (1945).

[9] G. M. Harris, J. Phys. and Colloid Chem. **51**, 505 (1947).

[10] K. Schaefer, "On the Thermodynamics of Rocket Propulsion, I," Headquarters, Air Materiel Command, Wright Field, Dayton, Ohio, 1947.

[11] S. Glasstone, K. J. Laidler, and H. Eyring, *The Theory of Rate Process* (McGraw-Hill Book Company, New York, 1941).

[12] F. Daniels *et al*, private communication, 1943.

[13] J. Zeldovich, Acta Phys. Chim., URSS **21**, 577 (1946).

[14] D. Frank-Kamenetsky, Acta Phys. Chim., URSS **22**, 27 (1947).

duced by chemical reaction. The corrections which should be applied to the thermodynamic treatment of the flow process when appreciable composition changes occur are usually not large. A detailed discussion of the method has been given elsewhere for an idealized system.[15]

II. REDUCED TEMPERATURE AS A FUNCTION OF NOZZLE DIAMETER

The adiabatic expansion of 1 mole of a perfect gas through a nozzle without friction losses is considered in the following discussion. From the condition that the flow occurs isentropically, it follows that

$$d\rho/\rho = dT/(\gamma-1)T, \tag{1}$$

where ρ represents the density, T is the temperature at any point along the nozzle, and γ is the ratio of the specific heat at constant pressure to the specific heat at constant volume. By the use of Eq. (1) together with the equation of continuity

$$dv/v + d\rho/\rho + dA/A = 0 \tag{2}$$

and the law of conservation of energy

$$Mvdv = -c_p dT \tag{3}$$

it can be shown that

$$\frac{dr}{dT_R} = \frac{r}{2}\left[\frac{1}{2(1-T_R)} - \frac{1}{(\gamma-1)T_R}\right]. \tag{4}$$

Here v is the velocity of flow parallel to the nozzle axis, A represents the cross-sectional area at any point which is assumed to be circular and of radius r, M is the molecular weight, c_p is the heat capacity per mole at constant pressure, and T_R is defined as T/T_c where T_c represents the chamber temperature. Equation (4) has been derived on the assumptions that $v=0$ at $T=T_c$ and that c_p is constant.***

From Eq. (4) the following well-known relations can be derived:

$$(r_e/r)^2 = (T_R/T_{R_e})^{1/(\gamma-1)}[(1-T_R)/(1-T_{R_e})]^{\frac{1}{2}} \tag{5}$$

and

$$T_{R_t} = T_t/T_c = 2/(\gamma+1), \tag{6}$$

where the subscripts e and t denote conditions at the nozzle exit and nozzle throat, respectively.

Calculations have been carried through to determine T_R as a function of r/r_e for a ratio of chamber pressure p_c to exit pressure p_e of 20:1 for gases with $\gamma=1.67$ and $\gamma=1.20$. The values of T_{R_e} were calculated by use of the customary adiabatic relation

$$T_{R_e} = T_e/T_c = (p_e/p_c)^{(\gamma-1)/\gamma}. \tag{7}$$

Results are summarized by the plots of Fig. 1. It should be noted that the minimum value of $r/r_e = r_t/r_e$, corresponding to the nozzle throat, occurs at greater values of T_R for smaller γ in accord with Eq. (6). Also the value of $T_{R_e} = T_e/T_c$ increases with decreasing γ according to Eq. (7). As the chamber entrance is approached where $T_R=1$, r/r_e increases without limit. This is the result of the assumption that $v=0$ at $T=T_c$, which was made in the derivation of Eq. (4).

III. REDUCED TEMPERATURE AS A FUNCTION OF AXIAL DISTANCE

Instead of expressing T_R as a function of r/r_e, it is possible to relate T_R to the linear distance from some arbitrarily chosen origin. It is convenient to choose the origin at the nozzle throat and to designate the direction toward the nozzle exit as the positive axis, as shown in Fig. 2.

Conventional designs of rocket nozzles are

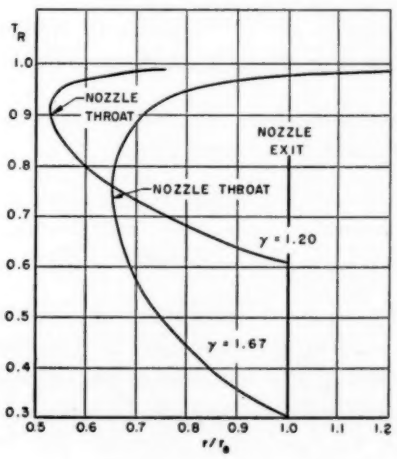

FIG. 1.

[15] S. S. Penner and D. Altman, J. Franklin Inst. **245**, 421 (1948).

*** The constancy of c_p and hence of γ is assumed in the present paper for the sake of simplicity. The replacement of an average γ for a given region by a variable γ which includes changes in internal energy states and chemical composition involves a second-order correction to the physical parameters discussed in this paper.

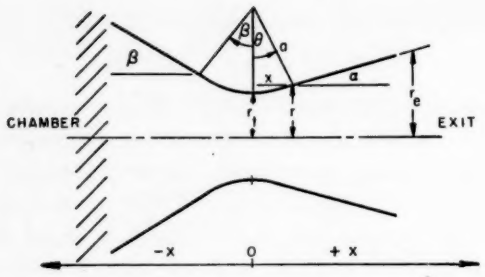

FIG. 2.

formed from two intersecting cones of half angles α and β. The throat region is rounded off with a radius of curvature a, which is frequently chosen as approximately equal to the throat diameter $2r_t$. In the present analysis, it will be assumed that $a=2r_t$, $\alpha=15°$, and $\beta=30°$.

Reference to Fig. 2 shows that if r is the radius of an arbitrary point in the region of the throat and subtends an angle θ, the following relations follow from trigonometry:

$$\left.\begin{aligned} r&=(a+r_t)-a\cos\theta=r_t+a(1-\cos\theta),\\ dr&=a\sin\theta d\theta,\\ x&=a\sin\theta,\\ dx&=a\cos\theta d\theta.\end{aligned}\right\} \quad (8)$$

Hence

$$dr=\tan\theta dx.$$

In general, it is evident that

$$dr=\tan\delta dx, \quad (9)$$

where

$$\tan\delta=\begin{cases}\tan\beta \text{ in the converging section}\\ \tan\theta \text{ in the throat region where the nozzle contour is circular}\\ \tan\alpha \text{ in the expanding section.}\end{cases}$$

By combining Eqs. (4) and (9) and replacing dx by $a\cos\theta d\theta$, it is found that

$$\frac{d\theta}{dT_R}=\frac{r[\frac{1}{2}(1-T_R)^{-1}-(\gamma-1)^{-1}T_R^{-1}]}{2a\sin\theta}. \quad (10)$$

According to de l'Hospital's rule, the limit of $d\theta/dT_R$ as θ approaches zero is determined by differentiating the numerator and denominator of Eq. (10) with respect to T_R and taking the limit as θ approaches zero of the resulting fraction. This procedure can be shown to lead to the relation

$$\lim_{\theta\to0}\left(\frac{r_t}{2a}\right)\left[\frac{1}{2(1-T_{Rt})^2}+\frac{1}{(\gamma-1)T_{Rt}^2}\right]=\frac{(\gamma+1)^3}{(\gamma-1)}\frac{r_t}{8a}, \quad (11)$$

where use has been made of Eq. (6). Since $r_t(\gamma+1)^3/8a(\gamma-1)^2$ is positive and finite, it follows that

$$\lim_{\theta\to0}(d\theta/dT_R)$$

must also be positive and finite. Therefore,

$$\lim_{\theta\to0}\frac{dx}{dT_R}=a\lim_{\theta\to0}\frac{d\theta}{dT_R}=\tfrac{1}{2}\left(\frac{\gamma+1}{\gamma-1}\right)\left(\frac{(\gamma-1)ar_t}{2}\right)^{\frac{1}{2}}. \quad (12)$$

It is interesting to note that as a approaches zero and the nozzle contour approaches that formed by the intersection of two cones, the reduced temperature gradient dT_R/dx approaches infinity at the throat.

IV. TIME SPENT BY AN ELEMENT OF GAS IN A GIVEN TEMPERATURE RANGE

The time dt spent by an element of gas in the reduced temperature range dT_R corresponding to the distance dx is $dt=dx/v$ where dx is always positive along the path of flow. Thus

$$dt/dT_R=(1/v)(dx/dT_R). \quad (13)$$

No correction has been made for the fact that the flow is not entirely parallel to the nozzle axis, since this correction is small for the chosen values of α and β.[1] Substituting Eqs. (3) and (10) with θ replaced in terms of x in Eq. (13) yields finally for the derivative of the residence time with respect to temperature

$$\frac{dt}{dT}=\frac{r(M/2c_pT_c^3)^{\frac{1}{2}}}{2\tan\delta}\times\left[\frac{1}{2(1-T_R)^{\frac{1}{2}}}-\frac{1}{(\gamma-1)T_R(1-T_R)^{\frac{1}{2}}}\right]. \quad (14)$$

The value of dt/dT at the nozzle throat is

TABLE I. Derivative of residence time with respect to temperature for two types of gases.

T_R	T (°K)	$(-dt/dT)\times10^8$ (sec./°K) for two gases: Predominantly helium ($\gamma=1.67$, $M=4$ g/mol)	Combustion gases of nitric acid-aniline motor ($\gamma=1.20$, $M=27$ g/mol)
0.99	2970	149	143
0.95	2850	7.94	14.2
0.909†	2727	—	7.12†
0.90	2700	3.35	6.18
0.85	2550	1.98	4.15
0.80	2400	1.25	4.65
0.750†	2250	0.95†	5.73
0.70	2100	0.90	6.97
0.65	1950	0.85	8.56
0.607††	1821	—	10.3††
0.60	1800	0.75	—
0.55	1650	0.95	—
0.50	1500	1.17	—
0.40	1200	1.76	—
0.302††	906	2.83††	—

† Denotes throat.
†† Denotes exit.

obtained from Eq. (14) by noting that $1-T_{R_t}=(\gamma-1)/(\gamma+1)$. The result is

$$\left(\frac{dt}{dT}\right)_t=\frac{1}{4}\left(\frac{\gamma+1}{\gamma-1}\right)^2\left(\frac{(\gamma-1)Mar_t}{c_pT_c^3}\right)^{\frac{1}{2}}. \quad (15)$$

Equations (14) and (15) have been used to calculate the derivative of the residence time with respect to temperature dt/dT for two types of gases. A calculation has been made for a gas consisting predominantly of helium where $\gamma=1.67$ and $M=4$ g/mol, and another calculation has been made for a typical gas composition encountered in a nitric acid-aniline combination where $\gamma=1.20$ and $M=27$ g/mol. For both systems the following design parameters were assigned: $\alpha=15°$, $\beta=30°$, $T_c=3000°K$, $p_c/p_e=20$, and $r_e=5$ cm. The results of these calculations are presented in Table I and shown graphically in Fig. 3.

Reference to Fig. 3 shows that the minimum values of $-dt/dT$ do not occur at the throat for a nozzle of the chosen contour but rather at the point of discontinuity in the expanding section of the nozzle where $\theta=15°$.

Data on the derivative of the residence time with respect to temperature as a function of temperature of the type shown in Fig. 3 may be combined with known values for reaction rates to determine the extent of changes in concentration which accompany flow through the nozzle. In general, there is not enough information concerning reaction rates to allow more than qualitative estimates of the importance of changes of concentration resulting from chemical reaction occurring during flow through the nozzle at the high temperatures of interest in the present study. A useful method illustrating a procedure for calculating changes during flow through the nozzle is given in the following section for the decomposition of nitric oxide.

V. DECOMPOSITION OF NITRIC OXIDE DURING FLOW THROUGH A ROCKET NOZZLE

The rate constant k_f for the decomposition of nitric oxide according to the reaction

$$2NO\underset{k_b}{\overset{k_f}{\rightleftarrows}}N_2+O_2 \quad (16)$$

has been determined experimentally in the temperature range between 1500 and 2500°K under conditions approximating those existing in a rocket chamber and nozzle.[12,13,14] Although the reaction represented by Eq. (16) is probably not a homogeneous bimolecular gas reaction, the over-all process has been shown to be kinetically of second order.[12,13,14] Daniels and co-workers have calculated the rate constant for the decomposition of nitric oxide using the theory of absolute reaction rates and making the assumption that the decomposition of nitric oxide is a homogeneous bimolecular reaction.[12] The theoretical relation was found to be in good agreement with the experimental results obtained in a nitrogen fixation furnace after proper adjustment of the frequency factor. Daniels' rate constant will be employed in the following

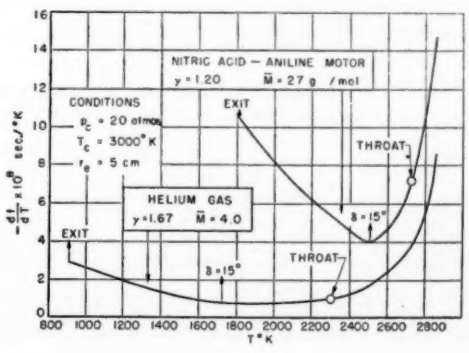

FIG. 3.

TABLE II. Equilibrium concentrations of NO, N_2, and O_2 in the rocket nozzle of a representative nitric acid-aniline motor.

T (°K)	$K_{eq}=n_{N_2}n_{O_2}/(n_{NO})^2$	n_{NO}	n_{N_2}	n_{O_2}
3000	66	0.0610	3.75	0.0655
2900	85	0.0552	3.75	0.0684
2800	110	0.0494	3.76	0.0713
2700	148	0.0436	3.76	0.0742

discussion in order to illustrate the method of application and also to predict approximately the approach to equilibrium of the NO decomposition reaction. Daniels' value for k_f is

$$k_f=1\times10^9 \times[\exp(-70{,}000/RT)]\ \text{atmos.}^{-1}\ \text{sec.}^{-1}. \quad (17)$$

If p_{NO}, p_{O_2}, and p_{N_2} represent the partial pressures of nitric oxide, oxygen, and nitrogen, respectively, which are present at any time during the expansion through the nozzle, then the rate of change of the partial pressure of nitric oxide with time resulting from chemical reaction is

$$-dp_{NO}/dt=k_f p_{NO}^2-(k_f/K_p)p_{O_2}p_{N_2}, \quad (18)$$

where the rate constant for the back reaction k_b has been replaced in terms of k_f and the equilibrium constant K_p is defined by the relation

$$K_p=p_{N_2}p_{O_2}/p_{NO}^2. \quad (19)$$

Although Eq. (18) should be used whenever calculations are carried out under conditions corresponding to a close approach to thermodynamic equilibrium, a simplification is justified when significant departures from thermodynamic equilibrium occur and the reformation of nitric oxide from oxygen and nitrogen can be neglected. In this case, Eq. (18) may be replaced by the approximate relation

$$\Delta p_{NO}/\bar{p}_{NO}=\bar{k}_f\bar{p}_{NO}\langle -dt/dT\rangle\Delta T, \quad (20)$$

where Δp_{NO} is the change in nitric oxide concentration which occurs in a temperature interval ΔT in which $\bar{p}_{NO}$, $\bar{k}_f$, and $\langle -dt/dT\rangle$ represent average values. It may be noted that the ratio $\Delta p_{NO}/\bar{p}_{NO}$ evaluated in Eq. (20) is also equal to the fractional change in the number of moles of nitric oxide, $\Delta n_{NO}/\bar{n}_{NO}$. The ratio $\Delta n_{NO}/\bar{n}_{NO}$, however, changes only as a result of chemical reaction and therefore provides a direct measure of the composition change produced by chemical reaction. Because the reformation of nitric oxide has been neglected in Eq. (20), the calculated values of $\Delta n_{NO}/\bar{n}_{NO}$ provide an upper limit for the true value of the term $\Delta n_{NO}/\bar{n}_{NO}$ and can therefore be used for establishing a conservative temperature below which composition changes caused by chemical reaction are negligible.

In a representative rocket motor using nitric acid and aniline as propellants, the number of moles of the various gases formed at equilibrium at a pressure of 20 atmos. and a temperature of 3000°K are $n_{NO}=0.0610$, $n_{N_2}=3.75$, and $n_{O_2}=0.0655$, while the partial pressure of nitric oxide is $p_{NO}^0=0.0610$ atmos. The equilibrium compositions at several other temperatures are summarized in Table II. These values were computed by use of the equilibrium constants given by Giauque and Clayton.[16] From the data listed in Table II it is possible to calculate the ratio $(\Delta n_{NO}/\bar{n}_{NO})_{equil.}$ for 100°K temperature intervals if thermodynamic equilibrium is maintained during expansion. The results of this calculation are contrasted in Table III with the actual changes produced by chemical reaction during flow, designated as $(\Delta n_{NO}/\bar{n}_{NO})_{kinetic}$, which were evaluated from Eq. (20). The average

TABLE III. Comparison between the kinetic and equilibrium values of $\Delta n_{NO}/\bar{n}_{NO}$.

T_2-T_1 (°K)	$\bar{k}_f$ (atmos.$^{-1}$ sec.$^{-1}$)	$\bar{p}_{NO}$ (atmos.)	$\langle -dt/dT\rangle\times10^8$ (sec. °K^{-1})	$(\Delta n_{NO}/\bar{n}_{NO})_{kinetic}$	$(\Delta n_{NO}/n_{NO})_{equil.}$
3000–2900	6.62×10^3	0.0531	52.6	0.01‡	0.0100
2900–2800	4.27×10^3	0.0400	14.2	0.0024	0.0111
2800–2700	2.76×10^3	0.0313	8.1	0.0007	0.0125

‡ The use of Eq. (20) in this temperature interval yields a value exceeding 0.01 since the back reaction has been neglected and the approach to equilibrium is very close. This value, therefore, was estimated from the complete Eq. (18).

[16] W. F. Giauque and J. O. Clayton, J. Am. Chem. Soc. 55, 4875 (1933).

value of the partial pressure of nitric oxide $\bar{p}_{NO}$ was calculated by taking into account the adiabatic change of state and a correction term for the extent of the chemical reaction by means of the equation

$$\bar{p}_{NO}=0.0610(\bar{T}/3000)^{\gamma/(\gamma-1)}-\Delta p_{NO}{}^{\bar{T}}, \quad (21)$$

where $\Delta p_{NO}{}^{\bar{T}}$ equals the reduction of partial pressure resulting from chemical reaction and $\bar{T}$ is the average temperature in the interval.

Comparison of the last two columns of Table II shows that significant departures from equilibrium occur in the temperature interval between 2900 and 2800°K and that the equilibrium

$$2NO \rightleftarrows N_2+O_2$$

is practically frozen below about 2800°K.

A calculation similar to the one just described has also been carried out for a gas with $\gamma=1.67$ and $\bar{M}=4$ g/mol using the same initial concentrations of N_2, O_2, and NO. Again it was found that practically no composition changes occur below about 2800°K. This result is not surprising since the thermodynamic constants of a gas do not produce a significant change in the term $(-dt/dT)$ or in the rate of decomposition of nitric oxide. Reference to Eq. (14) shows that the design parameters which affect some control over the composition changes are r and δ. In general, however, it is not practical to design a nozzle so as to give either constant-composition or equilibrium flow since design parameters r and δ are of secondary importance when compared with the reaction rate constants.

In conclusion, it should be emphasized that the present analysis is concerned only with the decomposition of nitric oxide according to Eq. (16). If gases are present which react chemically with nitric oxide, then the over-all composition change should be analyzed in terms of the composition changes associated with each of the individual reactions.

THE JOURNAL OF CHEMICAL PHYSICS VOLUME 17, NUMBER 1 JANUARY, 1949

The Kinetics of the Chromic Acid Oxidation of Isopropyl Alcohol: The Induced Oxidation of Manganous Ion

WARREN WATANABE AND F. H. WESTHEIMER
George Herbert Jones Laboratory, University of Chicago, Chicago, Illinois

(Received July 23, 1948)

1. Isopropyl alcohol "induces" the chromic acid oxidation of manganous salts to MnO_2. The limiting induction factor (ratio of moles of MnO_2 to moles of acetone formed) is one-half.

2. In the presence of manganous ion the rate at which chromic acid is reduced by isopropyl alcohol is decreased; the maximum decrease in rate observed under a wide variety of experimental conditions is 50 percent.

3. These facts, together with the previously determined reaction kinetics, demand the formation of an intermediate chromium compound in which chromium has the valence four or five.

4. Within chemically reasonable limits, *all* the reaction mechanisms involving such transitory intermediates have been examined. In the presence of manganous salts the only possible mechanism is

$$HCrO_4^-+CH_3CHOHCH_3 \rightarrow Cr^4+CH_3COCH_3,$$
$$Cr^4+Mn^{++} \rightarrow Cr^{+++}+Mn^{+++},$$
$$2Mn^{+++}+2H_2O \rightarrow Mn^{++}+MnO_2+4H^+.$$

In the absence of manganous salts several mechanisms (all of which are listed) are possible.

INTRODUCTION

IT has recently been shown[1] that, in the rate-controlling step of the chromic acid oxidation of isopropyl alcohol to acetone, one molecule of the alcohol reacts with one acid chromate ion and two hydrogen ions. In the over-all reaction, isopropyl alcohol undergoes a two electron oxidation; it follows, therefore, that the rate-deter-

[1] F. H. Westheimer and A. Novick, J. Chem. Phys. **11**, 506 (1943).

mining step must be either a reaction which produces a ketyl-free radical and a compound of pentavalent chromium, or a reaction which produces acetone and a compound of tetravalent chromium.[2] A complete mechanism for the chromic acid oxidation of isopropyl alcohol should identify the valence states of the chromium intermediates actually involved, and specify the further reactions by which these transitory intermediates are converted into the final reaction products. A tool with which to investigate the details of the reaction in question is supplied by the observation[1] that the chromic acid oxidation of isopropyl alcohol "induces"[3] the oxidation of manganous salts to manganese dioxide.

Chromic acid in dilute acid solution, or in acid solution containing acetone and a chromic salt, does not oxidize Mn^{++} to MnO_2. The active reagent in the reaction induced by isopropyl alcohol must therefore be one of the already

TABLE I. The induction factor: variation in Mn^{++} concentration.

Conc. of $MnSO_4$, mole/liter	Millieq. chromic acid reduced	Millieq. Mn^{++} oxidized (calc.)	Induction factor
0.053	0.137	0.036	0.36
0.106	0.141	0.040	0.40
0.213	0.148	0.047	0.47
0.331	0.153	0.050	0.50
0.426	0.149	0.048	0.48

postulated transitory compounds of tetravalent or pentavalent chromium. Furthermore, in the presence of manganous ion, the rate at which chromic acid is reduced is decreased by about fifty percent.[1] In the present investigation, the induced oxidation of manganous salts to MnO_2 and the concurrent decrease in reaction rate (hereafter called "inhibition") have been carefully studied. The results thus obtained show that the reaction sequence in the presence of manganous salts is that represented by Eqs. (1)–(3).

$$HCrO_4^- + H_2A \rightarrow Cr^4 + A, \quad (1)$$

$$Cr^4 + Mn^{++} \rightarrow Cr^{+++} + Mn^{+++}, \quad (2)$$

$$2Mn^{+++} + 2H_2O \rightarrow MnO_2 + Mn^{++} + 4H^+. \quad (3)$$

(In these and subsequent equations, acetone is represented by A, isopropyl alcohol by H_2A, the ketyl free radical by $HA\cdot$, compounds of pentavalent and tetravalent chromium by Cr^5 and Cr^4. Hydrogen ions are omitted wherever it is possible to do so without ambiguity.)

In the absence of manganous ions, Eq. (1) represents the first stage of the reaction; no decision can as yet be made among several possibilities for subsequent stages.

THE INDUCTION FACTOR

The oxidation of manganous salts to manganese dioxide by chromic acid alone is thermodynamically impossible[4] at $p\mathrm{H} > 0$. Under these conditions the reverse reaction occurs slowly (see below). Since isopropyl alcohol induces the chromic acid oxidation of manganous salts, the stoichiometry of the reaction must be represented by (4) or (5), or by a combination of (4) and (5).

$$2H_2A + 2Cr^6 + Mn^{++} \rightarrow 2A + 2Cr^{+++} + MnO_2, \quad (4)$$

$$H_2A + 2Cr^6 + 2Mn^{++} \rightarrow A + 2Cr^{+++} + 2MnO_2. \quad (5)$$

The ratio of the number of moles of MnO_2 produced to the number of moles of alcohol oxidized is called the "induction factor" for the reaction in question; the induction factor for reaction (4) is one-half, whereas that for (5) is two. Since experiment has shown that the induction factor is approximately one-half, Eq. (4) is stoichiometrically correct.

In every actual experiment, however, the value of the induction factor was found to be below 0.5; in fact this latter value was obtained only as a limit which was approached asymptotically when the manganous ion concentration was high, and when other special precautions (see below) were observed. Asymptotic approach to a definite induction factor has been observed in other cases,[3] and was here to be anticipated for the following reasons: In the absence of manganous ion the transitory chromium intermediates are

[2] For other cases in which compounds of pentavalent or tetravalent chromium have been described or inferred, see R. F. Weinland and M. Fiederer, Ber. **39**, 4042 (1906); C. Wagner and W. Preis, Zeits. f. anorg. allgem. Chemie **168**, 265 (1928); C. Wagner, *ibid.* **168**, 279 (1928).

[3] For other examples of induced chromic acid oxidations see C. F. Schönbein, J. pract. Chem. **75**, 108 (1858); F. Kessler, Pogg. Ann. **119**, 218 (1863); R. Lang, Zeits. anorg. f. allgem. Chemie **170**, 387 (1928); E. H. Land and J. Zwerina, *ibid.* **170**, 389 (1928).

[4] W. M. Latimer, *Oxidation Potentials* (Prentice-Hall, Inc., New York, 1938).

somehow consumed (e.g., by reaction with isopropyl alcohol). Consequently in the presence of manganous ion, isopropyl alcohol (or whatever it is with which the transitory compounds react) must compete for the transitory tetravalent or pentavalent chromium compounds. The manganous ion will compete successfully for the intermediate (and the stoichiometry will be that of Eq. (4)) only when the concentration of this ion is high; hence only under these conditions will the limiting value of the induction factor be attained.

In the experiments here performed, measured amounts of isopropyl alcohol in dilute perchloric acid solution were allowed to react essentially to completion with excess chromic acid and manganous ion. Then the amount of precipitated MnO_2 and the amount of unreacted chromic acid were independently determined. Since under like conditions but in the absence of manganous ion the oxidation of isopropyl alcohol to acetone is quantitative,[1] it was possible to compute the amount of manganous ion oxidized to MnO_2 from the amounts of chromic acid and alcohol consumed. Since the two methods led to the same result, both were employed. Table I gives the data and the induction factor obtained in a series of experiments in which the manganous ion concentration was varied and in which the other conditions were favorable to the formation of MnO_2. All the reaction mixtures had a total volume of 61 cc and were 0.0162 molar in chromic acid, 0.82 molar in perchloric acid, and 0.166 molar in isopropyl alcohol.

Although it was never possible to obtain an induction factor greater than 0.5, many experiments led to lower values for this factor. These low values were obtained not only in those experiments where insufficient manganous ion was used, but also in many experiments where the concentration of this ion was high. Careful tests, however, revealed that the MnO_2 produced in the induced oxidations is not indefinitely stable; in the solutions in which it is formed it slowly oxidizes chromic salts to chromates and isopropyl alcohol to acetone. Reaction (3) between Mn^{++}, Mn^{+++}, and MnO_2 was also considered; it proved, however, to be unimportant compared to the reactions of MnO_2 with chromic salts and isopropyl alcohol. When the induced

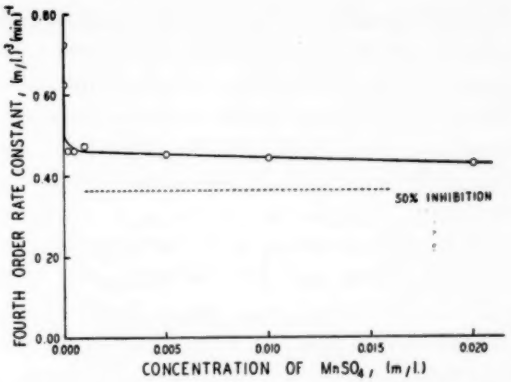

FIG. 1. Set of 8 determinations of the rate constant for the oxidation of isopropyl alcohol by chromic acid. Initial $(H^+) = 0.345M$, initial $(CH_3CHOHCH_3) = 0.200M$, initial $(CrO_3) = 0.0100M$; (Mn^{++}) shown in graph.

oxidation was allowed to proceed to completion, good yields of MnO_2 could be obtained only when the amount of alcohol oxidized was small. Hence there is evidently a relatively narrow range of concentrations of isopropyl alcohol and manganous salts over which the limiting value of 0.5 for the induction factor can actually be attained. (Some of the data leading to this conclusion are presented in the experimental section.) Since, however, the only two limiting values of the induction factors in question are 2.0 and 0.5, there can be no doubt that the latter is the correct one.

THE INHIBITION

It has already been noted that manganous ion decreases the rate at which chromic acid is reduced by isopropyl alcohol. This effect may easily be detected when solutions of manganous ion containing as little as 10^{-5} mole/liter are used. The maximum effect (a diminution in rate of about 50 percent) is achieved when the concentration of manganous ion is less than 0.01 mole/liter. A typical series of experiments is

TABLE II. Inhibition of the oxidation by Mn^{++}.

Chromic acid, mole/liter	Isopropyl alcohol, mole/liter	k_4, (mole/liter)$^{-3}$ min.$^{-1}$ No Mn^{++}	k_4, (mole/liter)$^{-3}$ min.$^{-1}$ $(Mn^{++}) = 0.01$ mole/liter	Percent inhibition
0.100	0.020	0.542	0.425	21.6
0.010	0.020	0.566	0.405	28.4
0.001	0.020	0.632	0.417	34.0
0.100	0.200	0.727	0.473	34.9
0.010	0.200	0.723	0.440	39.2
0.001	0.200	0.715	0.443	38.0
0.100	1.250	0.996	0.510	48.8
0.010	1.250	0.875	0.470	46.3
0.001	1.250	0.825	0.437	47.0

illustrated by Fig. 1. Here, with increasing concentration of manganous ion, the rate constant asymptotically approaches a limit, which is 61 percent of that obtained in the absence of manganous ion. The results obtained under widely differing experimental conditions are summarized in Table II.

A 50 percent diminution of rate is quite clearly the limit which can be obtained even under special conditions, i.e., when high isopropyl alcohol and manganous ion concentrations and low chromic acid concentrations are employed. If the reaction mechanism later advanced were precisely correct, then it would always be possible at high manganous ion concentrations to obtain a 50 percent diminution of rate. The slight but real deviation of the experimental from the theoretical results is considered in a later section (Secondary Effects).

At this point a word about rate constants is necessary. The statement (cf. Eq. (1)) that the effective oxidizing agent is the acid chromate ion, $HCrO_4^-$, is based on the application of a fourth-order kinetic equation,[1] (*N*), in which the value[5] of 0.023 mole/liter is assigned to the equilibrium constant for the hydrolysis (Eq. (6)) of dichromate to acid chromate ions.

$$Cr_2O_7^= + H_2O \rightleftarrows 2HCrO_4^-. \qquad (6)$$

The appropriate kinetic equation, (*N*), had previously been applied to results obtained at 40°; it applied equally well to those here obtained at 25° in the absence of manganous ion, or in the presence of either a very low (0.00001 mole/liter) or a considerable (0.01 mole/liter) concentration of manganous ion. But for intermediate concentrations (around 0.001 mole/liter) the rate constants, calculated by the use of Eq. (*N*), tended to drift downward during the course of each experiment; after one-half life these constants were 10–20 percent below the initial values.

These rather poor rate constants are somehow related to the precipitation of MnO_2 in the reaction mixtures. In the experiments where very little manganous ion is used no MnO_2 precipitates during the reaction. Since inhibition nevertheless occurs in these experiments, manganous ion must be oxidized and then regenerated. The manganic ions (or ions of tetravalent manganese) formed must be reduced, either by isopropyl alcohol or chromic ion or both. In experiments where the manganous ion concentration is high, manganese dioxide is promptly precipitated. However, in experiments where intermediate concentrations of manganous salts are used, only later does MnO_2 precipitate. The precipitation of the MnO_2 occurs approximately where the rate constant diminishes; further, if from the very beginning of the experiment MnO_2 is suspended in the solution, the lower rate constant is obtained throughout.

In order to be conservative, all the rate constants here reported are those which apply to the initial rate. If the average rate constant (or the rate constant obtained after MnO_2 had precipitated) had been used, the values of the calculated percent of inhibition would have been closer to 50 percent than those shown in Table II.

DISCUSSION

The experimental data just cited are consistent with the following reaction schemes: In the absence of manganous ion, the oxidation of isopropyl alcohol by chromic acid may occur by way of Eqs. (1) and (7)–(9).

$$HCrO_4^- + H_2A \rightarrow Cr^4 + A, \qquad (1)$$

$$Cr^4 + H_2A \rightarrow Cr^2 + A, \qquad (7)$$

$$Cr^6 + Cr^2 \rightarrow Cr^{+++} + Cr^5, \qquad (8)$$

$$Cr^5 + H_2A \rightarrow Cr^{+++} + A, \qquad (9)$$

or by one of several other paths to be later outlined. In the presence of manganous ion, the reaction occurs by way of Eqs. (1)–(3).

$$HCrO_4^- + H_2A \rightarrow Cr^4 + A, \qquad (1)$$

$$Cr^4 + Mn^{++} \rightarrow Cr^{+++} + Mn^{+++}, \qquad (2)$$

$$2Mn^{+++} + 2H_2O \rightarrow MnO_2 + Mn^{++} + 4H^+. \qquad (3)$$

The stoichiometry of Eqs. (1)–(3) is consistent with a limiting value of 0.5 for the induction factor; the two sets of equations together account for the fact that manganous ion cuts in half the rate at which chromic acid is consumed. This latter effect is explained as follows: In the reaction scheme represented by Eqs. (1) and (7)–(9), one acid chromate ion is consumed in

[5] J. D. Neuss and W. Rieman, J. Am. Chem. Soc. **56**, 2238 (1934).

reaction (1) and each molecule or ion of tetravalent chromium produced in (1) consumes (by way of reactions (7) and (8)) a second ion containing hexavalent chromium. On the other hand, if tetravalent chromium reacts with manganous ion instead of with hexavalent chromium (that is, if reaction (2) replaces reaction (7)), then the rate at which hexavalent chromium is consumed is cut in half.

Although the mechanism just presented accounts satisfactorily for the observed induction and inhibition effects, there remains the question of whether this scheme is the only one which does so, or whether it is merely one of many satisfactory possibilities. Usually it is difficult, if not impossible, to show that any given kinetic mechanism is unique. In the present case, however, the mechanism advanced for the reaction in the presence of manganous ion appears to be the only one falling within certain logically arbitrary but chemically reasonable limits referred to below as assumptions (*A*)–(*F*); the mechanism advanced for the reaction in the absence of manganous ion is one of a clearly designated small set. In order to show that such is the fact, *all* possible mechanisms consistent with the above-mentioned limitations are considered individually.

The oxidation of isopropyl alcohol by chromic acid may involve any or all of the following chemical species: compounds of hexavalent, pentavalent, tetravalent, trivalent, or divalent chromium, isopropyl alcohol, the ketyl free radical, the OH free radical, and acetone. (The H^+ ion, although it takes part in the reaction, may here be left out of account.) The first assumption (*A*) is that, for each valence state of chromium, there is only one effective oxidizing or reducing species; these are hereafter called Cr^6, Cr^5, Cr^4, Cr^3, and Cr^2.

Any step in the over-all oxidation must then be a reaction in which one or more of the nine substances just mentioned take part. The simplest steps would be bimolecular oxidation-reduction reactions; it is assumed (*B*) that only such reactions need be considered. If each species is paired with itself and with each of the other eight, there are forty-five possible combinations. The members of some of these pairs (e.g., $Cr^3+CH_3CHOHCH_3$, or Cr^6+Cr^6) are obviously stable toward one another, and some pairs are merely the products formed in more probable bimolecular reactions between members of the nine fundamental species. Elimination of pairs of the sorts just mentioned leads to a list of twenty-eight reactions; the list includes several cases where a given pair of reactants may react in two different ways to form two different sets of reaction products. The list may be further diminished by eliminating all reactions between two transitory intermediates (e.g., between a compound of tetravalent chromium and a ketyl free radical). Although this latter limitation seems drastic, it will later be shown to be equivalent to the reasonable assumption (*C*) that the transitory intermediates do not react preferentially with one another to the exclusion of their reaction with the stable species in solution.

It has further been assumed (*D*) that the chromium compounds containing Cr^4 and Cr^5 do not oxidize the solvent (water); except, perhaps, that tetravalent chromium may thus produce OH radicals.

$$Cr^4+H_2O\rightarrow Cr^3+HO\cdot. \qquad (10)$$

The experiments later described show that two electron oxidations of the solvent do not occur. Such oxidations would produce hydrogen peroxide. Even in the presence of isopropyl alcohol, this peroxide reacts with chromic acid to form perchromic acid which, under the experimental conditions here employed, decomposes[6] (see experimental section) to yield chromic ion and oxygen. It follows that, if hydrogen peroxide were formed, some of the oxidizing power of the solution would be lost as oxygen, and the yield of acetone, based on the chromic acid consumed, would not be quantitative. Since this yield is in fact quantitative, it follows that no peroxide (or oxygen) is formed. Finally, the reaction

$$Cr^5+H_2O\rightarrow Cr^4+HO\cdot \qquad (11)$$

is eliminated because it is unlikely that the oxidation portential of the Cr^5-Cr^4 couple is large enough to decompose water.

A fifth assumption (*E*) is that the reactions to be listed go essentially to completion in the direction indicated. The twelve reactions consistent with the assumptions (*A*)–(*E*) are listed

[6] N. D. Podobed, Chem. Abs. **32**, 25 (1938).

TABLE III. The mechanisms derived from the reactions of set (12).

(I) 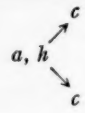

(II) a, f, g, c

(III) a, e, i, c

(IV) a, k, l, g, c

(V)

(VI) 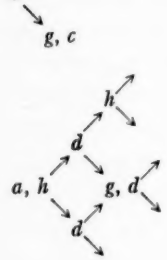

(VII) 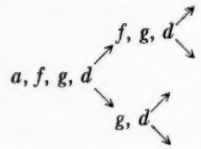

(VIII) 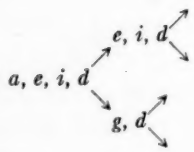

(XI) 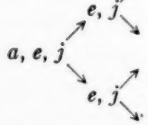

(X) 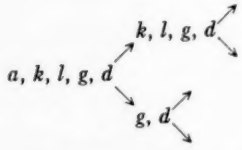

(XI) 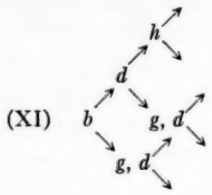

(XII) 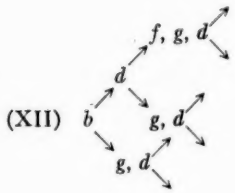

(XIII) 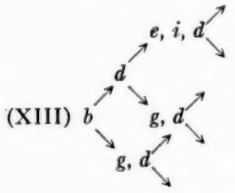

(XIV) 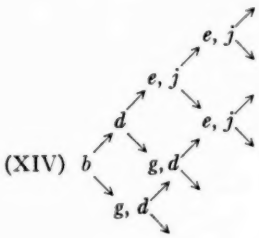

(XV) 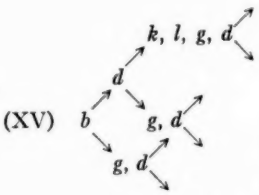

as set (12).

$$Cr^6+H_2A\rightarrow Cr^4+A, \quad (12a)$$

$$Cr^6+H_2A\rightarrow Cr^5+HA\cdot \quad (12b)$$

$$Cr^5+H_2A\rightarrow Cr^3+A, \quad (12c)$$

$$Cr^5+H_2A\rightarrow Cr^4+HA\cdot, \quad (12d)$$

$$Cr^4+H_2A\rightarrow Cr^2+A, \quad (12e)$$

$$Cr^4+H_2A\rightarrow Cr^3+HA\cdot, \quad (12f)$$

$$Cr^6+HA\cdot\rightarrow Cr^5+A, \quad (12g)$$

$$Cr^6+Cr^4\rightarrow 2Cr^5, \quad (12h)$$

$$Cr^6+Cr^2\rightarrow Cr^5+Cr^3, \quad (12i)$$

$$Cr^6+Cr^2\rightarrow 2Cr^4, \quad (12j)$$

$$Cr^4+H_2O\rightarrow Cr^3+HO\cdot, \quad (12k)$$

$$HO\cdot+H_2A\rightarrow H_2O+HA\cdot. \quad (12l)$$

In constructing mechanisms from these basic reactions, the following rules are applied: The total mechanism must account for the stoichiometry of the over-all reaction; the first (and rate-controlling) step must be either (12a) or (12b), since these alone are consistent with the known kinetics.[1] When these two rules are applied, fifteen different reaction schemes can be constructed from the twelve basic reactions of set (12). These mechanisms are collected in Table III; for brevity, the reactions are designated by letter. That is, the reaction scheme previously presented as Eqs. (1) and (7)–(9) is here written as a, e, i, c (mechanism III). Since the reactions b, d, h, and j lead to the formation of two unstable reactive intermediates, these reactions cause "branching." Whenever in Table III the arrows indicating branching do not lead to the symbol for any reaction of set (12), the mechanism is of the "chain branching" (autocatalytic) type.

Mechanisms VI–XV of Table III are of this chain-branching (autocatalytic) type. And, since the kinetics[1] of the over-all reaction show that it is not autocatalytic, these schemes must be discarded. Only mechanisms I–V remain.

It is on the basis of this conclusion that the reasonableness of restriction C rests. By this restriction all reactions between transitory intermediates are disregarded. Consider the three species, X, Y, and Z, of which X and Y are unstable intermediates and Z is a stable molecular species. If X reacts occasionally with Z and occasionally with Y, this latter chain-breaking step may serve to prevent autocatalysis of the simple-chain type, but cannot prevent autocatalysis of the branched-chain type. Only if X reacts almost exclusively with Y does this chain-

breaking mechanism serve to prevent autocatalysis of the branched chain type.[7] The autocatalytic mechanisms listed in Table III are all of the branched-chain type. Since they have been ruled out (by the fact that the chromic acid oxidation of isopropanol is not autocatalytic), only the following two hypotheses are possible:

(a) The unstable intermediates at least occasionally attack the stable molecular species. If such is the fact, then, since the over-all oxidation is not autocatalytic, only the mechanisms I–V listed in Table III are possible; and these would not be greatly modified by occasional reactions between two unstable intermediates (see Secondary Effects).

(b) The unstable intermediates react exclusively with one another. This behavior on their part would serve to prevent autocatalytic reactions of the branched-chain type such as VI–XV in Table III. But since these unstable intermediates are present only at very high dilution in the reaction mixture, it is extremely improbable that they would behave in the manner indicated. For this reason, assumption *C* appears highly plausible.

TABLE IV. Non-chain mechanisms using the reactions of sets (12) and (13) and giving the stoichiometry of Eq. (4).

XVI	(12a), (13c), (13g)	XXI	(13e), (12c), (13g)
XVII	(12a), (13d), (12i), (12c)	XXII	(13f), (12e), (12i), (12c)
XVIII	(12a), (12f), (12g), (13b)	XXIII	(13f), (12f), (12g), (12c)
XIX	(12a), (12e), (12i), (13b)	XXIV	(13f), (12k), (12l), (12g), (12c)
XX	(12a), (12k), (12l), (12g), (13b)		

Before trying to decide among mechanisms I–V, it is necessary to consider the possible mechanisms for the induced oxidation of manganous ion to MnO_2. It seems unlikely (assumption *F*) that the ketyl-free radical or the OH· free radical can oxidize Mn^{++} to MnO_2; the other possibilities are those of set (13).

$$Mn^2+Cr^5\rightarrow Mn^3+Cr^4, \quad (13a)$$

$$Mn^2+Cr^5\rightarrow MnO_2+Cr^3, \quad (13b)$$

$$Mn^2+Cr^4\rightarrow Mn^3+Cr^3, \quad (13c)$$

$$Mn^2+Cr^4\rightarrow MnO_2+Cr^2, \quad (13d)$$

$$Mn^2+Cr^6\rightleftarrows Mn^3+Cr^5, \quad (13e)$$

$$Mn^2+Cr^6\rightleftarrows MnO_2+Cr^4, \quad (13f)$$

$$2Mn^3+2H_2O\rightleftarrows MnO_2+Mn^{++}+4H^+. \quad (13g)$$

(Reactions (13e) and (13f) are here listed even though they are not reactions of manganous ion with an unstable chromium intermediate; they are eliminated by the argument given below.)

For the induced oxidation, the twelve reactions of set (12) and the seven of set (13) must be considered together. The conditions imposed on the system are the same as those previously used, except that the stoichiometry must correspond to Eq. (4), which implies an induction factor of one-half. Most of the conceivable mechanisms correspond to chain reactions. But no chain reaction (whether of the simple or of the branched-chain type) can be correct, since no such mechanism can account for the inhibition of the oxidation in the presence of manganous ion. All of the non-chain mechanisms which fall within the limits already proposed are listed in Table IV.

Mechanisms XXI–XXIV may be immediately eliminated, since they correspond to catalysis, not inhibition by manganous ion. Each of the mechanisms XVI–XX must be considered in combination with each of the mechanisms I–V of Table III. The correct mechanism (or mechanisms) must account for the fact that the upper limit of the inhibitory effect of manganous ion corresponds to a diminution of about 50 percent in the rate of consumption of chromate. It is a fortunate fact that of the mechanisms involving manganous ion only one (XVI = (1), (2), and (3) on p. 3) will account for any inhibition at all; this mechanism, as earlier noted, accounts for an inhibition of exactly 50 percent.

The choice of a mechanism for the induced oxidation facilitates the re-examination of the reaction schemes possible in the absence of manganous ion. Of these, I–IV begin with the same reaction (12a), which involves the formation of tetravalent chromium. In mechanism V, however, the only chromium-containing intermediate which appears contains pentavalent chromium. Since, in the induced oxidation, manganous ion is oxidized by tetravalent chromium, the latter species must appear somewhere in the complete reaction scheme. Hence mechanism V

[7] N. N. Semenov, *Chemical Kinetics and Chain Reactions* (Oxford University Press, London, 1935). H. D. Smyth, *Atomic Energy for Military Purposes* (Princeton University Press, 1945).

is eliminated and only mechanisms I–IV remain. These four mechanisms all start with the oxidation of isopropyl alcohol to acetone, accompanied by the reduction of acid chromate ion to a compound of tetravalent chromium; they differ as to the subsequent path by which the tetravalent chromium is reduced to chromic ion.

SECONDARY EFFECTS

In order to understand completely the mechanism of the oxidation of isopropyl alcohol by chromic acid, it is necessary to consider some of the slight but real variations in the rate constant, and to explain why the inhibition of the reaction by excess manganous ion is in some cases significantly less than fifty percent. These secondary effects can already be in part accounted for; in part they remain as subjects for future research.

The rate constant in the presence of manganous ion is certainly satisfactory, since 100-fold variations in the initial chromic acid concentration and 60-fold variations in the initial isopropyl alcohol concentration do not cause the rate constant to deviate by more than 10 percent from the average. Although this deviation is greater than the experimental error, the constancy of k over such wide variations in the concentrations of reactants is gratifying. The slightly larger rate constants observed at isopropyl alcohol concentrations of 1.25 mole/liter may be due to the fact that such high concentrations of alcohol (about 70 grams/liter) may cause an appreciable change in the properties of the solvent.

On the other hand, in the absence of manganous salts, the largest and smallest rate constants hitherto determined differ from the average by almost ±30 percent. This variation in the rate constant is the cause of the variation in the percent by which manganous salts inhibit the oxidation (see Table II). The results show an unmistakable trend; the inhibition approaches 50 percent when the isopropyl alcohol concentration is high and the chromic acid concentration low.

A possible explanation of the facts here observed is that the intermediate compounds of Cr^4 and Cr^5 disproportionate to a small extent. For example, the total rate at which chromic acid is consumed would be decreased by reaction (14).

$$Cr^4+Cr^5\rightarrow Cr^3+Cr^6. \qquad (14)$$

The rate of reaction (14) will be largest, relative to that of the normal reaction (e.g., mechanism III) when the isopropyl alcohol concentration is low and the chromic acid concentration high; the rate of (14) will be negligible when the chromic acid concentration is low and that of alcohol high. This explanation of a secondary effect is advanced only tentatively as a possible explanation for the low percent of inhibition observed under certain experimental conditions. However, this suggestion in no way invalidates the previous assumption (C) concerning the behavior of transitory intermediates. This assumption is only that transitory intermediates do not react with one another to the exclusion of their reactions with the stable species present. The tentative explanation here offered assumes only that transitory intermediates occasionally react with one another.

The reaction scheme which applies in the absence of manganous ion cannot now be selected with certainty. One of the four possible mechanisms, (II) involves the ketyl-free radical. This mechanism is not necessarily the correct one, despite the theory, recently advanced by Waters,[8] that chromic acid oxidations generally proceed by way of organic free radical intermediates. Waters showed that the chromic acid oxidation of many organic compounds is accompanied by the absorption of oxygen, and he stated correctly that many organic free radicals absorb oxygen. But many other compounds do so also. Further, it has been shown that the chromic acid oxidation of arsenious acid and of stannous salts is also accompanied by the reduction of oxygen.[9] Although these latter oxidations may proceed by way of transitory compounds involving, respectively, tetravalent arsenic and trivalent tin, it is possible (and with Cr^2 it is certain) that chromium compounds of valence other than six or three may also absorb oxygen.

Nevertheless, it seemed desirable to determine the effect of oxygen upon the rate of the chromic acid oxidation of isopropyl alcohol in aqueous solution. Careful experiments showed this rate

[8] W. A. Waters, J. Chem. Soc. 1151 (1946).
[9] R. Luther and T. F. Rutter, Zeits. anorg. f. allgem. Chemie 54, 1 (1907).

to be identical, within experimental error, under oxygen, under carbon dioxide, and in vacuum.

Other aspects of the chromic acid oxidation of isopropyl alcohol have been treated elsewhere.[10]

EXPERIMENTAL

Materials

The chromic acid used was Mallinckrodt reagent grade, purified by two recrystallizations from water;[11] solutions of chromic acid were standardized iodometrically. Mallinckrodt reagent grade 98 percent isopropyl alcohol was dried by refluxing over calcium oxide for 4 to 5 hours, quickly distilled, and again refluxed over fresh calcium oxide. The material thus treated was fractionated through a five plate distilling column; the fraction boiling at 82.0–82.1°, $\eta_D^{20}=1.3775$, was used in the experiments. Sodium perchlorate hydrate (G. F. Smith) was twice crystallized from water, dried, and weighed as the monohydrate. Manganous sulfate (General Chemical Company) was purified by crystallization from water slightly acidified with sulfuric acid; the salt was then dried, and analyzed for its manganese content by the bismuthate method.[12] All weighings of the dried manganous sulfate were made on the basis of the material thus analyzed. Perchloric acid (Mallinckrodt reagent grade 70–72 percent) was diluted to the approximate concentration required, and then standardized with carbonate-free base. In those experiments where MnO_2 was suspended in the reaction mixture before the start of the reaction, Merck reagent grade MnO_2, washed several times with water, was used.

Measurement of Induction Factor

The procedure employed to measure the induction factor was to pipette the requisite amounts of chromic acid, perchloric acid, isopropyl alcohol, and manganous sulfate solutions into an Erlenmeyer flask, and to allow the reaction to proceed undisturbed at room temperature. After a time had elapsed sufficient for all the isopropyl alcohol to be completely oxidized, the MnO_2 precipitate was filtered out on an asbestos mat and analyzed. The amount of chromic acid reduced during the reaction was determined by an iodometric titration of the filtrate against standard thiosulfate. The direct analysis of the MnO_2 precipitate was carried out by washing the asbestos mat together with the MnO_2 precipitate into a flask, digesting with a known excess of standard oxalate, and back titrating with standard permanganate.[13] The time required for the completion of the reaction varied from 40 hours to 80 hours, depending on the amounts of isopropyl alcohol oxidized.

Some experiments were also carried out at 40°, but here the amounts of MnO_2 precipated were smaller and the induction factors found were uniformly lower than in the corresponding experiments carried out at room temperature. When the acidity was reduced by one-half, a solution containing 25 cc 1.009N $HClO_4$, 25 cc 0.0999N H_2CrO_4, 10 cc 0.3M $MnSO_4$, and 1 cc 1.009N isopropyl alcohol gave 0.39 for the induction factor, again a value smaller than the limiting value noted in Table I.

TABLE V. Stability of MnO_2 precipitate.

Time in hr.	Millieq. isopropyl alcohol oxidized	Millieq. chromic acid reduced	Millieq. Mn^{++} oxidized (calc.)	Millieq. Mn^{++} oxidized (anal)
48	0.202	0.287	0.085	0.081
69	0.202	0.287	0.085	0.079
91	0.202	0.289	0.087	0.080
139	0.202	0.277	0.075	0.066
69	0.505	0.678	0.173	
91	0.505	0.645	0.140	0.144
139	0.505	0.621	0.116	0.110
196	0.505	0.607	0.102	0.091

TABLE VI. Induction factor.

Millieq. isopropyl alcohol oxidized	Millieq. chromic acid reduced	Millieq. Mn^{++} oxidized (calc.)	Millieq. Mn^{++} oxidized (anal)	Induction factor
1.009	1.080	0.071	0.079	0.07
0.909	1.039	0.130	0.126	0.14
0.808	0.961	0.153	0.146	0.19
0.707	0.896	0.189	0.182	0.26
0.606	0.784	0.178	0.174	0.29
0.505	0.676	0.171	0.177	0.34
0.404	0.566	0.163	0.164	0.40
0.303	0.430	0.127	0.131	0.43
0.202	0.301	0.099	0.091	0.47
0.101	0.153	0.052	0.048	0.50

[10] F. H. Westheimer and N. Nicolaides, in press.

[11] E. H. Archibald, *The Preparation of Pure Inorganic Substances* (John Wiley and Sons, Inc., New York, 1932), p. 279.

[12] W. F. Hillebrand and G. E. F. Lundell, *Applied Inorganic Analysis* (John Wiley and Sons, Inc., New York, 1929), p. 343.

[13] W. C. Pierce and E. L. Haenisch, *Quantitative Analysis* (John Wiley and Sons, Inc., New York, 1940), p. 195.

Stability of Precipitated Manganese Dioxide

Precipitated MnO_2 was suspended in 1.0*N* perchloric acid which contained an excess of chromic nitrate, and the mixture was allowed to stand for several days at room temperature. At the end of that time, most of the MnO_2 had disappeared, and solution (which had initially been a clear green) had turned greenish-yellow. After the residual MnO_2 had been removed by filtration, lead acetate solution was added to the filtrate, and a bright yellow precipitate of lead chromate was formed. Another sample of the filtrate, treated with H_2O_2, gave the blue color of perchromic acid.

The stability of the MnO_2 precipitate formed in the induced oxidation was tested under various experimental conditions; some of the data obtained are shown in Table V.

The values of the induction factor found under a variety of experimental conditions are presented in Table VI. Low values for this factor are found under those experimental conditions where MnO_2 is unstable.

RATE MEASUREMENTS

The measurements were made at 25°±0.01° and an ionic strength of 0.600; the technique was that previously[1] used. In the calculation of the ionic strength, as well as in the computation of the rate constants, the acid chromate-dichromate equilibrium was taken into account; the "concentration" equilibrium constant was estimated as 0.015 mole/liter. The concentration of acid was computed as the sum of that of the chromic acid and that of the added perchloric acid.

When MnO_2 precipitated in the reaction vessel, it was removed before the analyses by pipetting out samples through an attached tip packed with glass wool. Separate experiments were made to check the effect of acetone on the method of analysis, but the greatest amount of acetone likely to be formed in any of the experiments was found to be too small to affect the accuracy of the method.

The experiments in which a possible oxygen effect was sought were made by carrying out the reactions in thermostatted Drexel flasks into which either carbon dioxide or oxygen was bubbled. In order to minimize loss of isopropyl alcohol by evaporation, a train of two Drexel flasks was set up for each experiment, and identical reactions were carried out in both flasks. Before the reactions were started, carbon dioxide (or oxygen) was bubbled through the flasks for an hour in order to remove dissolved oxygen (or to saturate the solutions with oxygen). The reaction was started in the usual manner, and the rate of reaction in the second flask of each train was followed.

The experiments in vacuum were carried out in a closed H-shaped double flask, in which the cross-bar was attached by a ground glass joint to a vacuum line. One compartment of the double flask was filled with measured volumes of chromic acid and perchloric acid solutions; the other was filled with a solution of isopropyl alcohol and sodium perchlorate. These solutions were such that the desired concentration of all reactants would be obtained when the solutions were mixed. Each compartment was frozen with dry ice-acetone and degassed three times. The double flask was then sealed off the vacuum line at a pressure of about 10^{-5} mm of Hg, and thermostatted for several hours. The reaction was started by mixing together the solutions in the two arms of the flask. After the reaction had proceeded somewhat more than 50 percent, the flask was opened and the contents analyzed. All the experimental errors involved in this procedure (loss of water during degassing, distilling of isopropyl alcohol into the chromic acid compartment) tend to raise the observed reaction rate.

Effect of Hydrogen Peroxide

Aqueous H_2O_2 was added to solutions of chromic acid, perchloric acid, and isopropyl alcohol similar to those used in the kinetic experiments already recorded. The appearance of the blue perchromic acid was instantaneous; the color rapidly faded with evolution of oxygen. The amount of chromate consumed in the process was followed by titration. The initial loss of oxidizing power as a result of the reaction with H_2O_2 was the same in the presence as in the absence of high concentrations (1.25 mole/liter) of isopropyl alcohol; the rate of decomposition of the perchromic acid was approximately the same in the presence as in the absence of isopropyl alcohol.

THE JOURNAL OF CHEMICAL PHYSICS VOLUME 17, NUMBER 1 JANUARY, 1949

Rate of Nucleation in Condensed Systems

D. TURNBULL* AND J. C. FISHER*
General Electric Company, Schenectady, New York

(Received June 28, 1948)

On the basis of the nucleation theory developed by Volmer, Becker, and co-workers, and the theory of absolute reaction rates, an expression is derived for the absolute rate of nucleation in condensed systems.

BECKER[1] has proposed the following type of expression for the rate of nucleation in condensed systems (i.e., liquid-solid or solid-solid transformations)

$$r^*=K\exp[-(\Delta F_i^*+q)/kT], \tag{1}$$

where ΔF_i^* is the maximum free energy necessary for nucleus formation, q is the energy of activation for diffusion across the phase boundary (or within the solid solution when the transformation involves the separation of a phase having a different composition), and K is an undetermined constant. Although Becker and Döring[2] were able to evaluate semiquantitatively the factor corresponding to K for the rate of nucleation of a liquid from a supersaturated vapor, to the authors' knowledge no theory has been proposed for nucleation in condensed systems from which K can be specified.

It is the purpose of the present paper to derive an expression for r^*, applying to condensed systems, on the basis of the theory of absolute reaction rates.

Nucleation theory frequently leads to an expression of the form

$$\Delta F_i/kT=Ai^{\frac{1}{3}}-Bi \tag{2}$$

for the local free energy change associated with the formation of a region of a new phase β in a parent phase α. In this equation i is the number of atoms or molecules in the transformed region. A is proportional to the interfacial free energy per unit area of α-β-interface, and B is proportional to the bulk free energy difference between β and α in the absence of surfaces.

The curve of $\Delta F_i/kT$ *versus* i passes through a maximum $\Delta F_i^*/kT=4A^3/27B^2$ at $i^*=(2A/3B)$. then decreases without limit as shown in Fig. 1[3] Subcritical nuclei containing fewer than i^* atoms require free energy for further growth, while those containing more than i^* grow freely with decreasing free energy. Since nuclei generally grow one atom at a time as the result of statistical thermal fluctuations, it is evident that small nuclei with fewer than i^* atoms will usually disappear without reaching critical size. Only occasionally will a long chain of favorable energy fluctuations produce a nucleus exceeding the critical size.

The steady state rate of nucleation for a given transformation corresponds to constant equal net forward rates for the following set of reactions

$$\begin{aligned} m\alpha_1&\rightleftharpoons\beta_m,\\ \beta_m+\alpha_1&\rightleftharpoons\beta_{m+1},\\ \beta_{m+1}+\alpha_1&\rightleftharpoons\beta_{m+2},\\ \beta_{m+2}+\alpha_1&\rightleftharpoons\beta_{m+3},\\ &\vdots \end{aligned} \tag{3}$$

where α_1 represents an atom of phase α, β_i a nucleus of phase β containing i atoms, and where β_m is the smallest nucleus of phase β. Further, the concentration of β-nuclei must decrease to zero as the nucleus size increases,

$$\lim_{i\to\infty}[\beta_i]=0, \tag{4}$$

since otherwise the percentage of untransformed α will not differ from zero.

Consider the reaction

$$\beta_i+\alpha_1\rightleftharpoons\beta_{i+1} \tag{5}$$

at steady state. Referred to phase α as the standard state, the free energy of $\beta_i+\alpha_1$ is ΔF_i while that of β_{i+1} is ΔF_{i+1}. Assuming that the intermediate configurations between $\beta_i+\alpha_1$ and β_{i+1} correspond to free energies greater than either ΔF_i or ΔF_{i+1}, each path by which β_i and

* Research Associate, General Electric Research Laboratory.

[1] R. Becker, Ann. Physik, **32**, 128 (1938).

[2] R. Becker and W. Döring, Ann. d. Physik [5] **24**, 719 (1935).

α_1 can be combined to give β_{i+1} will have an intermediate configuration of maximum free energy. For one of these paths there will be a particular intermediate configuration corresponding to the least maximum free energy. This configuration may be called an activated complex. The free energy difference between the activated complex and the mean of ΔF_i and ΔF_{i+1} will be denoted by Δf^*.

Figure 2 indicates schematically the free energy variation associated with the combination of β_i and α_1 to give β_{i+1} (or the decomposition of β_{i+1} to give $\beta_i+\alpha_1$) by a path having the least possible maximum free energy. If n_i represents the steady state concentration of β_i nuclei, the rate of the forward reaction

$$\beta_i+\alpha_1\rightarrow\beta_{i+1}$$

can be written as

$$r^+=n_i a_1 i^{\frac{1}{3}}(kT/h)\exp(-\Delta f_1^*/kT) \qquad (6)$$

according to the theory of absolute reaction rates.[3] Here $a_1 i^{\frac{1}{3}}$ is the number of α-atoms in contact with each β_i nucleus, and $n_i a_1 i^{\frac{1}{3}}$ is therefore the concentration of α-atoms available for the reaction. $(kT/h)\exp(-\Delta f_1^*/kT)$ is the specific reaction rate for the formation of the activated complex with free energy increment Δf_1^* as shown in Fig. 2.

The rate of the reverse reaction $\beta_{i+1}\rightarrow\beta_i+\alpha_1$ can be written as

$$r^-=n_{i+1}a_2 i^{\frac{1}{3}}(kT/h)\exp(-\Delta f_2^*/kT), \qquad (7)$$

where $a_2 i^{\frac{1}{3}}$ is the number of β-atoms in contact with α per β_{i+1} nucleus. The net forward rate of the reaction is therefore

$$r^*=r^+-r^-=(kT/h)i^{\frac{1}{3}}[n_i a_1\exp(-\Delta f_1^*/kT) - n_{i+1}a_2\exp(-\Delta f_2^*/kT)]. \qquad (8)$$

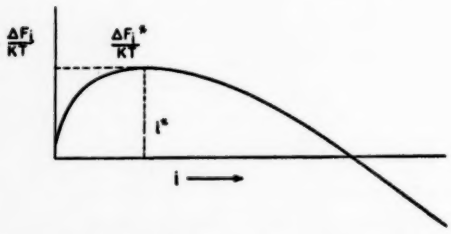

FIG. 1. $(\Delta F_i/KT)=Ai^{\frac{1}{3}}-Bi$ *versus* i.

[3] S. Glasstone, K. J. Laidler, and H. Eyring, *The Theory of Rate Processes* (McGraw-Hill Book Company, Inc., New York, 1941).

Equation (8) can be solved approximately for n_i by making the following simplifications:

(a) The number of α-atoms in contact with a β_i nucleus is not strictly equal to the number of β atoms in contact with α at the surface of a β_{i+1} nucleus. However, the difference is negligible for all but the smallest nuclei, and $a_1=a_2=a$ will be assumed.

(b) n_i and ΔF_i will be assumed smooth functions of i although they have meaning only for integral values of i. The change in n_i as i changes by one unit will be approximated by $(dn_i/di)\Delta i = dn_i/di$; similarly the change in ΔF_i will be approximated by $d(\Delta F_i)/di$. The approximation is good for all but the smallest nuclei.

(3) The quantities $(1/kT)d(\Delta F_i)/di$ and $(1/n_i)\times(dn_i/di)$ will both be assumed small in comparison with unity. Again the approximation is poor only for the smallest nuclei.

Noting that

$$\begin{aligned}\Delta f_1^* &= \Delta f^*+\tfrac{1}{2}(\Delta F_i+\Delta F_{i+1})-\Delta F_i\\ &= \Delta f^*+\tfrac{1}{2}(\Delta F_{i+1}-\Delta F_i)\\ &= \Delta f^*+\tfrac{1}{2}d(\Delta F_i)/di,\\ \Delta f_2^* &= \Delta f^*-\tfrac{1}{2}d(\Delta F_i)/di,\end{aligned}$$

$$r^*=(-akT/h)\exp(-\Delta f^*/kT)\times[n_i(\tfrac{2}{3}Ai^{-\frac{1}{3}}-B)+dn_i/di]i^{\frac{1}{3}}. \qquad (9)$$

Defining

$$R=r^*\Big/\left(\frac{akT}{h}\right)\exp(-\Delta f^*/kT), \qquad (10)$$

Eq. (9) reduces to the differential equation

$$dn_i/di+(\tfrac{2}{3}Ai^{-\frac{1}{3}}-B)n_i=-Ri^{-\frac{1}{3}}. \qquad (11)$$

The solution to Eq. (11) is

$$n_i=\exp[-(Ai^{\frac{1}{3}}-Bi)]\times\left[-R\int_{i_0}^{i}\exp(Ai^{\frac{1}{3}}-Bi)i^{-\frac{1}{3}}di + n_{i0}\exp(Ai_0^{\frac{1}{3}}-Bi_0)\right], \qquad (12)$$

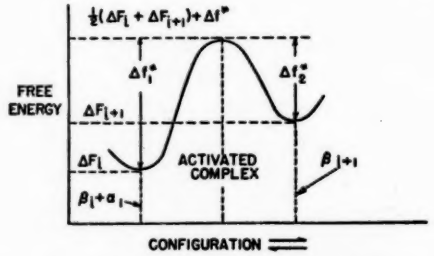

FIG. 2. Schematic representation of free energy of activation.

where n_{i0} is the steady state number of β_{i0} nuclei.

The steady state concentration of subcritical nuclei containing say one-third the critical number of atoms does not differ appreciably from the equilibrium concentration assuming no nucleation. Taking $i_0=i^*/3$,

$$n_{i0}=n\exp(-\Delta F_{i0}/kT)=n\exp[-(Ai_0^{\frac{2}{3}}-Bi_0)],$$

where n is the number of atoms of untransformed α. The expression for the steady state number of β_i nuclei reduces to

$$n_i=\exp(-\Delta F_i/kT)\times\left[-R\int_{i_0}^{i}\exp(\Delta F_i/kT)i^{-\frac{2}{3}}di+n\right]. \quad (13)$$

Since

$$\lim_{i\to\infty}\exp(-\Delta F_i/kT)=\infty,$$

and it is required that

$$\lim_{i\to\infty}n_i=0,$$

it must follow that

$$\lim_{i\to\infty}\left[-R\int_{i_0}^{i}\exp(\Delta F_i/kT)i^{-\frac{2}{3}}di+n\right]=0, \quad (14)$$

and hence that

$$R=n\Big/\left[\int_{i_0}^{\infty}\exp(\Delta F_i/kT)i^{-\frac{2}{3}}di+n\right]. \quad (15)$$

The exact location of the lower limit of integration in Eq. (15) is unimportant, since for i_0 intermediate between zero and i^* practically all the contribution to the integral comes from values of i very near i^*. Replacing $\Delta F_i/kT$ by a Taylor's expansion about $i=i^*$ and neglecting all terms after the third, the integral can be evaluated as

$$I=(9\pi/A)^{\frac{1}{3}}i^{*\frac{2}{3}}\exp(\Delta F^*/kT). \quad (16)$$

The steady state rate of nucleation is, therefore,

$$r^*=n^*(A/9\pi)^{\frac{1}{3}}(NkT/h)\times\exp[-(\Delta f^*+\Delta F^*)/kT] \quad (17)$$

nuclei per second per mole of untransformed material, where n^* is the number of surface atoms in the critical size nucleus. The quantity $n^*(A/9\pi)^{\frac{1}{3}}$ proves to be within a factor of ten of unity for most nucleation problems of interest, giving

$$r^*\cong(NkT/h)\exp[-(\Delta f^*+\Delta F^*)/kT] \quad (18)$$

nuclei per mole per second to an order of magnitude.

Equation (18) was derived for nucleation processes that do not require long-range diffusion. Δf^* is the free energy of activation for the short-range diffusion of atoms or molecules moving a fraction of an atomic distance across an interface to join a new lattice. However, long-range diffusion is to be expected in phase transformations that involve more than one component, since the new phase and the old are generally of different composition. Equation (18) approximates the rate of nucleation in a two or more component system when Δf^* is taken as the activation energy for diffusion of the most slowly moving component and when the expression is multiplied by the mole fraction of the precipitating component.

ACKNOWLEDGMENT

The authors are pleased to acknowledge some helpful conversations on this problem with Dr. Harvey Brooks of the Knolls Atomic Power Laboratory.

See footnote 12 in J. Chem Phys. 34, 820 (1961)

The Assignment of the Vibrational Spectra of the C_4 Hydrocarbons Butyne-1, Butene-1, and Vinyl Acetylene, to the Normal Modes of Vibration of These Molecules*

N. SHEPPARD**
Department of Physics, The Pennsylvania State College, State College, Pennsylvania

(Received June 25, 1948)

An attempt has been made to assign all the normal modes of vibration of the C_4 hydrocarbons butyne-1, butene-1, and vinyl acetylene, in terms of frequencies observed in the infra-red and Raman spectra. It has been found to be possible to do this in a satisfactory manner which takes into account the structural similarities of these and other hydrocarbon molecules. With the help of these assignments previous data on the frequency ranges characteristic of the various hydrogen deformation modes of the groups ethyl, vinyl, and $-C\equiv CH$ can be extended to include all such modes.

INTRODUCTION

THE detailed assignment of the vibrational spectra of the smaller hydrocarbons, together with the identification of the characteristic frequencies of particular structural groups in larger molecules, are two parallel methods which can be used to increase our understanding of the spectra of polyatomic hydrocarbons. The isolation and identification of characteristic frequencies in the infra-red and Raman spectra is in itself a method which can be applied with advantage as an aid to the complete analysis of the spectra of the smaller molecules. This has recently been shown in the case of *n*-butane,[1] and will be demonstrated again in the present communication. In recent years fairly complete assignments have been made for all the non-cyclic hydrocarbons of the C_2[2–5] and C_3[6–9] classes, and for the molecules *n*-butane,[1] isobutane,[10,11] isobutene,[7] *cis*- and *trans*-butene-2,[7] butadiene 1–2,[12] butadiene 1–3,[13] and dimethyl acetylene,[14] of the C_4 class. Assignments of a lesser degree of completeness have previously been made for the remaining well established C_4 hydrocarbons, and it is the purpose of this paper to bring up to date the work on these remaining molecules, with the exception of diacetylene (see reference 4, p. 323) for which further experimental work appears to be necessary. These three molecules, *viz.*, butyne-1, butene-1, and vinyl acetylene, also form a convenient series for examination as each of the structural groups, ethyl, vinyl, and $-C\equiv CH$, occurs in two of these molecules. An attempt will be made to assign specifically all the fundamental modes of vibration of these molecules in a manner which is consistent with the results on already reliably assigned molecules, and with the results of previous investigations on characteristic frequencies.

A. THE EXPERIMENTAL DATA

Experimental data on the infra-red and Raman spectra of all these molecules are now available.

In the case of butyne-1 (ethyl acetylene) Cleveland, Murray, and Taufen[15] have published

* This research was carried out on Contract N6onr-269 Task V of the Office of Naval Research.

** Now at Department of Colloid Science, Cambridge University, Cambridge, England.

[1] G. J. Szasz, N. Sheppard, and D. H. Rank, J. Chem. Phys. **16**, 704 (1948).

[2] F. Stitt, J. Chem. Phys. **7**, 297 (1939).

[3] W. S. Gallaway and E. F. Barker, J. Chem. Phys. **10**, 88 (1942).

[4] G. Herzberg, *Infra-Red and Raman Spectra of Polyatomic Molecules* (D. Van Nostrand Company, Inc., New York, 1945), p. 325.

[5] T. Y. Wu, *Vibration Spectra and Structure of Polyatomic Molecules* (Edwards Brothers, Inc., Ann Arbor, Michigan, 1946), p. 176.

[6] K. S. Pitzer, J. Chem. Phys. **12**, 310 (1944).

[7] J. E. Kilpatrick and K. S. Pitzer, J. Research Nat. Bur. Stand. **38**, 191 (1947).

[8] B. L. Crawford, J. Chem. Phys. **8**, 526 (1940).

[9] J. W. Linnett and W. H. Avery, J. Chem. Phys. **6**, 686 (1938).

[10] K. S. Pitzer and J. E. Kilpatrick, Chem. Rev. **6**, 686 (1938).

[11] N. Sheppard, J. Chem. Phys. **16**, 690 (1948).

[12] G. J. Szasz, J. S. McCartney, and D. H. Rank, J. Am. Chem. Soc. **69**, 3150 (1947).

[13] Aston, Szasz, Woolley, and Brickwedde, J. Chem. Phys. **14**, 67 (1946).

[14] B. L. Crawford, J. Chem. Phys. **7**, 555 (1939).

[15] F. F. Cleveland, M. J. Murray, and H. J. Taufen, J. Chem. Phys. **10**, 172 (1942).

the Raman spectrum together with the depolarization data for the lines. The infra-red spectrum has also been obtained recently.[16] Wagman, Kilpatrick, Pitzer, and Rossini[17] have previously made a semi-schematic assignment for this molecule.

The Raman spectrum of butene-1 (ethyl ethylene) has been independently determined by Kohlrausch and Stockmair,[18] and Bourguel and Piaux,[19] and the infra-red spectrum has been published by Rasmussen and Brattain.[20] A fairly detailed assignment has been made by Aston, Szasz, Woolley, and Brickwedde,[13] for the purpose of determining the contribution of the vibrational degrees of freedom to the thermodynamic properties of this molecule. This requires slight correction to bring it in line with data on the other molecules.

The Raman spectrum of vinyl acetylene has been studied by Glockler and Davis,[21] and Timm and Mecke,[22] and the infra-red spectrum has been obtained by Bartholomé and Karweil.[23] The most satisfactory previous assignment seems to be that of Kohlrausch,[24] made on the basis of the Raman frequencies.

There are possibilities of rotational isomerism in the case of the molecule butene-1. However, the number of lines in the infra-red and Raman spectra suggest that one form only is present in considerable quantity. It is probable that the energy difference between the two types of rotational isomer is greater than in the case of butane,[1] where several Raman frequencies caused by the higher energy form have been observed.

TABLE I. Collected experimental data on the vibrational spectra of butyne-1, butene-1, and vinyl acetylene.

Butyne-1		Butene-1		Vinyl acetylene	
Raman[a]	Infra-red[b]	Raman[c]	Infra-red[d]	Raman[e]	Infra-red[f]
3305 (2) 0.6	3300 (8)	3074 (4)	3075	3305 (1)	
2986 (5) 0.8		2998 (7)		3102 (2)	
2941 (8) 0.2		2968 (4)	2970	3012 (4)	
2919 (7) 0.2	2900 (10)	2936 (7)		2099 (6)	
2885 (5b) 0.4		2898 (7)		1595 (5)	1600 (8)
2851 (3) 0.4		2872 (4)		1405 (4)	1410 (2)
2118 (10) 0.5	2120	2850 (4)		1288 (4)	
1459 (3b) 0.8	1450 (9)	1636 (7)	1645 (9)		1245 (20)
1438 (4b) 0.8			1550 (1) *D*	1091 (2)	1090 (4)
1375 (1)		1450 (2)	1457 (9)		1058 (4)
1314 (4) 0.6	1325 (8) *D*	1416 (3)	1412 (½)		950 (30)
1252 (1b) 0.6	1250 (10) *PQR*		1391 (1)	928 (2)	935 (30)
1068 (6) 0.3	1070 (7) *D*	1376 (0)		875 (3)	
1023 (1)	1030 (½) *Q*		1307 (3) *PQR*	678 (2b)	
1005 (3) 0.6	1005 (1) *D*	1293 (5)		629 (4b)	
	910 (3) *PQR*	1257 (2)			615 (100)
840 (7) 0.2			1182 (1) *D*	538 (4)	535 (2)
784 (½)	783 (3) *PQR*	1166 (0)			515 (2)
642 (3b) 0.7	650 (6)		1135 (1)	309 (4b)	
563 (3) 0.5			1116 (1)	219 (4b)	
509 (4) 0.5		1068 (1)	1080 (4)		
348 (5b) 0.7		1019 (2)			
290 (1) *p*		(980) (2)	993 (9) *PQR*		
206 (8b) 0.7		908 (2)	912 (10) *PQR*		
		850 (4)	853 (1) *PQR*		
			802 (1)		
			788 (1) *D*		
		623 (½)			
		533 (0)			
		437 (2)			
		320 (0)			
		282 (½)			
		237 (0)			

[a] See reference 15.
[b] See reference 16.
[c] See reference 18.
[d] See reference 19.
[e] See reference 21.
[f] See reference 23.

In Table I are given the collected experimental data on vibrational spectra that have been used to make the assignments. In cases where several independent determinations of the spectra have been made, the values given are taken from the work of the authors of the most complete data, controversial frequencies being enclosed in brackets. The relative intensities of all the observed lines are given after the frequencies, and the degrees of depolarization or band contours of Raman or infra-red frequencies are given, when available, after the intensity values. *PQR* denotes an infra-red band with a marked *Q* branch, and *D*, a doublet contour. The designation *b* after the intensity value for a Raman line indicates a broad appearance to the line. Wherever possible, Table I is set out so that corresponding infra-red and Raman frequencies are opposite each other. The infra-red frequencies are estimated values taken from the center of each band contour. No frequencies greater than 3350 cm^{-1} are included, nor are any in the region 2800–1700 cm^{-1}, except for the obvious C≡C stretching frequencies, as it is well known that these regions are otherwise free of fundamentals.

[16] American Petroleum Institute Research Project 44, at the National Bureau of Standards. Catalog of Infra-Red Spectrograms. Serial No. 13, contributed by the Phillips Petroleum Company, Bartlesville, Oklahoma, and the University of Oklahoma Research Institute, Norman, Oklahoma.

[17] D. D. Wagman, J. E. Kilpatrick, K. S. Pitzer, and F. D. Rossini, J. Research Nat. Bur. Stand. **35**, 467 (1945).

[18] K. W. F. Kohlrausch and W. Stockmair, Zeits. f. physik. Chemie **B29**, 292 (1935).

[19] M. Bourguel and L. Piaux, Bull. Soc. Chem. Fr. **2**, 1958 (1935).

[20] R. S. Rasmussen and R. R. Brattain, J. Chem. Phys. **15**, 120 (1947).

[21] G. Glockler and H. M. Davis, J. Chem. Phys. **2**, 881 (1934).

[22] B. Timm and R. Mecke, Zeits. f. physik. Chemie **B35**, 442 (1937).

[23] E. Bartholomé and J. Karweil, Zeits. f. physik. Chemie **B35**, 442 (1937).

[24] K. W. F. Kohlrausch, "Ramanspektren," *Hand und Jahrbuch der Chemischen Physik* (Akad. Verlag Becker and Erler, Leipzig, 1943), Vol. 9, pp. 306, 309.

TABLE II. An assignment of the fundamental vibration frequencies of butyne-1, butene-1, and vinyl acetylene.

Group	Description of vibration	Frequency range previously assigned	References	*n*-butane[1]	Butyne-1	Butene-1	Vinyl acetylene	Frequency ranges from present assignments
	CH_3 symm. stretching	*ca.* 2870 cm^{-1}	29	2880, (2880)	2885	2872		2890–2870
	CH_3 asymm. stretching	*ca.* 2960	29	(2950), (2960), 2964, (2950)	2941, 2986	2936, 2968		2990–2935
	CH_2 symm. stretching	*ca.* 2850	29	2860, (2860)	2851	2850		2860–2850
Ethyl	CH_2 asymm. stretching	*ca.* 2930	29	2934, (2934)	(2925)	(2936)		2940–2920
	CH_3 asymm. deformation	1470–1440	26	1455(2), 1466(2)	1459, 1438	1457, 1450		1470–1435
	CH_3 symm. deformation	1390–1360	26	1370, 1390	1375	1391		1395–1365
CH_3-CH_2-	CH_3 wagging (in-plane)	1200–900	1	1148, 1134	1005	1019		1150–1000
	CH_3 wagging (out-of-plane)	1200–900	1	959, 956	910	(910)		960–900
	CH_2 bending	1470–1440	11	1455, 1466	1450	1450		1470–1440
	CH_2 wagging	1340–1290	11	1304, 1297	1325	1307		1330–1290
	CH_2 twisting	(1350–1100)	11	1244, (1250)	1252	1257		1260–1240
	CH_2 rocking	760–720	11	751, (740)	785	788		790–740
	CH_2 symm. stretching	*ca.* 2980	29			2998	3012	3020–2990
	CH_2 asymm. stretching	*ca.* 3080	29			3074	3102	3110–3070
Vinyl	CH stretching	*ca.* 3020	29			(2998)	(3012)	(3020–2990)
	CH_2 bending (in-plane)	1430–1390	28			1416	1410	1440–1380
	$-CH=CH-$ bending (in-plane)	1320–1280	28			1293	1288	1300–1270
$CH_2=CH-$	CH_2 rocking (in-plane)	?	—			1166	1090	1170–1090
	CH_2 wagging (out-of-plane)	920–900	28			912	935	940–900
	$-CH=CH-$ wagging (out-of-plane)	1010–980	28			993	950	1025–950
	CH_2 torsion (out-of-plane)	?	—			623	678	680–600
$CH\equiv C-$	CH stretching	*ca.* 3300	5, 8		3305		3305	*ca.* 3305
	CH deformation	700–600	5, 8		642, (605)		615, 629	650–600
	C–C stretching	1200–800	27	1058, 970, 835	1068, 840	1068, 850	875	1100–830
	C=C stretching	1700–1600	26			1645	1600	1650–1590
Skeletal and torsional modes	C≡C stretching	*ca.* 2050	26		2118		2099	2120–2090
	Skeletal deformation (in-plane)			432, (365)	509, 348	437, 320	538, 309	540–300
	Skeletal deformation (out-of-plane)	<600 cm^{-1}	26	?	206	282	219	(350)–200
	CH_3 torsion			200(?)	?	237 (?)		(240–200)

B. THE ASSIGNMENT OF FUNDAMENTALS

Our final assignments for these three molecules are summarized in Table II together, for comparison purposes, with that recently worked out for the *n*-butane molecule.[1] When the same frequency has slightly different values in the infra-red and Raman spectra, the infra-red frequency of the molecule in the gaseous state is usually chosen. Exceptions occur in the region above 2000 cm^{-1} where the resolution of the Raman spectra is usually superior, and in cases where it is difficult to estimate the precise center of an infra-red band contour. Detailed points with respect to the various assignments are discussed below region by region. Table II is subdivided into the frequencies of different molecular groups so that closely related frequencies in different molecules can be easily compared. The third and fourth columns of this table give, respectively, the characteristic frequency ranges which have previously been assigned to the various modes of vibration, and the appropriate references.[1, 5, 8, 11, 25–28] Although all of these molecules are asymmetric rotators and hence infra-red band contours are difficult to predict, the type *C* fundamentals of the planar molecules (see reference 4, p. 469), i.e., change in electric moment perpendicular to the skeletal plane of the molecule, would be expected to have fairly marked *Q* branches.

(a) The Region 3350–2800 cm^{-1}

It is generally recognized that the CH stretching modes of vibration occur in this region. Fox and Martin[28] have systematized the assignment of frequencies in this region to the specific CH stretching modes, and their conclusions are summarized in Table II, column 3. In addition to the frequencies listed there, others occur close to 2900 cm^{-1}, caused by overtones of the bending modes near 1450 cm^{-1}. The various assignments in this region shown in Table II have been made with these points in mind, and taking into

[25] See reference 4, p. 195, and discussions of individual hydrocarbon spectra.

[26] K. W. F. Kohlrausch and F. Köppl, Zeits. f. physik. Chemie **B26**, 209 (1934).

[27] N. Sheppard and G. B. B. M. Sutherland, Proc. Roy. Soc. (London) (to be published shortly).

[28] J. J. Fox and A. E. Martin, Proc. Roy. Soc. (London) **A175**, 208 (1940).

account the polarization data on the Raman lines they are fairly self-explanatory. When an insufficient number of lines have been observed schematic assignments have been made, and these values are enclosed in brackets. They are probably close to the correct values.

(b) The Region 2900–1700 cm^{-1}

The only fundamentals that can occur in this region are the C≡C stretching modes. This frequency occurs at 2118 cm^{-1} in butyne-1 and at 2099 cm^{-1} in vinyl acetylene. The slight lowering of this frequency in the latter molecule is probably due to a weakening of the linkage caused by conjugation with the neighboring C=C linkage.

(c) The Region 1700–1550 cm^{-1}

The C=C stretching modes occur in this region and are to be identified with the frequencies at 1650 cm^{-1} in butene-1, and 1600 cm^{-1} in vinyl acetylene. As in the case of the C≡C frequency discussed above, the C=C stretching mode of the conjugated molecule has a lower frequency than in the case of butene-1.

(d) The Region 1550–600 cm^{-1}

This is the most difficult region to analyze because of the occurrence of all the various CH deformation modes as well as the skeletal stretching vibrations of C–C linkages. The assignment of each molecule is discussed separately.

Butyne-1

This molecule is effectively made up of an ethyl group and a –C≡CH group. The latter will have only a few frequencies in this region, *viz.*, two CH bending modes between 700 and 600 cm^{-1} and a strong overtone or combination frequency involving these modes between 1300 and 1200 cm^{-1} in the infra-red.[5,8] The in-plane CH bending mode can be identified with the polarized Raman line at 642 cm^{-1}, and the infra-red frequency at *ca.* 650 cm^{-1}. The expected strong infra-red line occurs at 1250 cm^{-1}, and from this we deduce 608 cm^{-1} as an approximate value of the other CH bending mode. The remainder of the Raman lines and medium or strong infra-red lines in this region can probably be attributed to fundamental modes of the ethyl group. If we make the assumption that the two strong and highly polarized lines at 1068 and 840 cm^{-1} in the Raman spectrum correspond to the two skeletal stretching modes, the rest of the observed frequencies can be assigned with fair confidence using the correlation rules of Table II. The only Raman frequency in this region which has not been assigned to a fundamental is the weak line at 1023 cm^{-1}. This probably corresponds to the overtone of the 509-cm^{-1} frequency. The final assignment appears to be very satisfactory and is in most cases in agreement with the correlation rules, and with the previous assignment for *n*-butane.

Butene-1

The assignment for this molecule is fairly easily arrived at, taking into account the frequencies of the ethyl group found for butyne-1, and the correlation rules for the vinyl group modes. Apart from being satisfactory on these grounds, it also accounts for all the Raman lines in this region, and all the infra-red bands except a few weak absorptions of intensity (1) or less. One of the CH_3 wagging modes has been assigned in a schematic fashion by analogy with the butyne-1 spectrum. Although derived from a more extensive knowledge of the spectra of related molecules as summarized in the characteristic frequencies of Table II, this assignment is in good agreement with the earlier results of Aston, Szasz, Woolley, and Brickwedde.[13]

Vinyl Acetylene

The frequencies of the C≡CH group in this region can once again be picked out with little difficulty (CH bending modes at 615 and 629 cm^{-1}). The remaining frequencies of the vinyl group can be assigned as shown in a straightforward manner despite the fact that several of them are somewhat shifted from their usual positions. Although the infra-red data of Bartholomé and Karweil[23] did not give the contours of the lines, those of the closely similar spectrum of vinyl cyanide[29] help in the assignment of the out-of-plane modes of the vinyl group.

[29] H. W. Thompson and P. Torkington, J. Chem. Soc. (London) 597 (1944).

(e) The Region below 600 cm^{-1}

Butyne-1

In this region butyne-1 should have four fundamentals—three of them corresponding to bending modes of the carbon skeleton, and one to the methyl torsional mode. We have assigned the three strongest Raman lines (509, 348, and 206 cm^{-1}) to the skeletal modes, and the frequencies at 563 and 290 cm^{-1} may perhaps be the combination transitions 910–348 cm^{-1} and 509–209 cm^{-1}. A possible alternative would be to assign the 563-, 509-, and 348-cm^{-1} lines to the skeletal vibrations, and the 206-cm^{-1} line to the methyl torsion mode. Points against this latter assignment are that the methyl torsion mode is usually weak or non-observable in the Raman spectrum, and that it seems unlikely that both the in-plane (Raman, polarized) skeletal modes would be as high as 500 cm^{-1}.

Butene-1

This molecule should also have four low frequency modes of a similar type to those of butyne-1. We assign the lines at 437, 320, and 282 cm^{-1} to the skeletal modes, and that at 237 cm^{-1} to the methyl torsional oscillation. The weak line at 533 cm^{-1} can be explained as a difference band 853–320 cm^{-1}, although it may possibly be an in-plane skeletal bending mode of another rotational isomer.

Vinyl Acetylene

In this case there are just three observed Raman lines corresponding to the three skeletal modes, and the assignment is thus straightforward.

C. DISCUSSION OF RESULTS

The assignments given above for these C_4 hydrocarbons seem to be fairly satisfactory in that they explain all the strong infra-red and Raman frequencies of each molecule in a manner which is consistent with the assignments of corresponding frequencies in other structurally related hydrocarbons. Perhaps the most important advance is the systematization of the frequencies in the region 1500–600 cm^{-1}. It is clear that despite the effect of different neighboring groups on the hydrogen deformation frequencies of the ethyl, vinyl, and C≡CH structural units, these maintain a closely parallel series of fundamental frequencies in the infra-red and Raman spectra. The most notable exceptions are the higher frequency in-plane methyl wagging mode of the ethyl group, and the CH_2 in-plane rocking mode of the vinyl group. The variability of these frequencies is almost certainly due to the fact that these are the two hydrogen deformation modes which are closest to the frequencies associated with the C—C stretching modes for these molecules (1100–840 cm^{-1}). They will interact strongly with these skeletal modes as all of these are in-plane frequencies. Other deformation modes are either further away from the C—C stretching frequency range, or are out-of-plane modes which cannot interact with them.

The characteristic frequencies which were used as an aid in the assignments had been obtained from the spectra of closely related molecules. However, for such a characteristic frequency to be found consistently in the spectra of a series of molecules it must have some distinctive feature such as considerable strength in the infra-red or Raman spectrum. As a result, several frequencies cannot be found in this manner because of weakness in both types of spectra. Such cases are the CH_2 twisting mode of the ethyl group, the in-plane CH_2 rocking mode, and the torsional mode of the vinyl group. The detailed analysis of the spectra of these smaller molecules, however, has enabled these frequencies to be identified in the regions 1260–1240 cm^{-1}, 1170–1090 cm^{-1}, and 680–600 cm^{-1}, respectively. These values, together with the regions of the spectrum corresponding to the various other modes of vibration, are summarized in the last column of Table II, and have been taken directly from the data of the preceding columns. These data are supplementary to the data already given earlier in the third column of the same table on the characteristic frequencies of various modes, in that they are usually less precise in range. On the other hand, they are of wider application, and are probably fairly accurately obeyed in most hydrocarbon spectra.

The assignments that we have made in the frequency region below 600 cm^{-1} are probably the least reliable because of the lack of infra-red data.

The Assignment of the Vibrational Spectra of Ethyl Mercaptan and the Ethyl Halides, and the Characterization of an SH Deformation Frequency*

N. SHEPPARD**
Department of Physics, The Pennsylvania State College, State College, Pennsylvania
(Received June 25, 1948)

An assignment is given for all the fundamental modes of vibration of the ethyl mercaptan molecule from the observed vibrational spectra. By analogy the observed frequencies in the spectra of ethyl chloride, bromide, and iodide are also assigned to normal modes of vibration of these molecules.

Evidence is presented that one of the deformation modes of the SH linkage in mercaptans has a characteristic frequency lying between the limits of 800 and 900 cm^{-1}. This frequency is usually stronger in the Raman spectrum.

IN the course of an investigation of the infra-red spectra of an extensive series of organic molecules containing sulfur atoms, the infra-red spectrum of ethyl mercaptan has been obtained. This is a fairly small molecule whose vibrational spectra do not appear to have been analyzed, and it was decided to attempt this with a view to the identification of the normal modes of the ethyl group, and the characterization of the SH deformation frequency.

EXPERIMENTAL

The ethyl mercaptan used was a purified commercial sample (b.p. 36°C), contained in a gas cell with rocksalt windows. The infra-red spectrometer was a Hilger D 208 double-beam instrument used under standard conditions as described previously.[1] An absorption curve was obtained in close agreement with that published recently by Trotter and Thompson;[2] it is shown in Fig. 1. Our observed infra-red frequencies, together with the most recent Raman data as given by Wagner[3] and Kohlrausch,[4] are shown in Table I.

Both the infra-red and Raman spectra of ethyl mercaptan and of the ethyl halides are shown schematically in Figs. 2 and 3. The infra-red data for these halides has been taken from the work of Cross and Daniels,[5] and the Raman data from Wagner's compilation.[6]

THE ASSIGNMENT OF THE ETHYL MERCAPTAN SPECTRA

It is clear that the maximum symmetry that this molecule could have would be a single plane of symmetry (point group C_s). This would occur if one of the CH bonds of the CH_3 group and the SH group were to lie in the plane defined by the carbon and sulfur atoms, or alternatively if both of these groups were in free rotation about the C−C and C−S bonds, respectively. The selection rules for this symmetry group allow all the normal modes of vibration to be active in the infra-red and Raman spectra.

Ethyl mercaptan has nine atoms and hence 21

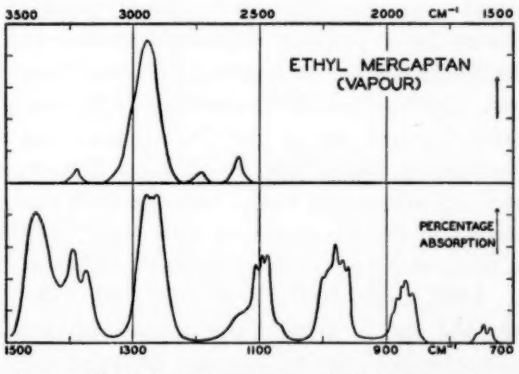

FIG. 1. The infra-red spectrum of ethyl mercaptan.

* This research was carried out in part on Contract N6onr-269, Task V, of the Office of Naval Research.
** Now at Department of Colloid Science, Cambridge University, Cambridge, England.
[1] N. Sheppard and G. B. B. M. Sutherland, J. Chem. Soc. 1540 (1947).
[2] I. F. Trotter and H. W. Thompson, J. Chem. Soc. 481 (1946).
[3] J. Wagner, Zeits. f. physik. Chemie **B40**, 439 (1938).
[4] K. W. F. Kohlrausch, "Ramanspektren," *Hand—und Jahrbuch der Chemischen Physik* (Akademische Verlagsgesellschaft, Leipzig, 1943), p. 239.
[5] P. C. Cross and F. Daniels, J. Chem. Phys. **12**, 48 (1933).
[6] J. Wagner, Zeits. f. physik. Chemie **B45**, 69 (1939).

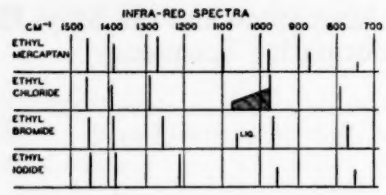

FIG. 2. The infra-red spectra of ethyl mercaptan and the ethyl halides.

normal modes of vibration. Of these, five will be C−H stretching modes which will occur in the region 2800–3050 cm^{-1}, and can be identified with the unresolved infra-red absorption and the Raman lines that lie in this region. Another will be the SH stretching mode which is well known (see reference 4, pp. 210–211) to correspond to the Raman and infra-red frequency at approximately 2575 cm^{-1}. This leaves fifteen modes to be identified, and as there are no multiple bonds present these will all lie below 1500 cm^{-1}. We can further account for the two asymmetrical CH_3 deformation modes and the CH_2 bending mode, as these are well known[7] to correspond to frequencies in the region 1400–1470 cm^{-1}. They can almost certainly be identified with the infra-red absorption between 1430 and 1480 cm^{-1}, which centers at 1453 cm^{-1}, and the broad Raman line centered at 1448 cm^{-1}. Thus we are left with twelve modes which should have frequencies below 1400 cm^{-1}. Two of these correspond to restricted rotations or torsional oscillations of the CH_3 and SH groups, and the remainder to stretching and deformation vibrations of the molecule. These modes of vibration can be described approximately in terms of group motions as follows: three CH_2 deformation modes (wagging, rocking, and twisting),[8] one CH_3 symmetrical deformation vibration, two CH_3 wagging modes (in and out of the CCS plane), one SH deformation mode, one C−C stretching mode, one C−S stretching mode, and one CCS skeletal bending mode. To correlate with these, we have ten frequencies which are probably fundamentals, *viz.*, 1385, 1269, 1097, 1049, 978, 870, 838, 745, 660, 332 cm^{-1}. Where frequencies have been detected in both the Raman and infra-red spectra, the latter frequencies have usually been chosen, as they correspond to measurements in the gaseous phase.

The Raman line at 332 cm^{-1} is certainly the skeletal bending mode in view of its low value, and that at 660 cm^{-1} is well known to be the C−S stretching mode (see Kohlrausch's[4] "Ramanspektren," p. 235). In addition, the strong line near 975 cm^{-1} in both the infra-red and Raman spectra is almost certainly the C−C stretching mode. This latter assignment is made on account of the magnitude of this frequency and its strength in the Raman spectrum. We have shown earlier that the CH_2 wagging and rocking modes in hydrocarbon molecules occur near 1300 and 750 cm^{-1}, respectively,[8] and on these grounds the

TABLE I. The observed frequencies in the infra-red and Raman spectra of ethyl mercaptan.

Infra-red frequency	Strength	Raman frequency[a]	Strength
		2966	Strong
2800–3050	Strong	2930	Strong
		2872	Strong
2730	V. weak	—	—
2580	Weak	2570	V. strong
1453	Strong	1448	Strong
1385	Strong	1374	Weak
1269	Strong	1265	Medium
1097	Medium	1092	Medium
—	—	1049	Medium
978	Medium	968	Strong
870	Medium	870	Weak
—	—	838	Weak
745	Weak	737	Weak
660[b]	Strong	657	V. strong
Not investigated		440	Weak
		332	Strong

[a] See references 3 and 4.
[b] See reference 2.

frequencies at 1269 and 745 cm^{-1} can very probably be assigned to these modes. The shifts of these frequencies from their normal positions in hydrocarbon molecules are very reasonable in view of the position of the CH_2 group next to the sulfur atom. Evidence will be presented below that the S−H deformation mode is to be identified with the Raman line at 838 cm^{-1}, and by analogy with many hydrocarbon molecules the frequency near 1385 cm^{-1} can be attributed to the symmetrical CH_3 deformation vibration. We are thus left with three frequencies at 1097, 1049, and 870 cm^{-1} to be assigned to the remaining CH_2 twisting and CH_3 wagging modes. Of these frequencies, the first and last are strong in the infra-red spectrum, and the middle line occurs only in

[7] G. Herzberg, Infra-Red and Raman Spectra (D. Van Nostrand Company, Inc., New York, 1945), p. 195.
[8] N. Sheppard, J. Chem. Phys. 16, 690 (1948).

the Raman spectrum. In view of the fact that methyl wagging modes in other sulfur-containing molecules (e.g., methyl mercaptan[9] and dimethyl sulfide)[10] are strong in the infra-red spectrum, we tentatively assign the frequencies at 1097 and 870 cm^{-1} to the in-plane and out-of-plane CH_3 wagging modes, respectively, and hence the 1049-cm^{-1} line is probably the CH_2 twisting vibration. In support of the above assignment of the methyl wagging modes, is the fact that a similar in-plane wagging mode in the more symmetrical propane molecule has been identified at 1152 cm^{-1} in the infra-red spectrum, on the basis of band contour data.[11] Unfortunately, ethyl mercaptan is a very unsymmetrical molecule, and it is more difficult to predict the band contours in this case. However the 870-cm^{-1} infra-red line has a complex structure (see Fig. 1) which may arise from the multiple Q branches of a perpendicular band in agreement with the above assignment.

There appears to have been no polarization data published on the Raman spectrum of ethyl mercaptan, but such data have been published for the very closely related spectrum of ethyl chloride (see Fig. 3). In this spectrum lines at 335, 656, 968, and 1071 cm^{-1} are appreciably polarized, and it is probably a fair extension to expect that accordingly the corresponding Raman lines at 332, 657, 968, 1092 cm^{-1} in the ethyl mercaptan spectrum have similar qualitative polarizations. The assignment described above for the ethyl mercaptan molecule was originally made without the help of these data, but it can be seen to be in accordance with them, as all these frequencies have been assigned to modes of vibration symmetrical with respect to the CCS plane. The wagging motion of the CH_2 group is also symmetrical with respect to this plane and occurs at 1265 cm^{-1} in the Raman spectrum of ethyl mercaptan and at 1281 and 1248 cm^{-1}, respectively, in the Raman spectra of ethyl chloride and bromide. This line in the ethyl bromide spectrum is also polarized in accordance with the assignment.

The only modes of motion which have so far not been spectroscopically identified in the ethyl mercaptan spectra are then the CH_3 and SH restricted rotations. However, it appears to be true that such modes are, in general, difficult to detect in these spectra. There is a weak line at 440 cm^{-1} which has not so far been assigned, but in view of its occurrence in the ethyl chloride spectrum also at 439 cm^{-1} it cannot be assigned to the SH torsional mode. It is possible that it may correspond to the methyl restricted rotation, but this appears to be a high value for such a mode. On the other hand, it can, like the other weak unassigned lines, be explained as a difference frequency.

THE IDENTIFICATION OF THE SH DEFORMATION FREQUENCY

The only previous assignment of an SH deformation frequency in mercaptan molecules seems to have been given in the analysis of the vibrational spectra of methyl mercaptan by Thompson and Skerrett.[9] A line at 805 cm^{-1} in the Raman spectrum of this molecule was identified as the SH deformation mode. An obvious first approach to the identification of the corresponding mode in the case of ethyl mercaptan was to look for a line near to the above frequency in the spectrum of this molecule, and which was not present in the very similar spectrum of ethyl chloride. Two lines at 838 and 870 cm^{-1} seemed to fulfil this condition. However, the fact that the latter occurred strongly in the infra-red spectrum also, whereas the former did not, suggested (by analogy with a similar behavior in the methyl mercaptan case) that the line at 838 cm^{-1} might be associated with this mode.

In view of the strong similarity between the Raman spectra of the methyl and ethyl mercaptans and chlorides, a comparison was likewise

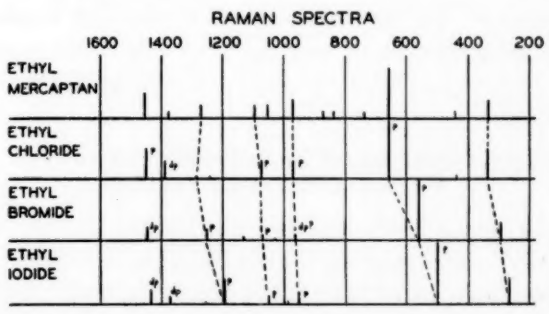

FIG. 3. The Raman spectra of ethyl mercaptan and the ethyl halides.

[9] H. W. Thompson and N. P. Skerrett, Trans. Faraday Soc. **36**, 812 (1940).
[10] H. W. Thompson, Trans. Faraday Soc. **37**, 38 (1941).
[11] V. L. Wu and E. F. Barker, J. Chem. Phys. **9**, 487 (1941).

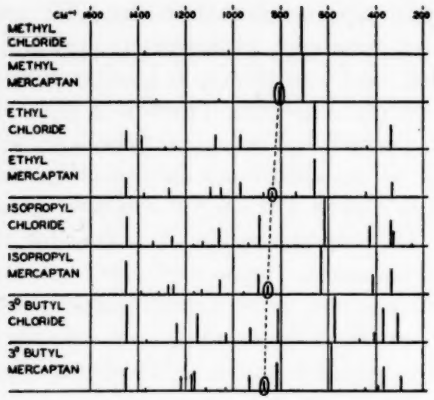

FIG. 4. The Raman spectra of the methyl, ethyl, isopropyl, and tertiary butyl mercaptans and chlorides. The circled lines are those assigned to the SH deformation frequency.

made between the Raman spectra of isopropyl and tertiary butyl mercaptans and chlorides (see reference 4, p. 240 *et seq.*) with a view to the picking out of extra lines in the mercaptan spectra that might correspond to SH frequencies. In Fig. 4 the Raman spectra of these various compounds are compared, and it can be seen that extra lines occur in the isopropyl and tertiary butyl mercaptan spectra at 856 and 866 cm^{-1}. These, together with the 805- and 838-cm^{-1} lines in the methyl and ethyl mercaptan spectra, are ringed in the figure and form a convincing series for assignment to the SH deformation mode. It is, of course, possible that in comparing the spectra of the chlorides and mercaptans extra lines should appear in the latter which are not caused by the extra SH group. However, it seems unlikely that an extra line should occur in approximately the same region with four structurally very different molecules if it were not due to this cause. We can conclude, therefore, that the deformation SH mode is to be expected to occur between the limits of 800 and 900 cm^{-1} in the Raman spectra of mercaptans. If it can be detected in the infra-red spectra it will probably be weak.

THE ASSIGNMENT OF THE SPECTRA OF THE OTHER ETHYL DERIVATIVES

The similarity between the Raman spectra of ethyl mercaptan and ethyl chloride has already been mentioned, and this extends to some extent also to the infra-red spectra. Thus many of the frequencies in the spectra of the chloride can be identified immediately by a direct comparison of the spectra, and the results of this are shown in Table II. There seems to be little doubt about the assignment of the frequencies in the case of the chloride except for the out-of-plane CH_3 wagging and CH_2 twisting modes. The former was strong in the infra-red spectrum of the mercaptan, but there is no corresponding absorption in the chloride spectrum and it seems likely that it may have shifted in position and has been lost in the strong absorption between 990 and 960 cm^{-1} caused by the C−C stretching mode. Clearly, no precise value can be given for this frequency, although a value near 960 cm^{-1} is suggested by the above reasoning. In the case of the CH_2 twisting mode there is no Raman line corresponding to the ethyl mercaptan frequency, but this has been tentatively assigned a value of 1030 cm^{-1} corresponding to an unidentified region of weak absorption stretching from 1000 to 1075 cm^{-1} in the infra-red spectrum of the chloride.

The spectra of ethyl bromide and ethyl iodide are also, on the whole, easily assigned by analogy with the ethyl chloride case. In carrying this out it has been assumed that changes in frequency will probably occur in progression in passing along the sequence chloride→bromide→iodide. As in the case of the chloride molecule, assignments for one of the CH_3 wagging and the CH_2 twisting vibration are more doubtful in all these molecules and have been made schematically by reference to the completely assigned mercaptan spectrum, but otherwise the spectra seem to be satisfactorily explained. The most recent attempted assignments of these molecules seem to

TABLE II. The assignment of the fundamental frequencies of ethyl mercaptan and the ethyl halides.

	C_2H_5SH	C_2H_5Cl	C_2H_5Br	C_2H_5I
CH_3 stretching	2966 (2) 2870	2966 (2) 2877	2980, 2960 2866	2965 (2) 2859
CH_2 stretching	2930 2870	2932 2877	2924 2866	2914 2859
CH_3 asymmetrical deformation	1450 (2)	1450 (2)	1440 (2)	1440 (2)
CH_3 symmetrical deformation	1385	1385	1385	1372
CH_3 wagging (in-plane)	1097	1071	1069	1049
CH_3 wagging (out-of-plane)	870	(960)	(960)	(960)
CH_2 bending	1450	1450	1440	1440
CH_2 wagging	1269	1290	1255	1210
CH_2 twisting	1049	1030	1027 (?)	985 (?)
CH_2 rocking	745	790	770	740
C−C stretching	978	968	960	955
C−X stretching	660	656	560	500
C(C)X bending	332	335	292	262
X−H stretching	2575	—	—	—
X−H deformation	838	—	—	—

have been made by Wagner,[6] and the present ones are in good agreement with his work, and in all cases extend his conclusions. Attempts have been made to deduce complete schematic assignments for the ethyl chloride molecule by Linnett[12] and Pitzer.[13] Our present results differ somewhat from the results of these authors in the assignment of non-observed frequencies.

[12] J. W. Linnett, Trans. Faraday Soc. **36**, 527 (1940).
[13] J. Gordon and W. F. Giauque, J. Am. Chem. Soc. **70**, 1506 (1948).

ACKNOWLEDGMENTS

The author would like to thank the Master and Fellows of St. Catharine's College, Cambridge, and the Dunlop Rubber Company Ltd., England, for financial aid during part of this investigation.

THE JOURNAL OF CHEMICAL PHYSICS VOLUME 17, NUMBER 1 JANUARY, 1949

Raman Spectra of Polycrystalline Hydrocarbons at Low Temperatures. Rotational Isomerism. II*

D. H. RANK, N. SHEPPARD,† AND G. J. SZASZ††
Spectroscopy Laboratory, Department of Physics, The Pennsylvania State College, State College, Pennsylvania
(Received August 3, 1948)

Making use of the low pressure, water-cooled Hg arcs as the source of nearly monochromatic radiation, a simple method was developed for the investigation of the Raman spectra of polycrystalline solids. The method was applied to the study of the first four normal paraffins. The Raman spectra of the solids between 600–1500 cm^{-1} are compared with those in the liquid phase. All these spectra undergo a marked simplification on solidification due to the disappearance of all but one of the rotational isomers. This process is shown to be discontinuous at the melting point.

IN the first paper[1] of this series we have calculated the energy difference of the rotational isomers of *n*-butane by measuring the relative intensity of "line pairs" as a function of temperature in the liquid range. Numerous considerations make it desirable to extend the investigation of the spectra of rotational isomers to the solid phase.

During the war work was done in Japan** on the Raman spectra of some hydrocarbons in the solid phase. These Japanese workers have reported that certain lines in the spectra disappear in the solid phase. In the light of this work and our observed behavior of line intensity ratios as a function temperature,[1] it would seem to be of importance to investigate whether the intensity ratio of "line pairs" varies continuously or not when one proceeds from the liquid to the solid phase.

It is relatively easy to obtain the Raman spectra of solids if they can be prepared as homogeneous glasses or single crystals. The preparation of solid hydrocarbons in an optically homogeneous state can and has been accomplished by a number of investigators. However, preparation of such solid samples will require practically a special investigation for production of satisfactory solids for each molecule studied.

Crystal powder methods of obtaining Raman spectra have been brought to a state of more or less perfection by Kohlrausch[2] and his coworkers. More recently Cabannes[3] and his col-

* This research was carried out on contract N6onr-269, Task V of the Office of Naval Research.
† Now at Dept. of Colloid Sciences, Cambridge University, Cambridge, England.
†† Now at U. S. Office of Naval Research, London, England.
[1] G. J. Szasz, N. Sheppard, and D. H. Rank, J. Chem. Phys. **16**, 704 (1948).
** T. Shimanouchi and S. Midzushima, J. Chem. Soc. (Japan) **63**, 1215 (1942); Chem. Abs. **41**, 3332 (1947); Sci. Pap. Inst. Phys. Chem. Research (Tokyo) **40**, 467 (1943), Chem. Abs. **41**, 6089 (1947); M. Takeda, J. Chem. Soc. Japan **62**, 896 (1941); Chem. Abs. **41**, 5390 (1947); H. Okazaki, J. Chem. Soc. Japan **63**, 1136 (1942); Chem. Abs. **41**, 3740 (1947). Unfortunately, the complete papers have been inaccessible to us so far.

[2] K. W. F. Kohlrausch, *Ramanspektren* (Akad. Verlag., Leipzig, 1943), p. 49.
[3] J. Cabannes, R. Lennuier, and M. Harraud, Comptes Rendus **223**, 301 (1946).

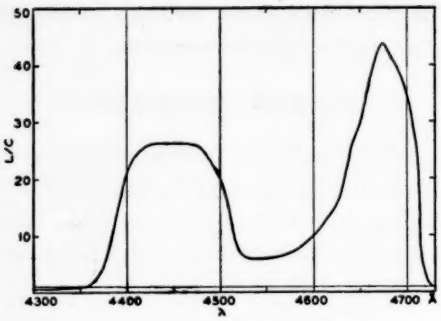

FIG. 1. Plot of the relative weakening of continuum compared to the exciting line *vs.* wave-length.

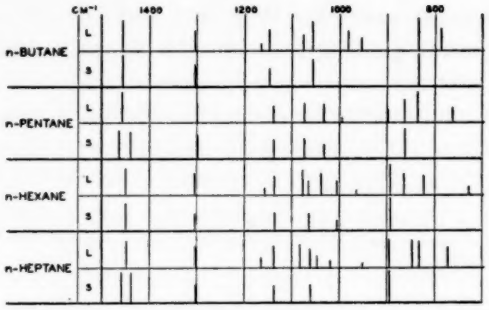

FIG. 3. Schematic representation of the Raman spectra of *n*-paraffins in the liquid (*L*) and solid (*S*) phases.

laborators have developed a crystal powder method which is elegant in principle. The method of Kohlrausch is very complicated both in arrangement of the optical system and in adjustment thereof. Cabannes' method makes use of a monochromator to illuminate the sample and the spectra produced are very feeble. Neither of the two methods of obtaining crystal powder spectra mentioned above seem to lend themselves easily to work at low temperatures.

The problem of obtaining Raman spectra of crystal powders essentially resolves itself to producing the excitation by means of sufficiently monochromatic light. The crystal powder will diffusely reflect a much greater percentage of the incident light than will be scattered by the individual molecules. The relative intensity of the continuum in a spectrum compared to the intensity of an ideal monochromatic line will vary inversely as the true resolving power of the spectrograph. In the case of Raman spectra, however, it is not possible to greatly weaken the continuum relative to the Raman line by simply increasing the resolving power of the spectrograph, since the Raman lines in general have considerable breadth.

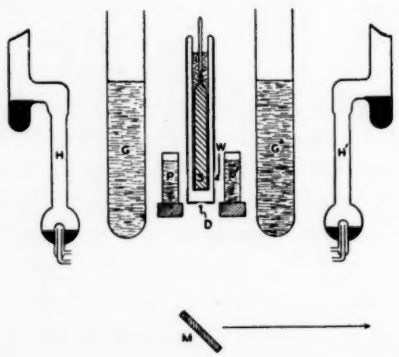

FIG. 2. The experimental arrangement used to obtain Raman spectra of polycrystalline solids.

A great deal of the work recorded in the literature on Raman spectra has been done, making use of relatively high pressure mercury arcs as light sources. It has been shown[4] that in the low pressure Hg arc the continuous spectrum is only about $\frac{1}{10}$ as strong as in the moderately high pressure sources. In addition it is possible to reduce the continuous spectrum on the long wave side of λ4358 very materially by means of a praseodymium ammonium nitrate filter. Figure 1 shows a plot of L/C as a function of wave-length for the praseodymium filter which we have used in this work. L is the fractional part of incident light of wave-length λ4358 transmitted by the filter and C is the transmission of the filter for wave-length λ. This curve shows the relative weakening of the continuum compared to the exciting line. From inspection of Fig. 1 it can be seen that the relative intensity of the continuous spectrum of the Hg arc can be reduced by more than an order of magnitude over most of the region from λ4400 to λ4700A by means of this filter.

A schematic diagram of the apparatus we have used to obtain the Raman spectra of polycrystalline hydrocarbons at low temperatures is shown in Fig. 2. The sample tube *S* is placed in the Dewar flask which is painted black, except for entrance windows for the incident light marked *W* in the figure. The light scattered and diffusely reflected from the polycrystalline solid passes out through the aperture *D* and is reflected into the

[4] D. H. Rank and J. S. McCartney, J. Opt. Soc. Am. **38**, 279 (1948).

spectrograph by means of the mirror *M*. *H* and *H'* are low pressure water-cooled Hg arcs similar to those described previously.[5] *G* and *G'* are cylindrical lenses containing sodium nitrite solution to suppress the short wave part of the Hg spectrum and *P* and *P'* are cells which hold the praseodymium ammonium nitrate filter solution. The thickness of the cells was 12 mm and they contained a solution of 50 percent by weight of crude praseodymium ammonium nitrate in water. (Specific gravity *ca.* 1.50.) The crude salt was obtained from the Lindsay Light and Chemical Company, West Chicago, Illinois.

The spectrograph employed in this work was a 3-prism glass instrument equipped with an *f*:3.5 objective lens. The dispersion of the instrument was about 30A per mm at λ4500. The objective produces very sharply defined images which allows the slit width to be kept to a minimum value consistent with the natural breadth of the Raman lines. In order to avoid halation as much as possible, the plates were backed with Eastman "opaque." The λ4358 line was prevented from falling on the plate by being absorbed by means of a diaphragm placed in front of the plate. Even though the direct image of this line could not fall on the plate the intensity of this line is so great that light of this wave-length produces an ill-defined image in the neighborhood of the line position as the result of scattering in the various parts of the spectrograph. For this reason it was not possible to observe any lines in the solid spectra when the frequency shift was less than 600 cm^{-1}.

By filling the Dewar shown in Fig. 2 with liquid air, the sample could be frozen into a polycrystalline mass and the spectrum photographed in the manner described above. Suitable plates of the crystal powder spectra could be obtained in four to five hours' exposures. It was possible to obtain spectra of the liquid hydrocarbons at low temperatures with this apparatus by cooling the sample to the desired temperature with cold dry air as described in our previous paper.[1]

The *n*-paraffins used were obtained from the Petroleum Refining Laboratory of this college (*n*-butane, *n*-pentane, and *n*-hexane) and from the Phillips Petroleum Company (*n*-heptane).

The spectra of the liquid and solid hydrocarbons are schematically represented in Fig. 3. There are several features apparent in these spectra which are of particular interest. In general, the lines are considerably sharper at the low temperatures. The much simplified spectra of the solid normal paraffins investigated seem to consist of lines which arise from a single rotational isomer. On comparing results obtained from photoelectric intensity measurements of line pairs as a function of temperature with the qualitative intensities obtained from the solid spectra, it is apparent that the intensity changes of the line pairs are discontinuous when going from the liquid to the solid state.

There are several obvious improvements which can be made in the crystal powder technique which we have described in this paper. However, the incorporation of these improvements will make the method considerably more complex. Since it is possible to secure usable solid spectra in the simple manner described in this paper, it was thought worth while to describe our method in sufficient detail so as to clearly bring out the advantages and limitations of this technique.

A detailed discussion of the quantitative results obtained on the liquid and solid spectra of some normal and branched hydrocarbons will be given in two subsequent papers.

We thank Dr. M. R. Fenske, Director of the Petroleum Refining Laboratory in this college and the Phillips Petroleum Company (Bartlesville, Oklahoma) for supplying the hydrocarbons used. The figures were prepared by Mr. E. Shull.

[5] D. H. Rank, N. Sheppard, and G. J. Szasz, J. Chem. Phys. **16**, 698 (1948).

THE JOURNAL OF CHEMICAL PHYSICS VOLUME 17, NUMBER 1 JANUARY, 1949

Spectroscopic Studies of Rotational Isomerism. III. The Normal Paraffins in the Liquid and Solid States*

N. SHEPPARD† AND G. J. SZASZ††
Spectroscopy Laboratory, Department of Physics, The Pennsylvania State College, State College, Pennsylvania
(Received August 3, 1948)

The Raman spectra of *n*-butane, *n*-pentane, *n*-hexane, and *n*-heptane have been investigated in the liquid phase between 310°K and their melting points, and also in the solid phase. The room temperature spectra clearly show the presence of appreciable concentrations of two rotational isomers in butane and pentane, and of three isomers in hexane and probably in heptane. In the solid phase only one of these isomers is present, and in agreement with previous conclusions based on spectroscopic and other evidence, this lowest energy form was assumed to possess the planar, *trans*-, zig-zag configuration. The spectra of the solids yield experimental values for the limiting skeletal stretching frequencies of the zig-zag form, and these were compared with values calculated by previously established methods. The photoelectric spectrograph was used for quantitative intensity measurements on selected line pairs of each molecule over appropriate temperature intervals, and from the results values were obtained for the energy difference, $-\Delta H$, between rotational isomers. The values obtained were 760 ± 100 cal. mole^{-1} in *n*-butane, 450 ± 60 cal. mole^{-1} in *n*-pentane, 520 ± 70 and 470 ± 60 cal. mole^{-1} in *n*-hexane. No quantitative result could be obtained for *n*-heptane. The observed gaseous heat capacities of *n*-butane, *n*-pentane, and *n*-hexane were compared with values calculated by statistical mechanics. It was found that for *n*-pentane and *n*-hexane the calculated values do not agree accurately with the experimental results, probably because of the simplified partition functions used to obtain the compositions of the isomeric mixtures.

I. INTRODUCTION

IN the first paper of this series[1] we have shown that the photoelectric Raman spectrograph[2] recently developed in this laboratory can be applied to a quantitative study of the rotational isomers in liquid normal butane. A value was obtained for the energy difference in good agreement with that previously used by Pitzer[3] in his treatment of the thermodynamic properties of hydrocarbons. In this manner it was also possible to separate the Raman spectra of the two isomers, and thus to make a complete assignment of frequencies for the low energy, *trans*-isomer of *n*-butane. In the preceding paper[4] a simple method of obtaining the Raman spectra of solids was described, and the results obtained on the *n*-paraffins were given.

In continuation of these studies it seemed of interest to make quantitative line intensity measurements on the *n*-paraffins. It was hoped to obtain values for the numbers of isomers present and for the energy differences between them. These results, together with the spectra of the solids,[4] should enable us to assign the appropriate frequencies to the skeletal stretching modes of vibration of the different rotational isomers. The improved techniques used in this work also made a reinvestigation of *n*-butane possible, to yield a valuable independent confirmation of our previous result.

II. EXPERIMENTAL

The work on the spectra of the liquids was done essentially as described before.[1] A great improvement was introduced, however, by utilizing the low pressure Hg arcs[5] in conjunction with the photoelectric measurements. The two advantages of these sources are their low general background and the very weak satellites of the 4358A Hg exciting line. This latter property was essential for quantitative work on the 835–789-cm^{-1} line pair of *n*-butane.[1] To obtain improved resolution for this work we further narrowed the spectrograph slits. The spectra of the solid paraffins were obtained by the general crystal powder method described in the preceding paper.[4]

* This research was carried out on Contract N6onr-269, Task V, of the Office of Naval Research.
† Now at Department of Colloid Science, Cambridge University, Cambridge, England.
†† Now with U. S. Office of Naval Research, London, England.
[1] G. J. Szasz, N. Sheppard, and D. H. Rank, J. Chem. Phys. 16, 704 (1948).
[2] D. H. Rank and R. Wiegand, J. Opt. Soc. Am. 36, 325 (1946).
[3] K. S. Pitzer, J. Chem. Phys. 8, 711 (1940).
[4] D. H. Rank, N. Sheppard, and G. J. Szasz, J. Chem. Phys. 17, 83 (1949).
[5] D. H. Rank, N. Sheppard, and G. J. Szasz, J. Chem. Phys. 16, 698 (1948).

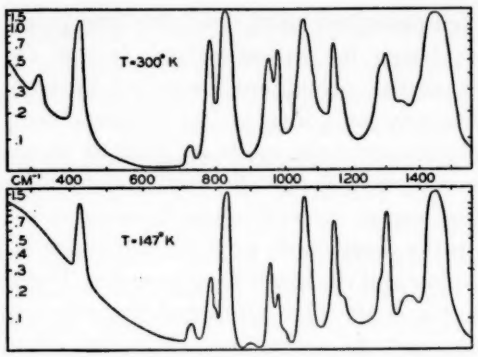

FIG. 1. Smoothed microphotometer curves of the Raman spectrum of liquid *n*-butane at 300°K and at 147°K.

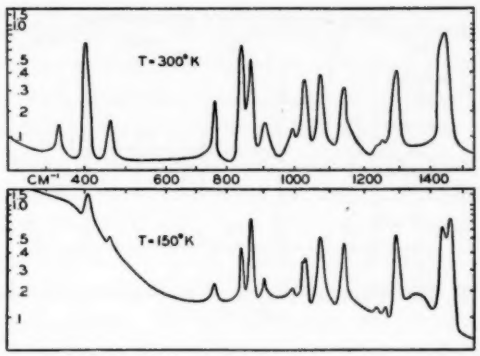

FIG. 2. Smoothed microphotometer curves of the Raman spectrum of liquid *n*-pentane at 300°K and at 150°K.

The normal paraffin samples were the same as used before.[1,4] They were stated to be 99+ percent pure and were used without further purification. The small amounts of water present produced slight cloudiness of the liquids below the icepoint, but because of the low background of Rayleigh scattering obtained with our sources, this did not interfere with any of the measurements.

III. THE EXPERIMENTAL RESULTS

A. The Raman Spectra

In Figs. 1–3 are shown the Raman spectra of *n*-butane, *n*-pentane, and *n*-hexane below 1500 cm^{-1} in the liquid phase at the higher and lower temperatures, respectively. These have been traced from the microphotometer curves as described before. A low temperature spectrum in the liquid was not obtained with the *n*-heptane sample. It can be seen at once that the spectra undergo marked changes with temperature. The spectra of the solid hydrocarbons between 1500 and 600 cm^{-1} are shown schematically in Fig. 4.[4] Although longer exposure times might bring up a few more weak lines in these spectra, the plates that we have obtained are sufficient to decide the behavior on solidification of all the strong lines in the room temperature spectra. This does not apply to frequencies below 600 cm^{-1} because in this region the increased background obscures all but the strongest lines.

The Raman spectra of *n*-butane, *n*-pentane, *n*-hexane, and *n*-heptane are summarized in Table I. This table has been arranged in such a way as to show the similarities in these spectra. Each frequency is followed by the relative intensity of the line, and in the case of the liquid spectra by a + or − sign, indicating a relative intensity increase or decrease of the line upon cooling. The asterisk indicates that the line splits upon cooling, and that the two components behave differently. It would be expected that all the lines marked + in the liquid spectrum would persist in the solid spectrum, and this appears to be the case for most of the lines observed. Those that do not seem to obey this condition are relatively weak in the liquid spectra, and might show in the solid spectra with longer exposures.

The frequencies listed for *n*-butane are taken from our first paper, and for the other compounds the values given by Kohlrausch[6] have been used. In a few cases we have observed weak lines not recorded by Kohlrausch, and these frequencies have been estimated to approximately 5 cm^{-1} by interpolation from the known values.

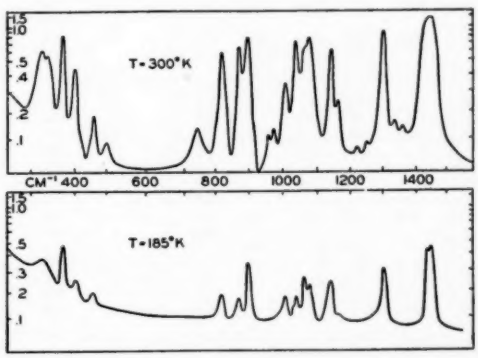

FIG. 3. Smoothed microphotometer curves of the Raman spectrum of liquid *n*-hexane at 300°K and at 185°K.

[6] K. W. F. Kohlrausch, "Ramanspektren," *Hand und Jahrbuch der Chemischen Physik* (Akademische Verlagsgesellschaft, Leipzig, 1943), p. 210.

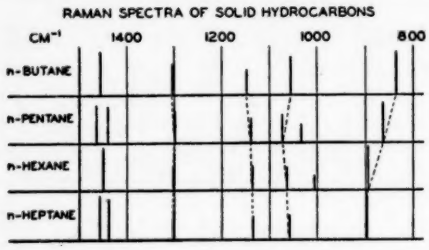

FIG. 4. The Raman spectra of normal paraffins in the solid state.

B. The Determination of the Energy Difference between the Rotational Isomers

The method used to obtain the energy differences was that of Langseth and Bernstein,[7] and the equations used for the calculations were given in our previous paper.[1] In this investigation we have restricted our attention to the strong polarized lines[8] between 780–900 cm^{-1}, as in all cases cooling produced marked relative intensity changes in this region.**

The results obtained on the energy differences, $-\Delta H$, are summarized in Table II, together with the temperatures used, and the line pairs that were chosen for investigation. In the case of *n*-hexane two prominent lines decreased notably in intensity on going to low temperatures, and measurements were made on each of these with respect to the 896-cm^{-1} line which did not behave in this fashion. Several measurements of the line-pair ratios were made for each substance at both the upper and the lower temperatures. The values given for $-\Delta H$ were computed from the average values, and the errors were estimated by taking into account the spread of our experimental results. The choice of the lower temperature was governed by considerations of convenience, and by the melting point of the hydrocarbon in question.

TABLE I. Observed Raman frequencies in liquid and solid *n*-paraffins (below 1500 cm^{-1}).

n-butane		*n*-pentane		*n*-hexane		*n*-heptane	
Liquid 300°K	Solid 90°K	Liquid 300°K	Solid 90°K	Liquid 300°K	Solid 90°K	Liquid 300°K	Solid 90°K
			{1463				{1457
1455 (10)+	1455	1450 (10)+	{1438	1450 (10)+	1450	1450 (10)	{1438
1370 (0)				1360 (0)			
				1337 (0)		1350? (0)	
1304 (4)+	1304	1299 (5)+	1299	1302 (7)+	1302	1302 (7)	1302
1282 (2)−							
		1260 (0)+		1265 (0)			
		1240 (0)+		1235 (0)			
1167 (1)				1165 (2)−		1161 (1)	
1148 (4)+	1148	1138 (4)+	1138	1136 (5)+	1136	1136 (4)	1136
1077 (3)−				1077 (6)−		1082} (6)	
1058 (9)+	1058	1073 (4)+	1073	1062 (4)+	1062	1060}	1060
		1033 (4)*	1033	1039 (5)−		1046 (3)	
						1019 (1)	
				1007 (3)+	1007		
981 (4)−		995 (1)		970 (1)			
956 (3)+		900 (2)+		950 (1)		951 (1)	
835 (10)+	835	862 (6)+	862	896 (10)+	896	899 (5)	899
		837 (8)−		867 (6)−		846 (3)	
				825 (5)−		831 (5)	
789 (5)−		762 (3)−		729 (1)		772 (2)	
				500 (0)			
432 (7)+	432	463 (2)+	463	460 (1)+		494 (0)	
				400 (3)−		447 (0)	
		399 (8)+	399				
						396 (1)	
325 (1)−		334 (2)		363 (5)+		350 (0)	
				323 (3)−		309 (3)	
				309 (4)		280 (0)	

[7] A. Langseth and H. J. Bernstein, J. Chem. Phys. **8**, 410 (1940).

[8] For detailed polarization data see *Report on the Raman Spectra of Hydrocarbons* (Petroleum Refining Laboratory, School of Chemistry and Physics, The Pennsylvania State College, May 1947).

** This was also observed by H. Okazaki, Bull. Chem. Soc. Japan **18**, 364 (1943); Chem. Abs. **41**, 4382 (1947).

IV. DISCUSSION

A. The Raman Spectra

In contrast to the *n*-butane case, it is not feasible to attempt complete frequency assignments for these larger hydrocarbons. However, it is still possible to pick out the Raman lines caused by the most stable rotational isomer, as these will increase in relative intensity on going to lower temperatures, and have hence been marked + in Table I. All the lines observed in the spectra of the solids belong to this class. It would only be possible to further assign the lines resulting from less stable molecular isomers (−) to particular non-stable configurations, if measurements of the energy difference were made in each case. This is not experimentally feasible except for the strong lines in the region 750–900 cm^{-1}, and our measurements on these are discussed in Section IV B.

The most notable feature of the solid spectra shown in Fig. 4 is the enormous simplification obtained when compared with the corresponding spectra of the liquids. This is probably due to the persistence of a single rotational isomer in the solid state in each case, and this is presumably the lowest energy, planar, zig-zag form,[4] as previ-

TABLE II. The energy difference between rotational isomers in *n*-butane, *n*-pentane, and *n*-hexane.

Compound	*n*-butane	*n*-pentane	*n*-hexane	
Line pair(s), cm^{-1}	835–789	862–837	896–867	896–825
Temperature, °K	155 310	154 310	186 310	186 310
Intensity ratio (average value)	12.5 3.63	0.69 1.44	2.45 1.39	2.53 1.53
Energy difference cal. $mole^{-1}$, $-\Delta H$	760±100	450±60	520±70	470±60

ously indicated by x-ray crystal analysis.[9] In the case of *n*-butane our previous spectroscopic evidence also points to this configuration.[1]

There are marked similarities between the spectra of all these hydrocarbons, and this has been indicated in Fig. 4, by dotted lines connecting related frequencies in the various compounds. From our previous detailed analysis of the *n*-butane spectrum it can be seen that the frequencies near 1450, 1300, and 1140 cm^{-1} are of the hydrogen deformation type corresponding, respectively, to CH_2 bending, CH_2 wagging, and in-plane CH_3 wagging modes. It further seems reasonable to assign the two series of frequencies near 1050 cm^{-1} and between 900 and 830 cm^{-1} to skeletal stretching modes of the chain. This is substantiated both by the *n*-butane assignment for the first members of these series, and by the fact that it is in just these regions of the spectra that the greatest numbers of lines disappear on solidification. It is reasonable to suppose that, in general, such skeletal modes would be more sensitive to changes in configuration than the hydrogenic modes, and would hence show up separately in the spectra at room temperature. It is interesting to note from Figs. 1–3 that the positions of the lines corresponding to the lowest skeletal stretching modes of the non-planar configurations in the region 900–750 cm^{-1} are all at lower frequencies than the planar ones. This will have to be taken into account in any complete theoretical treatment of these frequencies. The observed skeletal frequencies are assumed to be the upper and lower limiting frequencies of the stretching vibrations of each molecule. This is certainly true of *n*-butane, for which a detailed assignment has been made previously,[1] and is suggested for the other hydrocarbons by the dotted correlation lines of Fig. 4. Kohlrausch (see reference 6, p. 206) has also given the expected polarization data and selection rules for the skeletal modes of these hydrocarbons, and showed that the limiting upper and lower frequencies should all be Raman active in agreement with our assumption.

As in this manner we have obtained convincing experimental evidence for the assignment of some of the skeletal stretching modes of the planar zigzag form, it was of interest to compare these results with previous calculations. A considerable number of calculations have been made, but their correlation with experimental frequencies has previously been somewhat arbitrary because of the presence in the Raman spectra of a multitude of lines caused by other rotational isomers. Such calculations can be divided into two main types, those in which the skeletal modes have been computed on the assumption that no angle changes are involved during the vibrations,[10–13] and more complete treatments in which angle changes are also considered.[3,14–17]

The results of the most recent calculations made by these methods are shown schematically in Fig. 5 together with the observed limiting skeletal frequencies. This figure includes the results on all the normal paraffins up to C_8. The observed frequencies given for *n*-octane have been obtained from the liquid spectrum given by Kohlrausch[6] on the assumption that they are close to 1060 and 900 cm^{-1}, as is true for *n*-hexane and *n*-heptane.

The observed frequencies for each compound

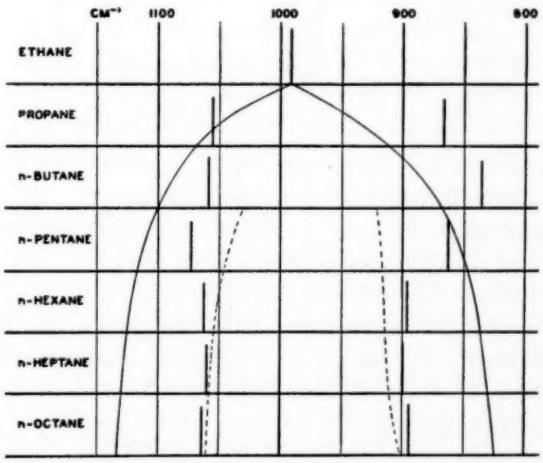

FIG. 5. Calculated and observed limiting skeletal stretching frequencies of the normal paraffins.

[9] See, for example, R. C. Evans, *Crystal Chemistry* (Cambridge University Press, Teddington, England, 1939), p. 326.

[10] E. Bartholomé and E. Teller, Zeits. f. physik. Chemie **B19**, 366 (1932).
[11] R. Mecke, Zeits. f. physik. Chemie **B36**, 347 (1934).
[12] B. I. Stepanov, J. Phys. Chem. (U.S.S.R.) **14**, 474 (1940).
[13] L. Kellner, Trans. Faraday Soc. **41**, 217 (1945).
[14] L. Kassel, J. Chem. Phys. **3**, 326 (1935).
[15] J. G. Kirkwood, J. Chem. Phys. **7**, 506 (1939).
[16] S. E. Whitcomb, H. H. Nielsen, and L. H. Thomas, J. Chem. Phys. **8**, 143 (1940).
[17] C. O. Ahonen, J. Chem. Phys. **14**, 625 (1946).

are indicated by the individual heavy lines. The calculated upper and lower limiting frequencies by the first method (assumption of no angle change) are given by the positions in which the continuous curve cuts the appropriate ordinates, and those by the second method (including angle changes) are likewise indicated by the dashed curve. The smooth curve has been drawn directly from the data given by Stepanov,[12] and the dashed curve from Ahonen's[17] calculations on *n*-butane, *n*-hexane, and *n*-octane, modified as described below.

In comparing the experimental frequencies with those calculated by Stepanov, it should be noticed that both tend to constant values with increasing chain length, but that the calculated separation (*ca.* 300 cm^{-1}) is much larger than the experimental separation (*ca.* 170 cm^{-1}). It is a general feature of the more detailed treatments that the calculated upper and lower limiting frequencies for the longer chain molecules do not have so great a separation and are hence in better agreement with our experimental value, but calculations that have so far been made do not in any case agree closely with experiment as regards the individual positions of the lines. For example, Ahonen calculates that these frequencies should occur between 1127 and 956 cm^{-1} for *n*-octane, as compared with the experimental limiting frequencies of 1064 and 894 cm^{-1}. In his calculations Ahonen used force constants derived from the propane molecule, and it is clear that a small change in the stretching constant would give very good agreement between the two sets of data. Accordingly, we have corrected Ahonen's figures in a semi-empirical fashion, assuming that a small change in force constant would give rise to a proportional shift of the frequencies (i.e., neglecting further effects due to angle bending). The factor that we used would correspond, on this assumption, to a change of the stretching force constant from 4.12×10^5 to 3.7×10^5 dynes cm^{-1}. We corrected, in a similar fashion, the frequencies given by him for *n*-hexane and *n*-butane, and have used these recomputed values to draw in the dotted curve shown in Fig. 5. It can be seen that in this way good agreement between theory and experiment has been achieved in both the positions and separations between the limiting frequencies in the hydrocarbons *n*-hexane, *n*-heptane, and *n*-octane. It is clear, however, that this treatment fails in the case of *n*-butane and, by interpolation, for *n*-pentane. Indeed it is difficult to see how either treatment could account for the peculiar behavior of these frequencies in the lower members of the series. It is probable that these can only be explained in a satisfactory manner by taking into account the fact that rather different bending and stretching constants will apply to the ends as compared to the inner portions of the chain.

TABLE III. Statistical weights of rotational isomers in *n*-paraffins.*

Compound	Energy above ground state: 0	*a*	*2a*	*3a*	*4a*	∞
n-butane	1	2	0	0	0	0
n-pentane	1	4	2	0	0	2
n-hexane	1	6(4, 2)	8	2	0	10
n-heptane	1	8(4, 4)	18	12	2	40

* This table is reproduced in part from Pitzer's work (see reference 3).

B. The Number of Rotational Isomers and the Energy Differences

As mentioned earlier, the improved techniques made possible a determination of the energy difference in *n*-butane using the line pair at 835–789 cm^{-1}. The result obtained was $-\Delta H = 760\pm100$ cal. $mole^{-1}$, which is to be compared with our previous value of 770 ± 90 cal. $mole^{-1}$. The exact agreement is perhaps fortuitous, but leaves no doubt as to the general magnitude of the energy difference. This value agrees remarkably well with Pitzer's prediction.[3] According to Pitzer's treatment the general picture for the first four hydrocarbons containing rotational isomers is shown in Table III. In this table are shown the statistical weights of groups of rotational isomers of the same energy, and the molecular compositions of these mixtures can be obtained to a first approximation from the formula

$$g_i \exp(-E_i/RT)/\sum_i g_i \exp(-E_i/RT).$$

In Pitzer's treatment E_i is the appropriate integral multiple of $a = 800$ cal. $mole^{-1}$, and g_i is the statistical weight given in Table III. Some of the isomers belonging to the same energy level can be further distinguished spectroscopically, because their different spatial configurations will lead to separate frequencies in the spectra. This subdivi-

sion is indicated in Table III for the first levels of *n*-hexane and *n*-heptane by the numbers in parentheses. It is easily seen from the molecular models that the maximum statistical weight of any spectroscopically identical species is four. Consequently, we have not carried out this separation for the higher energy isomers on the assumption that the $\exp(-E/RT)$ term will greatly reduce the populations of such states. On the basis of this picture we would predict the following number of strong, polarized Raman lines in the region 900–780 cm^{-1}: *n*-butane and *n*-pentane two, *n*-hexane and *n*-heptane three. This is based on the very probable assumption that each type of isomer present in quantity will give one such frequency in this region as is the case for the stable, planar, and zig-zag form. The experimental results for *n*-butane, *n*-pentane, and *n*-hexane in this region are shown in Figs. 1–3 and can be seen to be in excellent agreement with these predictions, and provide further evidence for the general correctness of Pitzer's treatment. Although in the case of *n*-heptane no complete spectrum was obtained at low temperatures, we did investigate the spectral region between 950–800 cm^{-1} on the photoelectric spectrograph. The curves, obtained at the high and low temperatures are shown in Fig. 6. In agreement with Kohlrausch,[6] we find three fairly strong frequencies at 899, 846, and 831 cm^{-1}, as predicted above. The weaker shoulder on the side of the 899-cm^{-1} line, which shows up more distinctly in the low temperature run because of the sharpening of the lines, is probably another, non-skeletal, frequency of the stable isomer. The photoelectric measurements on *n*-butane, *n*-pentane, and *n*-hexane were made on sufficiently well resolved lines to yield clear-cut results, the line pair separations given in Table II ranging from 25–46 cm^{-1}, as compared with the 15-cm^{-1} separation of these poorly resolved lines in *n*-heptane. These measurements lead to the energy differences summarized in Table II. No further discussion of the value obtained for *n*-butane is necessary. The energy differences obtained for *n*-pentane and *n*-hexane are distinctly lower than that for *n*-butane. In the case of *n*-pentane we are still dealing, as in *n*-butane, with rotation about the second C—C linkage, while beginning with *n*-hexane inner linkages are also contributing different rotational isomers. In the case of

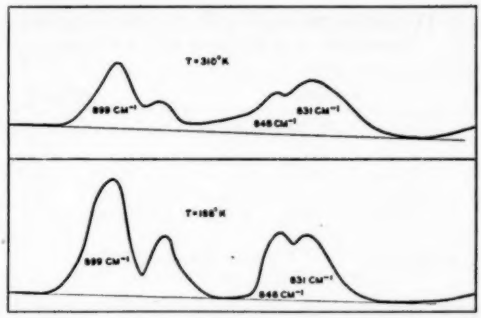

FIG. 6. Photoelectric intensity recording of the Raman spectrum of *n*-heptane, between 925 and 800 cm^{-1}, at 310°K and at 188°K.

n-hexane there are two spectroscopically different isomers at about the same energy above the ground state. It is not possible to decide unequivocally which of these is the butane analog and which is the new type, but the separation of the line pairs suggests that the 867-cm^{-1} line belongs to the *n*-butane type isomer, having a corresponding energy difference of 520 cal. $mole^{-1}$. It was, unfortunately, not possible to derive any quantitative results from our measurements in *n*-heptane, for, as can be seen from Fig. 6, the overlapping of the lines makes the intensity measurements extremely uncertain. The energy differences in *n*-pentane and *n*-hexane are identical within experimental error. As one of the *n*-hexane values corresponds to rotational isomerism about an internal C—C linkage, it seems likely that this value of about 500 cal. $mole^{-1}$ is the energy difference for all rotational isomers previously considered[3] at 800 cal. $mole^{-1}$ (i.e., those listed in the "*a*" column of Table III), except of course for the special case of *n*-butane.

Independent evidence of a less direct type has been cited by Beckett, Pitzer, and Spitzer[18] in support of the original choice of 800 cal. $mole^{-1}$ for the *n*-butane type energy difference. This was based on the heats of combustion[19] of the liquid dimethyl cyclohexanes and gave a value of 900 cal. $mole^{-1}$. No experimental evidence concerning the magnitude of these energy differences is so far available in the vapor, and it is possible that our values are not strictly applicable to this phase. On the other hand, it seems probable that in view of the relatively weak intermolecular forces the

[18] C. W. Beckett, K. S. Pitzer, and R. Spitzer, J. Am. Chem. Soc. **69**, 2488 (1947).
[19] E. J. Prosen, W. H. Johnson, and F. D. Rossini, J. Research Nat. Bur. Stand. **39**, 173 (1947).

TABLE IV. Experimental and calculated gaseous heat capacities of *n*-pentane and *n*-hexane.

	n-pentane			*n*-hexane		
T, °K	Cp exp[a]	Cp° calc. $-\Delta H=$ 500 cal. mole^{-1}	Cp° calc. $-\Delta H=$ 800 cal. mole^{-1}	Cp° exp[b]	Cp° calc. $-\Delta H=$ 500 cal. mole^{-1}	Cp° calc. $-\Delta H=$ 800 ca mole^{-1}
331	31.3±0.2	31.0	31.5	37.28±0.04	37.1	37.9
427	38.0±0.3	38.6	39.0	45.69±0.05	46.0	46.6

[a] See reference 21. [b] See reference 23.

energy differences in liquid and vapor hydrocarbons are not very different.

An obvious way to test our results was to compare experimental and calculated thermodynamic properties, using the rounded value of 500 cal. mole^{-1} for the parameter "*a*" in Pitzer's treatment.[3] In making these calculations, we used the following frequency assignment for the hydrogenic modes of the CH_2 and CH_3 groups (cf. our analysis of the *n*-butane spectrum[1]): CH_2 group, 2900(2), 1450, 1300, 1250, 750; CH_3 group, 2900(3), 1450(2), 1375, 1140, 950. The upper and lower limiting frequencies of the C–C stretching modes were taken from the solid spectra of the low energy form and from the frequencies of neighboring temperature-dependent Raman lines for the high energy forms. The intermediate stretching frequencies were computed using Stepanov's calculations[12] adjusted so as to fit the experimental values of the extreme frequency interval. The C–C bending modes for *n*-pentane were taken to be the three observed frequencies for all the isomeric forms, and in the case of *n*-hexane the four strong observed Raman lines were likewise used. The torsional modes were taken at 120 cm^{-1}. 3300 cal. mole^{-1} was used as the height of the sinusoidal potential barrier hindering the rotation of the terminal methyl groups.

For our purposes the gaseous heat capacity is the most useful thermodynamic property, as it is relatively insensitive to the low lying bending and torsional frequencies which are the least accurate in our assignment. On the other hand, it is sensitive to changes in population between the various energy states, as controlled by the energy difference in which we are interested.

In the case of *n*-butane our detailed frequency assignment gives almost identical heat capacity contributions with the earlier schematic one of Pitzer,[3] which was subsequently modified[20] to give better agreement with the experimental results on *n*-pentane.[21] While Pitzer's later assignment gives somewhat better numerical agreement with the experimental gas heat capacities of *n*-butane[22] than does our treatment, both calculations are within the experimental errors of the measurements. As they assume the same energy difference between the rotational isomers, the somewhat different results are of no significance from our present point of view.

The experimental gas heat capacities of *n*-pentane[21] and of *n*-hexane[23] were compared with calculated values, and the results are summarized in Table IV. No detailed comparisons were made for *n*-heptane.[24] In the case of both pentane and hexane, using 500 cal. mole^{-1} for the energy difference, the calculated and experimental curves cross between 330° and 430°K (the temperature range of Pitzer's experimental values for *n*-pentane). In both cases our slope is too high, i.e., the calculated heat capacity increases too rapidly with temperature. This slope could be decreased somewhat by adopting the value of 800 cal. mole^{-1} for the energy difference, but this would raise the calculated curve above the experimental one throughout the entire temperature range. In order to bring these curves into good agreement some modification of Pitzer's treatment appears necessary. In view of the important part played by the higher energy rotational isomers it seems probable that the appropriate energy differences are not represented with sufficient accuracy by simple multiples of the parameter "*a*." This seems physically reasonable for isomers derived from the planar zig-zag form by successive rotations about neighboring linkages.

ACKNOWLEDGMENTS

We wish to thank Dr. D. H. Rank for his encouragement and help throughout the progress of this research. We are also indebted to Dr. J. G. Aston, Director of the Cryogenic Laboratory in this college, for many discussions concerning various phases of this problem. The figures were prepared by Mr. E. Shull.

[20] K. S. Pitzer, Ind. Eng. Chem. **36**, 829 (1943).

[21] K. S. Pitzer, J. Am. Chem. Soc. **63**, 2413 (1941).

[22] B. P. Dailey and W. A. Felsing, J. Am. Chem. Soc. **65**, 44 (1943).

[23] G. Waddington and D. R. Dousline, J. Am. Chem. Soc. **69**, 2275 (1947).

[24] G. Waddington, S. S. Todd, and H. M. Huffman, J. Am. Chem. Soc. **69**, 22 (1947).

Spectroscopic Studies of Rotational Isomerism. IV. 2-Methyl Butane and 2,3-Dimethyl Butane*

G. J. Szasz† AND N. Sheppard††
Spectroscopy Laboratory, Department of Physics, The Pennsylvania State College, State College, Pennsylvania
(Received August 3, 1948)

The Raman spectra of 2-methyl butane and 2,3-dimethyl butane were investigated between room temperature and 90°K. In marked contrast to the behavior of the normal paraffins all the main lines persist in the solid phase. The slight change with temperture in the relative intensity of one line pair in liquid 2-methyl butane was investigated quantitatively with the photoelectric spectrograph. No measurable intensity changes were observed in the 2,3-dimethyl butane spectrum. The results were interpreted in terms of both a very small (<100 cal. mole^{-1}) and a very large (1600 cal. mole^{-1}) energy difference between the rotational isomers. Although both interpretations appear consistent with the spectroscopic results, neither affords a completely straightforward explanation of all the facts. It is shown for 2-methyl butane that accurate gaseous heat capacities would distinguish between these alternatives. The spectroscopic data on 2,3-dimethyl butane are inconsistent with a single molecular configuration possessing a center of symmetry.

I. INTRODUCTION

IN the preceding papers of this series[1–3] we have investigated the phenomenon of rotational isomerism in the *n*-paraffins by means of Raman spectroscopy. It seemed of interest to study the simplest branched paraffins in which the coexistence of rotational isomers would be expected on the basis of the previously established general picture. The obvious compounds to investigate from this point of view are the methyl substituted butanes. In this paper we report results on 2-methyl butane and 2,3-dimethyl butane. It would be expected that because of the trigonal symmetry introduced by the three identical groups attached to one of the carbon atoms of the central C−C linkage, there should be only one rotational isomer in the case of the other methyl substituted butanes (2,2-dimethyl, 2,2,3-trimethyl and 2,2,3,3-tetramethyl butane). This has been verified in the case of 2,2-dimethyl butane by the spectroscopic work of Mizushima, Morino and Takeda.[4] Pitzer[5] has previously estimated the energy difference between the possible isomers in the case of both 2-methyl butane and 2,3-dimethyl butane from steric considerations. He estimated an energy difference, $-\Delta H$, of 1600 cal. mole^{-1} in both these cases, and this would lead one to expect the presence of a rather small proportion (*ca.* 10 percent) of the higher energy isomer at room temperature. As in the case of the *n*-paraffins, we made a complete investigation of these compounds from room temperature down to the melting point and also extending into the solid phase.

The experimental procedures were identical with those described in the previous papers.[2,3] Low temperature measurements on liquid 2-methyl butane using the photoelectric spectrograph were made after the sample had been cooled from room temperature to 130°K in a few minutes, and also over a period of 5½ hours. This was carried out because of a recent discussion[6,7,8] of presumed hysteresis effects in some measurements of the liquid heat capacities of isopentane, and their explanation in terms of rotational isomerization as a slow rate process. If this

* This Research was carried out on contract N6onr-269, Task V, of the Office of Naval Research.
† Now at Department of Colloid Science, Cambridge University, Cambridge, England.
†† Now with U. S. Office of Naval Research, London, England.
[1] Szasz, Sheppard, and Rank, J. Chem. Phys. **16**, 704 (1948).
[2] Rank, Sheppard, and Szasz, J. Chem. Phys. **17**, 83 (1949).
[3] N. Sheppard and G. J. Szasz, J. Chem. Phys. **17**, 86 (1949).
[4] Mizushima, Morino, and Takeda, Sci. Papers Inst. Phys. Chem. Res. (Tokyo) **38**, 437 (1941).
[5] K. S. Pitzer, J. Chem. Phys. **8**, 711 (1940).
[6] J. G. Aston and S. C. Schumann, J. Am. Chem. Soc. **64**, 1034 (1942).
[7] G. B. Guthrie, Jr. and H. M. Huffman, J. Am. Chem. Soc. **65**, 1143 (1943).
[8] J. G. Aston, J. Am. Chem. Soc. **65**, 2041 (1943).

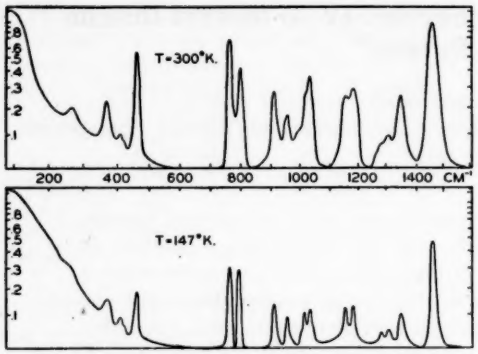

FIG. 1. Smoothed microphotometer curves of the Raman spectrum of liquid 2-methyl butane at 300°K and at 147°K.

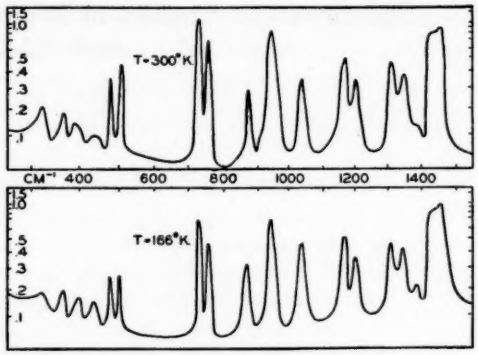

FIG. 2. Smoothed microphotometer curves of the Raman spectrum of liquid 2,3-dimethyl butane at 300°K and 166°K.

picture were true, the rate of cooling might conceivably affect the results at low temperatures.

Both the hydrocarbons used in this investigation were obtained from the Petroleum Refining Laboratory of this college. They were stated to be 99+ percent pure, and were used without further purification.

II. EXPERIMENTAL RESULTS

Figures 1 and 2 show the high and low temperature Raman spectra of 2-methyl butane and 2,3-dimethyl butane in the liquid state. These have been traced in the usual manner from microphotometer curves obtained from the original plates. The Raman spectra of the solid hydrocarbons have also been obtained, and show the presence of all the lines observed in the liquid between 600 and 1500 cm^{-1}, with the exception of the weakest line in the 2,3-dimethyl butane spectrum. It is probable that this would show up with longer exposure time. The heavy background accompanying the exciting line in the solid spectra did not permit the study of the spectral region below 600 cm^{-1} in any detail. However the strong frequency at 462 cm^{-1} in the 2-methyl butane spectrum could be observed on one of the plates.

Examination of Figs. 1 and 2 shows that these spectra do not undergo any marked changes on cooling. In the case of 2-methyl butane there are a few small changes in the relative intensity of the lines in the spectra, and in particular the intensity change of the two strong lines around 800 cm^{-1} seemed to warrant quantitative investigation on the photoelectric spectrograph. On the other hand in the case of 2,3-dimethyl butane there were no changes in the spectra outside of experimental error, and hence no photoelectric measurements were made on this compound.

As mentioned in the introduction, the quantitative measurements on isopentane were carried out with two very different rates of cooling. The results obtained are summarized in Table I.

It can be seen from this table that good agreement was obtained for the intensity ratio at low temperatures in both runs, showing the absence of any effects due to hysteresis upon our results.

TABLE I. Intensity ratio of the 763 and 796 cm^{-1} line pair of isopentane at different temperatures.

Temperature, °K	Intensity ratio	Cooling rate
310	1.30±0.05	—
130	1.02±0.04	Rapid
120	0.98±0.06	Slow

III. DISCUSSION OF THE SPECTRA

In marked contrast to the behavior of the normal paraffins it was found that there is very little change in the Raman spectra of 2-methyl butane and 2,3-dimethyl butane on cooling and solidification (cf. Section II). There are two possible explanations of this, either

(A) only a single molecular species is present in an appreciable concentration at temperatures up to 300°K, corresponding to a rather large energy content of the second isomer, or

(B) a mixture of two rotational isomers of almost equal energy exists, whose composition is approximately temperature independent.

2-methyl butane and 2,3-dimethyl butane are

analogous in terms of the number and relative configurations of their rotational isomers, and therefore the same hypothesis would be expected to explain all observations on both of these compounds. On the basis of our previous experimental work[1,3] we can conclude that the energy difference between the isomers must be less than *ca.* 200 cal. mole^{-1} or greater than *ca.* 1000 cal. mole^{-1}. Although the only previous estimate of this value by Pitzer was 1600 cal. mole^{-1} it will be shown below that the spectroscopic evidence can be interpreted in terms of either a high or a low energy difference. We shall accordingly discuss the spectra in the light of each of these hypotheses, and it will be shown that neither of them is completely satisfactory without making some *ad hoc* assumptions.

A. Assumption of a Single, Prevalent, Rotational Isomer (Large Energy Difference)

The fact that the spectra change only very slightly on cooling and on solidification finds a natural explanation in terms of this assumption. The Raman spectrum showed no observable changes on cooling in the case of 2,3-dimethyl butane, and in the case of 2-methyl butane there was a slight change in the relative intensity of the line pair at 796 and 763 cm^{-1}. This could be easily explained if it were assumed that a small percentage of the less stable form was present at 300°K and that one of its frequencies coincides with the 763 cm^{-1} line of the stable isomer.

In the case of 2-methyl butane the Raman[9] and infra-red[10] spectra below 1500 cm^{-1} can be interpreted as belonging to a single form without any difficulty as regards the numbers of frequencies and normal modes of vibration. There are, however, two strong polarized[11] Raman lines present between 700–800 cm^{-1} (796 and 763 cm^{-1}) whereas on the assumption of a single molecular form we would expect to find only one such line in this region, namely the lowest C−C stretching mode.[12] It would be possible to explain this extra line as due to a Fermi type resonance between the C−C stretching mode and a combination band of the two low skeletal modes at 366 and 415 cm^{-1}. However, this is an *ad hoc* assumption which does not easily lend itself to verification.

In the case of 2,3-dimethyl butane one of the possible staggered configurations possesses a center of symmetry, class C_2h, which would restrict the number of lines permitted in the infra-red and Raman spectra, and would prohibit the appearance of any coincidences between them. The observed spectra,[13,14] however, contain too many lines for such a symmetrical molecule and about half of these can be found in both the infra-red and Raman spectra. These arguments appear to exclude the possibility that 2,3-dimethyl butane consists of a single molecular species with a center of symmetry. If we assume that the low energy form has the other staggered configuration (no center of symmetry, class C_1) the above restrictions are removed and the observed 2,3-dimethyl butane spectra can be satisfactorily accounted for. Once again, however, there is a second strong polarized line between 700 and 800 cm^{-1} which is difficult to explain except in terms of a Fermi-type resonance.

B. Assumption of Two Rotational Isomers (Small Energy Difference)

The existence of a small energy difference between the two isomeric forms in 2-methyl butane and 2,3-dimethyl butane would lead to an almost constant equilibrium composition determined mainly by the statistical weights of the components, and by the presumably small differences in their rotational and vibrational partition functions. If this were the case the only experimental fact that is difficult to explain is the persistence of all the Raman lines upon solidification in marked contrast to the behavior of the normal paraffins.[2,3] The presence of both isomers in the crystalline phase can be explained in terms of separate crystallization or solid solution, of which the former is only possible if equilibrium be frozen. Solid solution formation between different branched chain paraffins has been demonstrated

[9] K. W. F. Kohlrausch, *Ramanspektren* (Akademische Verlagsgesellschaft, Leipzig, 1943), p. 210.
[10] American Petroleum Institute Research Project 44. Spectrogram No. 550, contributed by the U. S. Naval Research Laboratory, Washington, D. C.
[11] M. R. Fenske *et al.*, Ind. Eng. Chem. Anal. Ed. **19**, 700 (1947).
[12] N. Sheppard, J. Chem. Phys. **16**, 690 (1948).
[13] Rosenbaum, Grosse, and Jacobson, J. Am. Chem. Soc. **61**, 689 (1939).
[14] Reference 9, Spectrogram. No. 656, contributed by the U. S. Naval Research Laboratory, Washington, D. C.

recently in a series of studies by Aston and coworkers,[15] and it seems reasonable to suppose that it may occur with two different rotational isomers of a single branched hydrocarbon. The persistence of all the lines in the solid spectra would be a natural consequence of such a state of affairs. Such solid solution seems much more probable for these relatively compact branched hydrocarbons than for the elongated molecules of the normal paraffins, and may or may not possess a residual zero-point entropy, depending on the state of order of the lattice. Since the assumption of zero-energy difference corresponds to a two-to-one composition ratio, the formation of an ordered lattice (i.e., no residual entropy) may not be unlikely. In this connection the investigation of the zero-point entropy of established hydrocarbon solid solutions seems of great interest.**

The rest of the spectroscopic results can be easily explained in terms of the presence of two forms. Thus the measured change in the intensity ratio of the line pair at 796 and 763 cm^{-1} in 2-methyl butane then corresponds to an energy difference, $-\Delta H$, of 100 ± 50 cal. $mole^{-1}$ between the isomers, whereas in the case of 2,3-dimethyl butane we must conclude that the energy difference is even smaller than this value. Our previous experience with the normal paraffins showed[2,3] that only the skeletal modes gave rise to different spectral lines for the different isomers. On this basis we would expect only a few extra lines to appear if there are two isomers present, and hence the possible explanation of all the observed frequencies in terms of a single molecular species in each case is not conclusive evidence against this view. This expectation provides the most straightforward explanation of the doubling of the highly polarized Raman lines between 700–800 cm^{-1} in the spectra of both molecules, whose explanation was a difficulty on the first hypothesis.

IV. THERMODYNAMIC CONSIDERATIONS

It is probable that the most satisfactory way of distinguishing between the two hypotheses discussed in Section III is by comparing experimentally determined values of the thermodynamic properties of these molecules with the results of statistical calculations. The most sensitive property for our present purpose will almost certainly be the gaseous heat capacity (cf. the discussion on the normal paraffins in the preceding paper).[3] A single value of the gaseous heat capacity of 2-methyl butane has been given by Eucken,[16] but no values are available for 2,3-dimethyl butane. Although entropy values are available for both of these compounds,[17,18,19] it is not worth while to present a detailed discussion of the entropy comparisons because of uncertainties in the lower frequencies and particularly in the skeletal torsional mode.*** In the heat capacity calculations on 2-methyl butane the following frequencies and parameters were used: CH stretching 2900 cm^{-1} (12); CH_3 deformation (isopropyl group) 1462 (4), 1381, 1368, 1014, 949, 920, 910; CH_3 deformation (ethyl group) 1462 (2), 1381, 1140, 974; CH_2 deformation 1462, 1299, 1269, 764; CH deformation 1339, 1299: C–C stretching 1176, 1149, 1030, 796; skeletal deformation 463, 420, 366, 246; skeletal torsion 120 cm^{-1}; barrier restricting CH_3 torsion 3300 cal. $mole^{-1}$; reduced moment of CH_3 group 5.2×10^{-40} g cm^2. The same assignment has been assumed to be correct for both isomeric species, and this probably only involves considerable errors in the frequencies of the skeletal bending modes. However, this is of little consequence for the calculation of the gaseous heat capacity as this property is relatively insensitive to the precise values of these frequencies.

The calculations were carried out assuming both 0 and 1600 cal. $mole^{-1}$ for the energy difference between the isomers, the value of 1600 cal. $mole^{-1}$ being that assumed by Pitzer[5] previously. The results at 454°K are 40.7 cal. $deg.^{-1}$ $mole^{-1}$ for the assumed zero energy difference, and 41.2 for the large energy difference. These are to be

[15] J. W. Tooke and J. G. Aston, J. Am. Chem. Soc. **67**, 2275 (1945); Finke, Cines, Frey, and Aston, J. Am. Chem. Soc. **69**, 1501 (1947).

** Such an investigation is planned for the system 2,2-dimethyl butane—cyclopentane in the Cryogenic Laboratory of this college.

[16] A. Eucken and B. Sarstedt, Zeits. f. physik. Chemie **B50**, 143 (1941); Chem. Abs. **37**, 2648 (1943).

[17] S. C. Schumann, J. G. Aston and M. L. Sagenkahn, J. Am. Chem. Soc. **64**, 1039 (1942).

[18] D. R. Douslin and H. M. Huffman, J. Am. Chem. Soc. **68**, 1704 (1946).

[19] Ref. 10, Tables of selected values of properties of hydrocarbons, Table 2*t*, part 1.

*** In addition Dr. J. G. Aston has pointed out to us that a further uncertainty may arise in the interpretation of the observed entropies if the disordered solid solutions mentioned as a possibility above do, in fact, exist.

compared with Eucken and Sarstedt's experimental value[16] of 40.5±0.8 cal. deg.$^{-1}$ mole^{-1} at this temperature. Although an unequivocal decision between the two alternatives is not possible on these grounds because of the magnitude of the experimental error, it is clear that the problem could be decided if accurate gaseous heat capacities were available over a considerable temperature range.

ACKNOWLEDGMENTS

Our thanks are due Dr. J. G. Aston, Director of the Cryogenic Laboratory in this college, for helpful discussion and criticism, and to Dr. D. H. Rank for encouragement and help, particularly with the solid spectra. Dr. M. R. Fenske, Director of the Petroleum Refining Laboratory in this college kindly supplied the hydrocarbons used. The figures were prepared by Mr. E. Shull.

THE JOURNAL OF CHEMICAL PHYSICS VOLUME 17, NUMBER 1 JANUARY, 1949

The Transverse Boundary of the Random Coil

C. A. HOLLINGSWORTH
Department of Chemistry, University of Pittsburgh, Pittsburgh, Pennsylvania
(Received September 7, 1948)

The probability density for the distance of that link (or links) which is farthest from the line joining the ends of a random coil is obtained for the case in which the number of links is large. The most probable value and the averages of that distance are determined approximately.

INTRODUCTION

KUHN[1] considers h_2, the distance of the middle of a random chain from the line joining the ends, to be the transverse dimension of the chain. He obtained the probability density for h_2 and found the root-mean-square to be given by

$$(\bar{h}^2)^{\frac{1}{2}} = (N/6)^{\frac{1}{2}} l \sim 0.41 N^{\frac{1}{2}} l,$$

where N is the number of links in the chain, and l is the length of each link. Kuhn[2] later showed that in case the chain is undisturbed by external forces, h_2 is independent of the extension of the chain as long as the distance between the end links does not approach too near that of the completely extended chain. Extensions which are large enough to affect h_2 are extremely improbable for the undisturbed coil.

In this paper the probability density for the "transverse boundary" of a random chain is obtained by a method which has been described in a previous paper.[3] This boundary determines the distance ρ of that link (or links) which is most distant from the line joining the ends of the coil. The boundary is a cylinder with its axis along the axis of the chain and having a radius equal to ρ.

THE PROBABILITY DENSITY FOR ρ

Let $W(\mathbf{R}, N)dV$ designate the probability that a random coil of N links, starting at the origin, ends in the volume element dV which has the position vector $\mathbf{R}$. For large values of N the following relation holds:

$$W(\mathbf{R}, N) = (2\pi N l^2/3)^{-\frac{3}{2}} \exp[-3|\mathbf{R}|^2/2Nl^2], \quad (1)$$

which in cylindrical coordinates (r, θ, z) is

$$W(r, z, N) = (2\pi N l^2/3)^{-\frac{3}{2}} \times \exp[-3(r^2+z^2)/2Nl^2]. \quad (2)$$

It can be shown[4] that Eq. (2) satisfies the differential equation for heat flow (or diffusion), namely,

$$\partial W/\partial N = (l^2/6)\nabla^2 W. \quad (3)$$

Let $W(r, z, N; \rho)$ denote the probability that the chain, starting at the origin, ends in the volume element dV at (r, θ, z) with the added condition that the chain has at no point gone beyond the cylinder $r=\rho$. It can be shown[3] that $W(r, z, N; \rho)$ satisfies the differential Eq. (3)

[1] W. Kuhn, Kolloid Zeits. **68**, 2 (1934).
[2] W. Kuhn, J. Polymer Sci. **1**, 380 (1946).
[3] C. A. Hollingsworth, J. Chem. Phys. **16**, 544 (1948).
[4] S. Chandrasekhar, Rev. Mod. Phys. **15**, 1 (1943).

with the following boundary condition applying:

$$W(r, z, N; \rho)=0 \quad \text{when} \quad r=\rho. \tag{4}$$

The initial condition is

$$W(r, z, N; \rho)=W(r, z, N) \tag{5}$$

when

$$Nl=g(\rho, r, z). \tag{5a}$$

The function $g(\rho, r, z)$ is complicated and gives the minimum value of N which will enable the chain to start at the origin, touch the cylinder $r=\rho$, and then end at the point (r, θ, z). In place of this function a much more simple approximation,

$$g(\rho, r, z)=\rho, \tag{6}$$

will be used. Although this choice is somewhat arbitrary, it is a good approximation as long as N is sufficiently large and we are not concerned with chains having extensions considerably greater than the average.

Under these conditions the formal solution of Eq. (3) can be given in the following form:

$$W(r, z, N; \rho)=\int_0^\infty \cos\alpha z \sum_{j=1}^{\infty} J_0(\lambda_j r) A_j(\alpha) \times \exp[-(l^2/6)(\alpha^2+\lambda_j^2)(N-\rho/l)]d\alpha, \tag{7}$$

where

$$A_j(\alpha)=\frac{4}{\pi\rho^2[J_1(\lambda_j\rho)]^2}\int_0^\rho \int_0^\infty r W(r, z, \rho/l) \times J_0(\lambda_j r)\cos\alpha z dz dr, \tag{7a}$$

and $W(r, z, \rho/l)$ is given by Eq. (2). $J_0(\lambda_j r)$ and $J_1(\lambda_j r)$ are the Bessel function of the first kind of order zero and one, respectively. λ_j is the jth root of

$$J_0(\lambda\rho)=0.$$

The integrations of Eq. (7) over α and Eq. (7a) over z can be easily carried out, giving the result

$$W(r, z, N; \rho)=(2\pi Nl^2/3)^{-\frac{1}{2}}3/\pi l \times \exp[-3z^2/2Nl^2]\sum_{j=1}^{\infty} H_j(r, \rho), \tag{8}$$

where

$$H_j(r, \rho)=[J_1(\lambda_j\rho)]^{-2}\rho^{-3}J_0(\lambda_j r) \times \exp[-\lambda_j^2 l^2(N-\rho/l)/6]B_j(\rho), \tag{8a}$$

and

$$B_j(\rho)=\int_0^\rho r \exp[-3r^2/2\rho l]J_0(\lambda_j r)dr. \tag{8b}$$

Since $H_j(r, \rho)\to 0$ when ρ becomes much less than $N^{\frac{1}{2}}l$, ρ in the upper limit of the integral in Eq. (8b) can be replaced by ∞. Writing $J_0(\lambda_j r)$ in series form and integrating gives

$$B_j(\rho)\sim\rho l/3\sum_{m=0}^{\infty}(-1)^m(\lambda_j^2\rho l/6)^m/m! = \rho l/3\exp[-\lambda_j^2\rho l/6]. \tag{9}$$

The function $W(r, z, N; \rho)dV$ given by Eq. (8) gives the probability that a chain ends in the volume element dV, which is at the point (r, θ, z), without having gone beyond the cylinder $r=\rho$. Therefore,[3]

$$F(r, z, N; \rho)=\partial W(r, z, N; \rho)/\partial\rho \tag{10}$$

gives a probability density such that $F(r, z, N; \rho)d\rho dV$ is the probability that a chain passes through the cylinder $r=\rho$, but does not go beyond the cylinder $r=\rho+d\rho$, and at the same time ends in the volume element dV, which is at the point (r, θ, z). Of course,

$$\int\int F(r, z, N; \rho)d\rho dV=1.$$

In the present problem $r=0$, and, since $J_0(0)=1$, we have

$$F(z, N; \rho)=\frac{2\exp[-3z^2/Nl^2]}{\pi(2\pi Nl^2/3)^{\frac{1}{2}}}\sum_{j=1}^{\infty}F_j(N, \rho), \tag{11}$$

where

$$F_j(N, \rho)=\frac{\partial H_j(0, \rho)}{\partial\rho} =[J_1(x_j)]^{-2}\rho^{-3}(x_j^2Nl^2/6\rho^2-1) \times \exp[-x_j^2Nl^2/6\rho^2], \tag{11a}$$

and x_j is the jth root of $J_0(x)=0$; that is, $x_j=\lambda_j\rho$.

An interesting function can be obtained from Eq. (11) by dividing by $W(0, z, N)$. The result is

$$F(N, \rho)=(4Nl^2/3)\sum_{j=1}^{\infty}F_j(N, \rho). \tag{12}$$

$F(N, \rho)d\rho$ is the probability that a chain which ends at the point $(0, \theta, z)$ has passed the cylinder $r=\rho$, but has not gone beyond the cylinder $\rho+d\rho$, and

$$\int F(N, \rho)d\rho = 1.$$

In other words, $F(N, \rho)$ is the probability density for ρ when the extension of the chain is z.

It will be noted that $F(N, \rho)$ is independent of z. Obviously, therefore, $F(N, \rho)$ as given by Eq. (12) does not possess the correct limiting property that $\rho \to 0$ when $z \to Nl$. A function that does possess this property should be obtained if Eq. (3) were solved using the exact condition (5a), where $g(\rho, r, z)$ is a function of r and z as well as of ρ. Also, when $z \to Nl$, Eq. (1) no longer holds, and $W(\mathbf{R}, N)$ must be given by a more complex expression which has been obtained by Kuhn and Grün.[2,5] However, as has already been pointed out, such large values of z are extremely improbable for an undisturbed chain. Equation (12) should, therefore, apply to all probable configurations. Thus ρ, like Kuhn's h_2, is independent of the extension of the chain for moderate extensions.

THE MOST PROBABLE VALUE AND AVERAGES OF ρ

It is a simple matter to determine approximately the most probable value and the averages of ρ graphically using Eq. (12). Figure 1 is a graph of $N^{\frac{1}{2}}lF(N, \rho)$ as a function of $\rho/N^{\frac{1}{2}}l$.

[5] W. Kuhn and F. Grün, Kolloid Zeits. **101**, 248 (1942).

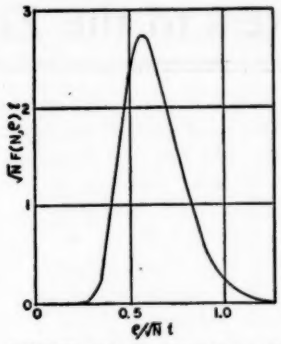

FIG. 1. $N^{\frac{1}{2}}F(N, \rho)l$ as a function of $\rho/N^{\frac{1}{2}}l$.

From this curve the most probable value of ρ is found to be given approximately by

$$\rho_{\text{m.p.}} = 0.55N^{\frac{1}{2}}l. \tag{13}$$

The area under the curve in Fig. 1 was measured by means of a planimeter and found to be 1.01 ± 0.01, which is to be compared with the theoretical value of unity.

By measuring the areas under appropriate curves the following approximate values of the averages were obtained:

$$\bar{\rho} = 0.62N^{\frac{1}{2}}l, \tag{14}$$

$$\bar{\rho}^2 = 0.41Nl^2, \tag{15}$$

and

$$(\bar{\rho}^2)^{\frac{1}{2}} = 0.64l. \tag{16}$$

Perhaps it should be pointed out that in case the equations developed here are to be applied to molecular chains, the link of the chain must be the appropriate "statistical chain element" introduced by Kuhn.[6]

[6] See, for example, W. Kuhn and H. Kuhn, J. Colloid Sci. **3**, 11 (1948).

Letters to the Editor

THIS section will accept reports of new work, provided these are terse and contain few figures, and especially few halftone cuts. The Editorial Board will not hold itself responsible for opinions expressed by the correspondents. Contributions to this section should not exceed 600 words in length and must reach the office of the Managing Editor not later than the first of the month preceding that of the issue in which the letter is to appear. No proof will be sent to the authors. The usual publication charge ($4.00 per page) will not be made and no reprints will be furnished free.

A Comparison of the Ionization Cross Sections of H_2 and D_2

NORMAN BAUER* AND J. Y. BEACH
California Research Corporation, Richmond Laboratories, Richmond, California
November 1, 1948

WE wish to correct an impression given in the opening sentences of a recent note by R. E. Honig[1] on "A comparison of the ionization cross sections of H_2 and D_2" which referred to our note on "Differences in mass spectra of H_2 and D_2."[2] We did not report a significant difference between the sensitivities for H_2^+ and D_2^+. Rather the difference observed (about 10 percent) was interpreted as being within the probable limit of mass spectrometer discrimination for the two masses. The difference observed (presumably caused by discrimination) was reported as about 10 percent—not 10 to 40 percent. Our note was not concerned with the question of correcting sensitivities by $M^{\frac{1}{2}}$, and the data were not obtained or discussed with that question in view.

* Present address, 1 Arlington Avenue, Berkeley, California.
[1] Richard E. Honig, J. Chem. Phys. 16, 837 (1948).
[2] Norman Bauer and J. Y. Beach, J. Chem. Phys. 15, 150 (1947).

Calculation of Transport Properties of Gases

I. AMDUR
Department of Chemistry, Massachusetts Institute of Technology, Cambridge, Massachusetts
November 10, 1948

HIRSCHFELDER, Bird, and Spotz[1] have recently reported a method for calculating transport properties of non-polar gases which leads to excellent correlation of experimental results. Since they did not compare their procedure with that previously used by Amdur[2] in calculating low temperature transport properties of the rare gases, it seems desirable to point out briefly the similarities and differences in the two approaches. The discussion will be limited to viscosity and self-diffusion, which should suffice to illustrate the major steps in the two treatments.

The classical, velocity dependent cross section for viscosity and thermal conductivity, $S_{\eta,K}$, may be defined as

$$S_{\eta,K}=2\pi\int_0^\pi G(\theta)\sin^3\theta d\theta, \tag{1}$$

and the classical, velocity dependent cross section for self-diffusion, $S_{D(1,1)}$, as

$$S_{D(1,1)}=2\pi\int_0^\pi G(\theta)\sin^2\frac{\theta}{2}\sin\theta d\theta, \tag{2}$$

where $G(\theta)$ is the solid angle scattering coefficient, and θ, the angle through which the direction of the relative initial velocity, v, of two colliding particles is turned by a collision. $G(\theta)$ may be defined by the statement that $2\pi NG(\theta)\sin\theta d\theta$ is the number of atoms deflected per second between θ and $\theta+d\theta$ from a stream of N atoms per unit area per second impinging upon a single scattering atom. The scattering angle, θ, may be calculated from classical treatment of the two-body collision problem if the potentiai energy of interaction as a function of distance is known, and, for a given value of the initial relative velocity, $G(\theta)$ may be evaluated from the known dependence of θ on r_0, the distance of closest approach of the two particles.[3]

The method of Hirschfelder, Bird, and Spotz consists, in effect, of evaluating functions such as $S_{\eta,K}$ and $S_{D(1,1)}$ from fundamental relations such as Eqs. (1) or (2). (They actually calculated reduced cross sections which are the ratios of velocity dependent cross sections to the hard sphere cross section, πr_0^2, which is independent of velocity.) Their method is direct and should give excellent results within the limitations imposed by their choice of a single analytical form for the interaction potential of all the non-polar gases which they consider, and by the validity of classical mechanics in treating the transport phenomena.

Amdur used an indirect approach in calculating $S_{\eta,K}$ and $S_{D(1,1)}$ by assuming that, at any given value of v, the *ratio* of these cross sections to the classical total collision cross section, S, is the same for a real gas as for a gas of hard spheres. In the latter case, $G(\theta)=r_0^2/4$, and since

$$S=2\pi\int_0^\pi G(\theta)\sin\theta d\theta, \tag{3}$$

the desired ratios are $S_{\eta,K}/S=\frac{2}{3}$ and $S_{D(1,1)}/S=\frac{1}{2}$. For real gases, S, as calculated from Eq. (3), is infinite if $G(\theta)$ is calculated from classical mechanics which does not allow for the diffraction effects which predominate at sufficiently small angles of scattering. Massey and Mohr[4] have shown, however, that classical mechanics may be used to calculate proper classical values of S by limiting the integration in Eq. (3) to angles greater than the "critical scattering angle, θ_c." This angle, above which diffraction effects are negligible, is equal to $\lambda/(2r_0)$ where λ is the deBroglie wavelength of the colliding system. Amdur's method reduces to calculation of total classical collision cross sections for real gases from

$$S=2\pi\int_{\theta_c}^\pi G(\theta)\sin\theta d\theta \tag{4}$$

on the basis of classical two-body collision theory, and use of the hard sphere ratios of $\frac{2}{3}$ and $\frac{1}{2}$ to obtain values of $S_{\eta,K}$ and $S_{D(1,1)}$ appropriate to the real gas.

The manner in which values of the velocity dependent cross sections are used to obtain actual transport properties does not differ in the two approaches. Both methods calculate transport cross sections which are functions of *temperature* by averaging over the Maxwellian distribution of ve-

locities, and then substitute these temperature dependent cross sections into the classical transport equations of Chapman[5] and Enskog.[6]

One would not expect Amdur's indirect approach to be capable of the same accuracy as that of Hirschfelder, Bird, and Spotz. The method does seem, however, to permit greater flexibility in the choice of forms for the potential energy function and does not require numerical integrations. The good agreement between calculated and experimental values for the transport properties of the five rare gases (for example, for viscosities in the range 14°–550°K the average absolute deviation is 4.8 percent) would appear to justify the assumptions used to obtain quantities such as $S_{\eta,\kappa}$ and $S_{D(1,1)}$ as functions of v. This seems particularly likely since care was taken to use potential energy functions whose constants were not evaluated from experimental values of the transport properties which were being calculated.

[1] J. O. Hirschfelder, R. G. Bird, and E. L. Spotz, J. Chem. Phys. **16**, 968 (1948).
[2] I. Amdur, J. Chem. Phys. **15**, 482 (1947); **16**, 190 (1948).
[3] E. H. Kennard, *Kinetic Theory of Gases* (McGraw-Hill Book Company, Inc., New York, 1938), Chapter III.
[4] H. S. W. Massey and C. B. O. Mohr, Proc. Roy. Soc. **A141**, 434 (1933).
[5] S. Chapman, Phil. Trans. Roy. Soc. **A211**, 433 (1912); **A216**, 279 (1915); **A217**, 115 (1917).
[6] D. Enskog, *Kinetische Theorie der Vorgange in massig verdunnten Gasen*, (Inaug. Diss., Upsala, 1917).

The Transport Properties of Non-Polar Gases

J. S. Rowlinson
Physical Chemistry Laboratory, Oxford University, England
November 4, 1948

In the October issue of this Journal, Hirschfelder, Bird, and Spotz[1] (HBS) have published extensive tables for calculating the viscosity and thermal conductivity of gases whose molecules have a van der Waal's interaction potential of the form $E(r)=Ar^{-12}-Br^{-6}$. Their tables now enable such data to be analyzed with almost the same precision as has been applied to second virial coefficient data since 1924. The purpose of this note is to report an independent and almost simultaneous investigation of the same problem which, although different approximation methods were used, confirms the results of these authors.

The dynamics of an encounter were treated by a method similar to that of Burnett.[2] His treatment could not be followed exactly as some of his substitutions are valid for repulsive force-fields only. χ, the angle of deflection, was computed as a function of two variables α and q. In the notation of HBS, α is given by

$$\alpha=1+(1+K)^{\frac{1}{2}} \quad \text{(cf. HBS Eq. (43))},$$

where K is the ratio of the relative kinetic energy to the maximum energy of interaction. q is a measure of $1/b$, where b would be the distance of closest approach if $E(r)$ were everywhere zero, and is given by

$$y_m=q(\alpha/2)^{1/6}.$$

For head-on collisions, $q=1$, and when molecules pass at infinite distance $q=0$. For each value of α and q, χ was computed by Gauss' method of approximate quadrature, using 6 ordinates. To avoid the complications of incipient "orbiting," the viscosity was only found for $kT/\epsilon \geqslant 0.5$ (HBS $kT/\epsilon \geqslant 0.3$). The largest value of χ was 475°. A function of $\sin^2\chi$, denoted by J (as in Eq. (6) of Burnett and corresponding to $S^{(l)}(K)$ of Eq. (53) of HBS) was then found by integration by Gauss' method, using 5 ordinates in each of the following ranges of q, 1.00–0.95, 0.95–0.90, 0.90–0.40, and 3 ordinates in the range 0.40–0.00. Finally the J terms were summed by the most accurate of Burnett's formulae (4-terms). Empirical formulae were used to give J as $f(\alpha)$ and interpolation was used at many of the temperatures. It is readily seen that $\frac{1}{2}\Sigma n_s J_s$ should be identical with $W^2(2)$ of HBS. The two are compared in Table I.

TABLE I.

kT/ϵ	0.5	0.6	0.7	0.8	0.9	1.0	1.2	1.4	1.6
$\frac{1}{2}\Sigma n_s J_s$	2.300	2.085	1.916	1.773	1.651	1.554	1.410	1.312	1.241
$W^2(2)$	2.257	2.065	1.908	1.780	1.675	1.587	1.452	1.353	1.279
kT/ϵ	1.8	2.0	2.2	2.4	2.6	2.8	3.0	3.5	4.0
$\frac{1}{2}\Sigma n_s J_s$	1.190	1.105	1.118	1.083	1.064	1.042	1.022	0.9864	0.9547
$W^2(2)$	1.221	1.175	1.138	1.107	1.081	1.058	1.039	0.9999	0.9700
kT/ϵ	4.5	5.0	5.5	6.0	7.0	8.0	9.0	10.0	
$\frac{1}{2}\Sigma n_s J_s$	0.9403	0.9262	0.9074	0.8950	0.8740	0.8562	0.8406	0.8265	
$W^2(2)$	0.9464	0.9269	—	0.8963	0.8727	0.8538	0.8379	0.8242	

The viscosity may be calculated from either of these functions by using Eq. (7) of HBS. No attempt was made to compute the small correction factor V, as $(V-1/V)$ is less than the probable error in $W^2(2)$.

In view of the length and complexity of these calculations, and the different methods used in each laboratory, the agreement is very satisfactory. The differences are small and irregular, and are almost certainly due to inaccuracy in the interpolation formulae used in this work and to the use of methods which were essential in a single-handed computation.

[1] J. O. Hirschfelder, R. B. Bird, and E. L. Spotz, J. Chem. Phys. **16**, 968 (1948).
[2] D. Burnett, Proc. Camb. Phil. Soc. **33**, 363 (1937).

Effect of Temperature on Mass Spectra

D. P. Stevenson
Shell Development Company, Emeryville, California
November 1, 1948

In a recent communication with a title similar to that of the present one, Fox and Hipple[1] describe the effect of temperature on the mass spectrum of isobutane. It is the object of this note to indicate the nature and origin of their observations.

An increase of temperature has two observable effects on the mass spectra of the substances thus far studied. These are:

1. The specific intensity of all ions decrease with increasing temperature.

2. The specific intensities of the "parent ion" decrease more rapidly with temperature than do the specific intensities of fragmentary ions, and within the accessible temperature range (75–350°C) this effect is more pro-

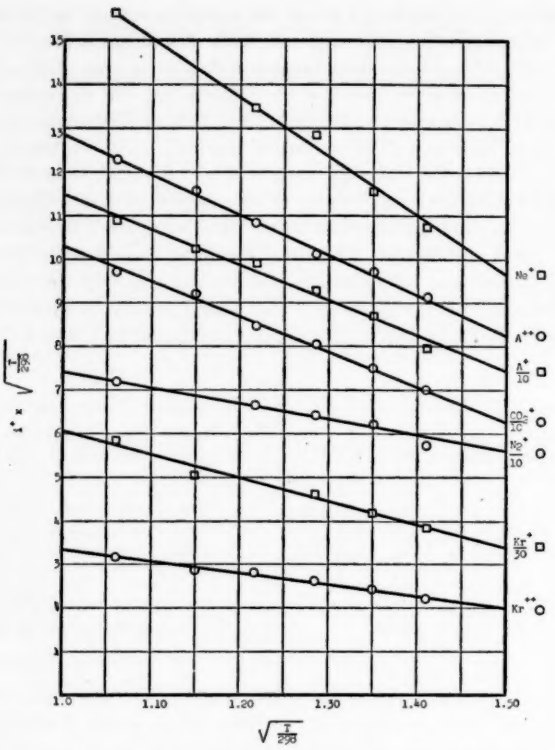

FIG. 1. The variation of specific ion currents (i^+) with absolute temperature (T) for various simple ions (Westinghouse type LV mass spectrometer, 75-volt ionizing electrons). Although the specific current units are arbitrary, the same units have been used for all substances and thus are consistent with the relative sensitivities of the various substances. The temperatures have been normalized to "room temperature" (25°C) to provide a more convenient scale.

nounced for complex than for simple molecules. The largest effects have been found in the mass spectra of branched chain paraffins.

Both 1 and 2 have their origin in the increase in energy of the molecules associated with the increase in temperature. The increase in kinetic energy ($\frac{3}{2}kT$) is the source of effect 1, while the increase in internal (vibrational) energy brings about effect 2.

The increase in kinetic energy of the molecules results in a decrease in the average number of molecules in the ionization chamber since the flow of gas through the mass spectrometer tube is effusive. This results in the ion current being proportional to $T^{-\frac{1}{2}}$. The increase of kinetic energy further results in the ions being formed with greater initial kinetic energy and since the discrimination losses in the ion source increase as $T^{\frac{1}{2}}$, the observed ion current decreases as $(1-\alpha T^{\frac{1}{2}})$, where α is a function of the ion source geometry, the ion accelerating fields, and the magnetic fields across the ionization chamber.[2] Thus the decrease of ion current with temperature is expressed as

$$i(T)=i_0T^{-\frac{1}{2}}[1-\alpha T^{\frac{1}{2}}]. \qquad (A)$$

Equation A has been found to represent the temperature variation of the ion currents in the mass spectra of neon, argon, krypton, nitrogen, and carbon dioxide over, $335 \leqslant T \leqslant 593$°K. This may be seen from Fig. 1, where $i\times(T/298)^{\frac{1}{2}}$ is plotted against $(T/298)^{\frac{1}{2}}$ for selected ions. It will be noted that for the rare gases (argon and krypton), the formula for the temperature variance of specific ion current fits singly and double charged ions equally well.

The increase in internal energy that accompanies increasing temperature results in an increased fraction of the molecules of a substance being in configurations which permit excitation to energy levels above dissociation limits of the states of the molecule-ion. This results in a larger fraction of the molecule-ions produced by electron impact dissociating, and thus the parent ion forms a smaller fraction of the total ion current. This effect, (2), is related to the greater probability of the breaking of C−H bonds than of C−D bonds in deutero-hydrocarbons.[3]

In Table I there are given the ratios, $i_p^+/\Sigma i_n^+$, where i_p^+ = specific intensity of parent ion, i_n^+ = specific intensity of any ion, and the summation is over all ions, including i_p^+, in the mass spectra of a number of hydrocarbons for $T=340$, 440, and 540°K. This ratio equals the fraction of ions formed which do not dissociate. These data were obtained with a Westinghouse type LV mass spectrometer, i.e., the same type used by Fox and Hipple.[1] The spectra were recorded by varying the magnetic field, and the ion intensities were not corrected for ion source discrimination. As would be expected, the less rigid the molecule the greater is the effect of temperature on the probability of dissociation of the molecule ion, i.e., the smaller the fraction of ions which do not dissociate.

TABLE I. Effect of temperature on the fraction of the mass spectra due to parent ions.

Substance	p[a]	75-volt ionizing electrons $T=340$	440	540°K
Methane	16	0.572	0.555	0.542
Acetylene	26	0.796	0.792	0.788*
Acetylene-d_2	28	0.829	0.821	0.820*
Ethane	30	0.164	0.152	0.135
Propane	44	0.154	0.132	0.108
n-Butane	58	0.095	0.071	0.048
i-Butane	58	0.0295	0.0204	0.0117

[a] p = molecular weight of parent ion.
* $T=575$°K.

[1] R. E. Fox and J. A. Hipple, J. Chem. Phys. 15, 208 (1947).
[2] For discussions of ion source discrimination, see Norman D. Coggeshall, J. Chem. Phys. 12, 19 (1944); H. W. Washburn and C. E. Berry, Phys. Rev. 70, 559 (1946).
[3] The differences in the mass spectra of such isotopic molecules arise in part from the greater amplitude of the zero-point vibrations of the −H bonds than of the −D bonds. See Evans, Bauer, and Beach, J. Chem. Phys. 14, 701 (1946); N. Bauer and J. Y. Beach, J. Chem. Phys. 15, 150 (1947); David P. Stevenson, J. Chem. Phys. 15, 409 (1947).

The Phase Transition and the Piezoelectric Effect of KH_2PO_4

T. NAGAMIYA AND S. YOMOSA
Department of Physics, Osaka University, Japan
November 1, 1948

ANOMALOUS behaviors of the dielectric constants[1,2] and the phase transition[3] at 122°K of KH_2PO_4 were treated by the methods of statistical mechanics by Slater[4] and others.[5,6] In this crystal, PO_4 groups are linked by hydrogen bonds which are directed nearly parallel to the

axis a or b. In Slater's model it is assumed that two hydrogen atoms (or protons) out of the four hydrogen bonds linking each PO_4 group to its neighbors lie nearer to it, and the resulting $(H_2PO)_4^-$ group has a dipole moment directed to one of the crystalline axes. Further, it is assumed that the energy of the crystal in the absence of external electric field is given by the number of those dipoles which are perpendicular to the c axis multiplied by a constant ϵ The number of configurations with the same energy and the same polarization was calculated by an approximate method, and a unique type of transition was predicted. His theory does not, however, account for the anomaly of the piezoelectric effect which was also observed[2,7] and was found to be very similar to the anomaly of the dielectric constants, although he considers it to be the primary cause of the λ-type broadening of the transition temperature. We must expect a close relationship between them.

Instead of assuming the energy of the $(H_2PO_4)^-$ dipoles directed to $+c$ and that of the dipoles directed to $-c$ as being equal, we took them in the form

$$\epsilon_+ = -\epsilon_0 - \beta x_y, \quad \text{and} \quad \epsilon_- = -\epsilon_0 + \beta x_y, \tag{1}$$

respectively, where ϵ_0 and β are constants and ϵ_0 stands for Slater's ϵ. x_y is the strain of the crystal. The assumption (1) is consistent with the point group symmetry of the crystal, V_d. Denoting the dipole moment associated with a $(H_2PO_4)^-$ group by μ, the external electric field by E, and the normal elastic constant corresponding to x_y by $N\alpha$, where N is the number of molecules of the crystal of unit volume, we can write the energy of the crystal as

$$U = N_+\epsilon_+ + N_-\epsilon_- - (N_+ - N_-)\mu E + \tfrac{1}{2}N\alpha x_y^2, \tag{2}$$

N_+ and N_- being the numbers of $(H_2PO_4)^-$ dipoles which are parallel to $+c$ and $-c$, respectively. To (2) we further added the term which is due to the induced polarization, and the term which represents the normal piezoelectric effect, namely,

$$-\tfrac{1}{2}\chi_1 E^2 - \zeta_1 x_y E, \tag{3}$$

χ_1 and ζ_1 being constants. The writers believe that the problem of the local field is cared for by the inclusion of the terms (3) and that the inclusion of the local field factor a in the form $\chi = a\chi_0 + \chi_1$ for the susceptibility, as was done by Slater, is not correct.

Combining the energy given above with the entropy formula derived by Slater, and minimizing the free energy with respect to N_+ and N_-, the equations for describing the equilibrium state can be obtained. Further, the polarization p in the direction of the c axis and the stress component X_y are derived from the free energy A through the equations

$$P = -\partial A/\partial E = N\mu z + \chi_1 E + \zeta_1 x_y, \tag{4}$$

$$X_y = -\partial A/\partial x_y = -N\alpha x_y + N\beta z + \zeta_1 E, \tag{5}$$

where $z = (N_+ - N_-)/N$.

The nature of the phase transition is practically the same as that predicted by Slater's theory in that the transition is accompanied by a latent heat and that the crystal is abruptly and spontaneously polarized below the transition temperature. However, our theory predicts a further fact that the crystal is spontaneously deformed with a constant shearing strain $x_y = \beta/\alpha$ below the transition temperature. In fact, the relation

$$x_y/z = \beta/\alpha \tag{6}$$

always follows from (5) when there is no stress and no external electric field.

From the condition of the minimum of the free energy we have

$$z = \frac{\sinh[(\beta x_y + \mu E)/kT]}{2\exp[-\epsilon_0/kT] - \cosh[(\beta x_y + \mu E)/kT]}. \tag{7}$$

If we substitute this into (4) and (5) and assume x_y and E to be small, we can derive the following equations:

$$P = \chi E - d_{36}X_y \quad \text{and} \quad x_y = d_{36}E - s_{66}X_y, \tag{8}$$

with

$$\begin{aligned} \chi &= N\mu'^2/(D - 2\delta) + \chi_1 + \zeta_1^2/N\alpha, \\ d_{36} &= (\beta\mu'/\alpha)/(D - 2\delta) + \zeta_1/N\alpha, \\ s_{66} &= (\beta^2/N\alpha^2)/(D - 2\delta) + 1/N\alpha; \end{aligned} \tag{9}$$

$$D = kT(2e^{-\epsilon_0/kT} - 1), \quad 2\delta = \beta^2/\alpha, \quad \mu' = \mu + \beta\zeta_1/N\alpha. \tag{10}$$

The three quantities of the Eqs. (9) can be written approximately in the form $A/(T - T_c) + B$ for the temperature range above the transition temperature which is of practical interest. The following numerical values explain all the results of Mason's[2] measurements:

$$\begin{aligned} &\beta/\alpha = 6.8 \times 10^{-3} = 23' \text{ in angle}, \\ &N\alpha = 7.04 \times 10^{10}[1 - (T - T_c) \times 6.7 \times 10^{-4}] \text{ dyne/cm}^2, \\ &\epsilon_0 = 1.22 \times 10^{-14} \text{ erg}, \\ &\mu' = 1.55 \times 10^{-18} \text{ c.g.s.e.s.u.} \end{aligned}$$

Figure 1 shows the computed and the measured elastic constant, the dotted curve corresponding to the constant value of $N\alpha$ (the term proportional to $T - T_c$ given above being omitted), and the full curve corresponding to $N\alpha$ given above. The Curie point of the clamped (i.e., strain-free) crystal is lowered by 3.5° as compared with that of the stress-free crystal, in agreement with Mason's result. A somewhat greater value of the dipole moment μ', which

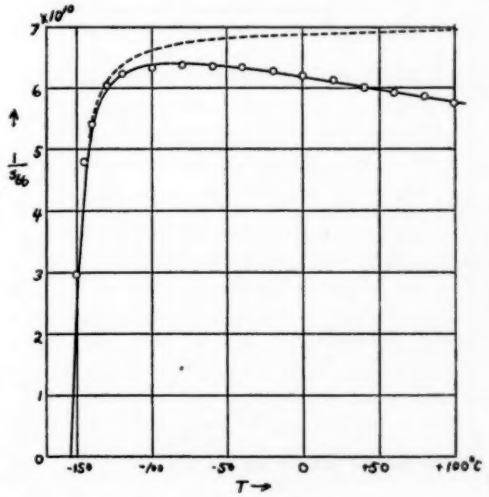

FIG. 1.

is practically equal to μ, compared with that which can be derived from the Busch[1] measured spontaneous polarization, namely, 1.25×10^{-18}, is to be interpreted as due to that not all the domains are parallel to the field in his experiment, or otherwise, as due to the experimental errors.

A detailed account will be published in Journal of the Physical Society of Japan or in Progress of Theoretical Physics.

[1] G. Busch, Helv. Phys. Acta **11**, 296 (1938).
[2] W. P. Mason, Phys. Rev. **69**, 173 (1946).
[3] J. C. Stephenson and J. G. Hooley, Phys. Rev. **56**, 121 (1939); J. Am. Chem. Soc. **66**, 1397 (1944).
[4] J. C. Slater, J. Chem. Phys. **9**, 16 (1941).
[5] H. Takahasi, Proc. Phys.-Math. Soc. Japan **23**, 1069 (1941).
[6] Y. Takagi, Sûbutu Kaisi (the Japanese journal of the Phys.-Math. Soc. of Japan) **17**, 280 (1942). This paper treats the theory of the dielectric constant in the direction of the a axis.
[7] W. Lüdy, Zeits. f. Physik **113**, 302 (1939).

Fundamental Vibrational Frequencies and Thermodynamic Functions for Vinylacetylene, Revised Thermodynamic Functions for Hydrogen Cyanide, and Thermodynamics of Two Reactions Involved in the Synthesis of Acrylonitrile

ROBERT F. STAMM, FREDERICK HALVERSON, AND JOHN J. WHALEN
Stamford Research Laboratories, American Cyanamid Company, Stamford, Connecticut
November 12, 1948

THE Raman[1,2] and infra-red[3] spectra of vinylacetylene (Fig. 1) have been reported in the literature, but no consistent assignment of the vibrational frequencies has been given. Using the recently published assignment for a structurally similar molecule, acrylonitrile,[4] as a basis, a reasonable choice for the fundamental vibrational frequencies of vinylacetylene can be made. This choice of frequencies, together with an approximate description of the vibrational modes, is given in Table I. The planar and non-planar bending vibrations of the C≡C−H group have been assumed degenerate, with the frequency 615 cm^{-1}.

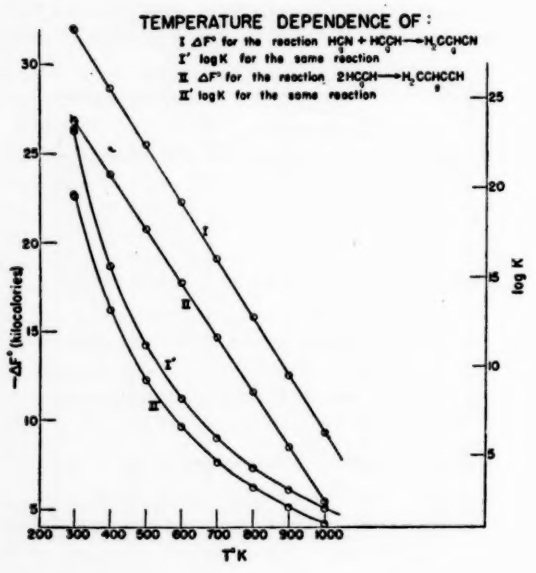

FIG. 1.

TABLE I. Fundamental vibration frequencies for vinylacetylene.

Description		Frequency
	Planar	
ν_1	≡C−H stretch	3305*
ν_2	≡C−H stretch	3102*
ν_3	≡C−H stretch	(3080)***
ν_4	≡C−H stretch	3012*
ν_5	C≡C stretch	2099*
ν_6	C=C stretch	1600**
ν_7	$=CH_2$ deformation	1410**
ν_8	≡C− rock	1288*
ν_9	$=CH_2$ rock	1090**
ν_{12}	C−C stretch	875*
ν_{14a}	C≡C−H bend	615**
ν_{15}	C=C−C bend	535**
ν_{17}	C−C≡C bend	219*
	Non-planar	
ν_{10}	C=C−C wag	950**
ν_{13}	C=C torsion	678*
ν_{11}	$C=CH_2$ wag	935**
ν_{14b}	C≡C−H bend	615**
ν_{16}	C−C≡C bend	309*

* Reference 1.
** Reference 3.
*** Estimated.

Using these frequencies and assuming the structural parameters given in Fig. 1, the thermodynamic functions calculated by the rigid rotator[5]-harmonic oscillator[6] approximation for vinylacetylene in the ideal gas state under one atmosphere pressure are given in Table II.

Values of the functions $(H°-H_0°)/T$, $(F°-H_0°)/T$, and $S°$ for HCN calculated by the rigid rotator[5]-harmonic oscillator[6] approximation, and by making corrections for anharmonicity, interactions, stretching, and integration error according to the method of Wagman *et al.*,[7] are given in Table III. Spectroscopic values given by Herzberg[8] were used ($\nu_1=2089.0$, $\nu_2=712.1$, $\nu_3=3312.0$ cm^{-1}; $d_1=1$, $d_2=2$, $d_3=1$; $\alpha_1=9.3\times10^{-3}$, $\alpha_2=-7\times10^{-4}$, $\alpha_3=10.8\times10^{3}$; $B_{(0)}=1.4784$ cm^{-1}, $D=+3.3\times10^{-6}$, $X_{11}=-52.0$, $X_{12}=4.2$, $X_{13}=14.4$, $X_{22}=2.85$, $X_{23}=19.53$, $X_{33}=55.48$). A com-

TABLE II. Thermodynamic functions for vinylacetylene (cal./mole/deg.).

Absolute temperature	$C_p°$	$H°-H_0°/T$	$-(F°-H_0°)/T$	$S°$
298.16	17.49	11.67	55.11	66.77
300	17.57	11.70	55.18	66.88
400	21.26	13.65	58.82	72.47
500	24.25	15.48	62.06	77.54
600	26.67	17.09	65.03	82.12
700	28.68	18.67	67.79	86.46
800	30.40	20.02	70.37	90.38
900	31.87	21.16	72.82	93.97
1000	33.16	22.39	75.10	97.48
1500	37.52	26.78	85.07	111.85

TABLE III. Values of thermodynamic functions for HCN in the ideal gaseous state (calories/deg./mole).*

T°K	C_p°	$(H°-H_0°)/T$			$-(F°-H_0°)/T$			$S°$		
	I*	I	II*	III*	I	II	III	I	II	III
298.16	8.58	7.41	7.408	7.410	40.80	40.811	40.763	48.22	48.219	48.173
300	8.59	7.42	7.416	7.413	40.85	40.856	40.810	48.27	48.272	48.223
400	9.38	7.82	7.817_5	7.812	43.04	43.046	42.997	50.85	50.863	50.809
500	9.98	8.19	8.199	8.191	44.82	44.832	44.781	53.02	53.031	52.972
600	10.47	8.53	8.544	8.534	46.35	46.356	46.305	54.88	54.900	54.839
700	10.91	8.84	8.859	8.848	47.69	47.697	47.646	56.53	56.556	56.494
800	11.30	9.12	9.149	9.134	48.89	48.898	48.845	58.01	58.046	57.979
900	11.65	9.39	9.418_5	9.401	49.98	49.989_5	49.936	59.36	59.408	59.337
1000	11.97	9.63	9.670	9.649	50.98	50.993	50.941	60.60	60.663	60.590

* The values in columns designated by I were calculated by the harmonic oscillator-rigid rotator approximation. The values in columns designated by II were calculated by the harmonic oscillator-rigid rotator approximation but were corrected in the manner discussed in the text. The values in columns designated by III are the values originally calculated by Gordon from older spectroscopic data and have been corrected here to take account of the latest values of the physical constants.

parison of these thermodynamic values with those calculated by Gordon[9] using his method[10] and slightly different spectroscopic data are also included in Table III. (Gordon's values have been corrected by the writers for changes in the best values of the fundamental and derived constants.[5])

Using these functions and relevant data from the literature, free energy changes and equilibrium constants have been calculated for two of the possible reactions in mixtures of acetylene and hydrogen cyanide.

I. $HCN(g)+HCCH(g)=H_2CCHCN(g)$. Data obtained in these laboratories[11] on the heats of combustion (ΔH_{298}(1 atmos.) $=-420.82$ kcal.) and vaporization ($\Delta H_{298}=+7.850 \pm 0.050$ kcal.) of acrylonitrile, combined with the standard[5] heats of combustion for C (graphite) and $H_2(g)$, yield $+44.040$ kcal. as the heat of formation for $H_2CCHCN(g)$ at 25°C. Heats of formation for $HCN(g)$ and $HCCH(g)$ at 25°C are taken to be $+31.00$ kcal.[9] and $+54.194 \pm 0.190$ kcal.[7], respectively. Using these values we obtain

$$HCN(g)+HCCH(g)=H_2CCHCN(g);$$
$$\Delta H_{298}=-41.154 \text{ kcal./mole.}$$

From the values of $(H°-H_0°/T)$ for these substances[4,7]

$$\Delta(H°-H_0°)_{298.16}=-1.383 \text{ kcal.}=\Delta H°-\Delta H_0°.$$

Lacking data necessary to correct for gas imperfections we set $\Delta H_{298}=\Delta H°_{298.16}$, thus getting $\Delta H_0°=-39.771$ kcal./mole as the difference in zero-point energies. This constant is employed with the values of $(F°-H_0°/T)$ for the three substances[4,7] to obtain the values of $\Delta F°$ and $\log K_p$ given in Table IV and Fig. 2 for various temperatures.

TABLE IV. Free energy changes and equilibrium constants for the reactions: I. $HCN(g)+HCCH(g)=H_2CCHCN(g)$; II. $2HCCH(g)=H_2CCHCCH(g)$.

T°K	$\Delta F°$		$\log K_p$	
	I	II	I′	II′
298.16	−31,986	−26,900	23.4453	19.72
300	−31,932	−26,900	23.2624	19.59
400	−28,799	−23,900	15.7349	13.06
500	−25,586	−20,800	11.1835	9.09
600	−22,335	−17,800	8.1354	6.48
700	−19,065	−14,700	5.9523	4.59
800	−15,779	−11,600	4.3161	3.17
900	−12,519	− 8,500	3.0400	2.06
1000	− 9,261	− 5,400	2.0240	1.18

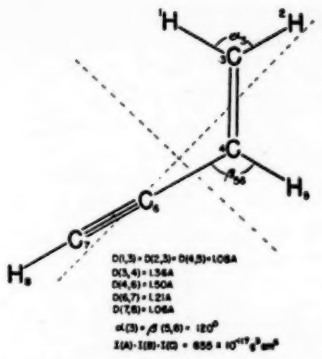

FIG. 2. Structural parameters for vinylacetylene.

II. $2HCCH(g)=H_2CCHCCH(g)$. The writers could find no experimental heat of combustion value for vinylacetylene. However, calculation of ΔH_{291} for reaction I using Pauling's[12] table of bond energies yields a value only 0.05 kcal. less than the experimental one. Because of the structural similarity of the compounds involved, it is assumed that the value $\Delta H_{291}=-35.6$ kcal./mole calculated for reaction II using bond energies[12] is good to ± 0.5 kcal. Combination of this ΔH with the values of $(H_0-H_0°/T)_{291°}$ yields $\Delta H_0°=-34.3$ kcal./mole for reaction II. The values of $\Delta F°$ and $\log K_p$ calculated for reaction II using this $\Delta H_0°$ are given in Table IV and Fig. 2.

[1] G. Glockler and H. M. Davis, J. Chem. Phys. **2**, 881 (1934).
[2] P. Gänswein and R. Mecke, Zeits. f. Physik **99**, 189 (1936).
[3] E. Bartholomé and J. Karweil, Zeits. f. physik. Chemie **B35**, 442 (1937).
[4] F. Halverson, R. F. Stamm, and J. J. Whalen, J. Chem. Phys. **16**, 808 (1948).
[5] Working equations given by Wagman *et al.*, J. Research Nat. Bur. Stand. **34**, 143 (1945) were used for the translational and rotational contributions.
[6] Tables given by J. G. Aston in Taylor and Glasstone, *Treatise on Physical Chemistry* (D. Van Nostrand Company, Inc., New York, 1942), Vol. I, p. 655, were used.
[7] D. D. Wagman *et al.*, J. Research Nat. Bur. Stand. **35**, 467 (1945).
[8] G. Herzberg, *Infrared and Raman Spectra of Polyatomic Molecules* (D. Van Nostrand Company, Inc., New York, 1945), p. 280.
[9] A. R. Gordon, J. Chem. Phys. **5**, 30 (1937).
[10] A. R. Gordon, J. Chem. Phys. **3**, 259 (1935).
[11] A. B. Bestul and D. J. Salley, American Cyanamid Company Technical Data Sheet (Dec., 1947).
[12] L. Pauling, *The Nature of the Chemical Bond* (Cornell University Press, Ithaca, New York, 1939), pp. 53 and 123.

On Rotation in Ammonium Halides

E. L. WAGNER AND D. F. HORNIG
Metcalf Chemical Laboratories, Brown University, Providence, Rhode Island

October 18, 1948

ALTHOUGH thermodynamic evidence[1] has been obtained which is opposed to the notion that the phase transition in NH_4Cl is due to the onset of free rotation of the NH_4^+ ions, Beck's grating studies[2] of the 1750-cm^{-1} bands in the infra-red spectra of NH_4Cl and NH_4Br showed fine structure in both room and low temperature phases which he interpreted as evidence of rotation.

We have studied the spectrum of both salts and of ND_4Cl in the temperature range, 28°C to −190°C, and find no evidence of rotational structure in any of the salts in either phase. The 1750-cm^{-1} band obtained with NH_4Cl is shown in Fig. 1. The spectra of the other salts are similar.

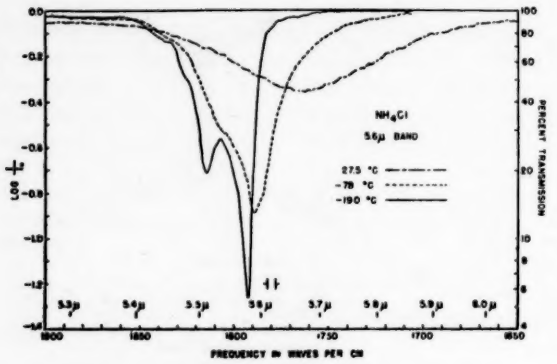

FIG. 1. 5.6μ band of NH_4Cl.

Our resolution in this region was better than 5 cm^{-1} and the reported rotational spacing was about 15 cm^{-1}.

It seems clear that the structure previously obtained was due to water vapor. Although the peaks reported do not coincide with water vapor peaks, the approximate separation is the same and we have observed that in spectra taken point by point apparent peaks are frequently obtained on the steep sides of lines in the background spectrum. Furthermore, it is noteworthy that although the band center in the bromide occurs at a frequency 50 cm^{-1} lower than in the chloride, peaks were reported at identical frequencies in both spectra.

Our data show no evidence of rotation in either phase. We have been able to interpret the major features of the low temperature infra-red spectrum of NH_4Cl on the basis of a body-centered lattice in which all NH_4^+ tetrahedra are similarly oriented, and the NH_4Br spectrum on the basis of a similar structure in two dimensions but with a screw axis replacing translation in the third dimension (i.e., space group D_{4h}^9). The splitting of the triply degenerate mode at 1400 cm^{-1} constitutes our chief evidence. These structures are both in accord with optical, piezoelectric, x-ray and Raman data obtained on these crystals.[3] The fact that the spectra of the room temperature phases of the two compounds are almost identical suggests that the room temperature modification of both salts has the same structure, in which the NH_4^+ ions are randomly distributed between the two possible orientations, and that the phase transition is a simple order-disorder transition.

Experimental work on ND_4Br is in progress and more detailed data and analysis will be published shortly.

[1] A. W. Lawson, Phys. Rev. **57**, 417 (1940).
[2] C. Beck, J. Chem. Phys. **12**, 71 (1944).
[3] A. C. Menzies and H. R. Mills, Proc. Roy. Soc. (London) **148**, 407 (1935). These data are conveniently summarized in this article. However, the NH_4Br model used by these authors does not account for the splitting of the 1400-cm^{-1} mode.

Physical Adsorption on Non-Uniform Surfaces

TERRELL L. HILL
Department of Chemistry, University of Rochester, Rochester, New York
November 11, 1948

IN a recent paper[1] with the above title, G. Halsey has discussed several aspects of adsorption including the BET theory and "cooperative adsorption." The writer would like to make a few comments on these two points.

Halsey makes the following statement which, it seems to the writer, may lead to some confusion: "$\cdots$ the hypotheses of the BET theory lead to substantially no adsorption beyond the first layer if $E_2=E_L$, and stepwise isotherms if $E_1>E_2>E_3\cdots>E_L$." Now actually the *hypotheses of the BET theory*[2] lead, as is well known, to multimolecular adsorption for any value of the BET constant c for p/p_0 sufficiently close to unity, and in no case to stepwise isotherms. Halsey's statement actually refers to a mixture of BET hypotheses and somewhat refined hypotheses. In summary, although the BET model assigns extremely unrealistic properties[2] to the liquid state, the model *does* lead to multimolecular adsorption. The present writer, in other words, is by no means defending the BET model, but is defending the deductions which have been made *from the model.*

Halsey discusses cooperative adsorption (i.e., adsorption in which horizontal as well as vertical interactions are taken into account so that condensation phenomena are possible[2]) and in this connection accepts the reality of stepwise adsorption near the surface—although he feels that the non-uniform nature of the surface will tend to smooth out these steps. This is a new and interesting point of view. It should be pointed out, however, that a closely related approximate *quantitalive* approach to the problem of "cooperative" adsorption on a uniform surface (for mathematical simplicity) has already been given,[3] though not mentioned by Halsey in his discussion of cooperative adsorption. Stepwise adsorption was encountered in the mathematical equations and was discussed, although it was not felt that the model was sufficiently refined to come to a definite conclusion concerning the physical significance of this aspect of the approximate theory.

[1] G. Halsey, J. Chem. Phys. **16**, 931 (1948).
[2] These can probably be outlined most clearly in terms of a statistical mechanical model. See: (1) T. L. Hill, J. Chem. Phys. **14**, 263 (1946), Eqs. (3)–(5), (28) (29), and Fig. 1; (2) J. Chem. Phys. **15**, 767 (1947), Eq. (18).
[3] T. L. Hill, J. Chem. Phys. **15**, 767 (1947).

A New Equation for the Non-Stationary Shock Wave

F. CAP
Davos-Platz, Switzerland
November 2, 1948

IN analogy to the "Stoßpolare" of Busemann[1] for the stationary shock wave of two dimensions I found an equation for the non-stationary shock wave of one dimension.

We start from the well-known hydrodynamic equations

$$(w-\mu)\rho=(\rho-\bar{u})\bar{\rho}, \tag{1}$$

$$(w-u)^2\rho+p=(w-\bar{u})^2\bar{\rho}+\bar{p}, \tag{2}$$

$$\frac{a^2}{u-1}+\frac{(w-u)^2}{2}=\frac{\bar{a}^2}{u-1}+\frac{(w-\bar{u})^2}{2},$$

where w is the speed of the shock wave, u the velocity of the gas, ρ the density, p the pressure, a the velocity of sound, and $a^2/u-1=i$, the enthalpy of a perfect gas; the bar refers to the quantities behind the shock wave. By

dividing (2) by (1) one obtains

$$\bar{u}=\mu\pm\left(\frac{1}{u}\left[-(a^2+\bar{a}^2)+\left((\bar{a}^2+a^2)^2-\frac{4u^2}{u-1}\left[\frac{1}{u}-\frac{1}{u-1}\right](a^2-\bar{a}^2)^2\right)^{\frac{1}{2}}\right]\right)^{\frac{1}{2}},$$

where use has been made of the relation $a^2=up/\rho$. For large values of $\bar{a}(\bar{a}\gg a)$ we have the limiting relations (if $u=0$)

$$\frac{\bar{u}}{\bar{a}}=\left(\frac{1}{u}\left[1+\left(1-\frac{4u^2}{u-1}\left[\frac{1}{u}-\frac{1}{u-1}\right]\right)^{\frac{1}{2}}\right]\right)^{\frac{1}{2}};\quad \frac{w}{\bar{a}}=\frac{\bar{u}}{\bar{a}}\cdot\frac{u+1}{4}.$$

If $k=1.40$ (air), we have

$$\bar{u}/\bar{a}=1.89(w/\bar{a})=2.27\frac{w}{\bar{u}}=1.20.$$

A comprehensive publication of this topic will appear in Helvetica Physica Acta. Since sometimes the opinion is expressed that there is no limiting law for w, it might be of interest to point out that there is such a limiting relation.

[1] Lectures in the department of aerodynamics, Aachen 1929.

The High Frequency Factors of "Unimolecular" Reactions

M. Szwarc
Department of Chemistry, University of Manchester, Manchester, England
November 18, 1948

It was shown by Polanyi and Wigner[1] that the frequency factor of unimolecular reactions should be of the order 10^{13} sec.$^{-1}$. The further elaboration of this subject[2] introduced various coefficients (e.g., the transmission coefficient, the quantum restrictions, and so on), which may account for the changes in the magnitude of the frequency factor, and in particular enable us to explain the low values of this quantity. Indeed, a review of the experimental data shows that the frequency factors of the "true" unimolecular reactions are preferentially of the order of 10^{12}–10^{14} sec.$^{-1}$, and the data obtained for reactions in which molecules are decomposed by the breaking of one bond only[3] are especially illuminating.

It was claimed, however, that in some "unimolecular" reactions (these include decomposition of some explosives) the frequency factors attained values as high as 10^{24} sec.$^{-1}$.* As the treatment mentioned before does not offer any explanation of such high values of the frequency factor, we suggest here an approach which, we hope, will provide a basis for further elaboration.

In order to illustrate our suggestion we shall make use of a purely hypothetical scheme for the thermal decomposition of propylene as follows:

$$CH_2=CH-CH_3\rightarrow CH_2=CH-CH_2\cdot+H, \quad (1)$$

$$CH_2=CH-CH_2\cdot\rightarrow CH_2=C=CH_2+H, \quad (2)$$

$$CH_2=CH-CH_3+H\rightarrow CH_2=CH-CH_2\cdot+H_2. \quad (3)$$

The investigation of the pyrolysis of propylene[4] seems in fact to indicate that the reactions (1), (2), and (3) represent the first steps in the thermal decomposition of that compound. Let us now assume that reaction (3) is much faster than reaction (2), while the latter is much faster than reaction (1), and that reaction (2) is *the only* one which consumes allyl radicals. Such assumptions lead to a decomposition mechanism in which the allyl radicals *do not attain* the stationary concentration. Their concentration increases as a consequence of reaction (1), whereas the net result of the reactions (2) and (3) does not affect the concentration of allyl radicals.

To find the rate of the over-all reaction we shall discuss first a special case, in which the percentage of decomposition is kept so low that we can consider the concentration c of propylene as a constant throughout the whole time of the reaction (this can be achieved by using a very short time of contact). The rate of formation of allyl radicals is given by $2k_1\cdot c$,** and the concentration of allyl radicals after time t is, therefore, $2k_1\cdot c\cdot t$. The rate of the over-all reaction (which on our assumptions is equal to the rate of formation of allene or H_2) is, therefore:

$$\text{rate of the over-all reaction}=k^{**}=2k_1\cdot k_2\cdot c\cdot t.$$

Let us examine this result more closely. The rate of the reaction is proportional to the first power of the concentration of propylene, and the reaction is, therefore, of the first order for a constant time of contact. On the other hand, the constants k_1 and k_2 represent the constants of the "true" unimolecular reactions (1) and (2), and thus they will have frequency factors of the order of 10^{12}–10^{13} sec.$^{-1}$, and energies of activation E_1 and E_2, respectively. As a result, k^{**} will have a frequency factor of the order of 10^{24}–10^{26} sec.$^{-1}$, and an energy of activation E_1+E_2.

We suggest that this type of reaction is responsible for the very high frequency factors found for some "unimolecular" decompositions. This type of reaction is further characterized by the increase of the rate with the time, which is a principal feature of the decomposition of explosives, and can be expressed in another way by the statement: the quantity of material decomposed is proportional to the square of time.

The generalization of this example is quite simple. The conditions which must be fulfilled in order to obtain the required kinetics are:

1. The molecule A decomposes into B and C; B decomposes easily into the molecule D and a reactive species C_1, while both C and C_1 react rapidly with A, regenerating B.
2. The decomposition of B should be much more probable than any other reaction in which B can participate. This demands a very low reactivity of B and a very low energy of activation for its decomposition, and leads in consequence to the *non-stationary state* for the species B.

In the case discussed the reactivity of the allyl radical is very low (the radical is stabilized by its high resonance energy), and it is probable that at a high enough temperature and a very short time of contact the required conditions would be fulfilled.

The discussion of these kinetics for the case not restricted to a very low percentage of decomposition reveals some interesting features. Returning to our example, let us denote the initial concentration of propylene by C_0 and the concentration of allyl radicals and allene after time t as x and y, respectively. The previously suggested mechanism leads to the following system of differential equations:

$$dx/dt=2k_1\cdot(C_0-x-y) \quad (a)$$

$$dy/dt=k_2\cdot x. \quad (b)$$

These can easily be solved by differentiating (a) and substituting in the resultant equation for dy/dt from (b). We thus obtain:

$$\frac{d^2x}{dt^2}+2k_1\frac{dx}{dt}+2k_1\cdot k_2\cdot x=0,$$

and the initial conditions are that for $t=0$, $x=0$, and $dx/dt=2k_1\cdot C_0$. Since our initial assumption was that $k_2>k_1$, the discriminant $k_1^2-2k_1k_2$ is negative and, therefore, the solution has a form similar to that obtained for a damped oscillator

$$x=2k_1\cdot c_0/\alpha\cdot e^{-k_1\cdot t}\cdot\sin\cdot(\alpha\cdot t),$$

where $\alpha^2=2k_1\cdot k_2-k_1^2$.

The solution for y is obtained by simple integration:

$$y=c_0-c_0/\alpha\cdot(2k_1\cdot k_2)^{\frac{1}{2}}\cdot e^{-k_1t}\cdot\sin\cdot(\alpha\cdot t+\vartheta),$$

where

$$\sin\vartheta=\alpha/(2k_1\cdot k_2)^{\frac{1}{2}}.$$

As can easily be verified, both y and dy/dt are 0 for $t=0$. Therefore, for very small values of t, y is given by the square term of Taylor's series, i.e.,

$$y\sim\tfrac{1}{2}\left(\frac{d^2y}{dt^2}\right)_{t=0}\cdot t^2=k_1\cdot k_2\cdot c_0\cdot t^2.$$

The appearance of the trigonometric functions in chemical kinetics is rather unusual. It should be noted, however, that since obviously $x+y$ cannot be greater than C_0 the expressions given above break down at a time $t_f<\pi/2\alpha$, i.e., before $\sin(\alpha\cdot t)$ reaches its maximum value of 1.

* I am indebted to Professor C. E. H. Bawn for this information.
** The factor 2 arises from reaction (3) which produces allyl radicals from H atoms formed in reaction (1).
[1] M. Polanyi and E. Wigner, Zeits. f. physik Chemie **A139**, 439 (1928).
[2] See Glasstone, Laidler, and Eyring, *The Theory of Rate Processes; The Kinetics of Chemical Reactions, Viscosity, Diffusion and Electrochemical Phenomena* (McGraw-Hill Book Company, Inc., New York, 1941).
[3] Ziegler, Orth, and Weber, Annalen **504**, 131 (1933); Ziegler, Leib, Kuoevangel, and Anders, *ibid.* **551**, 161 (1942); E. T. Butler and M. Polanyi, Trans. Faraday Soc. **39**, 19 (1943); M. Szwarc, J. Chem. Phys. **16**, 128 (1947); and the following papers.
[4] M. Szwarc, J. Chem. Phys. (in press).

Ultraviolet Absorption Spectra of Phenanthrene in Various Solvents.

WILLIAM FRANCIS MADDAMS AND ROBERT SCHNURMANN
Physics Department, Manchester Oil Refinery, Limited
Manchester, England
November 8, 1948

IN a recent letter Vodar and Robin[1] described the ultraviolet absorption spectra of phenanthrene dissolved in compressed gases (nitrogen and argon). They illustrate in the case of argon at constant temperature the displacement of the absorption bands as a function of the density of solvent, showing a red shift with increasing density.

As part of a comprehensive program[2] on the ultraviolet absorption spectra of aromatic hydrocarbons, we examined phenanthrene[3] in various solvents (iso-octane, ethyl alcohol, chloroform, and benzene) with the interesting result at room temperature of displacements of the absorption bands (predominantly red shifts when using iso-octane as the reference solvent) of pronounced regularity (Fig. 1), and also of characteristic changes in the absorption intensities (expressed as $\Delta(\log_{10}\epsilon)$, where ϵ = molecular extinction coefficient) of the various bands (Fig. 2).

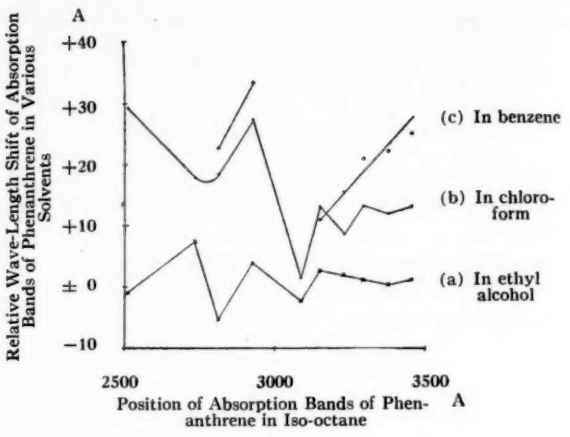

FIG. 1.

In agreement with the results obtained on other aromatic hydrocarbons,[4] and in particular with the still more regular wave-length shifts in the absorption spectra of anthracene, there is no clear hint of the connection of this definitely existing solvent effect (even in cases where there is no chemical reaction taking place between the solute and the solvent) either with the dipole moment, or the refractive index, or the density of the solvent.

In the present case the concentration of the phenanthrene solutions in iso-octane was 1 part in 272,440 by weight for the measurement of the short wave-length end of the spectrum, and 1 part in 1308 by weight for the long wave-length end. The accuracy of the wave-length determination of the absorption peaks is within ±4A, and the absorption intensities are determined to about ±5 percent. It appears from Fig. 1 that the red shift at the long wave-length end of the spectrum is very small in ethyl alcohol, whereas it is considerable in chloroform and still larger in benzene. Table I shows that the distances between neighboring absorption bands are very similar in the four solvents except for bands A[5] and D, both of which exhibit a large red shift in chloroform and therefore give compara-

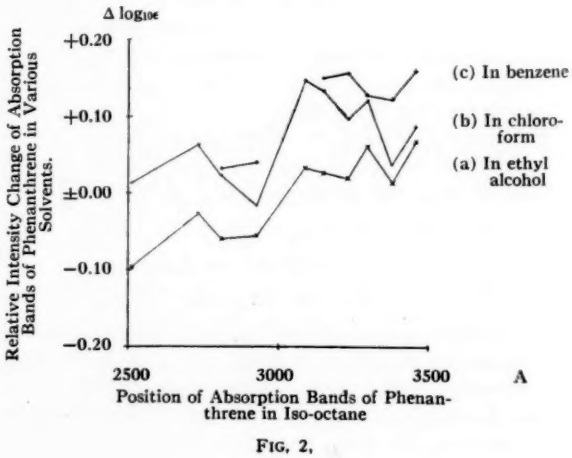

FIG. 2.

TABLE I. Distances between neighboring absorption bands in A.

Solvent	Distance between adjacent bands A–B	B–C	C–D	D–E	E–F	F–G	G–H	H–I	I–J
Iso-octane	223	78	114	161	62	80	66	83	78
Ethyl alcohol	232	65	124	155	67	80	65	82	79
Chloroform	212	78	123	135	74	76	71	82	79
Benzene	—	—	125	—	—	85	71	84	81

tively smaller distances from their long wave-length neighbors.

Of some interest is also the *percentage* change in absorption intensity on passing from iso-octane to one of the other three solvents. All three give rise to an increase in absorption intensity at the long wave-length end of the spectrum (Table II), and only ethyl alcohol seems to weaken the absorption at the short wave-length end.

TABLE II. Percentage change of absorption intensity in the ultraviolet spectrum of phenanthrene in various solvents both below and above 3000A as compared to phenanthrene in iso-octane.

Solvent	Maximum percentage change of absorption below 3000A	above 3000A
Ethyl alcohol	−6 to −20	+3.5 to +17
Chloroform	−3.5 to +15.5	+9.1 to +40.4
Benzene	+9.5 to +10.1	+32.3 to +45

[1] B. Vodar and S. Robin, J. Chem. Phys. **16**, 996 (1948).
[2] R. Schnurmann and S. Whincup, Petroleum **8**, 122 (1945).
[3] We are indebted to Dr. M. Sulzbacher of the Grosvenor Laboratory, London, for the synthesis of this particular sample of phenanthrene.
[4] A detailed account of this work will be published elsewhere.
[5] The phenanthrene bands are here lettered alphabetically beginning with *A* at the short wave-length end of the spectrum.

An Effect of Isotopic Mass on the Rate of a Reaction Involving the Carbon-Carbon Bond*

PETER E. YANKWICH** AND MELVIN CALVIN
*Department of Chemistry and Radiation Laboratory, University of California, Berkeley, California****
November 12, 1948

INVESTIGATION on the effect of the difference in mass between isotopes upon the rate of a chemical transformation has been limited entirely to the very lightest of the elements, especially hydrogen, although the effect of isotopic mass upon the rate of many physical processes has been extended throughout the periodic table.[1] The effect of isotopic mass on certain chemical equilibria has been used to separate the isotopes of carbon and nitrogen. Recently, the isotope effect on the rate of a chemical reaction has been observed by Beeck[2] who demonstrated in the course of a study of the isomerization of propane that the dissociation probability of the $C^{12}-C^{12}$ bond was increased 77 percent, and that of the $C^{13}-C^{12}$ bond decreased 12 percent from the dissociation probability of the $C^{12}-C^{12}$ bond in unlabeled propane. Further experiments[3] by the same authors yield a $C^{12}-C^{12}/C^{13}-C^{12}$ rupture ratio of 1.08 for thermal cracking at 500°, contrasted with 1.22 for electron impact rupture.

Decarboxylation reactions can be made to take place at moderate temperatures, and for a given reaction the isotope effect should increase with decreasing temperature. If a symmetrical dicarboxylic acid, labeled in only one carboxyl group, is decomposed to form a monocarboxylic acid and carbon dioxide, the primary competition for reaction is between the different functional groups in the same molecule. Assuming the same type of bond strengthening and weakening noted above, the carbon dioxide evolved would be impoverished in the label, while the mono-acid produced would be similarly enriched in label. Since the isotopic constitution of the remaining di-acid is unaffected, this result of symmetry can be used to "retire" part of the "chemically active" label and produce a level rate of isotope label enhancement with a constant net effect at any stage of the decarboxylation process.

Singly labeled malonic acid was prepared from chloracetic acid and active cyanide after the procedure of Weiner.[4] The product was recrystallized from diethyl ether—60° petroleum ether mixtures; m.p. 135°. A part of this acid was treated with bromine in moist ether, and the bromomalonic acid formed recrystallized from acetone and benzene. (The bromomalonic acid finally employed was not of great purity.)

A few hundred mg of acid was placed in the bottom of a pear-shaped flask, which could be swept throughout with nitrogen. The flask was heated in an oil bath ~10° above the decomposition temperature of the acid; carbon dioxide was swept through dry-ice-acetone traps (which served to collect much of the product mono-acid) into sodium hydroxide-filled absorption bubblers. After apparent completion of the reaction, the mono-acid was transferred to a combustion train. Two malonic acid experiments were performed, using 6 and 10 moles, respectively; one 2.1 mole bromomalonic acid decarboxylation was carried out.

The results of the experiments are shown in Table I. The frequency of rupture ratios was obtained by pairing each of the specific activity figures with those remaining, and the approach to identity of the three quotients thus obtained is a measure of the internal consistency of the experimentally derived data. The three bases noted are: *A*, carbon dioxide and di-acid; *B*, mono-acid and di-acid; *C*, carbon dioxide and mono-acid.

It is to be noted that the above ratios, that is 1.12 for malonic acid and 1.4 for the bromomalonic, are considerably larger than any isotope effects that have been observed in chemical equilibria. It is, of course, to be expected that the effect of the zero-point energy difference on a chemical rate process should be larger than its effect on an

TABLE I.

Compound	F_{12-12} basis *B*	F_{12-14} basis *A*	*A*	F_{12-12}/F_{12-14} basis *B*	*C*
Malonic acid	0.531 ±0.016	0.474 ±0.015	1.13 ±0.03	1.11 ±0.03	1.12 ±0.03
Bromomalonic acid	0.61 ±0.04	0.44 ±0.03	1.30 ±0.11	1.57 ±0.15	1.41 ±0.08

equilibrium, because the zero-point energy differences are also found in the product of an equilibrium as well as in the reactants while in a rate process presumably only the zero-point energy difference of the reactants is effective. However, if one tries to attribute the above-observed ratios entirely to differences in activation energy for the splitting off of the two different carboxyl groups, one arrives at a value of 96 calories for the difference in malonic acid and 250 for the difference in bromomalonic acid. These differences are rather larger than can be accounted for in terms of the effect of mass on the carbon-carbon stretching vibration (approximately 1000 wave numbers), and it is evident that the situation is more complex than that.

The assistance of Mr. Wilbur Melbye in the bromomalonic acid experiment is gratefully acknowledged.

* This paper is based on work performed under Contract No. W-7405-Eng-48 with the Atomic Energy Commission in connection with the Radiation Laboratory, University of California, Berkeley, California.

** Present address: Department of Chemistry, University of Illinois, Urbana, Illinois.

*** This paper has been presented at the 113th National Meeting of the American Chemical Society, Chicago, Illinois, April, 1948 and at the meeting of the Pacific Intersectional Group of American Chemical Society Sections of the Pacific Division of the American Association for the Advancement of Science, Berkeley, California, June, 1948.

[1] H. C. Urey, Record Chem. Progress **9**, 69 (1948).

[2] O. Beeck, J. W. Otvos, D. P. Stevenson, and C. D. Wagner, J. Chem. Phys. **16**, 255 (1948).

[3] D. P. Stevenson, C. D. Wagner, O. Beeck, and J. W. Otvos, J. Chem. Phys. **16**, 993 (1948).

[4] N. Weiner, *Organic Synthesis* (John Wiley and Sons, Inc., New York, 1943), Coll. Vol. II, p. 376.

Errata: "Raman Spectrum of Tetraethyl Orthosilicate" and "Raman Spectrum of Trimethyl Silicon Chloride"

[J. Chem. Phys. **16**, 1006, 1009 (1948)]

JULES DUCHESNE, A. MONFILO, AND CLAUDE ANSPACH
Faculty of Science of the University, Brussels, Belgium

THE names and addresses of the authors of these papers were incorrectly given. They should have appeared as "Raman spectrum of tetraethyl orthosilicate" by Jules Duchesne and A. Monfilo, Faculty of Science of the University, Brussels, Belgium, and "Raman spectrum of trimethyl silicon chloride" by Claude Anspach and Jules Duchesne, Faculty of Science of the University, Brussels, Belgium.

The following note should have appeared with both articles.

"One of us (Jules Duchesne*) wishes to express his sincere thanks to the University of Brussels for its kind hospitality during the tenure of his professorship there."

* Present address: Department of Chemical Physics of the University of Liege, Belgium.